Structure-Property Relationships in Polymeric Materials Generated by Electron Beam Processing

by

Robert W. Greer IV

Dissertation submitted to the Faculty of the
Virginia Polytechnic Institute and State University
in partial fulfillment of the requirements for the degree of

DOCTOR OF PHILOSOPHY

in

Chemical Engineering

APPROVED:

_____
Garth L. Wilkes, Chairman

_____ _____
Richey M. Davis Eva Marand

_____ _____
David A. Dillard Judy S. Riffle

November 18, 1997
Blacksburg, Virginia

Structure-Property Relationships in Polymeric Materials Generated by Electron Beam Processing

by

Robert W. Greer IV

Garth L. Wilkes, Chairman
Chemical Engineering

(ABSTRACT)

The work presented in this dissertation is in the subject area of radiation chemistry of polymeric materials and begins with a literature review of that subject. Along with the general literature review, three smaller and more specific reviews are presented for background information relevant to the three systematic studies addressed in the authors research. Following the literature review, these three studies involving the electron beam processing and subsequent characterization of various polymeric materials are presented.

The first study involves the generation of cellular materials by electron beam irradiation. A technique was developed for generating a cellular structure in a radiation curable composition prior to irradiation, extruding the composition, and then curing the froth in the electron beam accelerator, thus locking into place the cellular structure. A systematic study of different monomer/oligomer systems was conducted with mono-, di-, and triacrylate model systems utilized for comparative purposes.

The second study is a follow up investigation of previous work in the area of physical aging of polymers. A unique phenomena was discovered in

which a physically aged polymer displaying a typical excess enthalpic aging peak by DSC was observed to deage when exposed to electron beam irradiation. The goal of the presented work was to investigate what, if any, volumetric changes were occurring in these materials and to further explain the observed phenomena.

The third study involves the irradiation of high density polyethylene films having simple and well-defined stacked lamellar morphology without a distinct presence of row-nucleated fibril structures. These materials have been utilized to carry out investigations into the effects of radiation on their solid state structure-property relationships. These materials were characterized (as a function of radiation dose) with respect to the following areas with the utilized characterization technique(s) following: tensile behavior (Instron), dynamic mechanical behavior (DMS), melting behavior (DSC), lamella thickness (SAXS, TEM, and HSEM), orientation (WAXS) and microporous membrane formation (HSEM).

Acknowledgments

I would like to thank my advisor, Professor Garth L. Wilkes, for the education he has given me for even though I have learned much from him, he has also taught me how much more I have to learn. I thank him for his guidance, patience, friendship, and most importantly the knowledge he has given me over the last five years. I count myself as truly fortunate to have had the honor and privilege of being one of his students.

I thank my committee members for their helpful discussions and time during the course of my research.

I thank Professor Vivian Thomas Stannett of North Carolina State University for the research background in radiation chemistry of polymers he gave me during my last year at NCSU and his encouragement for me to continue my education with Professor Wilkes. I am grateful for his helpful consultations, his friendship and continued mentorship during my course of study at Virginia Tech.

I am grateful for the help I received from the departmental staff. I thank Billy Williams and Wendel Brown for their help in designing and repairing experimental apparatus, Dr. Conger for supporting my admission, Steve McCartney for his help in the microscopy lab and Sandy Simpkins for all her help supporting my work.

I thank my former and present lab colleagues Srivatsan Srinivas (Watson), Brian Risch and David Rodrigues for their help in getting me off to a quick start and trained on the lab's equipment. I thank Kurt Jordens, Chris Robertson, David Shelby and Jim Dounis for their helpful discussions and friendship over the years.

I thank my wife, Janice, for her love, friendship and daily unconditional support of my work. I thank my parents, Robert and Janel Greer of Greensboro NC for giving me life, continuing to support my education with their hopes and prayers, and for always being there for me over the years, without which this document could not exist. I also thank my brother, Matthew Greer of Lake Jackson Texas, my in-laws and extended family for their support.

I am thankful for the friendship I received from the many people I met here in Blacksburg who are too numerous to list. I am especially grateful for the people at Blacksburg Christian Fellowship and Blacksburg United Way Shelter Home for their friendship, support and prayers over the years.

Finally, I praise God for giving me my savior Jesus Christ and for blessing me with the strength and ability to attain this accomplishment.

> "Ever since the creation of the world His eternal power and divine nature, invisible though they are, have been understood and seen through the things He has made."
> Romans 1:20

Table of Contents

List of Tables

List of Figures

1 Introduction

The rapid growth of the nuclear industry over the past fifty years has given impetus to the study of the effects of the high energy ionizing radiation produced by these facilities and on the materials exposed to them. In addition, there continues to be a great deal of interest in improving the properties of these materials as a result of exposure to radiation. While one might initially think that nuclear physics would have predominate concern with these changes, nuclear physics is primarily concerned with the arrangement and interaction of particles with the nucleus of the atom. Most of the radiation induced changes that occur in materials come as a result of changes in electrons relative to nuclei.[1] Radiation chemistry is therefore a science that studies the changes that occur in materials as a result of exposure to high energy ionizing radiation.[2] High energy ionizing radiation is classified into two groups, particulate and photon radiation.[2-5] Particulate radiation includes the charged particles of electrons, protons, α-particles and heavy ions. Interactions with both particulate and photon radiation produces ionization and some excitation so these particles and photons are often grouped together under the term "ionizing radiations".[3] Photon radiation includes X-rays and γ-rays.[6] Visible and ultraviolet photons do not produce ionization and are therefore termed "nonionizing radiations".[3] These types of radiation will be briefly contrasted in a later section. The amount of energy transferred to a material by interaction with high energy radiation is highly dependent on the type of radiation (see Figure 1-1 and Table 1-1).

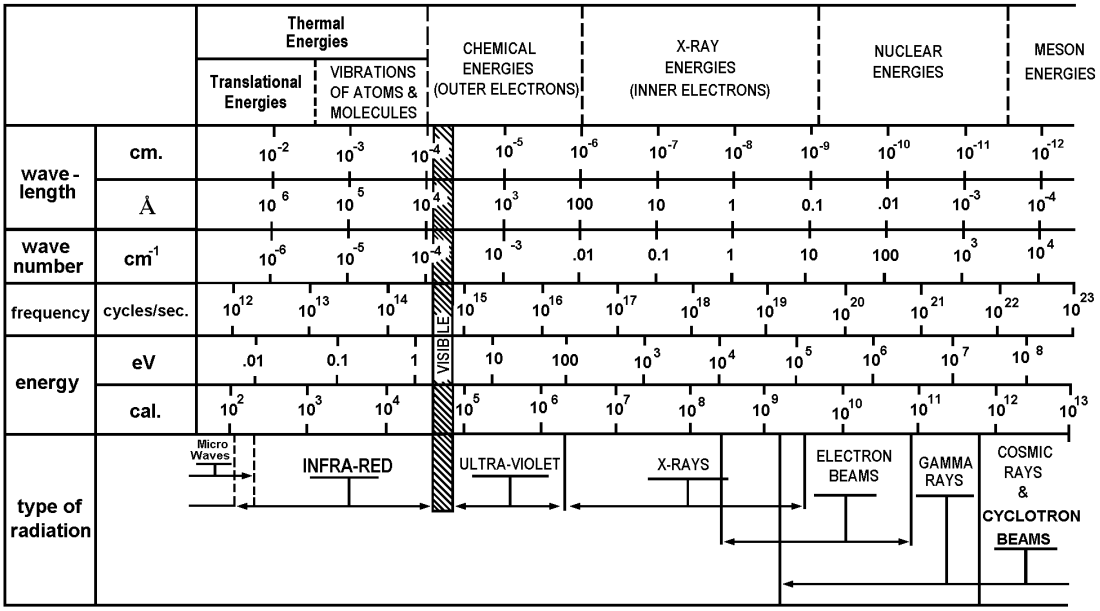

Figure 1-1 The X-ray region of the electromagnetic spectrum.[7]

Table 1-1 Subdivision of the Electromagnetic Spectrum in Terms of Wavelength, Frequency, Energy and Source[8]

Wavelength λ, nm	Frequency ν, sec^{-1}	Energy eV	Source
1.25×10^{-5}	2.4×10^{22}	1.0×10^{8}	Hard X-rays
1.0×10^{-4}	2.9×10^{21}	1.2×10^{7}	High end γ range
6.0×10^{-4}	5.3×41^{20}	2.2×10^{6}	Y^{90} β electrons
4.0×10^{-3}	7.5×10^{19}	3.1×10^{5}	Co^{60} β electrons
1.25×10^{-2}	2.4×10^{19}	1.0×10^{5}	High end soft X-ray
2.5×10^{-2}	1.2×10^{19}	5.0×10^{4}	Low end λ range
6.8×10^{-2}	4.4×10^{18}	1.8×10^{4}	H^{3} β electrons
1.25×10^{-1}	2.4×10^{18}	1.0×10^{4}	Low end soft X-ray
1.25×10^{2}	2.4×10^{15}	10	Photon UV
2.5×10^{2}	1.2×10^{15}	4.9	Hg lamp

With the exception of neutrons, radiation interacts with orbital electrons only. Therefore, deposition of this high energy radiation is dependent of electron density for which mass density typically provides a good approximation.[9]

The interaction of high energy radiation with matter takes place by three main processes:[10]

- Reaction with the nucleus which typically produces new nuclear arrangements or structures.
- The displacement of these nuclei which gives a new atomic or molecular arrangement.
- The further interaction with orbital electrons, and any atomic rearrangement that occurs indirectly due to the different electron system. In this step, there is no change in nuclear structure. Radiation chemistry deals primarily with the last of these processes, which results in chemical changes in the system.

History of Radiation Chemistry

Nature has given us the opportunity to observe radiation chemistry since man's first recorded history. One of the earliest known observations in radiation chemistry was that of Homer, who observed a sulfur-like smell in the air after lightning. This smell was due to ozone and oxides of nitrogen produced by reactions initiated by the lightning. However, radiation chemistry did not begin on a scientific basis until the late 1800's.[11] In 1874 the formation of an inert solid (which we now know to be polymeric) when acetylene was exposed to an electric discharge was observed. Wollaston and Berzelius were two of the first to investigate radiation in materials in their study of thermal luminescence in materials containing radioactive elements.[1] However,

radiation chemistry is typically credited with having it's origins in the discovery of X-rays by Wilhelm Conrad Roentgen November 8, 1895. [12]

Roentgen was interested in obtaining information about the nature of cathode rays, and was carrying out experiments on the discharge of electricity through gases when he noticed that a sheet of paper coated with barium platinocyanide fluoresced when the discharge was operating. Covering the discharge tube with black paper which absorbed any ultraviolet light from the discharge did not prevent this fluorescence. He concluded that the fluorescence was thus due to some previously unknown type of radiation, which he labeled "X-radiation."[13]

Roentgen was able to reveal some of the properties of X-rays in further experiments. He found that X-rays were very penetrating and could pass through substances which were opaque to ordinary light. He found that all substances reduced the intensity of the rays, and further found that the absorbing power of a material depended to some extent on its density and its relative atomic mass. Roentgen showed that the X-rays had the power to blacken a photographic plate wrapped in black paper. He also showed that a gold leaf electroscope could be discharged when exposed to X-radiation. Thomson also noticed this phenomena, and the cause was soon traced to the ionization of air molecules in the electroscope. It was thus shown that X-rays were capable of causing ionization of gases.[13]

Roentgen had shown that X-rays could produce fluorescence in several substances, and he had also reported that the X-rays radiated from that part of the discharge tube opposite the cathode and that the inner wall of the tube in this region fluoresced. It was this connection between X-rays and fluorescence which attracted the attention of Becquerel in 1896.[14] Becquerel had been interested in the phenomena of fluorescence for some time, and several years earlier he had prepared potassium uranyl sulfate and noticed its pronounced

fluorescence under the influence of ultraviolet light. Becquerel performed the photographic plate experiments and found that the blackening on the plate could be caused by these salts and the blackening was proportional to the amount of uranium in the sample. Other important work in 1896 was done by J.Perin, who measured X-ray intensity using an air-ionization chamber.[15]

In 1898, Pierre and Marie Curie reported that radiation of glass caused color changes and that irradiation of oxygen produced ozone.[16] The finding that some materials change color upon irradiation lead to the use of materials that have this property in dosimetry. They also showed that the radiation emitted by uranium compounds was an atomic phenomena which did not depend on the chemical or physical state of the active element. The phenomenon was termed *radioactivity* by the Curies. In 1899 Rutherford used an apparatus similar to the one Marie Curie had used to study the nature of radiation. Rutherford was able to show that there were two types of radiation by interposing metal foils between the source of radiation and the detector. Whereas one of these was absorbed completely by a few thousandths of a centimeter of aluminum foil, the other required about a hundred times this thickness for absorption. The first type was named α-radiation and the second type β-radiation. At about the same time, Villard showed that a third type of radiation, much more penetrating than β-radiation, could be obtained from some radioactive elements. This was called γ-radiation.[17]In 1900, Giesel observed decomposition of water and the coloration of alkaline halides. By late 1900, alpha, beta, and gamma rays had been distinguished with regard to their charges and their respective abilities to ionize and penetrate various materials.[18]In 1901, Becquerel observed the effects of β and γ radiation and compared their effects to that of light. In 1906, Jorrissen and Ringer[19] demonstrated that hydrogen and chlorine combine at room temperature by radiation and Jorrissen and Woudstra[20]showed that the penetrating radiation from radium caused the

coagulation of some colloid solutions. In 1925, Collidge irradiated various organic materials with cathode rays and reported on the formation of solid deposits on the walls of his equipment, alluding to the ability of radiation to induce polymerization.[21]In 1929, E.B. Newton subjected rubber to cathode rays demonstrating that crosslinking could be achieved by radiation exposure.[22]It should be noted that most of this early work was carried out before the development of powerful radiation sources.

Radiation chemistry truly began to flourish after the Manhattan Project and atomic bomb along with the first nuclear reactor was built in Chicago after World War II.[23]After these events, interest in nuclear fission and the effects of radiation environments on materials exposed gave renewed interest to the area of radiation chemistry. In addition, there was large concern over the then unknown effects of radiation on biological systems. Radiation sources became more powerful and were readily available as non-natural radioisotopes (e.g. cobalt-60), were produced in atomic reactors.

The discovery of crosslinking reactions by Dole and Rose[24]during 1947-1949 led to the first systematic study of the radiation chemistry of polymers and the property changes that occur in them. Dole and Rose observed that polyethylene chains were crosslinked by radiation and this induced notable effects on the mechanical properties of polyethylene. Perhaps the most significant contributions to the field of radiation chemistry were produced by Charlesby, who in 1952 published his first paper on the effects of radiation on polymers. In his first paper, Charlesby demonstrated that polyethylene could be transformed into an insoluble, crosslinked material with high thermal stability.[25]In 1960, Charlesby authored what is, to date, the treatise which best describes the theoretical and experimental aspects of crosslinking and scission for polymers subjected to radiation.[1] Charlesby's brilliant treatment of the mechanisms and consequential aspects of radiation induced modifications in

various polymers is best appreciated by considering that his analysis is as valid now as it was almost forty years ago.

Today, the effects of radiation on polymeric materials is an area of increasing interest to many high technology industries.[26-27]From radiation sterilization, microlithography, thin film applications, crosslinking of wire and cable, to satellites in orbit, the response of polymeric materials to irradiation is critical in design and system lifetime determination.

Polymers can respond to ionizing radiation in one of three ways. First, no reaction may occur and these types of polymers are in high demand for many applications. As mentioned above, the polymer can react by degradation (main chain scission) or crosslinking - but more often a combination of scission and crosslinking. The types of polymers that have the ability to resist degradation are termed "rad-hard" and are also of interest in increasing the lifetime of polymeric materials used in the automotive industry. In addition, rad hard polymers are required in aerospace programs where radiation resistant polymers are desired as the need for longer lifetimes of satellites and other space vehicles are increased. In the biomedical field, radiation sterilization is becoming more popular as concern for the toxicity of chemical sterilants increases.[28] In this field, the need for more radiation resistant polymers is required as the polymers that are commonly used in implantable surgical devices tend to undergo some radiation-induced degradation leading to discoloration and loss of properties.[29] Polymers that respond to radiation by scissioning are also commonly used in positive resist microlithographic applications. The need for better microlithographic resist materials is demonstrated in Figure 1-2. These resist materials are typically positive resists although negative resist materials are becoming more popular as decreasing linewidths merit.[27] Further, Intel® production guidelines indicate that the number of transistors on their mass produced microprocessors should

double every eighteen months. This rule has held since the early 1970's and is known as *Moore s Law* after Intel's chairman. One consequence of this "Law" is that the space the transistors occupy must also be reduced to accommodate the overall chip size and thus the polymer resist material plays a key role in this process by allowing higher resolution lithography.

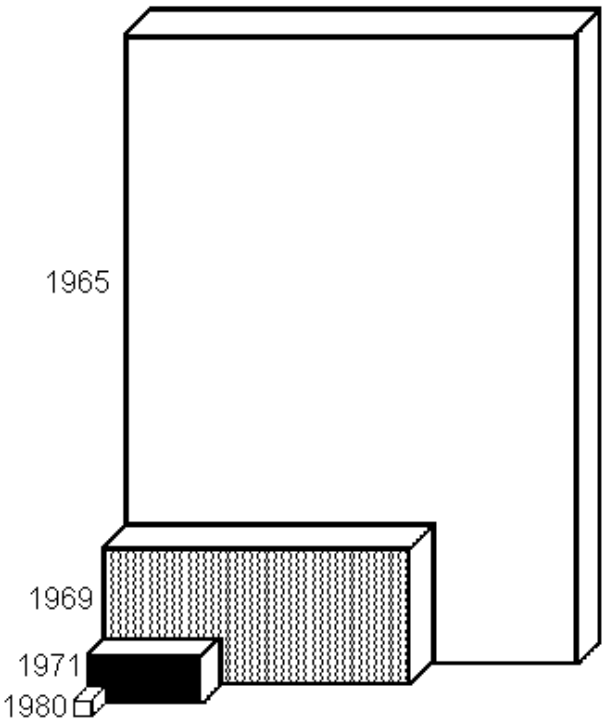

Figure 1-2 Relative size of circuitry required to produce the calculator logic chip in 1965 vs. 1980. [30]

Polymers that respond to radiation by crosslinking are useful in many other applications, such as surface coatings and wire and cable applications. The ability to crosslink a polymer can lead to improved abrasion resistance and increased solvent resistance. The use of polymer radiation to crosslink polymers, notably PE for cables, heating pipes, and shrinkable packaging film has become well established over the last 30 years. Further applications include irradiated polyethylene for cardiovascular systems, and hip prosthesis with long term dimensional stability, low friction and no brittleness, while the grafted system (polyethylene powder with acrylic acid graft) can be used to improve adhesion of PE to metals, e.g. aluminum. Polymers with a hydrophilic graft are used to control the release rate of drugs for other medical purposes. Numerous other applications have been suggested, either as novel ideas or as alternative techniques for producing an existing well-established product.[31]

The purpose of this introduction has been to acquaint the reader with the history and background for the study of radiation chemistry. It is hoped that some appreciation has been gained for the advances that have been made as well as the work that needs to be done. The following chapters will cover the system of units for radiation chemistry and the fundamental aspects of particle and photon interactions. In subsequent sections, a comparison of various types and sources of radiation, some general features of the interaction of radiation with condensed organic systems, radiation response of polymers, polymerization, grafting, electron beam processing of polymers, cellular materials, physical aging, and some general features of semi-crystalline polymers will serve as background information in the form of a literature review for the work presented. Following the literature review, experimental results and conclusions are reported on: (1) the generation of cellular materials by electron beam irradiation, (2) the apparent reversal of physical aging in irradiated glassy polymers, (3) the electron beam irradiation of high density polyethylene extruded tubular films having a well defined stacked lamellar morphology.

2 Literature Review: Radiation Chemistry of Polymeric Materials

2.1 Introduction

Chapter two is a literature review of radiation chemistry of polymeric materials. Section 2.1 contains some background information as well as the history for the field and a discussion of the system of units for radiation chemistry. Section 2.2 discusses fundamental concepts of the interactions of the two types of radiation; particulate and photon radiation. In section 2.3, the absorption of radiation is covered and in section 2.4 the sources for radiation are discussed. Section 2.5 includes the radiation response of polymers. Finally, sections 2.6 through 2.10 cover polymerization, grafting, irradiation in a solvent, and physical aging.

2.1.1 Background

The current literature dealing with radiation effects cover a very wide range, from basic radiation chemistry of polymers, on low molecular weight organics which serve as simple models, to kinetic reactions , and to potential applications. Some more fundamental subjects of interest in the field of radiation chemistry of polymers follow. This should give the reader some idea of the present state of the art of the fundamental aspects in the field.

- There is interest in the influence of chemical and physical structures on energy absorption. e.g. crystallinity, orientation, side groups, etc.
- Why is polystyrene observed to be relatively resistant to radiation in comparison with most other polymers? The accepted answer is energy transfer, however there is debate over whether or not this is adequate enough of an explanation.

- Ionization typically produces an excited system with electron recapture but can be largely affected by chemical structure, molecular arrangement, and especially electron density which is of interest to those who desire a predetermined radiation response from synthesized molecules.
- Trapped electrons can cause radiation induced conductivity and can also lead to bulk property changes with time.
- What happens between the initial energy absorption (which is considered to be random) and the highly selective bond which is affected? For example, in polyethylene (PE) it is the side C-H bond which is broken. However in polyisobutylene it is the main chain C - C bond which scissions. Precise knowledge of why this occurs can lead to better design of molecules with a desired radiation response.
- Prediction of lethal doses for biological molecules can lead to some surprising results. For example, it only takes one "event" per polymer chain to lead to dramatic changes in properties. The higher the molecular weight, the lower the required dose for these changes. This analysis is also true for larger molecules (e.g. DNA@10^9), which just on molecular weight considerations alone, requires a very low dose relative to typical synthetic molecules for damage to its structure.[32]

These items are just a few of those concerning radiation polymer chemists; however, they represent the more fundamental areas of current focus in the field. While the area of research is more engineering in nature, it is important to mention and discuss the fundamental science that motivates a lot of the work in the field.

2.1.2 System of Units for Radiation Chemistry

Many different units are used in radiation chemistry. As the field has progressed, many units have been outdated and replaced with more up to date units reflecting the use of metric and SI standards. These units are used to describe the intensity of a radiation source, absorbed dose, and the chemical changes that occur as a result of absorbed energy. It has been observed that for energies greater than 20 keV, the number of events that occur in a material does not depend very much upon the nature or energy of the radiation used.[33] This concept is important for comparison of the results from different sources of radiation. Keep in mind that environmental conditions (e.g. temperature, oxygen) will still play a critical role as will be discussed in later sections. What follows is a listing of the classical and modern units used to describe these items.[34]

2.1.2.1 Intensity of Radiation Source:[33]

1 curie (Ci) = 3.7×10^{10} disintegrations per second (classical)

1 Becquerel (Bq) = 1 disintegration per second (SI)

The activity of a radioactive nuclide is expressed in terms of the number of nuclear transformations which occur in unit time. The unit of activity is the curie (Ci) corresponding to 3.7×10^{10} events, or disintegrations, per second. (s^{-1} = Hz)[33]

2.1.2.2 Absorbed Dose[33,35,36]

The absorbed dose is most commonly expressed in terms of a unit called the rad. The International Commission of Radiological Units and Measurement in 1959 recommended the adoption of the rad as the unit of absorbed dose of any ionizing radiation.[37] The rad corresponds to an energy

absorption of 100 erg (10 μJ) per gram of material irradiated (10^{-2} J/kg). The dimensions are (length)^2 x (time)$^{-2}$. Electron volts (eV) per gram is also used, mostly for electron accelerators.

1 eV = 1.6 x 10^{-19} J

1 rad = 0.01 J/kg

1 gray (Gy) = 1 joule/kg (SI)

1 Gy = 100 rad

1 rad = 100 ergs of energy absorbed per gram of material irradiated.

1 rad = 6.24 x 10^{13} eV/g

2.1.2.3 Amount of Chemical Change[32,33,35]

The *G* value represents the average number of "events", or more usefully, reactions per 100 eV of absorbed energy. Most G values lie between 0.1 and 10. Higher values usually indicate a chain reaction.[33]

"G" value = # of events per 100 eV of energy absorbed

1.0 μ mol /J = 10 G

2.1.2.4 Linear Energy Transfer(L.E.T.)[33]

Linear energy transfer (LET) is the average energy locally imparted to the medium by ionizing radiation of specified energy in traversing a certain distance. It is expressed as energy per unit distance, e.g. eV/A or aJ/nm, and is different for each type of radiation (1 eV/A = 1.6 aJ/nm).

For X-rays or γ-rays the exposure at any point is expressed as roentgen (R). One roentgen produces a total of 2.58 x 10^{-4} coulomb of electrical charges on all of the ions of one sign in one kilogram of air. An exposure of one roentgen

corresponds to an absorbed dose in air of 86.9 erg/g. One roentgen of 1 MeV γ-radiation deposits 96.5 erg in water, but this figure varies with the energy of the radiation and with the material being irradiated. The rad is the measure of energy absorbed in the system and is preferable to the roentgen. The roentgen is rarely used in radiation chemistry. The absorbed dose in a system in rads is numerically the same as the exposure in roentgen, within a few per cent. [33]

2.2 Interaction of Ionizing Radiation With Matter

The fundamentals of the interaction of radiation with matter have been reviewed in several texts. [33, 38-44] Expressed in its most basic form, high energy ionizing radiation interacts with materials to produce ionization, excitation and lattice defects.[33] The resulting species can further react to give free radicals, which can cause monomers to polymerize, or cause polymers to crosslink and degrade, and, in mixtures, monomers to graft to polymers. While the chemical nature and morphology of the material determines which of these reactions are predominant, it is also important to consider the environment in which ionizing radiation occurs as this can influence reactions in many cases.[45]

Ionizing radiation deposits energy that is large and highly localized therefore chemical bonds can be often easily broken and/or reconfigured after a very short time interval (see Table 2-2). In addition to ionization, the mechanism of excitations causes these radiations to deposit energy in an absorber. In this process, an atom or molecule is raised to a higher energy level by the interaction without gaining the necessary energy for an electron to be ejected.

Each molecular species has well-defined quantised electron energy levels. Therefore, the energy required to ionize will depend on the orbital from which the electron is ejected and may vary from a few electron-volts (eV) for

the least tightly bound electron, to several thousand electron volts (keV) for inner shell electrons in a heavy atom. The average energy required to ionize an atom is given by E_1, the mean excitation/ionization potential for the atom. The following formula can be used to estimate E_1 for an atomic element of number Z:

$$E_1 = \begin{cases} 19.0 \text{ eV} & Z=1 \\ (11.2 + 11.7Z) \text{ eV} & 2 \leq Z \leq 13 \\ (52.8 + 8.7Z) \text{ eV} & Z > 13 \end{cases}$$

The parameter defined as W is the average energy expended in producing a single ion pair and also contains the energy used in excitation interactions between ionizations. Its value depends on the type of radiation and on the absorbing material. The accepted value of W in air is 33.8 eV, for water 29.6 eV and for methane 27.3 eV.[46] Since excitations involve smaller amounts of energy, it follows that the excitation rate far exceeds the ionization rate. It is more difficult to measure W in liquids and solids than in gases since the charges of opposite sign are more difficult to collect. In solid conductors, the electrons released by the radiation are a very small proportion of the total which would be collected in an electric filed, whereas in polymeric insulating materials it becomes extremely difficult to collect and measure the number of ions formed. A proportion of the energy of the incident radiation may also be used to create photons in solid materials.[47]

The two types of ionizing radiations, particulate and photon (sometimes called electromagnetic) radiation are sometimes referred to as directly ionizing (particulate) and indirectly ionizing (photon) radiations. The major difference between the interactions of directly ionizing and indirectly ionizing radiations is that for indirectly ionizing radiation there are few collisions and each involves a large energy loss, whereas directly ionizing radiation involves a very

large number of interactions, with little loss of energy each time.[47] Particulate radiation includes the charged particles of high energy electrons, protons, deuterons, α-particles, β-particles, and heavy ions as well as electrically neutral particles (neutrons). Photon radiation includes gamma radiation and X-rays. High energy electromagnetic radiations, such as 1 MeV γ-rays, and neutrons can penetrate through about a meter of solid material. The charged particles can penetrate only about a few millimeters in solids. X-rays and γ-rays penetrate intermediate distances. As mentioned before, with the exception of neutrons, radiation interacts with orbital electrons. Table 2 shows data for the penetration of 1 MeV radiations in water and in air.[33] Reasonably extensive descriptions of the nature of these radiations, their sources, and their interactions with polymers have been published.[48,49]

The effects produced in a pure polymer by the absorption of a given amount of energy per gram are typically independent of radiation type, energy, intensity, energy transfer efficiency, and source. The first reason for this has to do with how radiation transfers energy to a polymer. This process occurs primarily by ionization (ejection of electrons from molecular orbitals) and by subionizing excitation of the orbital electrons. Ionization and subionizing excitation are of comparable magnitude in the dissipation of radiant energy and total to an average of approximately 34.5 eV per ion pair produced. Most of the ion pair formation is accomplished by the initially ejected electrons which ionize and excite molecules along their paths before slowing down and being captured by positive ion sites. 1 e.v. per molecule is equivalent to 23.05 kcal/mole so that at a neutralization site there is sufficient energy available to cleave many chemical bonds. A large part of this cleavage should be homolytic, thus yielding free radical species capable of undergoing their characteristic reactions. Due to the large amount of available energy, some nonradical, molecular detachment reactions are also possible.[50]

The second reason is the apparent "caged" reaction which exists. This reaction depresses the effect of concentration of reactive species upon the reaction efficiency. Therefore, densely ionizing radiations (α-particles, protons, deuterons) which have a high linear energy transfer in the polymers do not exhibit greatly reduced chemical reaction efficiency within their tracks. Likewise, variations by many orders of magnitude in the intensities of penetrating radiations (γ-rays and X-rays) does not significantly change the reaction efficiency on the basis of energy absorbed. Therefore, the interaction between reactive species in different ionization tracks within solid polymers is not usually evident.[50]

Table 2-1 Penetration of 1 MeV radiations[51]

Type of Radiation	Penetration	In Water (cm)	In Air (cm)
X or γ	hvt	10	7000
β or Electron Beam	Range	0.5	400
Alpha	Range	0.0005	0.2
Proton	Range	0.002	2.3
Neutron	hvt	1.5	Large
Fission fragment	Range	0.01	2.5

hvt = half value thickness

Table 2-2 shows the time scale of the principal events occurring in radiolysis. These times depend to a small extent on the particular substrate and are therefore approximate.

Table 2-2 Time scale of events in radiation chemistry.[37]

Time(s)	Event
10^{-18}	Ionizing radiation traverses one molecule.
10^{-15}	Time interval between successive ionizations.
10^{-14}	Dissociation of electronically excited species. Transfer of energy to vibrational modes. Ion-molecule reactions beginning.
10^{-13}	Electrons reduced to thermal energies.
10^{-12}	Radicals diffuse one jump.
10^{-11}	Electron is solvated in polar media.
10^{-10}	Fastest diffusion controlled reactions are complete.
10^{-8}	Molecular products complete.
10^{-5}	Scavenging of radicals by reactive scavengers.
10^{-3}	Reactive decay of triplet states.
1	Most reactions are complete. In some systems, post-irradiation reactions may continue for several days.

It will be seen that, apart from the earliest events, many of these processes can be studied using the technique of pulse radiolysis. In the solid state, some of the reactive intermediates are trapped and can be analyzed by conventional spectroscopy.

What follows is a review of the two fundamental interactions in materials, particulate and photon.

2.2.1 Particle Interactions in Materials

As mentioned in the section 2.2, particulate radiation includes the charged particles of electrons, protons, α-particles, and heavy ions. Beta-particles and electron beams are high-energy (high-velocity) electrons.[33] An

electron beam accelerator is used as the radiation source in the presented research. Although discussed in the next section, high energy electrons can also be produced by Compton and photoelectric processes in material irradiated by γ-rays. [52]

Energetic charged particles can deposit energy in a medium in several possible ways, but the one that concerns radiation chemistry the most is through the interaction with the electrons of the medium. Such electrons can be excited to higher energy levels, or they can be ionized; and these processes constitute the most important mechanism for the loss of energy by the charged particles.[52]

It is well known that charged particles form tracks as they deposit energy in a medium. For example, particle tracks in photographic emulsions are well understood, and each track is characteristic of the charge and velocity of the particle that forms it. In high-energy particle studies, such tracks are used in particle identification. Similarly, many results of radiation chemistry can be understood in terms of "initial" track structure. By this term it is meant that the geometrical pattern of energy deposition at the instant the energy is transferred to the medium. In order to describe this pattern, terms such as spurs, blobs, short tracks, and branch tracks are used. Based on these concepts, a general description for the track structures of all charged particles can be made.[52]

Ionization is typically considered as the phenomenon which results when high-energy radiation which interacts with matter. However, during a glancing collision, insufficient energy may be transferred to eject an electron completely, i.e. to effect ionization. If an electron is raised to a higher orbital, the molecule will be electronically excited. The secondary electrons towards the end of their paths are more likely to cause excitation than ionization. Consequently, there is a zone of excitation surrounding the zone of ionization along the track of an ionizing particle.[53] (see Figure 2-1)

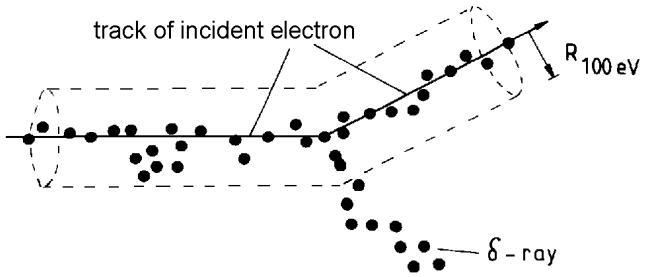

Figure 2-1 Schematic representation of ionization and excitation sites produced by an energetic electron in an absorbing medium.[53]

If one electron is ejected and another in the same atom is excited an excited ion results. If two partners of an ion pair recombine, i.e. an electron and its parent positive ion, an excited molecule will be produced. A large proportion of the energy deposited in a material appears as heat, i.e. as other forms of excitation (vibrational, rotational and kinetic), but electronic excitation is probably more important because it can lead to chemical reaction.[33]

In contrast to the photon, the energy of which may decrease considerably in every act of interaction with the molecules of the medium it traverses, the electron loses its energy very gradually in ionizing and exciting a large number of molecules. In the interaction of a fast electron with a water molecule, an electron is often ejected and the incident electron continues its travel with a smaller energy on account of the ejected electron. If a very fast electron happens to pass by an atomic nucleus, which is rather an infrequent case under conditions in which radiation-chemical experiments are carried out

(low Z of the medium and electron energies mostly less than 5 MeV), then the electron may be suddenly decelerated. The corresponding energy loss is manifested in the form of *bremsstrahlung* which may be later absorbed by the material. A small amount of energy is also lost as Cerenkov radiation - a characteristic blue glow when high-energy electrons are slowed down to the speed of light in materials of refractive index greater than one. As to the fate of low-energy incident electrons or secondary electrons produced in one of the processes mentioned previously, they chiefly lose their energy in the following ways: they excite molecules, neutralize the positive ions present, attach themselves to neutral molecules, or polarize the medium and become hydrated. Capture of an electron by a positive ion or by a neutral molecule may be accompanied by dissociation of the product obtained.[54]

The range of high-energy electrons in a material is directly proportional to their energy and inversely to the density of the material. For 1-MeV electrons the maximum penetration in water is 5-6mm. As with γ-radiation, electrons do not produce their maximum effect at the surface of the irradiated material. The incident electrons eject orbital electrons by the process of Coulombic interaction, producing ionization. Thus, the primary electrons are slowed down and cascades of secondary, tertiary, etc., electrons are produced. The ionization density is higher than for γ-rays, but still not very high, except towards the ends of the tracks, where the electrons are moving more slowly and make more frequent collisions.[54]

Although electron interactions are of primary concern in the proposed research, it is important to recognize other forms of charged particles and their interactions with matter.

2.2.1.1 Heavy Charged Particles.

Alpha-particles, proton beams, etc., consist of the positively charged nuclei of atoms shorn of their orbital electrons. They have short ranges, and hence produce very intense ionization along their tracks. They transfer their energy to the medium in the same way as electrons, ionizing and exciting molecules in a number of successive collisions. This proceeds until the charged particles are so much slowed down that they may be neutralized by reaction with electrons, whereby their travel is stopped.[48] Alpha particles are produced from some radioactive heavy elements. They consist of helium nuclei, $^{4}_{2}He^{2+}$, and have discrete energies. [54]

2.2.1.2 Protons and Deuterons

Protons ($^{1}_{1}H^{+}$) and deuterons ($^{2}_{1}D^{+}$), are the nuclei of ordinary and heavy hydrogen atoms respectively. When produced directly by accelerating machines they are mono-energetic, but when produced by the slowing down of fast neutrons in hydrogenous material such as water or paraffin wax they have a range of energies. [54]

2.2.1.3 Fission Fragments

Fission fragments are formed whenever fissile materials, such as uranium-235 or plutonium-239, capture neutrons, for example in a nuclear reactor. Fission fragments are produced when the compound nuclei split in two. They are the nuclei of elements in the middle of the periodic table, partially shorn of electrons so that initially they each carry a net charge of about +20. They have enormous energies (up to about 100 MeV = 10 pJ) and form extremely dense ionization tracks. The range of heavy particles in water is very short. For 1-MeV particles the ranges in water are 5 microns (5 uM) for

alpha particles and about 30 microns for protons. The range of fission fragments is about 0.1mm (100 um). [54]

The processes by which heavy charged particles lose energy are similar to those for light charged particles, leading to ionization of the molecules of the medium. Since all the energy is deposited in a short distance, the ionization density is very high, particularly towards the end of the range.

2.2.1.4 Neutrons

In contrast to the case of the radiations considered previously, the primary interaction of neutrons with a medium involves not the electron shells but the nuclei of the atoms. Neutrons with energies larger than that of thermal motion give up their energy in elastic collisions with nuclei. The smaller the mass of the nucleus encountered, the larger the energy loss. [54]

Neutrons arise from fission events in atomic reactors or when α-particles, accelerated charged particles, high-energy x-rays or γ-rays impinge on certain targets. Because they are uncharged, neutrons do not interact with orbital electrons. They lose their energy by elastic collision with atomic nuclei- the lighter the nuclei, the greater the amount of energy transferred. Fast neutrons penetrate several centimeters in water, and along their tracks produce "knock-on" protons, which act in just the same way as would accelerated protons in the same locations. [54]

After several collisions the neutrons have been slowed down and no longer displace atoms. Finally they reach thermal energies (0.025 eV = 0.004 aJ) and may be captured by certain elements. Following the capture, excess energy may be emitted as a γ-ray and the capturing atom may recoil out of its molecule. This recoiling atom is called a 'hot atom' and acts like a heavy charged particle. Certain elements, after capturing a neutron, emit α-particles.

These elements are sometimes called 'energy converters'. Thus boron-10 after absorbing a neutron decomposed into lithium-7 and an α-particle.[35,54]

Reactor Radiation Reactor, or pile radiation is a mixture of γ- and neutron radiation. This makes the chemical effects of the radiation rather difficult to interpret, hence it is not suitable for basic studies. [54]

2.2.1.5 Inelastic Collisions of Electrons

At lower energies electrons lose their energy by inelastic collisions with electrons of the stopping material resulting in ionization and excitation in the material. The equation describing the rate of energy loss of an electron by ionization and excitation was first derived by H.A. Bethe and is given by:

$$\frac{dE}{dx} = \frac{2\pi Ne^4 Z}{m_0 v^2}\left\{\ln\frac{m_0 v^2 E}{sI^2(1-\beta^2)} - \ln 2\left(2\sqrt{(1-\beta^2)} - 1 + \beta^2\right) + 1 - \beta^2 + \frac{1}{8}\left(1-\sqrt{(1-\beta^2)}\right)^2\right\} \quad (2\text{-}1)$$

where: E is the energy of the electron
x is the distance traveled by the electron in the material
N is the number of atoms per cm^3
e is the charge of the electron
Z is the atomic number of the stopping material
m_o is the rest mass of the electron
v is the velocity of the electron
I is the mean excitation potential for atoms of the stopping material
and β=v/c where c is the velocity of light.

The quantity dE/dx, i.e. the rate of loss of energy with distance, is usually known as the linear energy transfer (symbol LET) and is a very important quantity in describing the behavior of any radiation.[37]

2.2.1.6 Elastic Collisions of Electrons

Electrons, because of their small mass, are readily deflected by the Coulombic field of a nucleus. Although there is no energy loss in elastic collisions of this kind, such collisions are important in that they result in a non-linear passage of the electron through the medium. Elastic collisions are important for low-energy electrons in materials of high atomic number. [37]

2.2.1.7 Effect of LET

The LET of all particles increases as the energy of the particle decreases. It is, however, convenient to characterize radiations by their mean LET values, i.e. the total energy of the radiation divided by the distance traveled by the radiation before coming to rest. Mean LET values for different radiations are given in Table 2-3. Usually LET values are in units of eV per angstrom.[37]

Table 2-3 Mean LET values for water.[37]

Radiation	Mean LET (eV A^{-1})
2 MeV electrons	0.021
1.25 MeV gamma rays (60Co)	0.021
0.018 MeV Beta-particles (3H)	0.32
5.3 MeV alpha particles (210Po)	13.6
1 MeV alpha particles	18.9

It is instructive to follow the passage of a high-energy electron (~2 MeV) through a typical liquid, e.g. water. Secondary electrons will be produced along the primary track as a result of inelastic scattering. Some of these electrons will have relatively low energies, about 100 eV, and this energy will be

dissipated rapidly as ionization and excitation within a relatively short range, about 20Å. Such ionizations and excitations are said to lie within a spur and for electrons of LET 0.02 eV $Å^{-1}$, such spurs will lie on average 5000Å apart. The energy required to create an ion pair is about 30 eV and about three ion pairs will be produced within a spur. Other secondary electrons will have relatively high energies with characteristic low LET and will form tracks of their own branching off from the primary track. Such tracks are known as δ-rays. Towards the end of a track when the energy of the electron falls below 500 eV, the LET will be much higher and the region of ionization both bigger and denser. These are sometimes referred to as blobs. With more densely ionizing radiation, the spurs will be produced in such proximity that they overlap each other resulting in the production of a high concentration of ions and excited molecules along the primary track.[37]

2.2.1.8 Radiation Induced Conductivity

The formation of radicals in irradiated polymer is the sequence of a series of events initiated by the absorption of energy from the incident high energy photon or electron. Not always is the electron ejected from the parent molecule recaptured by the polymer molecule to give a radical; it may become a mobile electron, away from its parent molecule, or it may be trapped and released far later. The physical effects include radiation induced conductivity and thermoluminescence.[55]

Considerable research effort has gone into studying the conductivity of polymers under a range of conditions other than during radiation, e.g. with a strong electrical field, but studies using radiation have notable advantages. Electrons are liberated uniformly throughout the specimen, and one can determine the effect of temperature and dose rates.[55]

2.2.1.9 Mass Stopping Powers

When energetic electrons penetrate materials, they lose energy by two mechanisms-collision loss where energy is given to electrons in the atoms of the material, and radiation loss involving the conversion of electron kinetic energy to photons of X-radiation in the field of an atomic nucleus. As the high energy incident electron traveling through the material might pass by a particular atom in about 10^{-18} s, it is able to exert large Coulomb forces on the atomic electrons and impart energy to them. The energy transfer may be sufficient to allow the electron to leave the parent atom, and so cause ionization, which is completed within about 10^{-15} s. Alternatively, the atomic electron may be excited to a higher state. These inelastic collisions are the most important mechanisms of energy loss.[56]

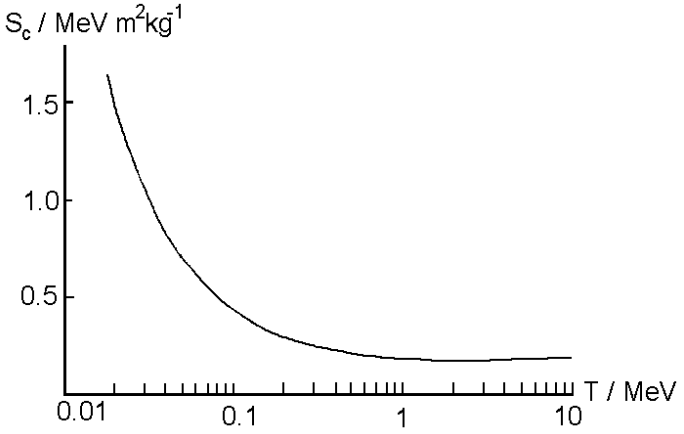

Figure 2-2 Variation of mass collision stopping power with electron kinetic energy for polyethylene.[56]

2.2.1.10 Depth Profile

When the secondary electrons produced by ionization processes from an incident beam of high-energy electrons are randomly directed in space, equilibrium is just under the surface of a polymer in contact with an environment of much lower density. Therefore, the absorbed radiation dose increases to a maximum at a distance from the surface (e.g. 2mm for 1 MeV electrons) which depends on the energy of the electrons. The energy deposition then decreases towards zero at a limiting penetration depth.[57] See Figure 2-3 and Figure 2-4.

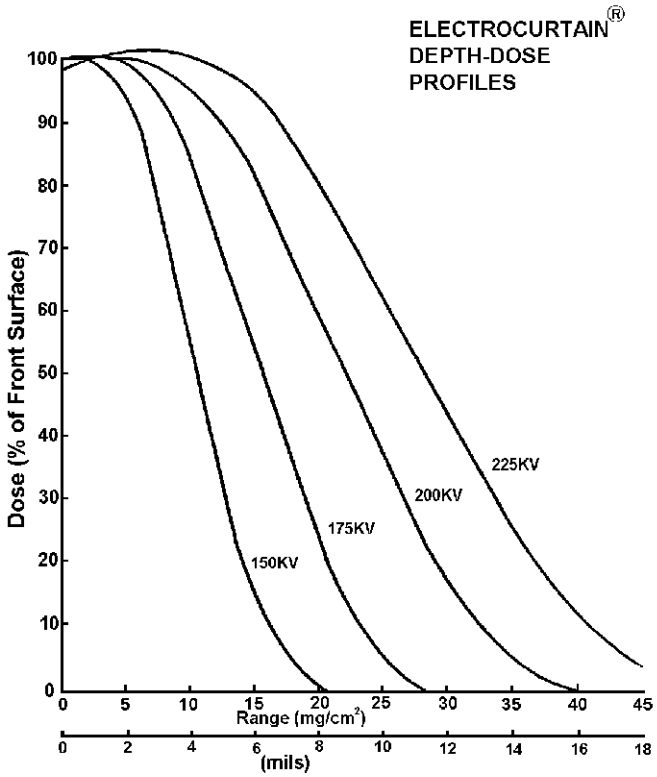

Figure 2-3 Energy Sciences Electro-Curtain Depth-Dose profile.

Much further work remains to be done on the behavior of electrons in irradiated polymers, since this may provide valuable information on leakage currents and the electrical breakdown in polymeric insulators, as well as on the behavior of charges in solids.

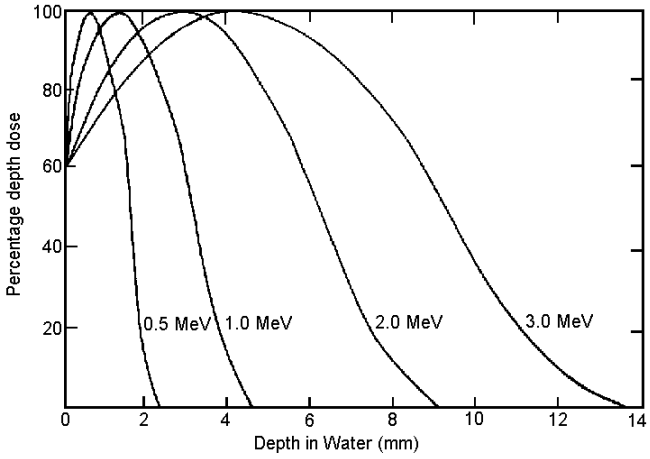

Figure 2-4 Percentage depth dose in water for high-energy electrons. [58]

2.2.2 Photon Interactions in Materials

Gamma rays are electromagnetic radiation of very short wavelength, about 0.01Å for a 1 MeV photon. When high-energy photons (X-rays or γ-rays) interact with matter, most of the energy is absorbed in the medium and ejects electrons from the atoms of the material. This process is predominately dependent on the atomic composition and not on molecular structure.[70]

Unlike electrons, photons are electrically uncharged and do not lose energy in a continuous manner as they penetrate a material. The distance which a photon travels before interacting is determined statistically by an interaction probability per unit length of travel. This probability depends on the effective atomic number Z and density ρ of the absorber as well as the photon energy E. If each atom in the material is representative of an effective microscopic cross-sectional area σ to the photon beam, and there are N target atoms per unit volume, then a measure of the probability of a photon interacting in unit thickness of the absorber is $\mu=N\sigma$. In terms of the Avogadro constant N_A, density ρ and relative atomic mass A_r of absorber:

$$\mu = \frac{N_A \rho \sigma}{A_r} \tag{2-2}$$

where μ is the macroscopic interaction probability and has units of m^{-1}. In general, μ increases with Z and ρ, and decreases with photon energy E. [70]

When a photon interacts with a target, it may be absorbed and disappear, or it may be scattered - typically with a loss of energy. Therefore, attenuation is a combination of absorption and scattering. Since the linear attenuation coefficient depends directly on the density of the medium, it has different values for each different physical state of a chemical species. Also, absorbers of similar atomic number, but different densities, have widely differing values of μ. Because of this, the interaction coefficient is more usefully quoted in terms of unit mass of absorber. The mass attenuation coefficient is: $\mu/\rho = N_A\sigma/A_r$ and has units of m^2kg^{-1}.[59]

In some cases, no energy is absorbed from a photon, and the decrease in intensity is due to scattering only. In this case, the incident wave changes its direction with no effect in the medium. This type of scattering induces no chemical change in the system. A photon cannot be partially stopped by the atoms of a medium. Some of the photons in a beam may be close enough to the location of an atom to interact and removed from the rest, or they may not be affected at all. This all-or-none process results in an exponential law between the intensity of the beam before absorption, I_0, and the final intensity, I, after absorption. This behavior can be expressed by the equation known as the Beer-Lambert Law:[60]

$$I = I_0 e^{-\mu c} \tag{2-3}$$

where I, I_0 are the intensities of the transmitted and incident radiations, x is the thickness of the absorber and μ is the linear absorption coefficient. If the

thickness of the absorber is expressed in cm, μ will have the units cm^{-1}. The linear absorption coefficient depends on the density of the absorber and it is convenient to define the mass absorption coefficient by

$$\mu_{mass} = \mu_{linear}/\rho \qquad (2\text{-}4)$$

where ρ is the density of the material. The mass absorption coefficient (units cm^2g^{-1}) is the same for the different physical states, i.e. gaseous, liquid and solid, of the absorber.[61]

The total absorption coefficient is the sum of three separate coefficients representing the three main processes of energy absorption by γ-rays. These processes are the photoelectric effect, the Compton effect, and pair production.[37,62-64] The regions where each process dominate are shown in Figure 2-5. Photon radiation undergoes energy absorption by pair production for high energies greater than 4 MeV, Compton scattering and the photoelectric effect for low energies less than 0.2 MeV. In the photoelectric effect, all of the energy of the incident photon is transferred to an electron ejected from the valence shell, whereas in Compton scattering there is also a scattered photon of lower energy. Thus, the radiation chemistry of photons occurs mainly through interactions of secondary electrons with the polymer molecules.[65]

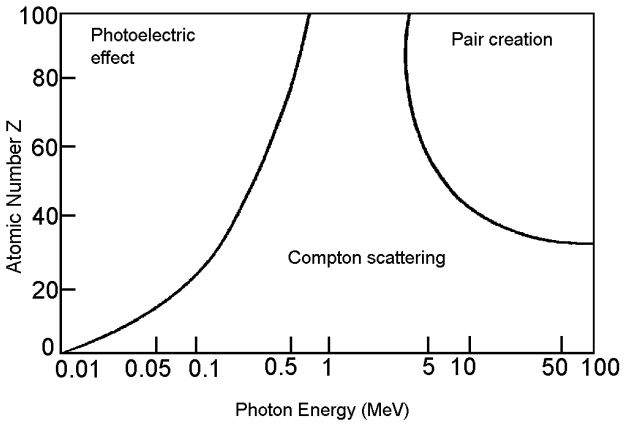

Figure 2-5 Region where each of the three photon process is dominate.[61]

High energy photons lose a considerable part of their energy in every elementary act of interaction with the atoms of the medium they traverse. The way in which they lose energy depends mainly on the energy of the incident photon. At lower energies (see Figure 2-5) the dominate process is the

photoelectric effect, in which the energy of the incident photon is entirely transferred to the electron ejected from the atom encountered. If the photon in collision does not transfer all its energy to the electron, but only a part of it, which allows it to continue its travel in a deviated path, then the process is known as the Compton effect. The third process is called pair production. Pair production can occur when the energy of the photon exceeds 1 MeV, but it becomes important only at much higher energies. In this case the photon is completely absorbed near the nucleus, and its disappearance is accomplished by the production of a pair of charged particles - an electron and a positron. [66]

It has been observed that the electrons produced in a substance by γ-radiation undergo the same sorts of interactions as do the electrons from β-particles or electron beams. Therefore γ-rays, x-rays, beta particles and electron beams yield a similar microscopic track. They do differ in penetration, but at the location of the interaction with the medium there is little difference between them.[33]

2.2.2.1 The Photoelectric Effect

At the beginning of the century it was known that when UV or visible light is incident on a metal surface, electrons will be ejected from the surface. This phenomenon is in itself not surprising since we know that light is electromagnetic radiation, and we may thus expect that the electric field of the light wave could exert a force on the electrons in the metal surface and cause some of these to be ejected. It is surprising, however, to find that the kinetic energy of the ejected electrons is independent of the intensity of the light, and instead depends increases linearly with frequency. In other words, an increase in the intensity of light increases the number of electrons emitted per unit time, but not their energy. This is difficult to understand in a classical sense as one would expect that as the intensity of the light wave increases, then the electrons would be accelerated to higher velocities. These facts had been

established before 1905 by P. Lenard and others. Precise measurements of the relationship between the frequency of the light and the energy of the ejected electrons were carried out in 1916, when the subject was studied by R.A. Millikan.[69]

In 1905 Albert Einstein suggested an explanation of these phenomena.[67]According to this explanation the energy in a beam of monochromatic light comes in parcels of magnitude $h\upsilon$, where υ is the frequency; this "quantum" of energy can be transferred completely to an electron. The electron acquires the energy E=$h\upsilon$ while it is still inside the metal.[68]If we now assume that a certain amount of work, W, has to be performed to remove the electron from the metal, then the electron will emerge from the metal with the kinetic energy = E - W = $h\upsilon$ - W.[69]

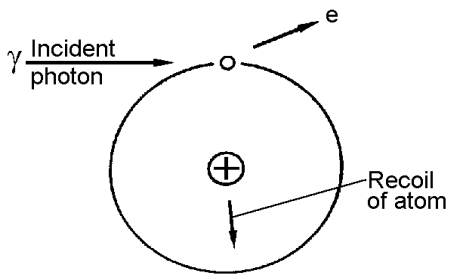

Figure 2-6 Photoelectric effect - below 60 keV.[33]

The photoelectric process is shown in Figure 2-6. Note that, as explained above, the incident photon is shown giving up all its energy to one of the inner electrons in an atom, which is then ejected from the atom. The electron then proceeds in the medium with an energy equal to that of the original quantum less the binding energy of the electron in the atom. The direction in which the electrons are ejected from the atom depends on the photon energy. At low energies, the tendency is for emission perpendicular to the direction of the photon, but at higher energies these photoelectrons tend to be emitted in the forward direction. The photoelectric effect is greatest for low photon energies, < 0.1 MeV, and for elements of high atomic number.[37]

The positively charged ion which remains is energetically unstable, having a vacancy in one of the inner electron shells. This is filled by an electron

falling from an outer orbit, with the emission of energy. This emission often appears as an X-ray photon having energy equal to the difference in binding energies of the two electron levels.[70]

2.2.2.2 Compton Scattering

If a photon interacts with one of the outermost electrons in the atom, the photon transfers a some of its energy to the electron, which is then ejected from the atom. The incident photon is scattered and proceeds with an energy equal to that of the original quantum less the recoil energy of the electron. The scattered photon may then undergo subsequent absorption either by the Compton effect or the photoelectric effect. The photon being scattered from its original direction with reduced energy E'. The electron kinetic energy depends on the angle of scattering. The scattering is shown schematically in Figure 2-7 and results in an electron energy spectrum which is continuous from zero to some maximum value corresponding to a head-on collision between photon and electron. The higher the photon energy, the greater the tendency for the electrons to be emitted in the forward direction.[70]

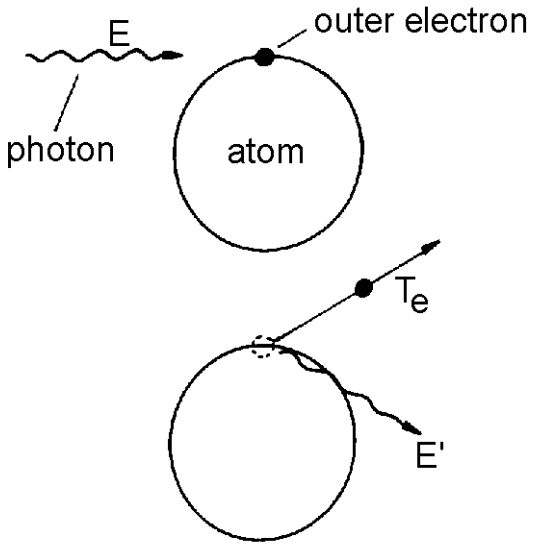

Figure 2-7 Compton scattering of an incident photon.[70]

Figure 2-8 shows the relative importance of the three interaction processes in carbon as a function of photon energy. It is shown that over the range from 20 keV to 20 MeV, Compton scattering is the major energy loss mechanism. This relationship holds for low Z elements, although in heavier elements the energy range of its dominance becomes gradually reduced, it is the main process in all elements between 0.8 and 4 MeV.[70]

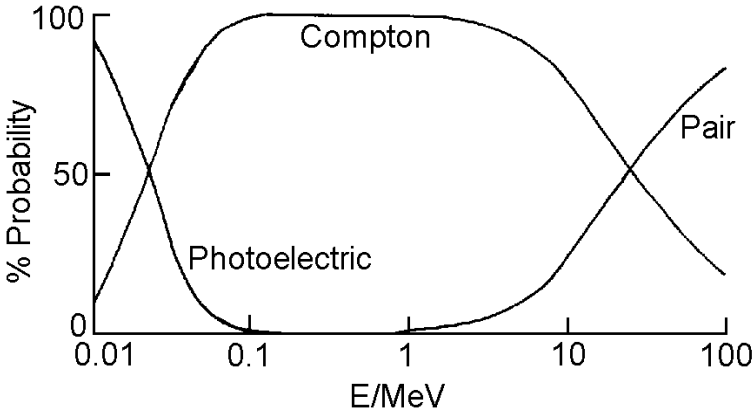

Figure 2-8 The relative probabilities of the three interaction processes in carbon at different photon energies.[70]

Compton absorption is more important for photons of higher energies and is, for example, the only absorption process for the interaction of ^{60}Co Gamma-rays with water.[37]

2.2.2.3 Pair Production

In pair production a gamma-ray photon with energy at least 1.02 MeV is absorbed close to the atomic nucleus and produces a positron-electron pair. Any excess energy of the photon appears as kinetic energy of the electron and positron. The positron and electron, after being slowed down, recombine with each other resulting in the production of two 0.51 MeV gamma rays - which is termed annihilation radiation. Pair production becomes more probable with increasing photon energy E and increases with atomic number approximately as Z^2.[37]

The positron deposits its kinetic energy in the absorber by the same mechanisms as an electron, and after this event decreases its velocity. At this

stage it combines with an electron to form positronium, a bound system consisting of the electron-positron pair rotating about its center of mass. The lifetime of positronium is of the order of 10^{-10} s, before the electron annihilates with its antiparticle, the positron. The two electron masses are converted into annihilation radiation, comprising two photons each of energy 0.511 MeV. The net effect of the total interaction is to transfer energy $E - 2m_0c^2$ to the immediate environment.[70]

Whatever the mechanism of energy loss of the gamma ray photon, secondary electrons with considerable kinetic energy are produced. Subsequent energy absorption processes, which account for most of the energy of the incident photon, are characteristic of electrons and will therefore be similar to those occurring when the material is bombarded directly with electrons.[71]

2.3 Absorption of Radiation

2.3.1 Reactions

The absorption of high-energy radiation depends only on the electron density of the medium. Mass density is a reasonable first approximation to electron density. More accurately, and conveniently, the average value of the ratio Z/A for the atoms, where Z is the atomic number and A is the atomic mass, can be used to calculate relative dose.[72]

The depth-profile of photon absorption is analogous to that for UV-visible light, i.e. I=Io exp(-Ad), where the mass energy absorption coefficient, u/g is used instead of the extinction coefficient. Particulate energy absorption can be described by relative stopping powers.[72]

2.3.1.1 Primary Reactions

Absorption of high-energy radiation by polymers produces excitation and ionization and these excited and ionized species are the initial chemical reactants. The ejected electron must lose energy until it reaches thermal

energy. Recombination with the parent cation radical may then occur and is more likely in substrates of low dielectric constant. The resultant excited molecule may undergo homolytic or heterolytic bond scission. Alternatively, the parent cation radical may undergo spontaneous decomposition, or ion-molecule reactions. The initially ejected electron may be stabilized by interaction with polar groups, as a solvated species or as an anion radical. The radiation chemistry of polymers is therefore the chemistry of neutral, cation and anion radicals, cations and anions, and excited species.[72]

2.3.1.2 Secondary Reactions

The reactions of the free radicals include (1) abstractions (of H atoms with preference for tertiary H, and of halogen atoms), (2) addition to double bonds, which are very efficient scavengers for radicals, (3) decompositions to give both small molecule products, such as CO_2 and (4) chain scission and crosslinking of molecules.[72]

2.3.1.3 Cage Effects

When the main-chain bond scission occurs in polymer molecules in the solid state to form two free radicals, the limited mobility of the resultant chain fragments must mitigate against permanent scission. This concept is supported by the increased yields of scission in amorphous compared with crystalline polymers. Similarly, the scission yields are increased above, the glass transition temperature, Tg, and melting, Tm, temperatures. There is also evidence from NMR studies of the changes in tacticity in PMMA that racemization occurs at a higher rate than permanent scission of the main chain, consistent with initial main-chain bond scission, rotation of the newly formed chain-end radical, and geminate recombination.[33,72]

2.3.2 Absorbed Dose

We have seen that the end result of the interactions of incident electrons and photons in an absorbing material is the deposition of energy in that material by ionizations produced by the secondary electrons. This energy deposition produces the effects in polymeric materials which subsequent chapters will describe. In order to clarify the relation between cause and effect, it is necessary to define a quantity called absorbed dose, which is a measure of the energy deposited per unit mass of material.

The ICRU has defined the absorbed dose as:

$$D = \frac{d\bar{\varepsilon}}{dm} \tag{2-5}$$

where $d\bar{\varepsilon}$ is the average energy imparted to an absorbing material of mass dm. The differential form implies that absorbed dose D can be defined at any point in the material, and so it is effectively a microscopic quantity. The energy ε imparted by ionizing radiation to a given volume of matter is defined as the difference between the total energy (kinetic and rest mass) of all radiations (particles and photons) entering the volume and the total energy of all radiations leaving the volume, less any increase in rest mass energy in the volume following nuclear reactions. In most cases, this formal definition simplifies to:

ε = Total energy input - Total energy output

The unit of absorbed dose is the gray, where 1Gy corresponds to and energy absorption of 1 J kg^{-1} of material. Although this has been the recommended unit for some time the previous unit, the rad, is still used. As absorbed dose of 1 rad is an energy deposition of 10^{-2} J kg^{-1}, and so 1 Gy = 100 rad. [70,73]

When ionizing radiation is used to affect the properties of polymeric materials, the desired end-points depend on the transfer of energy from the penetrating beam to the body of the material. Dosimetry is the range of techniques for measuring the absorbed dose. Radiation dosimetry is essential in radiation research in that both the doses and dose rates must be accurately measured on order to relate the observed effects to absorbed dose levels.[73]

The experimental measurements of absorbed dose fall into two groups - absolute and secondary. An absolute measurement of dose can be made using an ionization chamber. Basically this consists of two electrodes separated by a space containing a suitable gas which is ionized by the incident radiation. Ions produced in the gas are collected at the electrodes by means of an applied potential and the number of ions collected can be counted. Provided the energy required to create an ion pair in the gas is known, the absorbed dose can be calculated. Alternatively, the beam of X- or gamma-rays can be absorbed in a block of material and the resultant temperature rise measured. Clearly the material needs to be such than none of the energy goes into chemical reaction. Moreover it should have high thermal conductivity so that the temperature is uniform. Metals and graphite satisfy these criteria.[74]

Since absolute measurements of dose involve very careful techniques, they are not suitable for routine measurements where ease and speed are essential. For this reason secondary methods are usually employed. The most common dosimeter in use in radiation chemistry laboratories is the Fricke dosimeter. This consists of an air-saturated aqueous solution of 10^{-1} M sodium chloride and 0.4m sulphuric acid. Triply distilled water and A.R. purity reagents are used in making up the solution. It is known by comparison with calorimetric measurements that G (FE (III)) for this solution when irradiated with ^{60}Co gamma-rays is 15.6. The ferric ion is conveniently determined from the optical density at 303nm, where its extinction coefficient is 2.20×10^3 m^{-1}

cm^{-1} at 298 K. The sample to be irradiated is then placed in an identical position to the dosimeter. For ^{60}CO gamma-rays the absorption is entirely by the Compton process and the energy absorbed is proportional to the electron density of the sample. [74]

Other chemical dosimeters have been described but generally are not so convenient. N_2O is extensively used in the dosimetry of gases. Where only approximate measurements of dose are required, solid-state dosimeters may be used. The color produced in silver-activated phosphate glass is a measure of dose. Workers in radiation chemistry usually wear a film badge and the fogging produced in the photographic film is a measure of the dose received by the operator.[74]

A dosimeter is an instrument used to measure absorbed dose and dose rate. It is a transducer, in that the effect of energy deposition within the dosimeter is to produce an output signal related to the absorbed dose. The output signal may be a temperature rise (calorimeter), an electric current (ionization chamber) or a color change (Perspex dosimeter), for example.[36]

As with any measuring instrument, the presence of the dosimeter alongside the sample should not affect the dose deposition within the sample. This requirement indicates the need for a small, compact instrument. This is further emphasized by reference to Figure 2-9, which shows a typical absorbed dose profile for an electron beam. A large volume dosimeter as shown would provide a value for absorbed dose average over the total effective volume of the instrument. This situation may be contrasted with the use of a physically smaller instrument where a series of sequential measurements in the positions shown would allow the dose distribution to be measured.[36]

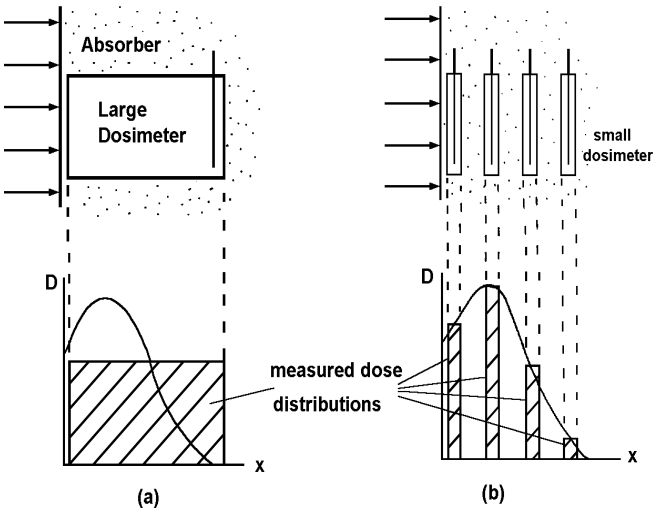

Figure 2-9 Measured electron beam absorbed dose distribution using (a) a large volume dosimeter, and (b) a compact dosimeter in several positions along the absorbed dose profile.[70]

Unless the elemental composition and density of the dosimeter correspond to those of the irradiated sample, the measured dose D_D will not be the same as the actual sample dose D_S. If the effective atomic number of the dosimeter differs from that of the sample, the pattern of energy deposition will not be the same, due to the different energy spectra of secondary electrons and Compton-scattered photons. Conditions for electronic equilibrium will change and in general the relationship between D_D and D_S will be difficult to establish without resort to use of a special analysis called cavity theory,[75] which enables the dose absorbed in one material to be calculated from that measured in a material of different elemental composition.

Ideally, the sensitivity of a dosimeter, i.e. the change in output signal per unit absorbed dose, should be constant. This would imply a linear response over the dose range of interest. Also, the output should depend on absorbed dose alone, but in many practical dosimetry systems this requirement is not satisfied and the output may depend on such factors as absorbed dose rate, energy spectrum of the radiation beam, and post-irradiation effects.[70]

2.4 Types of Radiation Sources and Processing

Ionizing radiation is a powerful tool in industrial polymer processing and in the sterilization of food and medical products. It is commercially important that the radiation sources used are able to provide the required integrated dose at a sufficiently high dose rate to allow adequate throughput of product. The absorbed dose should also be uniformly distributed throughout the material. [70,76]

As mentioned in section 2.2, there are two types of high energy ionizing radiation, photon and particulate radiation.[77] Particles include electrons, protons, α-particles, and heavy ions. Photons include X-rays and γ-rays.[78] Gamma rays have the advantage of deep penetration while trade off with the disadvantage of low dose rate. X-ray radiation, typically obtained from electron accelerators, while lower in energy (and therefore a lower depth of penetration) has a much higher dose rate so is more practical for industrial purposes. Radiation sources are of two types: isotope and machine source. Isotope sources provide continuous radiation and machine sources may provide continuous or intermittent radiation. Radioisotopes may be either naturally occurring or artificially produced. The characteristics of the more important radioisotopes are described in Table 2-4 below.[79]

Table 2-4 Radioisotopes used as radiation sources.[79]

Source	Half Life	Radiation	Energy (MeV)
^{60}Co	5.27 years	β	0.314
		γ	1.332
		γ	1.173
^{137}Cs	30 years	β	0.52
		γ	0.662
^{90}Sr	28.0 years	β	0.544
^{32}P	14.22 days	β	1.710
^{3}H	12.26 years	β	0.018
^{222}Rn	3.38 days	α	5.49
^{226}Ra	1620 years	α	4.777
^{210}Po	138 days	α	5.304

Most irradiation studies have been carried out using γ-emitters since very powerful sources can be obtained and dosimetry is relatively easy. In addition, because of their great penetrating power it is possible to irradiate relatively large samples in a fairly homogeneous fashion. However, because of their penetrating power, such sources need adequate shielding. The half value thickness (i.e. the thickness of absorber required to reduce the intensity of the radiation by one half) for ^{60}Co γ-rays for lead, concrete and water are respectively 1, 5 and 11 cm.[79]

Most sources use ^{60}Co which, as may be seen from Table 2-4, emits monoenergetic γ-rays of energies 1.17 and 1.33 MeV and has a half life of 5.27 years. It is prepared by neutron bombardment of ^{59}Co in a nuclear reactor. A few sources use ^{137}Cs which has the advantage of being readily available as a product of the fission of uranium. The β-particles emitted from both ^{60}Co and ^{137}Cs are usually filtered out by the metal canisters in which the sources are

contained. Typically the sources used range from activities of tens of curies in the smaller research laboratories to 650,000 curies in the Westminster Carpet Company's irradiation plant in New South Wales. The dose rates of these sources range from 10^{17} - 10^{21} eV $l^{-1}s^{-1}$.[79]

The most useful sources of β-particles are ^{90}Sr, ^{32}P, and ^{3}H. The penetrating power of β-particles is much less than that of gamma rays so that considerably less protection is required. The maximum range for β-particles from ^{90}Sr is 0.18 cm in water and 185 cm in air. However, care in handling the sources is still extremely importance since there is some danger of ingesting the material. ^{90}Sr is particularly hazardous in that it is readily taken up by bone. β-sources typically range in activity from a few millicuries to 1 curie. They may be used either as external sources or in some cases as internal sources for which purpose either the source encapsulated in a thin walled vessel is placed within the sample to be irradiated or a suitable compound of the radioisotope is mixed with the sample. It follows that compounds containing such radioisotopes must necessarily be irradiated by their own β-particles and the self decomposition of compounds containing particularly ^{14}C and ^{3}H has been studied in some detail.[79]

The earliest systematic studies in radiation chemistry around 1900 were primarily concerned with alpha particles since the radioelements radium, radon and polonium which had just been discovered were convenient sources of these. The alpha particles from a given emitter are monoenergetic. The range of alpha particles depends on their energy and is generally very small. For example, alpha particles from ^{210}Po have a range in air and water of 3.8cm and 3.9×10^{-3} cm respectively. For this reason, sources had either to be contained in capsules with very thin walls or else mixed with reactants. The gas radon was a convenient source for the study of reactions in the gas phase since it could be mixed directly with the gas to be studied.[79]

The earliest machine source of radiation was the X-ray tube. it is still a convenient source of continuous irradiation particularly for studies in the energy range 0.1-0.3 MeV, as provided by a conventional medium voltage X-ray tube. X-rays are produced whenever high energy electrons are rapidly decelerated, as occurs when they pass through the electric field of an atomic nucleus. In the X-ray tube, electrons from a filament are accelerated in vacuo towards a water-cooled metal anode. X-rays are emitted when the electrons collide with the anode. Although medium voltage X-ray sets should be housed in a room separate from the operator, they require no special shielding and have the advantage that they can be rendered inactive by simply switching off the voltage. Higher energy X-rays can be generated using fast electron generators by these then require special shielding and do not possess any particular advantage over conventional gamma-ray sources.[79]

In considering the various types of high energy radiation as they are most relevant to the irradiation of polymers, attention is very largely focused on fast electrons, obtained from various types of accelerators, and on gamma-radiation, almost always from a Co-60 radioisotope source. Other types of high energy radiation have been used to study reactions in polymers (e.g. α-radiation from a radioisotope), but primarily as a research project of academic interest. Studies of this nature can be of great value in nuclear design engineering, as indeed in radiobiological studies, but are not of large-scale direct polymer interest, and will not be discussed in detail here. X-rays can be usefully employed in these studies, and have an appropriate penetration. However, they are less convenient in reproducibility than gamma-rays from cobalt-60, and are expensive (since the conversion from fast electrons to X-rays is a very inefficient process except at very high voltages, well in excess of a few million electron-volts). At such voltages, the electron accelerator is very expensive, and may even induce radioactivity, a most undesirable feature,

which is always avoided with the gamma-ray from cobalt-60, or the fast electrons of up to 10 MeV. So practical interest is largely confined to electrons of 300-4000 keV and the cobalt-60 gamma ray at 1.3 MeV. The electron penetrates about 4mm per MeV of energy, with a further tail which has a far lower intensity and cannot therefore be used.[32,79]

2.4.1 Electron Beam Processing

Accelerated electrons were first used to cure coatings in the 1930's. It was not until the late 1960's that serious commercial interest in such a process was taken.[80] Electron beams are produced by various accelerating machines. Electrons from a hot filament acquire energy by passing through a high-voltage field in a vacuum. Their energy corresponds to this voltage and they are mono-energetic. A thin window is usually provided to that the beam may pass from the vacuum chamber and into the system being irradiated.[33] There are several categories of accelerator, two important ones being the linear accelerator (linac), which produces electrons of energy up to 10 MeV and typically has a total beam power of about 20kW, and the dynamitron[81]with a more modest electron energy (up to 6 MeV), but a high integrated beam power of perhaps 300kW. The electron beam may be continuous or pulsed.

A 1MCi ^{60}Co source produces a constant dose rate of about 5 Gy s^{-1}, whereas electron accelerators are capable of much higher dose rates. This may be exaggerated by the microstructure of the electron beam. For example, in a linac delivering electrons in short bursts of microseconds or less, the important dose rate parameter is the absorbed dose per pulse, which may be in the region of 10^{10}-10^{12} Gy s^{-1}. [70,82]

The central axis absorbed dose profiles in water for electron beams of various energies are shown in Figure 2-10. The penetration increases with incident kinetic energy T_e, and the general shape has been explained on the basis of electron scattering.[83] When a narrow beam of electrons enters a material, electrons are scattered away from the central axis and the absorbed dose decreases continually. However, for broad beam irradiation, this loss of electrons from the central region is more than compensated for by the gaining of electrons which have been scattered from surrounding annuli and so the absorbed dose initially increases until it reaches a maximum value. Thereafter, the absorbed dose decreases as further attenuation occurs.[84] A more uniform axial dose distribution may be achieved by placing a prescattering material in front of the irradiated sample material to increase the surface dose in the sample. In general, if the irradiated samples are thin relative to penetration depth, a high degree of uniformity may be achieved with under- utilization of available beam power. Conversely, if all the beam energy is absorbed, then the absorbed dose will vary significantly with depth.[70]

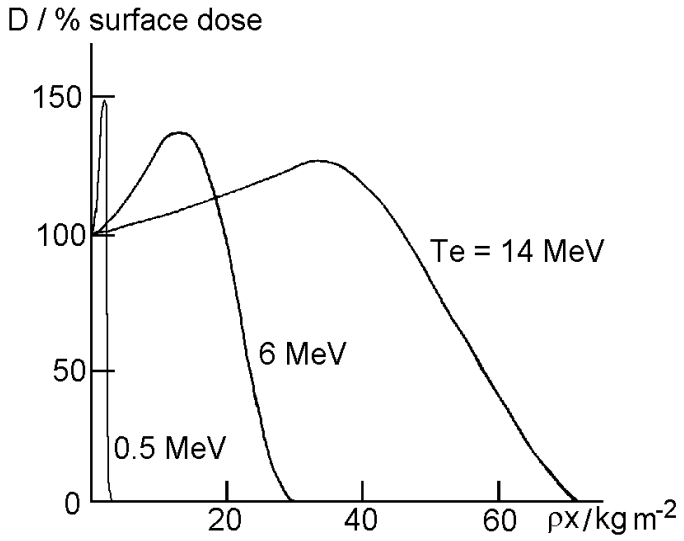

Figure 2-10 Broad beam central axis absorbed dose profiles in water for electron beams of several energies.[36]

2.4.2 Gamma Irradiation Processing

Gamma-radiation has found its principal industrial application to lie in its microbicidal properties. The pioneering work in this area began in the 1940's after the Manhattan project. The lethal effects of gamma-irradiation on microorganisms were well known, and the two gamma sources with relatively long half-lives, caesium-137 (30 years) and cobalt-60 (5.3 years) were thought to have practical industrial potential for this purpose. Caesium-137 formed in spent fuel rods was first considered to be the more likely of the two sources to be exploited. However, expensive separation processes would have been necessary to make sufficient caesium-137 available in a form acceptable for gamma processing. For cobalt 60, absorption of one neutron per atom converts cobalt-59 into radioactive cobalt-60; separation from other radioactive elements was unnecessary, and therefore cobalt-60 became the predominate industrial gamma source, although caesium-137 also has limited usage.[85]

In the early days of industrial irradiation, it was the possibility of food preservation that excited greatest interest. However, the first commercial applications were for medical device sterilization. It was at this time that interest began into the effects of exposure on the materials used and for the shielding used in these facilities. Table 2-5 illustrates the half value and tenth value thickness layers for shielding in the two most common facilities, for different shielding materials.[85]

Table 2-5 Approximate Half-value Layers (*HVL*) and Tenth-value Layers (*TVL*) of Shielding Materials Used in Large-scale Gamma-irradiators.[85]

Shielding Material	Shielding Thickness (mm)			
	Caesium-137		Cobalt-60	
	HVL	TVL	HVL	TVL
Lead	7	22	12	40
Steel	16	53	21	70
Concrete	48	157	62	200
Water	150	540	200	700

For fundamental studies in radiation chemistry, gamma radiation is often utilized. It has the disadvantage of possessing a low dose rate, however, it has the advantage of utilizing almost any container for the irradiated sample, including ultra-high vacuum containers. Caesium-137 is also utilized which is a fission product of uranium-135.[86]

The radionuclides ^{60}Co and ^{137}Cs emit γ-rays which are used in radiation research and processing. When a ^{60}Co nucleus undergoes radioactive decay, it emits two γ-rays of energies 1.17 and 1.33 MeV, whereas 85% of^{137}Co disintegrations result in the emission of a 0.66 MeV photon. The physical properties of these two γ-ray sources are compared in Table 2-6.[70]

Table 2-6 Properties of ^{60}Co and ^{137}Cs Photon Sources.[36]

Property	^{60}Co	^{137}Cs
Photon energy (MeV)	1.17; 1.33	0.66
Photons per disintegration	Each 100%	85%
Physical State	Metallic	CsCl
Half life (years)	5.3	30
Annual activity reduction	12%	2%
Activity per kW power output (kCi)	68	301

Caesium-137 has the advantage of a longer half-life, which necessitated a lower source replenishment rate, whereas cobalt-60 has a higher power output per unit activity and its higher average γ-ray energy indicates greater penetration and absorbed dose uniformity. Cobalt-60 is produced by reaction in a nuclear reactor, the Atomic Energy of Canada Limited (AECL) being the major supplier,[87] whereas ^{137}Cs is a fission product, and its availability depends on reprocessing facilities. Both the metallic ^{60}Co and the $^{137}CsCl$ sources are doubly encapsulated in stainless steel, and the photon beam geometry is defined by suitable collimation using a high Z, high density material (e.g. lead) as shielding.[70]

2.4.3 Ultra-Violet Processing

The absorption of energy from light waves including very soft x-rays, generally depends on the molecular structure of the medium and only indirectly on the atomic composition. Such a difference in the effects of atomic

composition or molecular binding constitutes a fundamental difference between ionizing radiation and nonionizing radiation.[88]

In contrast with the ionizing radiations discussed in previous sections, visible or near ultraviolet photons interact with matter by predominately producing excited states. Thus visible and ultraviolet photons are called "nonionizing radiations" and the chemical reactions produced by them are in the domain of photochemistry.[88]

However, it is interesting to compare radiation chemistry with photochemistry. In photochemistry the radiation will usually be monochromatic and one quantum of the radiation will be entirely absorbed by one molecule leading to the initial production of only one excited state. The nature of the excited state will be dictated by the optically allowed transitions. The absorption of radiation will generally be highly specific so that, even in a dilute solution, all the radiation may be absorbed by the solute. The excited states produced will be distributed homogeneously in the solution.[88]

In radiation chemistry the radiation may or may not be monochromatic, but even if it is initially monochromatic, the processes of energy loss are such that it will pass through a spectrum of lower energy states. In so doing, the initial quantum state of the particle will bring about the excitation and ionization of many molecules. Excitation of molecules by slow electrons is not governed by the optical selection rules, and states that are not readily observed in photolysis, e.g. triplet states, may be readily produced. The absorption of radiation will be non-specific and in a solution each component will absorb energy in proportion to its electron fraction. In a dilute solution most of the energy is absorbed by the solvent. The reactive species produced are not distributed homogeneously in the solution.[89]

2.5 Radiation Response in Polymers

The two principal changes occurring when a polymer is irradiated are degradation and crosslinking. In addition some decomposition to give gaseous products, usually of small molecules such as hydrogen, methane, carbon monoxide, or carbon dioxide, may be observed.[89]

Polymers have been classified into two groups according to their behavior under irradiation-those which predominantly crosslink and those which degrade. For vinyl-type polymers degradation usually occurs when there is a tetra-substituted carbon in the main chain, e.g.

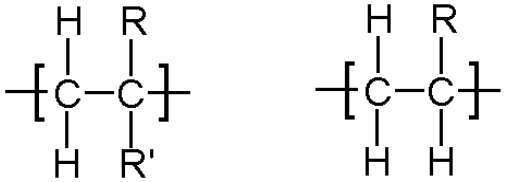

degrade crosslink

Thus poly(methyl methacrylate) and poly(isobutene) degrade, but poly(ethylene) crosslinks. However, there are many exceptions to this rule (most notably polypropylene which undergoes scission). It has been suggested that a more fundamental factor is the free energy of propagation. When this is low, steric and electronic factors favor degradation. Usually, both degradation and crosslinking occur and the ratio is affected by temperature, crystallinity, stereoregularity and air.[33]

2.5.1 Factors Influencing the Radiation Response

Many factors influence the radiation response of polymeric materials. Among these are oxygen (presence or absence), temperature, molecular weight, crystallinity, and structure.

2.5.1.1 Oxygen

Fundamental research on radiation effects on polymers is typically performed with samples sealed under vacuum. However, polymers may, in practical applications such as electron beam processing, be subjected to irradiation in air. The effect of irradiation is usually substantially different in air, with increased scission at the expense of crosslinking, and the formation of peroxides and other oxygen-containing structures. Diffusion rates control the access of oxygen to radicals produced by the radiation, and at high dose rates, as in electron beams, and with thick samples, the behavior may be similar to irradiation in vacuum (see Figure 2-12). Surface changes may be quite different from bulk due to the relative availability of oxygen.[90]

Sometimes scavengers are deliberately added to a system to react with primary radical species. Some scavengers are specific for one particular species (e.g. the electron). Other scavengers are less specific, and interpretation of product yields in terms of the primary species can be quite complex. [33]

2.5.1.2 Temperature

There is increasing interest in the utilization of polymer materials in radiation environments which are significantly above ambient temperatures, including aerospace applications.[91] The deterioration in the properties of polymers may be markedly increased by relatively small rises in temperature. The rates of chemical reactions normally show a positive temperature dependence, which is due to the activation energy barrier and can be described by an Arrhenius relationship. In polymers, the activation energy may show considerable variation and reflect both chemical and physical effects on the reaction. The temperature dependence of reactions in polymers is likely to show discontinuities, especially at the glass transition and crystalline melting temperatures. The reaction rates may be quite different in crystalline and amorphous polymers, and between the glassy and rubbery amorphous states.

There is increasing interest in the properties of the interfacial material between the amorphous and crystalline regions, which may have non-crystalline structure.[94]

Temperature effects on radiation chemistry have been studied by several workers. Charlesby and Moore[92] found that the yield of scission, G(S), in poly(methyl methacrylate) increased from 1.6 at 0°C to 3.8 at 180°C, and followed an Arrhenius relationship without any discontinuity at Tg. However, Wundrich,[93] in a study of PMMA over a wider temperature range down to 77 K, found three distinct temperature regions with different activation energies. Wundrich also studied poly(isobutene) and obtained similar results.[94]

Polymers which give high values of G(S) at ambient temperature frequently undergo depropagation to monomer during thermal degradation. Both types of behavior have been attributed to the large steric strain in these polymers, which usually arise from a quaternary carbon atom in the repeat unit of the main chain and a related low enthalpy of polymerization. Thus, initiated by main-chain scission and degradation by depropagation are both favored in these polymers.[95]

Bowmer and O'Donnell have shown that main-chain scission occurs on irradiation of poly (olefin sulfone)s with a high value for G(S) at temperatures from -196 to 100°C, and that depropagation to the two monomers increases rapidly above the ceiling temperature for propagation/depropagation equilibrium.[96]

2.5.1.3 Molecular Weight

Molecular weight plays an important role in the response of a polymer to radiation. In Figure 2-11, inverse of gel dose is plotted against molecular weight for a resist material. The general relationship holds that for a given dose, higher molecular weight species will be more sensitive to radiation than lower molecular weight polymers. For the case of both chain scission and crosslinking, a lower molecular weight polymer will be more resistant in terms of property affects than a higher molecular weight polymer.[97]

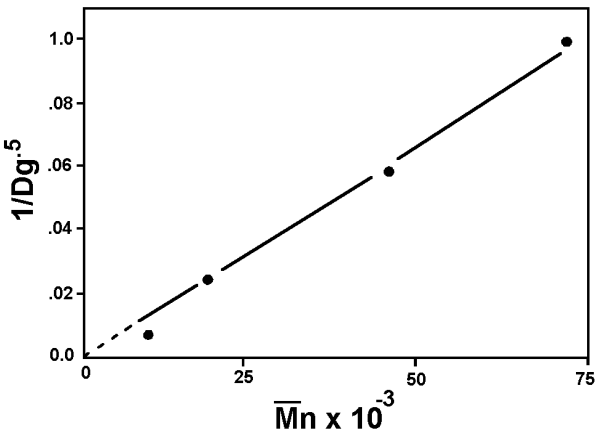

Figure 2-11 Sensitivity as a function of M_n for a resist material.[97]

2.5.1.4 Crystallinity

It has been found that for many polymers in the crystalline state, the critical dose for incipient gelation (calculated according to the theory of Flory[99]and Stockmayer[100]) shows poor agreement with theory. In one study,[101] for almost all samples of polyethylene tested, the critical dose was much less than the theoretical prediction. One possible explanation for this is the general belief that crosslinking occurs primarily in the amorphous regions of the polymer.[102]This is likely the result of an increased probability of radical pair recombination in the crystalline phase due to the dense packing and ordered structure of this state.

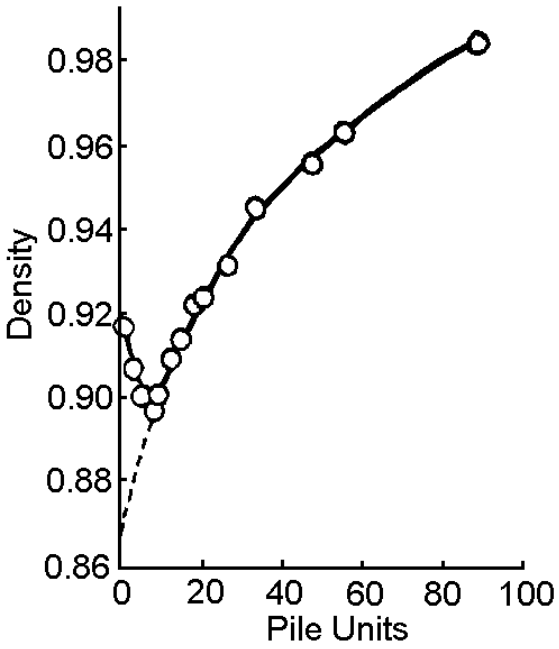

Figure 2-12 Influence of the dose of reactor radiation on the density of high pressure polyethylene. [98]

Figure 2-12 shows the influence of reactor radiation on density of polyethylene. Pile radiation was used early on (1940's and 50's) as a radiation source and samples were typically irradiated in air. What is shown is the increase in PE density to main chain scission in the presence of oxygen which results in previously entangled and restricted chains crystallizing resulting in higher density. The initial decrease in density is likely due to a delayed scission affect due to the sample thickness which resulted in crosslinking before diffusion of oxygen into the sample allowed the scission reaction to dominate.[98]

2.5.1.5 Structure

Although the absorption of radiation energy is dependent only on the electron density of the substrate and therefore occurs randomly on a molecular scale, the subsequent chemical changes are not random. Some chemical bonds and groups are particularly sensitive to radiation-induced reactions. They include COOH, C-Halogen, $-SO_2-$, NH_2, and C=C. Enhanced radiation sensitivity may be designed into polymer molecules by incorporation of radiation sensitive groups, and this is an important aspect of research in electron beam lithography.[103]

Aromatic groups have long been known to give significant radiation resistance to organic molecules.[103] There was early work on the hydrogen yields from cyclohexane (G=5) and benzene (G=0.4) in the liquid phase, and of their mixtures, which showed a pronounced protective effect. A substantial intramolecular protective effect by phenyl groups in polymers is shown by the low G values for H_2 and crosslinking in polystyrene (substituent phenyl) and in polyarylene sulfones (backbone phenyl), as well as many other aromatic polymers.[103] The relative radiation resistance of different aromatic groups in polymers has not been extensively studied, but appears to be similar, except that biphenyl provides increased protection. Studies on various poly(amino acid)s indicate that the phenol group is particularly radiation resistant. It is also possible to combine radiation-sensitive and radiation-resistant groups. Halogen substitution of the phenyl group results in high radiation sensitivity with inter-molecular crosslinking.[103]

2.5.2 Chain Scission in Polymers

One type of molecular change in polymers resulting from radiation-induced chemical reactions is chain scission. Chain scission results in a decrease in molecular weight. Many material properties of polymers are

strongly dependent on molecular weight, and are substantially changed by chain scission. For example, tensile and flexural strength - decrease and solubility increases.[103]

Small molecule products resulting from scission followed by hydrogen abstraction or combination reactions, can give valuable information on the mechanism of the radiation degradation. Gaseous products, such as CO_2, may be trapped in the polymer, and this can lead to subsequent crazing and cracking due to accumulated local stresses and a depression of Tg due to plastization. Contamination of the environment, e.g. by HCl liberated from poly(vinyl chloride), can be a significant problem in electronic devices. Further, the formation of these small molecules can result in significant changes in material properties. Development of color is a common form of degradation.[103]

In addition to main chain scission, other chemical changes are promoted by radiation. In PMMA, for example, side chains can be disrupted and reorganized, but such affects appear less significant than, for example, the effect of a single main scission in the molecular weight of PMMA or polyisobutylene.[103] Shown in Figure 2-13 illustrates the radiation chemistry of PMMA. Shown is the radiation induced scission which occurs in PMMA.[104]

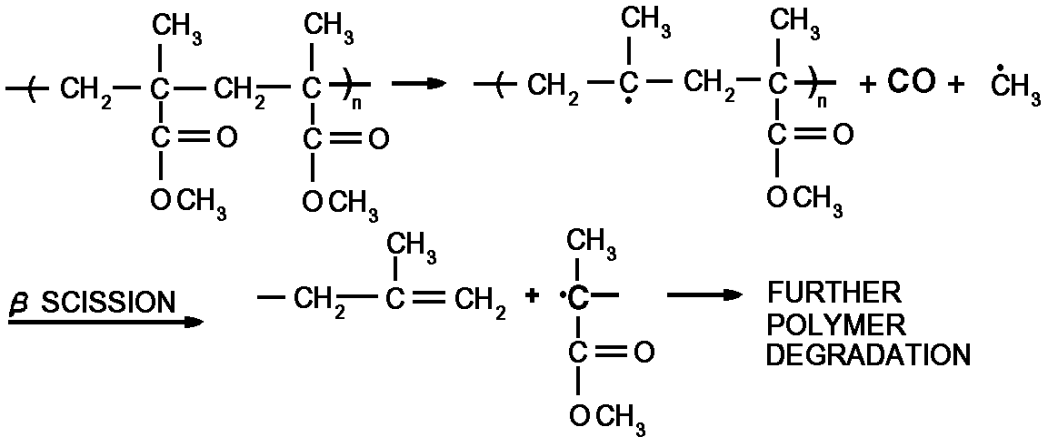

Figure 2-13 Schematic representation of the radiation chemistry of PMMA. [104]

Scission is usually promoted by the presence of oxygen which acts by forming peroxides:

$$\text{-A-A}\cdot + O_2 \rightarrow \text{-A-A-}O_2\cdot$$

and thus effectively prevents any recombination of the radical ends of the chains. As would be expected from the general rule, polymers which degrade include poly(isobutene), poly(methyl methacrylate), poly (tetrafluoroethylene), poly (α-methyl styrene) and cellulose. However, polystyrene degrades when irradiated in air, but crosslinks in vacuum. Polystyrene and poly (methyl methacrylate) are examples of polymers that undergo degradation. Typically, the yield of main-chain breaks, G(scission), ranges from 16, for poly-(α-methyl cellulose), to 0.3 for poly-(α-methyl styrene).[105]

Hydrogen is also produced in the radiolysis of poly-(methyl methacrylate). At doses below 50 Mrad, there is no visible formation of bubbles in the polymer, but if the polymer is heated above the second-order transition point, it expands forming a white brittle material which may be several times its original size, consisting of a mass of bubbles. [105]

The degradation that results from scission typically causes a loss of plasticity and structural strength and is usually an undesirable process. By incorporating a few per cent of aniline of substituted thiourea in the polymer, the extent of degradation can be reduced. These protective agents probably function by an energy-transfer mechanism. Free radical scavengers such as butylated hydroxy toluene (BHT) are also utilized.[105]

PTFE consists of a series of crystalline regions, held together by interleaving molecular chains winding from one crystal to another through the amorphous regions between crystallites. When irradiated, the chains in the amorphous regions scission preferentially. On heating to melt the crystallite, and then recooling, the crystallite reforms, but less restricted by these amorphous links. Thus, initially there is a slight increase in crystallinity, but

subsequent heating greatly increases it. Irradiated PTFE has a much weaker mechanical structure than initially, but has greatly improved lubricating properties. The effect of this secondary heating above the melting point must be ascribed to the reduced molecular weight which, therefore, reduces the number of chains linking adjacent crystals, thereby interfering with crystallization. In cellulosics likewise, one may expect to find a differential scission behavior as between the crystalline and amorphous fraction, possibly because the two fractured sections of the same molecule in a crystallite are held together and the damage can be repaired. [105]

A normal molecular weight distribution (and the relationship between Mn, Mw and Mv) is shown in Figure 2-14. Random scission produces such a normal distribution from any initial distribution. Deviation of the initial polymer from a normal distribution is shown by a negative intercept, which is sometimes called a virtual dose. Serious errors in the calculated G(s) will result if molecular weights are determined by viscosity measurements and there is a change in the molecular weight distribution. [105]

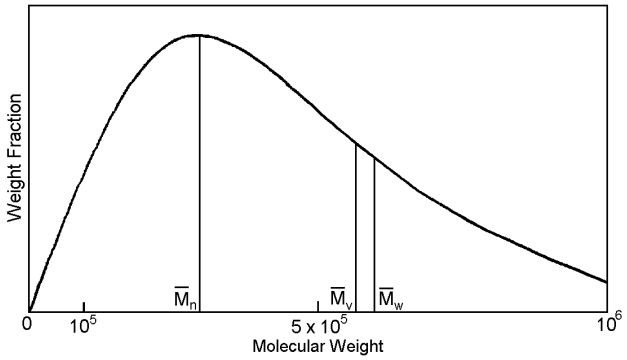

Figure 2-14 Most probable of normal molecular weight distribution for a polymer.[105]

G(s) values for polymers that scission when irradiated are shown in Table 2-7. The value for cellulose is much higher than for the others, probably due to specific cleavage of weak, inter-unit linkages. The temperature of irradiation does not generally have much affect on the amount of scission. [105]

Table 2-7 G (scission) at 20°C for polymers which degrade under irradiation.[105]

Poly (isobutene)	4
Poly (methyl methacrylate)	2
Poly (α-methyl cellulose)	16
Poly (tetrafluoroethylene)	-
Cellulose	11
Poly (α-methyl styrene)	0.3
Poly (ethylene oxide)	-

If main chain bonds in polymer molecules are broken during irradiation, either directly or as a result of subsequent reactions, the possibility of recombination would be expected to be high, especially in the solid-state. The Frank-Rabinowitch cage effect would be very effective when such large fragments are involved. Early workers considered that only C-H bonds could be permanently broken during irradiation of polymers. Indeed, it has been shown that the number of other permanent breaks is much smaller then the number of repaired breaks.[105]

2.5.3 Crosslinking

One type of change in polymers resulting from radiation-induced chemical reactions is crosslinking. Crosslinking causes an increase in molecular weight. Continued crosslinking of molecules will results in the formation of a three dimensional macroscopic network and the polymer is no longer completely soluble, the soluble fraction decreasing with radiation dose.[106]

Crosslinking occurs when radical sites in adjacent molecules combine. Such radical sites may be produced by two processes.

(1) Loss of a hydrogen atom from the irradiated polymer.

(2) Addition of a hydrogen atom to an unsaturated group.

The radical site may be localized or it may migrate along the chain until it encounters a radical site on another molecule when crosslinking will occur.[106]

The G(crosslinking) value for polyethylene varies with temperature from 1 at 173K to 3 at 296 K. Crosslinking results in increased tensile strength and greater insolubility for polymers. Since these are generally desirable properties there is considerable industrial interest in radiation-induced crosslinking. For example, unirradiated polyethylene softens in the range 360-370 K and melts at about 390 K, it can be heated up to 520 K without losing its shape if given a dose of 2 x 10^6 rads.[107]

Changes due to crosslinking have created interest in specialized applications. With low relative doses, the first changes due to crosslinking are increases in the average molecular weight and degree of branching. A point is soon reached, however, at which the "percolation threshold" or gel point is reached and a closed network is formed. Dramatic changes now occur in the physical properties of the material. It becomes partially insoluble in the usual solvents, and if the polymer is flexible, takes on rubber-like elastic properties. The reaction is similar to that obtained when rubber is vulcanized chemically, but is of much wider applicability. Advantages of the radiation technique include the complete control of density of crosslinking, the formation of crosslinks in the solid state, no need for catalysis or other additives, no heat treatment and the ability to crosslink polymers which because of the absence of unsaturated groups are largely resistant to conventional treatment. Crosslinking results in insolubility, increased strength and, depending on thermal history, elimination of the melting point. These desirable effects have led to industrial interest. For instance, when poly(ethylene) bottles are given a

30 Mrad dose of γ-radiation, heating the bottle to 120°C does not effect it while the same unirradiated bottle collapses. [107]

The mechanism of crosslinking is the subject of considerable controversy and varies between different polymers. Three main radical processes have been suggested. [107]

(1) Cleavage of a C-H bond on one polymer chain to form a hydrogen atom, followed by abstraction of a second hydrogen atom from a neighboring chain to produce hydrogen. Then, the two adjacent polymeric radicals combine to form a crosslink.

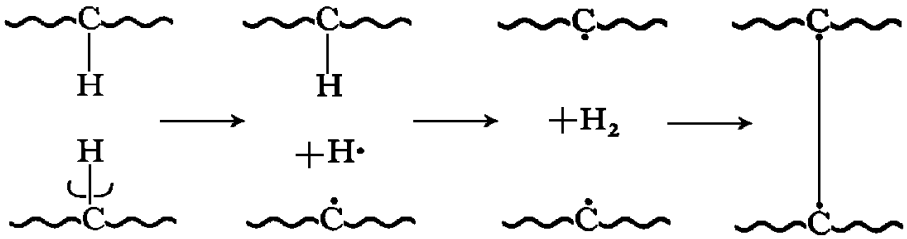

2) Migration of radical sites, produced by C-H bond cleavage, along the polymer chains until two of them are adjacent, when they combine to form the crosslink.

3) Reaction of unsaturated groups with hydrogen atoms to form polymeric radicals which can then combine.

Crosslinking is often accompanied by some degradation (scission), and the ratio of G (scission) to G (crosslink) can be obtained from a plot of the type shown in Figure 2-15 (a Charlesby-Pinner plot). There is a linear relationship between $S + S^{1/2}$ and 1/dose for a polymer with a molecular weight distribution of 2. This intercept at 1/dose = 0 is G(s)/G(x), and the gel dose corresponds to $S + S^{1/2} = 2$. Other molecular weight distributions give non-linear plots, but the same intercept and gel dose. [107]

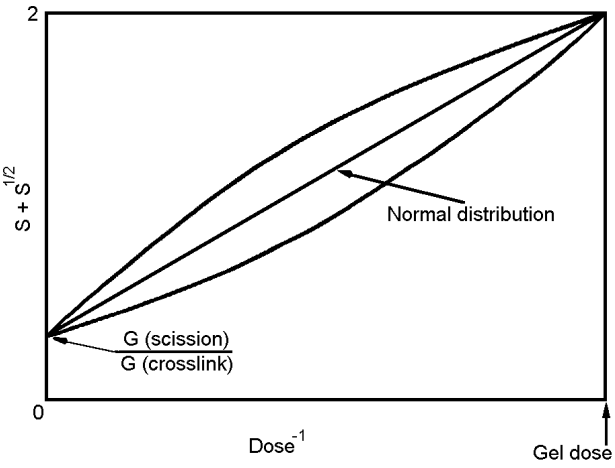

Figure 2-15 Determination of gel dose and ratio of G(scission) to G(crosslink) for irradiated polymer. S = soluble fraction.[33]

An interesting aspect of crosslinking in polymers is the memory effect. A polymer is crosslinked by irradiation and then heated and stretched. If cooled while stretched it retains this size or shape. However, any subsequent heating above the softening point causes shrinkage to the original dimensions. This technique has been used industrially for poly(ethylene) film and tube.[33]

This behavior was first discovered by A. Charlesby. It is used primarily with polyethylene in a variety of formulations and shapes, and relies on the fact that at room temperature the polymer is largely crystalline. Once it is melted and these crystallites disappear, the polymer is converted to a highly viscous liquid which can take up any desired shape. On cooling again, crystallization occurs and the polymer takes up a rigid shape similar to the one it held above T_m. [33]

When PE is irradiated beyond the gel point, few changes can be observed in its physical behavior at room temperature, and the melting point is typically unaltered (although for some special cases involving oriented PE as

shown in Chapter 5 this is not always true). At higher temperature, the crosslinks serve as a restraining force operating on the molecules so that instead of melting to a viscous liquid, it acquires the properties of an elastic rubberlike network. Above the melting point, irradiated polyethylene acquires highly elastic properties, many of which have been evaluated in great detail from thermodynamic analysis. In particular the elastic modulus increases linearly with dose (i.e. crosslink density) up to very high doses, but with corrections for end segments of polymer molecules, and if necessary non-network molecules, which can act as a diluent or solvent. [33]

If this elastic network is cooled and recrystallized while kept in a deformed state, it will retain this deformed state, held in position be the newly crystallized structure, even for a period of many years. However, if it is ever reheated again above the melting point to remove these crystallites, the elastic properties can become dominant, and the specimen will attempt to return to its original shape for purely thermodynamic reasons. This memory effect is an excellent example of the theory of highly elastic network systems, but has also been widely used for practical purposes. For example, repair strips for electrical wiring; a small length of irradiated tubing, with increased diameter (using this memory effect) is slipped over the junction of two cables, and heated. It will then shrink firmly over the two wires and retain this tight bond. [33]

The mechanical properties of flexible polymer networks are dependent on the density of crosslinking. Starting with the uncrosslinked material, for which the elastic modulus is theoretically zero (apart from entanglements) increased radiation doses beyond r_g first gives a highly elastic but weak rubber-like material, then a stronger rubbery material of higher modulus, at higher doses an over cured material, and eventually a brittle glassy structure.

The relationship between Young's modulus E and the crosslink density (inverse of the average molecular weight between crosslinks M_c) is:

$$E \sim 3\rho RT/M_C \qquad (2\text{-}6)$$

in the rubber like region. This formula is reminiscent of the gas law P=RT/MV, where P is pressure, R the gas constant, T the absolute temperature, M the molecular weight and V the volume, (replaced in the elastic modulus equation by the recripocal of the density ρ).[108]

$$M_C \sim 0.96 \times 10^6 / Gr \text{ if } r >> R_g \qquad (2\text{-}7)$$

The change in molecular weight may promote dramatic changes in physical properties. To follow these quantitatively, it is necessary to consider the various definitions of molecular weight. Each average is measured in a differently and differs according to the relative importance given to smaller and larger molecules. For scission, it is the number average which decreases; for crosslinking, it is the weight average which is important.[108]

For simple radiation-induced crosslinking, the number of such intermolecular crosslinks is proportional to dose over a very wide range, and they are distributed at random. At low radiation doses and crosslink density, there is an increase in average molecular weight, especially for the higher averages, since the larger the molecule, the more likely it is to take part in a crosslink. [108]

Much effort is expended on measuring the relationship between radiation dose and network (gel) fraction, since this determines the efficiency of crosslinking, the G(x) value, and even whether these crosslinks are random and no other reaction such as simultaneous scission is involved. The general relationship has been derived for any initial molecular weight distribution. [108]

$$g = \mathrm{d}g - \frac{1}{2!}\mathrm{d}^2 g^2 \frac{M_z}{M_w} + \frac{1}{3!}\mathrm{d}^3 g^3 M_4 \frac{M_n}{M_w^2} \cdots \qquad (2\text{-}8)$$

where $M_n = M_2$; $M_z = M_3$; M_4, M_5 . . . , etc. For an initially uniform distribution, when all three averages are equal:

$$g = \mathrm{d}_g - \frac{\mathrm{d}^2 g^2}{2!} + \frac{\mathrm{d}^3 g^3}{3!} \tag{2-9}$$

which can be written:

$$1 - g = s = e^{-\mathrm{d}g}; \mathrm{d} = \frac{r}{r_g} \tag{2-10}$$

The quantity, 1-g, while for a random distribution, can be obtained as in the case for random scission or termination by:

$$s + \sqrt{s} = \frac{2}{\mathrm{d}} = \frac{2r_g}{r} \tag{2-11}$$

Figure 2-16 shows this Charlesby-Pinner type of plot, also the effect of simultaneous random crosslinking and scission, with a higher 1/δ at gel and s + $s^{.5}$ per infinite dose. [32]

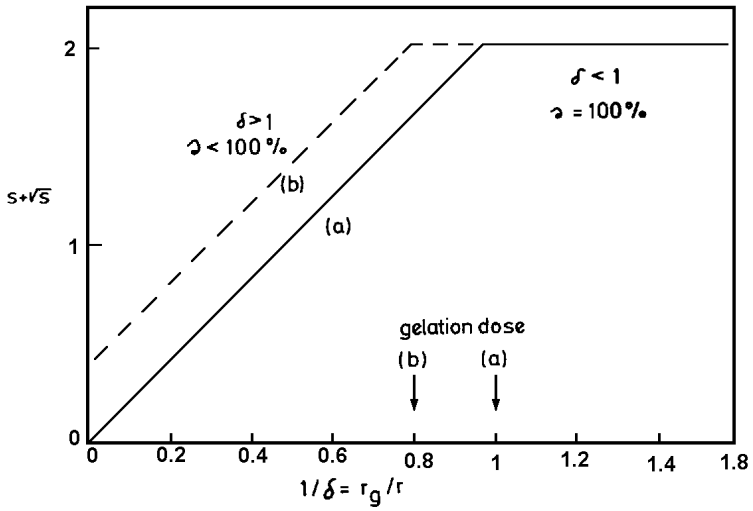

Figure 2-16 Charlesby-Pinner plot of sol fraction *s* for an initially random distribution. [32]

The relationship for an initial random distribution, referred to as a Charlesby-Pinner plot, is by far most generally used because a plot of $s + s^{1/2}$ versus 1/r immediately leads to r_g. In addition, the linearity of the plot confirms the assumption of initial distribution and also when radiation induced random scission also takes place. When the scissions are also random the ploy of $s + s^{1/2}$ versus 1/r gives a linear plot, which extrapolates for $r \rightarrow \infty$ to the ratio of scission to crosslinking, so that both G(x) and G(s) can be derived. The divergence from linearity at low doses alone also provide information on how far the initial molecular weight distribution departs from a random one (i.e. $M_w/M_n = 2$). [32]

2.5.3.1 Some Properties of Crosslinked Polymers

The following briefly describes some specialized properties of polymers modified by crosslinking. Although crosslinking is often be produced by chemical methods like vulcanization, radiation processing has considerable advantages. Some of these are: (1) the very extensive range of concentrations available; (2) the absence of any chemical catalysts or residues; (3) the wide range of temperatures at which the reactions can be induced, with little dependence on the temperature of irradiation; and (4) the differential effect which can be induced over a single specimen. Some examples of the use of these techniques and other advantages follow.[108]

2.5.3.1.1 Differential Irradiation

The elastic modulus above the melting point of PE is generally directly proportional to crosslink density (and therefore to dose). Thus, it becomes possible to fabricate items, with different elastic moduli over its surface or depth, by choosing an appropriate selection of doses over the surface, or in depth (e.g. by irradiation with electrons of different voltages and penetration).

To have a rubber specimen with different elastic properties over its surface, or in different directions, might be expected to offer many advantages for certain applications.[32,109]

2.5.3.1.2 Fillers

Mechanical properties can be improved for many polymer systems by the addition of fillers to the polymer before crosslinking. In the vulcanization of rubber, for example, carbon black is used, while for silicones, fine silica powder is often incorporated. This improvement takes place whether the crosslinking is induced by chemical means or by radiation. [32]

It is surmised that these changes are due to the introduction of these particles in between chains in the network. Under stress these will intervene in the deformed lattice, holding the orientated polymer chains apart. Therefore, the direction of stresses will be altered but without necessarily involving any chemical interaction.[32]

2.5.3.1.3 Creep and Deformation Recovery

A polymer below the glass transition or melting point can still be deformed under stress, but will partially retain this deformation when the external stress is removed. Lengthy periods under stress will give rise to an increasing, non-recoverable deformation, known as creep. If the polymer has been crosslinked, there is always a built-in elastic property, and there is an increasing tendency for any deformation to recover slowly when the external stress is removed. Radiation crosslinking of polymers therefore has the potential property advantages of creep resistance and elastic recovery, which increase with radiation dose. [32]

2.5.3.2 Time Temperature Transformation (TTT) Diagram

By far the most useful tool to develop the framework for understanding and comparing the various aspects of the cure process is the Time Temperature Transformation (TTT) diagram. The concept of TTT diagrams have been used extensively in materials science for studying the phase changes in metals and metal alloys for some time.[110,111]However, its application to thermosets originated with Gillham at Princeton University over the past fifteen years.[112-118]

A generalized TTT diagram is shown is Figure 2-17. This TTT diagram shows the majority of the important features that represent the cure of thermosets. In the most simple terms, a TTT diagram can be looked upon as a map showing the existence of various states of the material arising from different combinations of temperature and time of cure. Additional secondary events such as the onset of phase separation, isoviscosity, and full cure may also be represented on this diagram. In terms of radiation chemistry and curing, consideration of the TTT map may be important as irradiation may result in a material which can undergo transformations described by the TTT (e.g. curing a high functionality monomer which may result in a lower Tg due to the temperature of cure).[119]

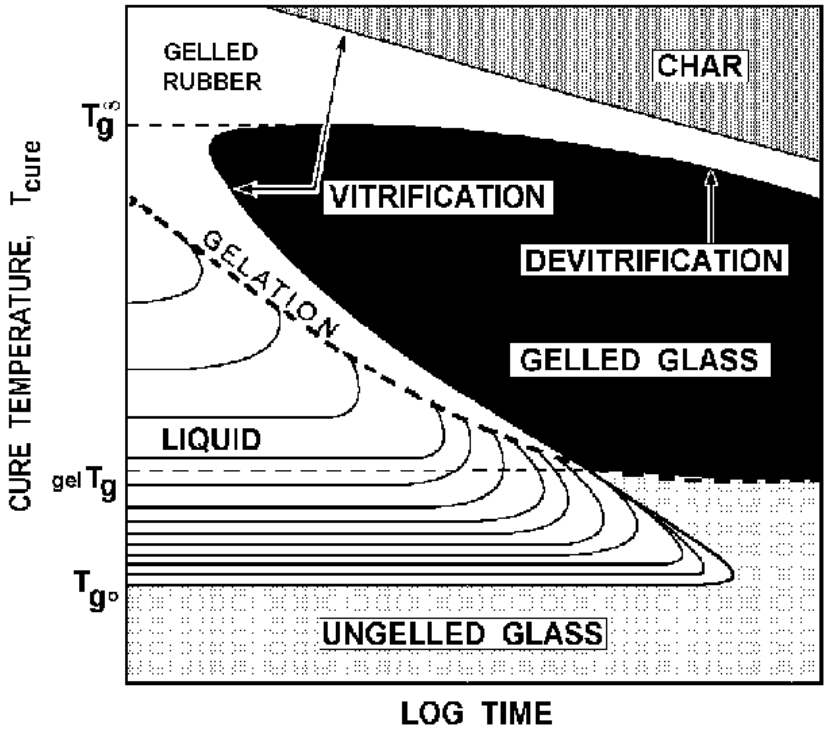

Figure 2-17 Time-Temperature-Transformation Diagram proposed by J.K. Gillham. Shown are three critical temperatures (T_{g0}, $_{gel}T_g$, and T_g) and distinct regions of matter (liquid, sol/gel rubber, sol/gel glass, gel glass, sol glass, char). The full cure line ($T_g = T_g$) separates the sol/glass from the gel glass region, and the sol/gel rubber from gel elastomer region, respectively. Also displayed are the degradation events of devitrification and char formation, and isoviscous lines. [119]

2.5.4 Measurement of Scission and Crosslinking

Any changes in molecular weight that occur with radiation may be used to determine yields of scission and crosslinking. Average molecular weights may be obtained by viscometry, osmometry, light scattering, gel permeation chromatography and sedimentation equilibrium. Equations have been derived which relate G(s) and G(x) to changes in Mn, Mw and Mz. Crosslinking produces branched molecules and the relative hydrodynamic volume (per mass unit) decreases compared with linear molecules. Therefore, molecular weights derived from viscometry and gel permeation chromatography will be subject to error.[120]

The equations relating Mn and Mw to radiation dose which are most frequently used apply to all initial molecular weight distributions for Mn, but only to the most probable distribution for other initial distributions, especially for representation by the Shultz-Zimm distribution equation. [120]

The use of Mz has been largely neglected in the evaluation of crosslinking and scission in polymers due to difficulty in utilization of the equations for Mz. However, it should be noted that Mz is particularly sensitive to higher molecular weight molecules produced by crosslinking. Mz can be obtained from sedimentation equilibrium experiments in the ultracentrifuge.[120]

If crosslinking predominates over scission [when G(x) > 4 G(s)], the decrease in soluble fraction above the gel dose, may be used to derive G values for both processes. The equation derived by Charlesby and Pinner can be used to predict the most probable molecular weight distributions.[121]

Crosslinking yields can also be derived from the extent of swelling of the irradiated polymer (if the hydrodynamic interaction factor, X, between the polymer and the solvent in known accurately), or from stress relaxation measurements on elastomers.[121]

2.5.5 Post-Irradiation Effects

Most irradiated polymers show a continuing change in properties for a long period after irradiation. These post-irradiation effects may be attributed to (1) trapped radicals which react slowly with the polymer molecules and with oxygen which diffuses into the polymer (2) peroxides formed by irradiation in the presence of air or trapped within polymers irradiated in vacuum or an inert atmosphere that slowly decompose with formation of reactive radicals and (3) trapped gases in glassy and crystalline polymers which cause localized stress concentrations. [121]

The consequences of post-irradiation effects in polymer materials are progressive reduction in strength, cracking and embrittlement. Some reduction

in these effects can be achieved by annealing of the trapped radicals, addition of appropriate scavengers, release of trapped gases, and control of the morphology of the polymer. [121]

2.6 Radiation Induced Polymerization

In 1874, the observation was made of the formation of an inert solid from acetylene after exposure to an electric charge. We now know that this was a polymeric material. Since that first observation, the polymerization of a wide variety of monomers by ionizing radiation has been investigated. Small amounts of radiation can produce relatively large effects in monomers or polymers. The radiation initially produces ions and radicals with radiation chemical yield (G value) of 1-10. These ions and radicals may initiate polymerization or copolymerization in monomers and degradation or crosslinking in polymers. It was found that radiation could initiate the reaction by the production of radicals, which then start a conventional polymerization sequence comparable with that obtained with a chemical catalyst acting as initiator.

There are several major advantages in radiation. An enormous range of intensities and hence initiation rates is possible and this will result in very different products; the effect of temperature is relatively unimportant for radiation initiation, so that its effect on propagation rate (which is not controlled by radiation) can be better assessed and controlled. For many reasons this can be very important, since the exotherm resulting from propagation can react back on the chemical initiation, and greatly complicate the reaction kinetics. The lack of any chemical initiator means that the product is not contaminated by any by-products. The effect of additives, solvents, etc. can be readily assessed, using a wide range of radiation dose rates and temperatures.

Radiation may be used to initiate all types of polymerization processes. These include gas phase, heterogeneous and emulsion polymerization. There is considerable interest is radiation-induced polymerization of aqueous emulsions because the heat of reaction is removed by the water, the molecular weight of the polymer is high and the final product is free of residual chemical initiator. There appears to be a wide variety of kinetic schemes applicable to different monomers.

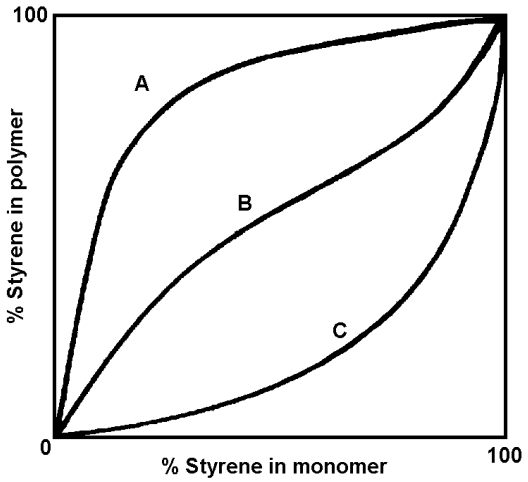

Figure 2-18 Variation in polymer composition with co-monomer composition for methyl methylacrylate-styrene mixtures polymerized by different mechanisms. (A) cationic, (B) free radical, (C) anionic.[33]

When a mixture of two monomers is irradiated, the composition of the polymer formed from different co-monomer compositions can be a sensitive test of the reaction mechanism. (see Figure 2-18).

Polymer formation during irradiation of liquid monomer follows a sigmoidal curve with time. This is illustrated in Figure 2-19. The rate of polymerization increases with dose rate, but may not show much temperature dependence. This is because the initiation rate (production of radicals or ions) is usually independent of temperature and the

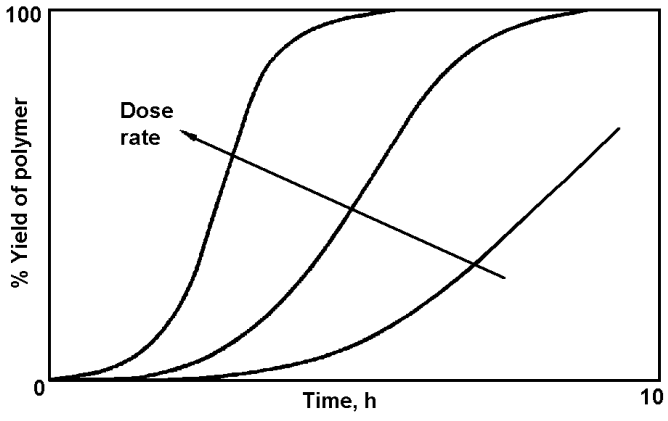

Figure 2-19 Polymerization of a monomer during irradiation.[33]

increase in propagation rate at higher temperatures is opposed by the increase in termination rate. Ionic polymerizations are frequently best carried out at low temperatures.[122]

Radiation of oligomers (low molecular weight polymers) is effectively a type of polymerization. It is the basis of radiation curing of surface coatings. Radiation-sensitive groups, such as double bonds in acrylates and methacrylates, enhance polymerization and chain extension. High dose rates are used, mainly with electron irradiation, to achieve high conversions in a few seconds and to take advantage of relatively low diffusion rates to avoid oxygen inhibition.[123] Much work has been done in the area of reactive oligomers both in the area of radiation curing and by other means.[124]

2.7 Grafting

Ionization or radical formation in a substrate polymer can initiate graft copolymerization of another monomer having different properties to give a product combining desirable features of both. For example, films of non-polar polymers like poly(ethylene) and poly(propylene) can have monomers with polar substituents grafted on to them which is then utilized in printing applications. Synthetic fibers can be similarly treated so that they can be satisfactorily dyed. The permeability of plastic films to particular gases can be reduced by grafting on a monomer which produces an impermeable polymer layer. This close combination of two very diverse polymer chains promises useful new products, and several have in fact been developed. One is in the form of membranes used in chemical filtration or other plants; PE is the base material, and provides the physical stability, while the grafted side chain, often polyacrylic acid, provides the hydrophilic medium for the reaction. The crystallinity in the PE fraction would be expected to impart rigidity in the graft copolymer, and several variables such as dose in PE, concentration and chain

length of the grafted acrylic acid chain, as well as thickness, will influence the properties the membrane can provide. [32]

By graft modification of the polymer surface, one can change the polymer's wettability,[125,126]adhesion,[127,128] printability, metalization, anti-fog properties,[129]anti-static properties,[130-132]and biocompatibility.[133-137] Bulk graft modification of the polymer has been used to improve water absorbency,[138-140] fire retardancy,[141] and to produce battery separators,[142-150] ion exchange and ion trap materials,[151-155] separation membranes,[156-158] deodorant materials and immobilized enzymes.[159-161]

The chief ways of producing a graft copolymer are:[162]

(1) The polymer is irradiated in the presence of the monomer, which may be present as vapor, liquid or in solution. Considerable amounts of homopolymer are usually produced. this method is suitable for monomers, such as styrene, for which G(initiation) in the monomer is low.

(2) The polymer is irradiated and then the monomer is added. This reduces homopolymer formation unless chain transfer to monomer is significant.

(3) The polymer is irradiated in air and then heated with the monomer. Peroxides are produced during irradiation, and these decompose on heating.

(4) Two polymers are irradiated in an intimate mixture. This produces crosslinking between the two types of chains.

The amounts of grafted copolymer vary greatly, but 100% increase in weight can be obtained. Swelling of the substrate greatly increases the amount of grafting. Increases in grafting at high temperatures are usually attributed to greater swelling. If a monomer-polymer mixture is irradiated and radicals are readily produced in the graft chains, then autoacceleration may occur.

Figure 2-20 shows a typical reaction for a multifunctional acrylate in the presence of gamma radiation. Although gamma radiation is illustrated, it

should be noted that other types of radiation have been used to graft with acrylates.

It is well known that graft polymerization can be initiated by many methods, for example, high energy (gamma ray, electron beam) irradiation, plasma treatment, ultraviolet light radiation, decomposition of chemical initiations and oxidation of the polymers. Among these methods, electron beam irradiation may be the most convenient and effective for industrial usage because of its high irradiation dose rate, ease in generating active sites in many kinds of polymers, effective penetration into the polymer and moderate initiation reaction conditions (room temperature and pressure). Electron beam irradiation induced graft copolymerization can be used to modify either the surface or the bulk of the polymer.[164]

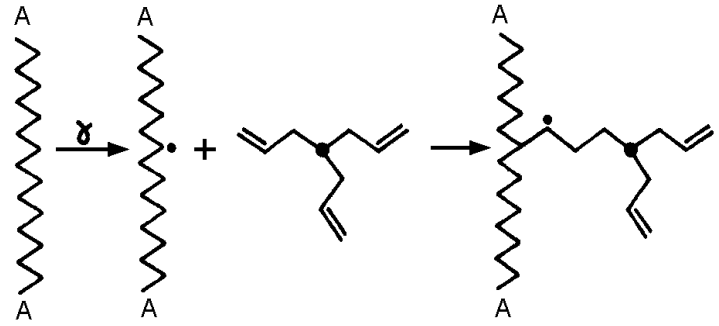

Figure 2-20 Interaction of multifunctional acrylate with polymer radical by gamma irradiation.[163]

2.8 Irradiation in a Solvent

When a polymer is irradiated in a solution, three reactions are involved; (1) primary reactions in the polymer, (2) primary reactions in the solvent and (3) mutual interaction of the products from the primary reactions. The effect of solvent is particularly prominent when a polymer is dissolved in water. Some of the reactive groups found in the water then not only react with each other, but also with the dissolved polymer, giving more radicals on the latter. This is referred to as the indirect effect and is of major importance in radiobiological research. [165] In some cases, solvents have been observed to catalyze

crosslinking reactions, but in most cases solvents act as a chain transfer agent and inhibit radiation chemistry events.

2.9 Cellular Materials

2.9.1 Introduction to Cellular Materials

Cellular materials compose approximately ten percent of all structural materials and have applications ranging from foam insulation and packing to structural applications. Foam production is also important in froth-flotation separations, the manufacture of cellular elastomers, plastics, and glass, and in certain special applications.[166] The majority of cellular polymers used in industry are polyurethanes, polystyrene, poly(vinyl chloride), and polyolefins. Polymer foams have been classified by their cellular morphology, mechanical behavior, composition, or cellular structure such as cell openness. In closed-cell foams, the gas phase is discrete and the polymer phase continuous. In open-cell materials, both the solid and fluid phases are continuous.

The most important feature of cellular solids is the relative density of the foam. Relative density is defined as the density of the cellular material ρ^* divided by that of the solid from which the cell walls are made ρ_s. Polymeric foams are typically between 0.05 and 0.2. Gibson and Ashby describe a transition at about 0.3 to a material which is better thought of as a solid containing isolated pores.[167]

Berkman and Egloff have pointed out that foam is produced in systems possessing the proper combination of interfacial tension, viscosity, volatility, and concentration of solute or suspended solids.[168] In addition, foam production requires the creation of small bubbles in a liquid capable of sustaining foam.[169]

2.9.2 Formation Theory

A bubble is a globule of gas or vapor surrounded by a mass or thin film of liquid. Globular voids in a solid are also sometimes called bubbles. A foam is

a group of bubbles separated from one another by thin films, the aggregation having a finite static life. Although often non-technical literature regarding these materials do not distinguish between a foam and froth, a technical distinction is often made. A highly concentrated dispersion of bubbles in a liquid is considered a froth even if its static life is substantially nil (i.e. it is mechanically maintained); thus all foams are also froth, whereas the reverse is not true. The term lather implies a froth that is worked up on a solid surface by mechanical agitation; it is seldom used in technical discussions. Gibson and Ashby provide a further distinction between a foam and a solid with dispersed voids through the consideration of relative density; a foam being defined as having a relative density less than 0.3. Thin walls of bubbles comprising a foam are called laminae or lamellae.

Bubbles in a liquid originate from one of three general sources: (1) they may be formed by de-supersaturation of a solution of the gas or by the decomposition of a component in the liquid; (2) they may be introduced directly into the liquid by a bubbler or sparger, or by mechanical entrainment; (3) they may result from the disintegration of larger bubbles already in the liquid.[169]

2.9.3 Foam Generation

Spontaneous generation of bubbles of gas or vapor from a homogeneous liquid is theoretically impossible.[170] The appearance of a bubble requires a gas nucleus as a void in the liquid. The nucleus may be in the form of a small bubble or of a solid carrying absorbed gas, examples of the latter being dust particles, boiling chips, or a solid wall. A void can result from cavitation, mechanically or acoustically induced. Blander and Katz have thoroughly reviewed bubble nucleation in liquids. [171]

Theory permits the approximation of the maximum size of a bubble that can adhere to a submerged horizontal surface if the contact angle between bubble and solid (angle formed by solid-liquid and liquid-gas interfaces) is

known[172,173] Unfortunately, bubbles that rise from a surface are typically smaller than those so calculated and the contact angle is seldom known, therefore the theory is not directly useful.[174]

2.9.4 Bubble Formation at an Orifice

For the formation of bubbles at an orifice or capillary immersed in a liquid, there are three regions of bubble production:[175] (1) Single bubble, (2) Intermediate, and (3) Jet. Perry's Chemical Engineer's Handbook provides extensive detail into the theory, equations and regions for which bubble formation in these regions occur.

2.9.5 Entrainment and Mechanical Disintegration

Gas can be entrained into a liquid by either a solid or liquid falling into the liquid from the gas phase. In addition, surface ripples or waves or the vertical swirl of a mass of agitated liquid about the axis of a rotating agitator can also entrain gas. Small bubbles probably form near the surface of the liquid and are then caught by turbulent eddies. The disintegration of a submerged mass of gas takes place by the turbulent tearing of smaller bubbles away from the exterior of the larger mass or by the influence of surface tension on the mass when it is deformed by inertial or shear forces into a cylindrical or disk form.[176]

2.9.6 Foams

A foam is formed when bubbles rise to the surface of a liquid and fail to coalescence or rupture. The formation of foam consists of the formation, rise, and aggregation of bubbles. The life of foams can vary from seconds to years but is in general finite. Therefore, maintenance of a foam is a dynamic phenomena. The maintenance of the foam is helped by gravity (bubbles rise and separate from liquid) and harmed by interfacial tension which favors coalescence and therefore bubble destruction.

The viscosity of the liquid opposes the drainage of the film and its displacement by coalescing bubbles. The higher the viscosity, the slower will be the film-thinning process. If the liquid in a foam system is changed to an impermeable solid membrane, the film viscosity can be regarded as having become infinite and the resulting "solid foam" will be permanent. In addition, if the liquid is a Bingham plastic or a thixotrope and does not have its yield stress exceeded, then the foam will be permanently stable. For other non-Newtonian fluids and for all Newtonian ones, no matter how viscous, the viscosity can only delay foam disappearance.[177]

Bikerman rejects the idea that foam films drain to a critical thickness at which point they burst spontaneously. He reasons that foam stability is instead linked to the existence of a surface skin of low interfacial tension immediately overlaying a solution bulk of higher tension, latent until it is exposed by rupture of the superficial layer.[178] Such a phenomena of surface elasticity, resulting from concentration differences between bulk and surface of the liquid, accounts for the ability of bubbles to be penetrated by missiles without damage.

The ability of some finely divided, insoluble solids to stabilize foam has long been known.[179,180] Bartsch found that the presence of fine galena greatly extended the life of air foam in aqueous isoamyl alcohol, and the finer the solids, the greater the stability. [181] 50μm particles have been shown to lengthen the life of some systems from 17s to several hours. This behavior is consistent with theory, which indicates that a solid particle of medium contact angle with the liquid will prevent the coalescence of two bubbles with which it is in simultaneous contact. Berkman and Egloff have shown that some additives increase the flexibility or toughness of bubble walls to render them more stable.[182]

Methods of gas dispersion and spargers are covered extensively in Perry's Chemical Engineer's Handbook, Chapter 18. While these are important industrially, only mechanical agitation will be used in the proposed research. Mechanical agitators are used primarily (1) to disperse gas into a liquid for the purpose of promoting mass transfer and (2) to create a foam. For producing foam many different agitators are available, and are most commonly utilized by manufacturers catering to the food industry. Wire-whip agitators are used quite extensively to aerate a liquid through and produce a uniform foam. Several other agitator types (serrated disk, disk, turbine, etc.) were tested by Fundy and Bates[183]in producing a liquid-liquid dispersion. Their findings have been quite useful for scale-up purposes.[184]

In conventional chemical foaming, a suitable chemical foaming agent is incorporated in the polymer, and its reaction is initiated by a temperature increase. If a chemical catalyst is also present, to initiate crosslinking at high temperature, there is the difficulty that this rise will initiate both reactions of crosslinking and foaming.. With radiation no such difficulty is involved. The polymer is crosslinked at approximately room temperature, and the temperature is then raised to initiate foaming above the melting temperature.. The size of the pore is determined by the radiation dose, and the gases released fill these pores. On cooling to room temperature, the polymer re-crystallizes, but the pores incorporating the foam gases retain the open structure. The size of the pores is determined primarily by M_c, the molecular weight between successive links, and is, therefore, chosen according to the crosslinking dose.

Typical methods of producing foams rely on chemical or physical blowing agents to generate a cellular structure in a polymer melt. However, as outlined in the above section, mechanical dispersion is possible. In addition, previous work[185-189] has shown that it is possible to generate cellular materials by electron beam irradiation techniques without a blowing agent by pre-foaming

using mechanical entrainment and then immediately curing of the froth using radiation. It is proposed that a fundamental study of the foaming and curing process is needed to further understand the process-structure-property relationships that govern these foams.

2.10 Physical Aging and the Glass Transition

2.10.1 Introduction

A brief review of physical aging and the glass transition is presented. In Chapter 4, an understanding of the subject of physical aging is required to help interpret the research material, therefore it is important to briefly cover some general aspects of physical aging in the literature review section. It is not the intent to completely cover the physical aging literature in detail, but to give an overview of various aspects, theories, consequences and manifestations of it.

2.10.2 The Non-Equilibrium Nature of Glassy Polymers

Cooling a polymer from the equilibrium liquid state will quench in some free volume which results in a non-equilibrium glassy state (see Figure 2-21). If one were to quench the polymer in question through the glass transition Tg and age at temperature Ta (at least 10°C below Tg) the amount free volume will slowly decrease over time. The rate of this decrease depends on the aging temperature relative to the glass transition temperature (Tg) of the polymer. The rate of aging generally increases up to 5-10°C below Tg, where it slows down considerably (see Figure 2-22 and Figure 2-23).

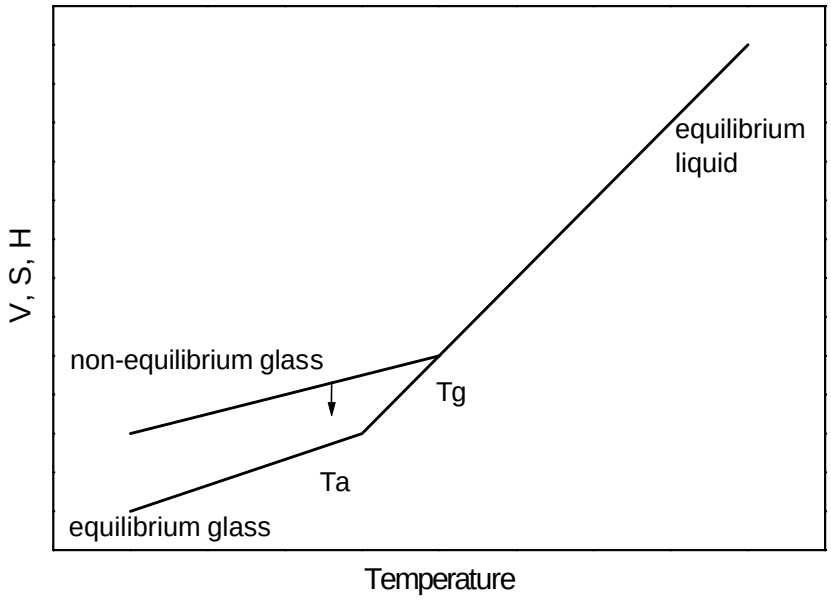

Figure 2-21 Volume-temperature curve for a polymer showing the non-equilibrium state below the Tg and quenched in free volume.

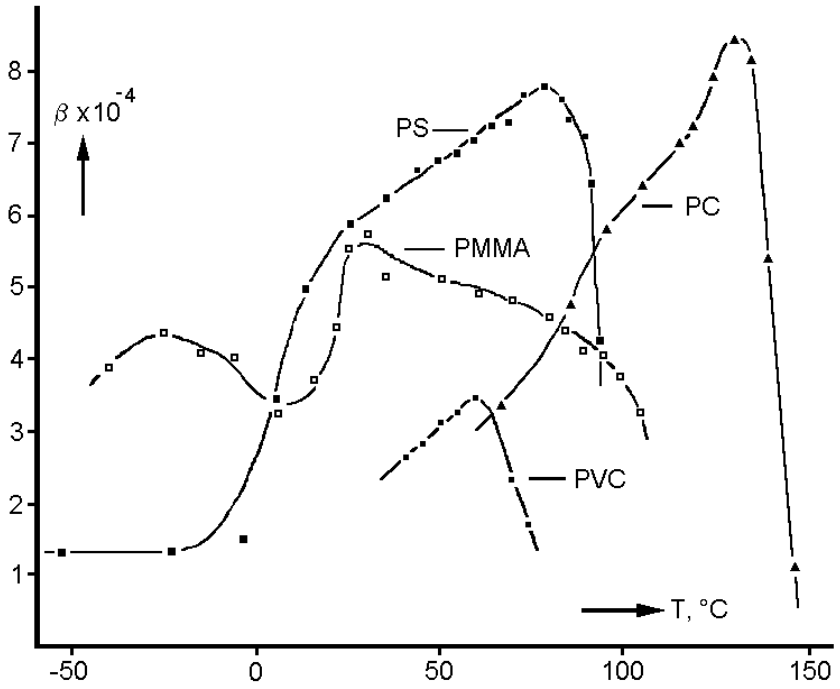

Figure 2-22 Volume relaxation rates for various polymers as a function of aging temperature.[190]

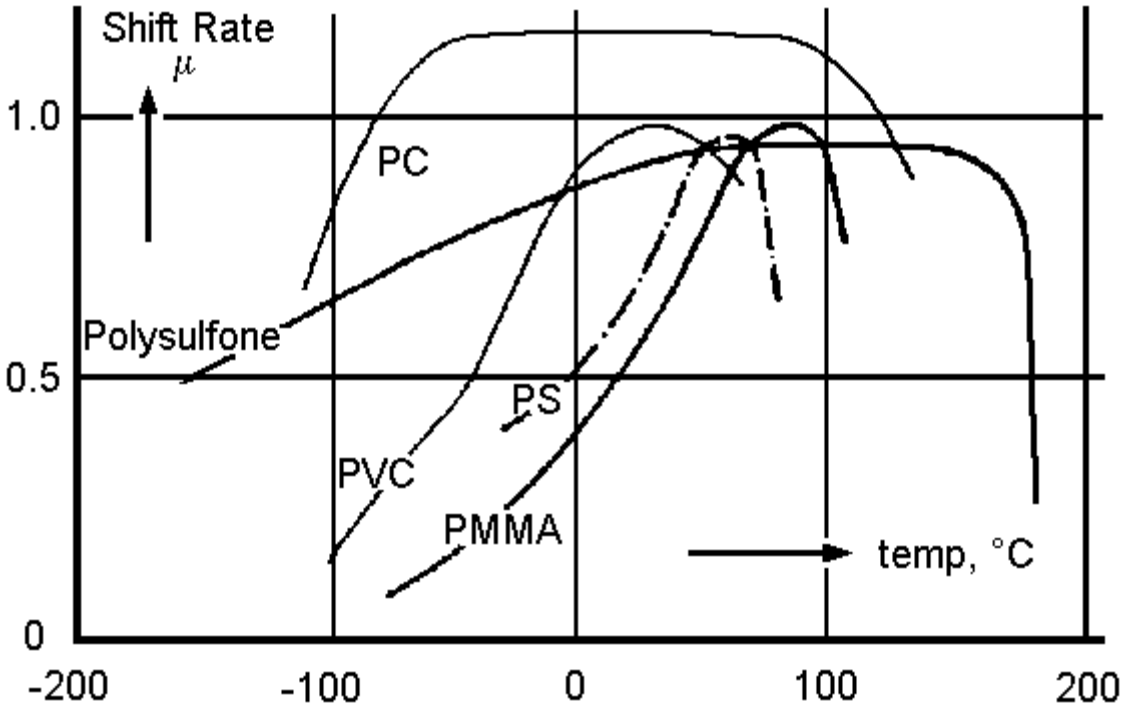

Figure 2-23 Mechanical shift rates for various polymers as a function of isothermal aging temperature.[191]

2.10.3 The Glass Transition

The glass transition temperature is generally defined as the temperature where the volume-temperature curve changes slope.[192-194] Physical aging is the phenomena that describes this free volume reduction and occurs at temperatures below Tg in the amorphous phase of polymers. It is closely interrelated with the glass transition in polymers and theories that describe and predict physical aging have often been closely tied to these glass transition theories. Theories of the glass transition have been separated by McKenna[195] into thermodynamic[196-198] and kinetic/free volume theories.[199-204] Because there is not a universally accepted theory of the glass transition in polymers or other materials as well, physical aging is also not completely understood. Further work is required to enable one to understand the role the

various molecular variables play in physical aging. There are many theories that have been developed to describe the glass transition, but none of them are completely adequate in predicting all aspects of physical aging.

Theories of the glass transition can be divided into two groups, thermodynamic theories and free volume/kinetic theories. Any successful thermodynamic theory of the glass transition will have to, in addition to predicting Tg, resolve Kauzmann's paradox.[205] Kauzmann showed that when the equilibrium entropy of a supercooled glass-forming liquid is extrapolated to low temperatures, the resulting entropy is less than the entropy of the crystalline solid, which is impossible (see Figure 2-24). Kauzmann, therefore, rejected any thermodynamic explanation of the glass transition and preferred kinetic models. There is no denying the fact that there is a time dependent effect involved in the glass transition. One only has to observe the effect of Tg measurement to the time frame of the experiment. One theory to successfully resolve Kauzmann's paradox is the thermodynamic theory of Gibbs and DiMarzio.[206-208] This theory will not be described in detail, but their method of resolving Kauzmann's paradox was to allow for a second order thermodynamic transition to occur at which the configurational entropy reaches and remains zero. Their theory has been used to predict influences of various molecular parameters (such as molecular weight and crosslinking) on Tg as well as the change in heat capacity at the glass transition.[209-216] The theory does utilize an infinitely slow heating rate to predict Tg, which results in Tg predictions 50°C below that of finite heating rate results making practical predictions somewhat more difficult.

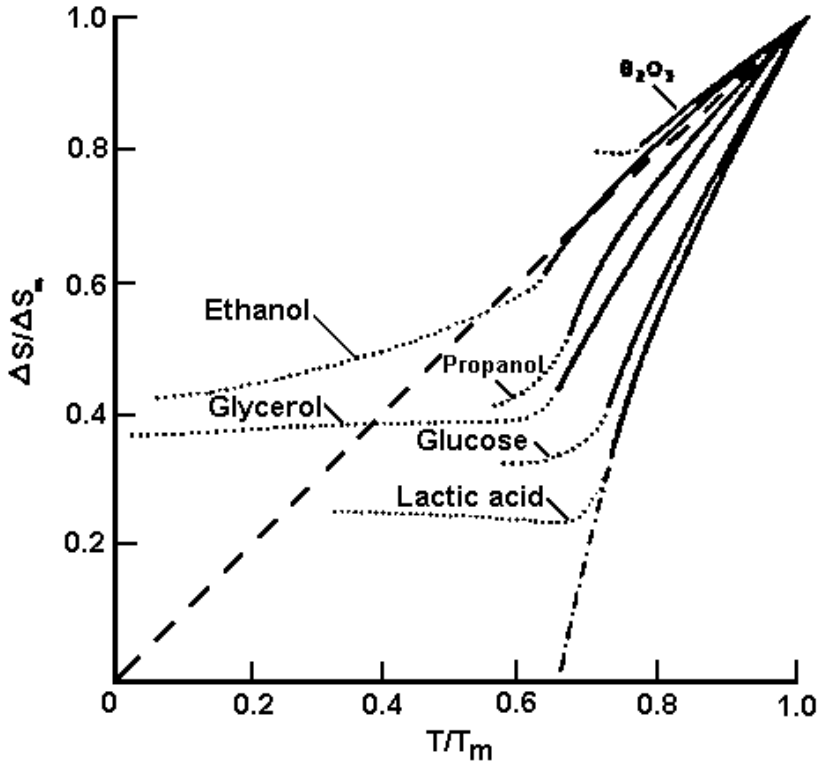

Figure 2-24 Data showing Kauzman's paradox for several glasses.[217]

2.10.4 Free Volume

Free volume is the volume not occupied by the polymer molecules and is due to inefficient packing of the polymer chains. This volume allows mobility of the molecules for diffusion, mobility, and energy dissipation. Free volume theory based on the Doolittle equation result in the well known Williams-Landel-Ferry equation (WLF) which, above Tg, can be used to accurately predict relaxation time and free volume but is lacking below Tg. Further refinements of the WLF equation were accomplished by Cohen and Turnbull[218,219] Several modifications to these theories have been proposed.[220,221] As with the thermodynamic theories, free volume theories

have successfully predicted the effects of molecular weight and crosslinking on Tg.[222-226]

Free volume theory has unfortunately failed to predict some aspects of physical aging. Struik found the free volume models to be lacking in their application which he believes to be a result of not taking into account the distribution of "holes" vs. the free volume model which assumes that one can utilize an average size.[227] This would be akin to comparing a highly disperse polymer with number average molecular weight (Mn) equal to that of a monodisperse polymer and expecting them to have similar behavior since they have an equal Mn.

From a practical standpoint, physical property changes are well known to occur over time in many amorphous polymers and reflect the reduced free volume and molecular mobility that occur with physical aging. Because of this reduced molecular mobility, physical aging can be described as a self-limiting process. As free volume is reduced, molecular mobility is lessened and the ability for chains to cooperate and "squeeze" out free volume slows with time. Therefore, it will take near infinite times in most cases for the system to reach equilibrium and most data is plotted in terms of log of the aging time to make the data analysis manageable. Changes in the mechanical properties and permeation of gases in glassy polymers over time are common and are often a result of physical aging.[228-229] It is therefore important for the engineer to have an understanding of physical aging in designing products manufactured from amorphous or semicrystalline polymers where the usage temperature is below the glass transition temperature. In addition, exposure of polymers to radiation in their working environment is becoming more commonplace and it is especially important to account for any additional changes that may occur in these materials when exposed to radiation.[230-232]

2.10.5 DSC Study of Physical Aging

Physical aging is also associated with enthalpy relaxation and is, therefore, observable thermally by differential scanning calorimetry (DSC) by the well known excess endothermic relaxation peak that often occurs. It is well known that the amount of volume relaxation is often roughly proportional to this peak at Tg.[233] Therefore, one can typically measure the extent of physical aging by measuring the area under the endothermic peak at the glass transition. The work in Chapter 4 is largely concerned with measuring thermodynamic properties of aged and irradiated polymers and the resultant changes in the enthalpy relaxation. Figure 2-25 shows typical aging data for aging of a bis-phenol-A polycarbonate sample (Tg 150°C). Samples were aged at 120°C for times of 0.1, 1.0, 10.0, and 200 hours and the corresponding data is shown. Note that the 0.1 hr. time corresponds roughly to the freshly quenched sample, but the 1 hour time already shows a significant aging peak. To reverse this physical aging - as observed by the DSC traces, one can heat the sample above Tg, where in the liquid state it will "forget" it's prior thermal history. Once quenched below Tg the sample will not show the aging peak if immediately heated through Tg again. Figure 2-26 shows the relationship between the heat capacity as measured by DSC and the resulting enthalpy. Note the similarity between the enthalpy curves and the free volume curve in Figure 2-21.

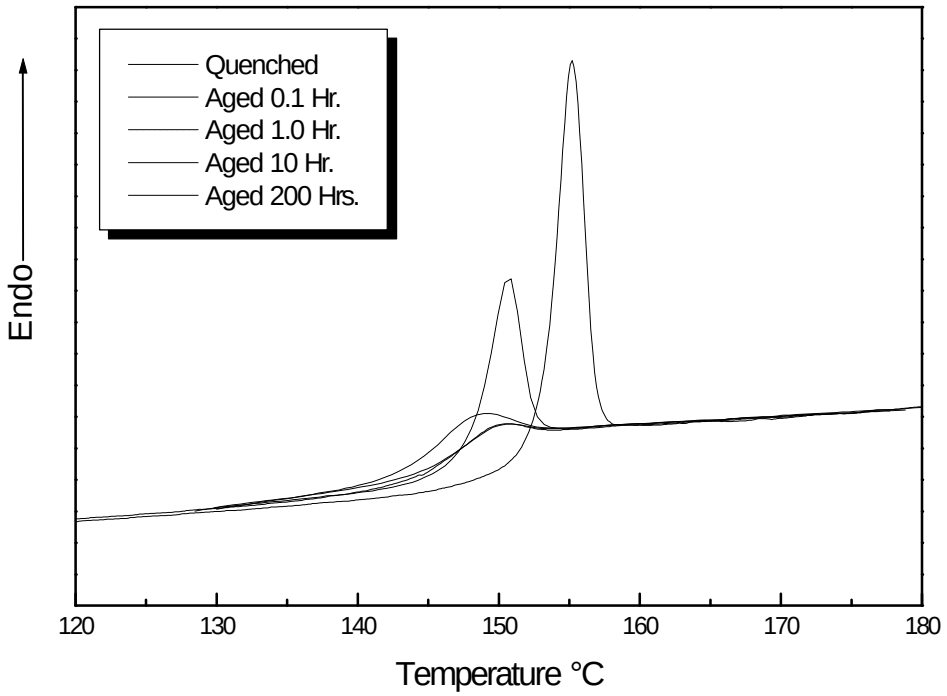

Figure 2-25 Physical Aging of polycarbonate at 120°C. Data for aging times of 0.1, 1, 10, and 200 hr. are shown. The heating rate was 10°C/min.

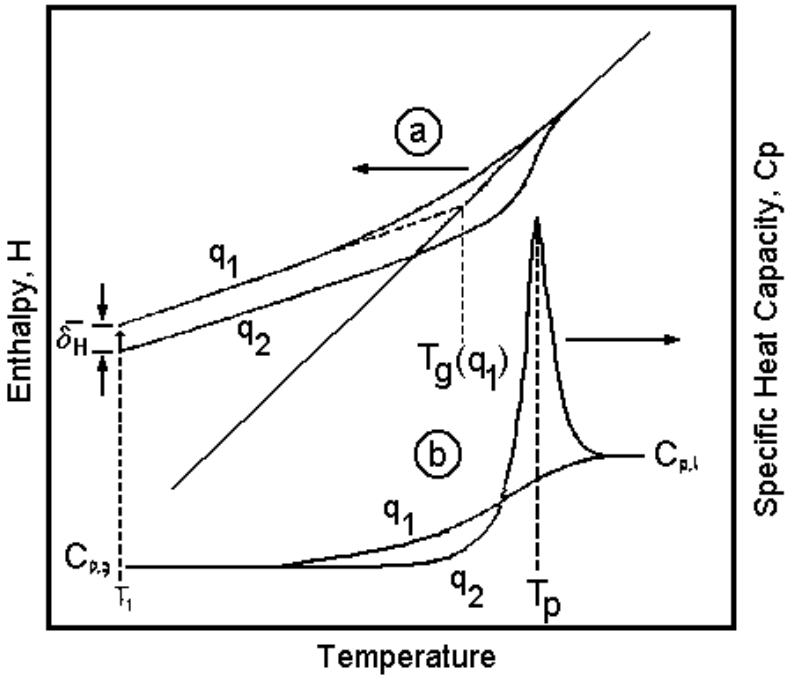

Figure 2-26 Schematic illustration of the variation of enthalpy (a) and specific heat (b) with temperature in a three step thermal cycle.[234]

Clearly, physical aging is an important phenomenon to be studied by the scientist and is just as important for the engineer to take into account when designing applications that utilize amorphous polymers. Because of this, theories to adequately describe the glass transition and physical aging are needed. One of the goals of the work in Chapter 4 is to make some contribution towards further understanding of the phenomena and the role of internal energy in the enthalpic state of the polymer as well as the effect of radiation itself on the process.

This concludes the literature review for this dissertation. Several topics have been discussed, ranging from the fundamental interactions between radiation and organic materials to the changes in materials that may or may not result. Specialized topics of polymeric foams, phase separation and physical aging have been presented to give the reader background information relevant to the experimental research that will now be presented.

3 Process Structure Property Relationships in Electron Beam Generated Cellular Materials

3.1 Introduction

Previous work[235-239] has shown that it is possible to generate cellular materials by utilizing electron beam irradiation techniques. While there are several different methods of producing cellular materials in this fashion, all of the processes are based on a principal of pre-frothing a radiation responsive mixture and then feeding this mixture into the electron beam radiation source, which cures the system. Some general advantages of using these techniques are having the ability to go from starting materials to final product in one step, and in principal, to do this in a continuous manner. Unfortunately, no systematic studies have been carried out to determine the effects of the type of different processes and the effect of processing variables on the structure property relationships for these materials. It is convenient to categorize the different processes as follows for the purposes of introducing this work:

Methods of Producing Cellular Materials by
Electron Beam Irradiation Techniques

- Chemical Blowing Agent[240,241]

  Processes that fall into this category rely on the addition of a compound to a polymer or a radiation curable monomer/oligomer blend. This compound decomposes upon irradiation and releases a gas which creates a cellular structure in the material by nucleation and growth of the cells.

- Physical Blowing Agent [242,243]

  These processes either utilize pressurized gas, which has saturated a polymer melt or radiation curable monomer/oligomer blend, or an agent, which releases a gas upon heating. The mixture is extruded (and preheated in the case of the thermally decomposable agent) which causes the system to expand into a cellular structure. Immediately after extrusion, the system is passed under the electron beam which sets the cellular structure in place before collapse. Unlike the previous category, the system has the cellular structure prior to irradiation.

- Pre-froth polymer by mixing[244]

  This process would be limited to polymers which crosslink in response to radiation, such as polybutadiene or polyisoprene. Also included in this category are systems that contain a polymer not normally thought of as a radiation cross-linker (such as PVC) and a reactive cross-linking plasticizer to cross-link the system, locking in the cellular structure, when irradiated. One would first melt the polymer, then mechanically entrain air, for example, by mixing with a dual high speed mixer. Once the system has generated sufficient froth, then one may extrude the froth into the electron beam, cross-link the system and thereby produce the cellular material.

- Pre-froth monomer by mixing[245,246]

  There are actually two separate techniques that start from a monomer. The first technique, which will be termed the "surfactant method" relies on a surfactant and a low molecular weight, low viscosity radiation curable monomer. First, air is blown through the mixture of the surfactant and the monomer which generates a froth. This froth is

then extruded to a fixed thickness and passed through the electron beam, which locks in the cellular structure. The key to this technique is that the surfactant stabilizes the cellular structure prior to irradiation.

The second technique in this category is the principal focus of the work discussed in this chapter. It does not rely on a surfactant, but instead is similar to the "pre-froth polymer by mixing" process. Starting with a high viscosity system of a radiation curable oligomer or a monomer/oligomer blend, one froths the system with a dual high speed mixer, then extrudes the froth into the electron beam for curing. One of the significant differences between the techniques is what “stabilizes” the cellular structure prior to irradiation, either a surfactant or the viscosity of the mixture.

As one can see from the above descriptions, much of this previous work has relied on the use of surfactants or blowing agents, which make the process more complex and expensive. In this work, focus has been placed on the generation of cellular materials from radiation curable materials without the use of heat, surfactant, or blowing agents. This technique relies on a sufficient viscosity to hold the cellular structure in place after it has been mixed as opposed to using a surfactant which relies on surface tension to stabilize the cellular structure in place before curing. Details of this viscosity requirement were studied in detail. In addition, it is possible to polymerize into the material blends of radiation curable species with different properties in order to custom tailor the material for a specific range of applications (e.g., high or low Tg, high modulus, etc.) Although it is possible to synthesize surfactants that have radiation curable functionality, common surfactants do not have radiation responsive groups (e.g. allylic groups), and, therefore, most previous work has relied on surfactants that do not respond to a

radiation cure and become part of the structure by reacting into the network.[247]

The advantages of the mixing process over the other techniques outlined previously are that no preheating is involved and no prepolymerization of the mixture before irradiation is required. In addition, no blowing agent (chemical or physical) and no surfactant are required for producing the cellular structure. While this technique (termed "mixing" process) has been the primary focus of this work, it is important to contrast this with the technique utilizing a surfactant (termed "surfactant" process) because the importance of the viscosity of the radiation curable mixture which determines which process is appropriate.

It is the purpose of this work to examine what process-structure-property relationships exist between these materials. It is hoped that this can provide additional information about understanding these materials and the potential applications for them.

3.2 Experimental

3.2.1 Reactant Materials and their Characterization

Acrylated functionalized materials were generously supplied by Radcure, a manufacturer of electron beam and UV curable coatings, under the commercial names of β–CEA, TMPTA, HDODA, Ebecryl 4827, and Ebecryl 1701. The structures of these compounds are outlined in Figure 3-1. It was desirable to compare monomers of different functionality in this work; therefore, a monoacrylate (β–CEA), diacrylate (HDODA), and a triacrylate (TMPTA) were selected. Ebecryl 4827 and 1701 are acrylated urethane oligomers of unknown structure, but for the purpose of this work, the most noted difference is their molecular weight and viscosity. A fluorochemical surfactant was obtained from 3M Inc. under the tradename of FC-430. FC-430 was selected because it was utilized in previous work[248] involving the "surfactant" process with monomers similar to the ones shown in Figure 3-1. Thin films of the monomers and oligomers were cast using a scalpel or ”doctor blade” on glass and cured in an ESI 175 KeV Electrocurtain electron beam accelerator using

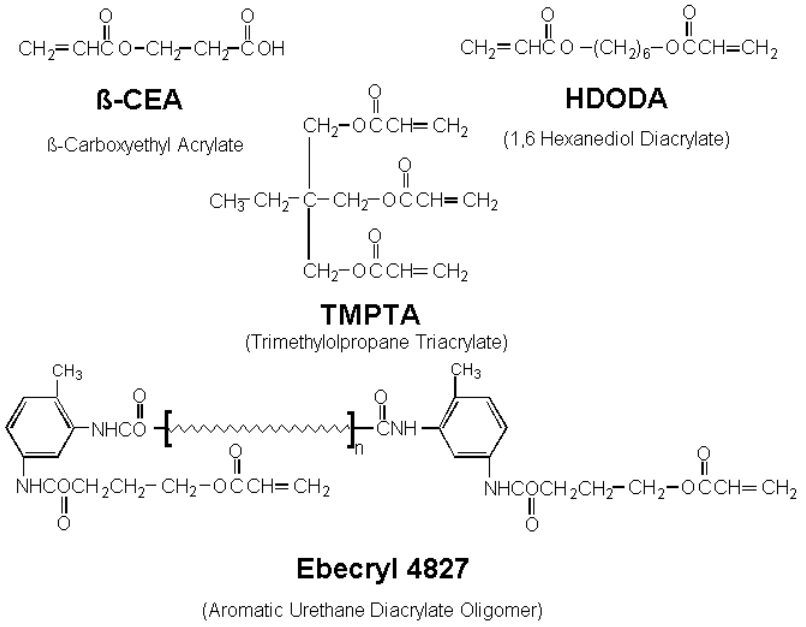

Figure 3-1 Structures of the materials used in this study.

doses of 0.625, 1.25, 2.5, 5, 10, 20, and 40 Mrad. Two samples were irradiated to higher doses. It should be noted that typical doses seen in industrial applications range up to 20 Mrad, with 5-10 Mrad being typical for most curing operations. They were then characterized according to their cured Tg's as a function of dose using differential scanning calorimetry (DSC) on a Seiko model 220C. These measurements were coupled with FTIR using a Nicolet 510 FT-IR spectrometer, also as a function of dose. Viscosity measurements were determined at 25°C using a Bohlin CS rheometer with cone and plate geometry. Viscosity results are summarized in Table 3-1. For the range of shear rates that these materials were tested (up to 661 s^{-1}), the data indicated Newtonian behavior. Due to instrumentation limitations on the upper limit of generated shear stress, these higher shear rates were not accessible for the oligomers.

Table 3-1 Summary of the rheological properties of the reactive chemicals used in this study.

Material Name	Description	ρ (g/cc) at 25°C	MW (g/mol)	Shear Rates Tested (s^{-1}) at 25°C	μ (Pa·S) at 25°C
β–CEA	β-Carboxyethyl Acrylate	1.21	144	2.89-661	0.20
HDODA	1,6 Hexanediol Diacrylate	1.02	226	2.89-661	0.0054
TMPTA	Trimethylol-propane triacrylate	1.10	296	0.888-99.90	0.094
Ebecryl 4827	Aromatic urethane diacrylate oligomer	1.11	1500	0.106-2.892	269.0
Ebecryl 1701	Arcylated Acrylic Oligomer	1.10	27,000	0.0837-1.125	1,200

3.2.2 Cellular Material Preparation

Figure 3-2 outlines the process used to produce the cellular materials. First, materials were selected based on their viscosity and *cured* Tg. This step is critical as it largely determines the final material properties. For example, if a stiff structural material is desired, then more rigid, high Tg (upon curing) materials should be selected; however, if a more flexible material is desired, then materials having a low Tg upon curing should be selected. The materials were then processed depending on the viscosity of the selected materials. In the case of the materials termed "mixing process" the materials were combined with a dual mixer at high speed until such time as a stable froth was generated, then the froth was cast on a substrate with a doctor blade set at a fixed height. The casting thickness was set at 16-20 mil and determined roughly as four times the uniform depth of penetration for the Energy Sciences Inc. Electrocurtain 175 KeV electron beam accelerator (4 mils). The "average" froth generated for this process had approximately 50% air, therefore, a casting thickness of ~8 mils would allow sufficient exposure to assume uniform exposure. However, to produce thicker samples, the froth was cast at 16 mils and irradiated on both sides. Because of the depth-dose profile, the first pass was typically sufficient to solidify the cellular material.

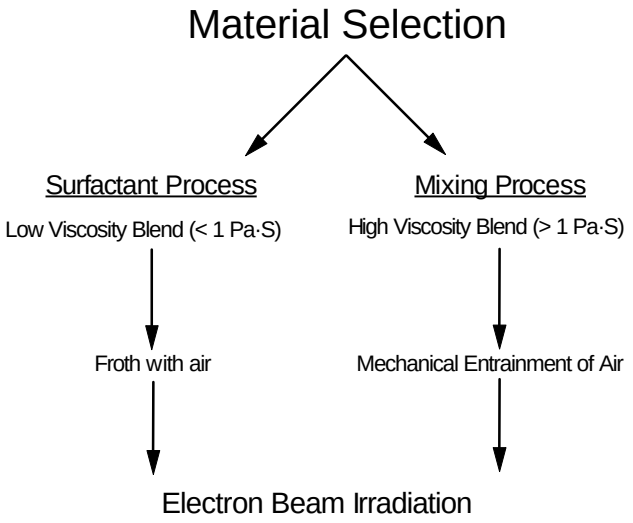

Figure 3-2 Qualitative outline of the E-Beam cellular material generation process involving the mixing technique.

The second pass on the other side which assured a relatively even cure. For comparative purposes, another type of cellular material was generated via the above mentioned surfactant method (also outlined in Figure 3-2) from a low viscosity mixture of only monomers with a small amount of the acrylated fluorochemical surfactant (Fluorad FC-430). In this case the surfactant was added to a monomer and then nitrogen was bubbled through the mixture. The froth was then poured onto a petri dish and immediately cured in the electron beam accelerator using the dual pass method described above.

3.2.3 Cellular Material Characterization

Scanning electron microscopy (SEM) studies of the resulting cellular materials were performed using a Cambridge Instruments Ltd. Stereoscan 200 microscope. Mechanical testing in tension was performed at ambient conditions in a Instron model 1122. The crosshead speed used for all tensile testing was 0.1 mm/min. 10 mm by 2.75 mm dogbone samples were cut for all specimens. Sample thickness varied from about 3 mils for the films and about 20 mils for the cellular materials.

3.3 Results and Discussion

3.3.1 Level of Cure for a Given Dose

The goal of this analysis was to determine the range of Tg's the cured materials had and, therefore, aid in selecting materials for stiff structural type applications or more flexible applications. In addition, it was desirable to know what the sensitivity to these materials was to a given dose, and to determine what percent residual double bonds exist in the materials as uncured acrylate monomer would contribute to network defects which would result in less than optimal mechanical properties. The additional concern for acrylate monomer diffusing out of these materials motivated these

experiments. Finally, because of the low dose desired from an practical and environmental viewpoint, dose-cure level optimization was required. This analysis was performed utilizing FTIR and DSC as a function of dose, starting with a dose of 0.625 Mrad and doubling the dose up to 20 to 80 Mrad, depending on the material.

Information on thermal stability and extent of reaction of the monomers was desired and acquired utilizing the technique of thermogravimetric analysis via a Seiko TG/DTA with a heating rate of 10°C/min in a nitrogen atmosphere. It should be pointed out that a nitrogen atmosphere tests the thermal stability of the chemistry, vs. an oxygen atmosphere which would test the resistance to oxidation. Figure 3-3-Figure 3-6 show the results for the three monomers and Ebecryl 4827 oligomer.

Indicated in all four figures is the onset of weight loss at about 200°C. β-CEA shows the quickest weight loss, as would be expected since it has the lowest molecular weight, highest vapor pressure and functionality 2. It lost about 95% of it's weight before significant polymerization had occurred. For the diacrylate (HDODA), about 50% weight loss from evaporation occurs before polymerization. The triacrylate (TMPTA) only lost about 5% before polymerization. The significance of these plateaus and weight losses gives information on the relative extent of reaction of the monomers. For example, a monomer that is capable of thermally curing, initial heating would cause some weight loss from evaporation if the monomer is has a significant vapor pressure at room temperature, with a significant observable endotherm observable on the DTA trace. At some point, thermolysis would cause the double bonds to react, polymerizing the monomer. One would observe a large exotherm on the DTA trace, with no accompanying weight loss. Finally, degradation of the polymer would occur at even higher temperatures, observable by continued and immediate weight loss. Indeed, one does observe

this behavior for the three monomers with different amounts of evaporation according to the relative extent of reaction. Maximum evaporation for all three monomers occurs at 200°C, with β-CEA evaporating the most, followed by HDODA and then TMPTA. Since these materials are all acrylate liquids at room temperature with similar vapor pressures, this should not be surprising. From the amount of monomer polymerized at this temperature (as measured by the second plateau) one can say that approximately 5% of the β-CEA reacted before it could evaporate, followed by HDODA (about 50%) and then TMPTA (about 95%). Finally at about 450°C, whatever had polymerized now degrades, resulting in dramatic and rapid weight loss.

From this analysis, one can make some qualitative observations that, with respect to the monomers, TMPTA is the most responsive to heating (i.e. the largest extent of reaction at a given temperature), followed by HDODA and β-CEA. This should be intuitive for a triacrylate, with a functionality of 6, has a much better probability of reacting with another triacrylate molecule than a monoacrylate, which has a functionality of two. (assuming equal mobility and functional group reactivity) A gel point/percolation threshold analysis leads to the same conclusion, with α_c = 1.0 for β-CEA, 0.33 for HDODA, and 0.2 for TMPTA. Similar behavior, in terms of reactivities was observed in the FTIR and DSC analysis, which will be discussed in the following section.

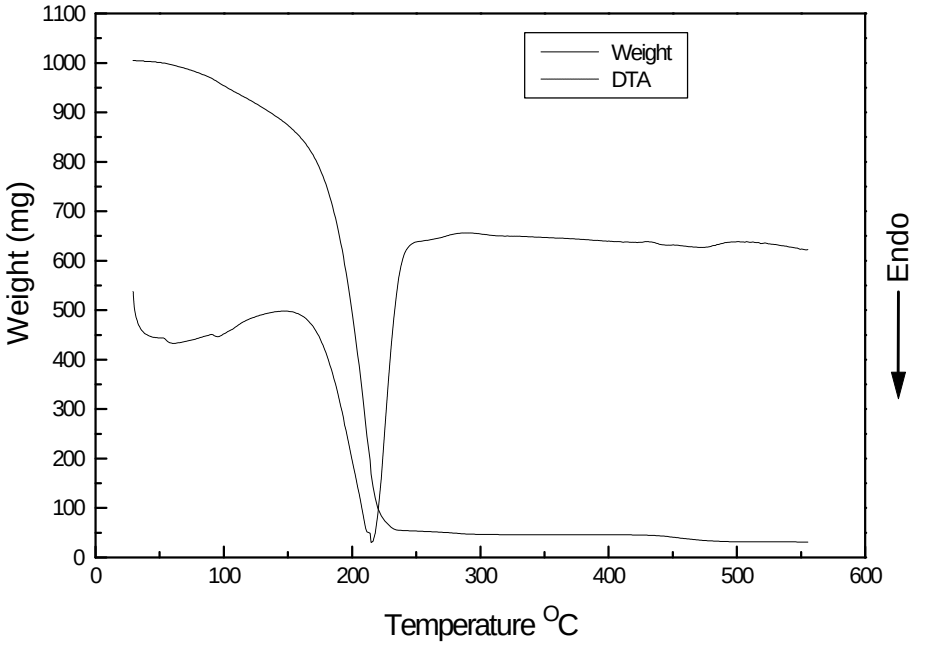

Figure 3-3 TG/DTA Scan for β-CEA. Heating rate = 10°C/min.

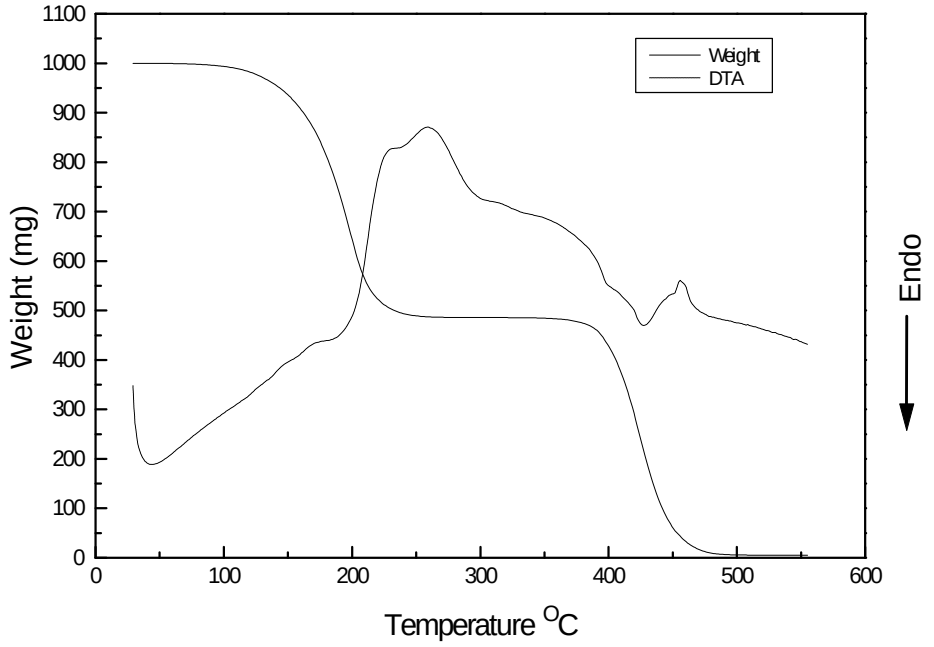

Figure 3-4 TG/DTA scan for HDODA.

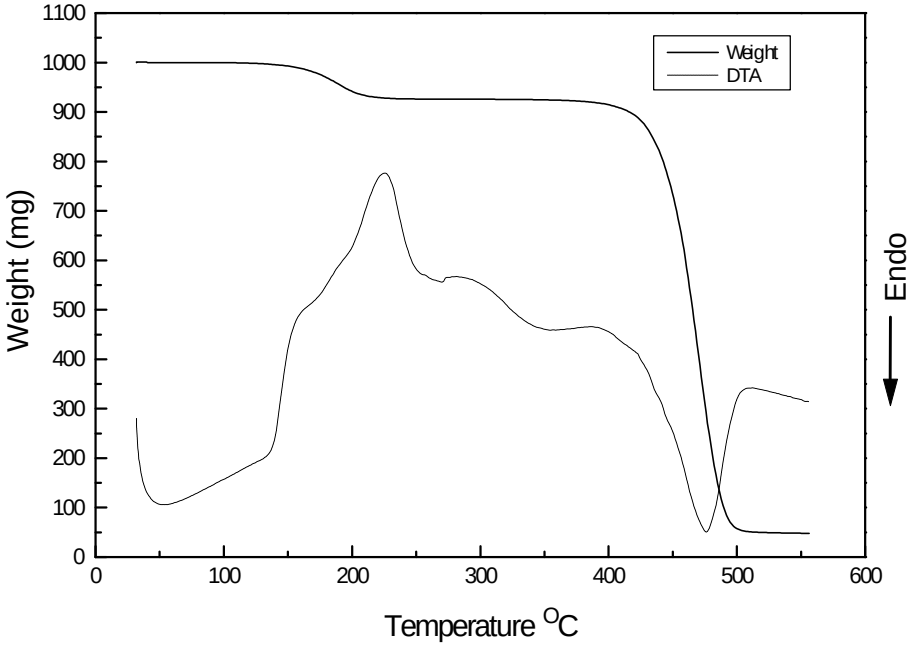

Figure 3-5 TG/DTA scan for TMPTA.

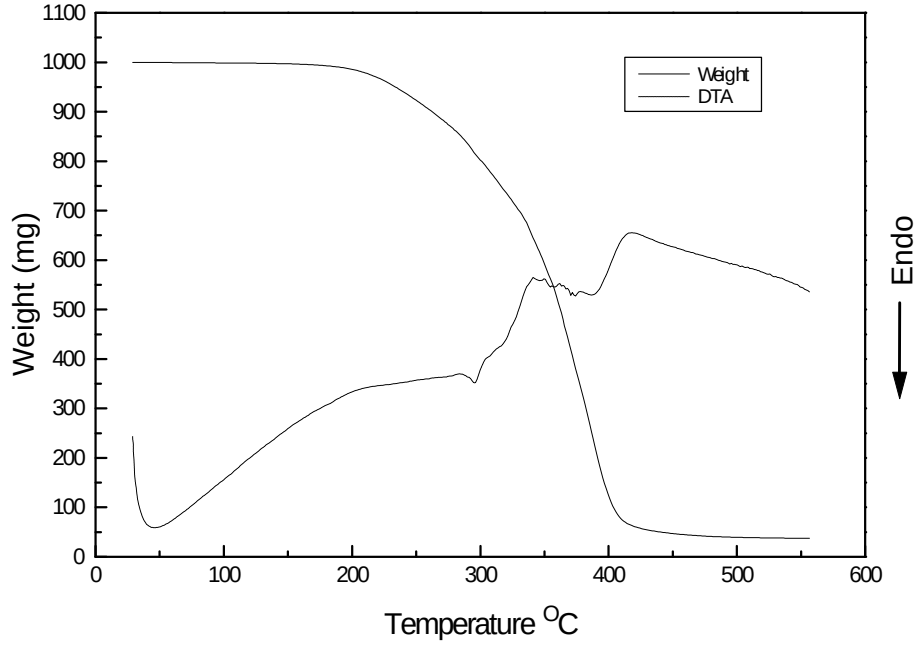

Figure 3-6 TG/DTA scan for Ebecryl 4827.

Figure 3-7-Figure 3-11 show DSC scans as a function of dose for the three monomers and one oligomer (Ebecryl 4827). The figures show DSC traces for doses from 0 to 40+ Mrad. The “0 Mrad” (uncured) materials were only run up to room temperature to avoid curing reactions which would damage the DSC cell. What is shown in each figure for the uncured system is some transitional behavior (Tg or Tm) as well as a heat of reaction. Next, each transition “climbs” in temperature as the dose increases and then either stops increasing at some point or keeps increasing. One notes that the oligomer has a significantly lower cured Tg than either of the two monomers (below room temperature) and that the multifunctional monomers have cured Tg's well above room temperature. While pinpointing the Tg for these materials is difficult, two monomers (HDODA and TMPTA) both had cured Tg's in excess of 100°C while the oligomer's Tg was approximately -25°C. The difficulty in observing transitions arises in that for a high functionality monomer, Tg becomes very "flat" and it is hard to observe a change in heat capacity. At lower doses, a Tg may be observable, but one has to recognize the fact that there may be residual unreacted monomer present that is plasticizing the system which would lower the Tg as measured. In Figure 3-8, data for HDODA is shown. A melting point occurs at approximately 0°C for the sample with no cure (0 Mrad). For the next two curves which result for the 0.625 and 1.25 Mrad dosage levels, the melting point is still observable, indicating residual monomer is present. For these two curves, a reaction exotherm occurs at 125°C. This reaction exotherm can only occur if the system has attained the cooperative segmental backbone motion associated with Tg. Increasing the dose causes this exotherm to disappear until a flat line DSC trace is observed, which is very typical of crosslinked systems. One can see the trend of the Tg's of the lower dose samples "climb" and then disappear. If one assumes the same trend of Tg continues with respect to

dose, one can approximate the Tg for this material at 225°C +/- 25°C. Using a similar analysis for TMPTA, one can observe the same trend in Figure 3-9 however, the curves for the "high" doses do not flatten out as they did with HDODA. Assuming this trend continues, a fully cured sample of TMPTA should have a Tg_{∞} around 300°C+. A full cure, defined as every molecule reacting as part of the network, is not realistic, since with *f*=6, a full cure would never happen at or close to room temperature due to time temperature transformation (TTT) effects and the high cured Tg of TMPTA. The monoacrylate sample, β-CEA, showed a Tg that did not increase with dose. It is believed that this is due to it's low functionality and lack of any potential cross-linking groups other than one acrylate group per molecule.

Using the Fox equation, which weights the Tg of a blend according to the Tg's of the pure components, one can estimate the cured Tg's for blends of these reactants and, therefore, custom tailor the cellular materials to specific temperature range applications. The Fox Equation is shown in the following equation:

$$\frac{1}{Tg} = \frac{W_a}{Tg_a} + \frac{W_b}{Tg_b} \qquad (3\text{-}1)$$

Where: W_a = weight fraction homopolymer of component 1
W_b = weight fraction homopolymer of component 2
Tg_a = Glass transition temperature of component 1
Tg_b = Glass transition temperature of component 2

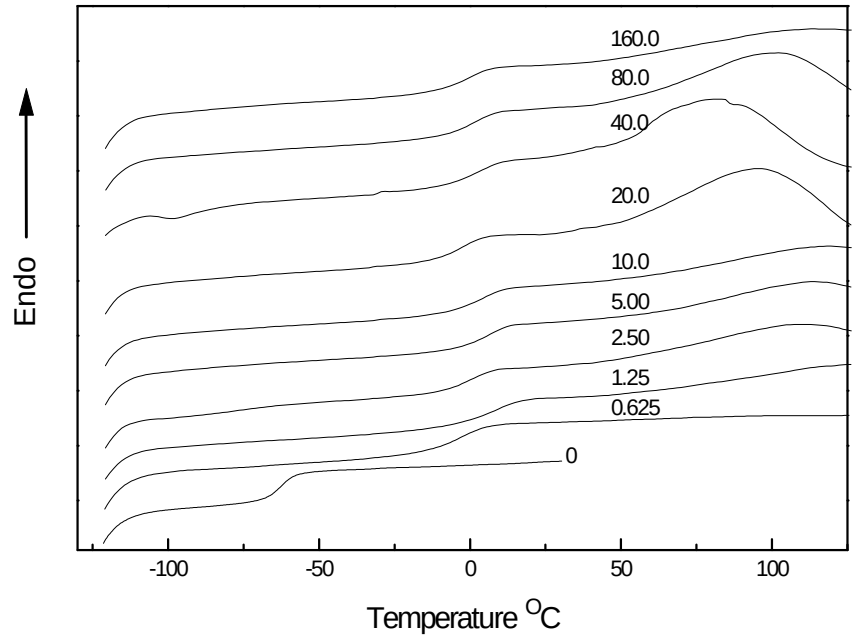

Figure 3-7 DSC scan for β-CEA as a function of dose. Heating rate = 10°C/min Numbers indicate the sample dose in Mrad

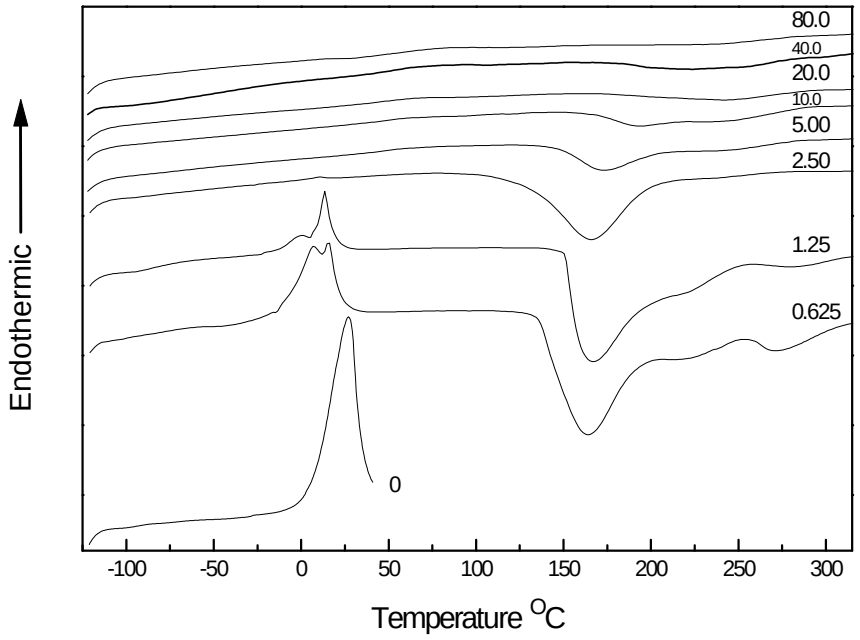

Figure 3-8 DSC for HDODA as a function of dose. Dosage values are in Mrads.

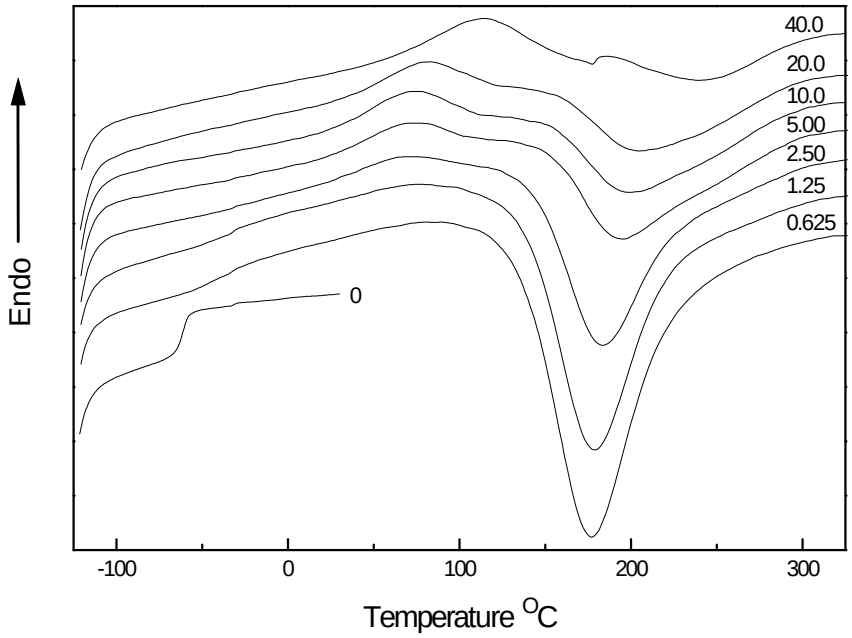

Figure 3-9 DSC scans for TMPTA as a function of dose. Dosage values are in Mrad.

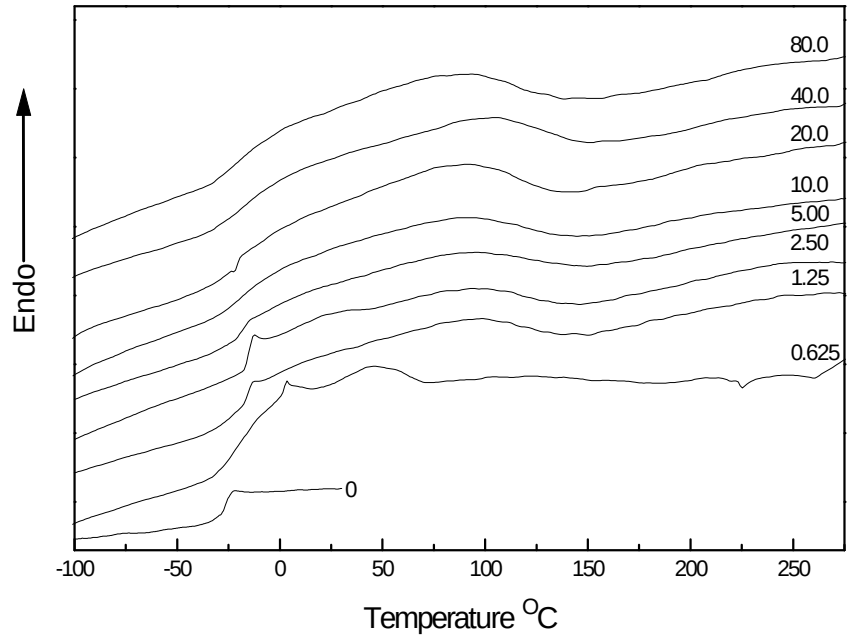

Figure 3-10 DSC scans for Ebecryl 4827 as a function of dose. Dosage values are in Mrad.

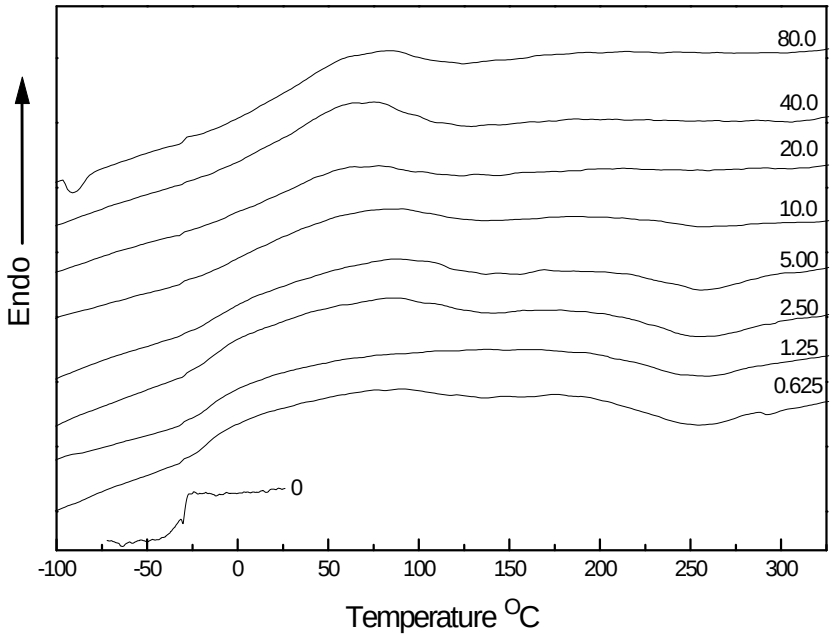

Figure 3-11 DSC scans for Ebecryl 1701 Oligomer as a function of dose. Dosage values are in Mrad

Figure 3-12 through Figure 3-17 show data from the FTIR analysis. This analysis was coupled with DSC primarily to follow residual double bond content as a function of dose. The acrylate peak at 810 cm^{-1} was used for this analysis and normalized on the ester peak at ca. 1750 cm^{-1}. Samples of each monomer or oligomer were coated on a KBr pellet and a scan was taken. To assure that quantitative work could be performed on the scans, the coating on the KBr pellet was made thin enough so that no absorbance peak was above 1.0. The same sample was then irradiated at 0.625 Mrad, then scanned in the FTIR, and the dose increased (doubling each time) until a total dose of 40-160 Mrad was reached. Higher doses were given to some samples to see if any further reduction in the acrylate peak or other reactions took place.

Figure 3-12 shows data for β-CEA. The entire spectrum is shown in this figure to show that in these materials, the significant changes occur

primarily in the fingerprint region from about 600 to 1900 cm^{-1}. Like the oligomers, increasing dose beyond a few Mrad did not significantly decrease the acrylate peak.

This material was particularly unique in that increasing the dose continued to quickly reduce the number of residual double bonds present even though the exotherm in the DSC trace appeared to disappear at ca. 20 Mrad. Figure 3-13 shows that at 20 Mrad there is still a visible acrylate peak in HDODA. The triacrylate material (TMPTA) showed both residual double bonds and a significant DSC exotherm at 20 Mrad (see Figure 3-9). Both oligomers showed an immediate reduction with very low doses and then no significant reduction in double bonds with increasing dose.

The FTIR analysis is summarized in Figure 3-17. Note that in all the materials there are significant unreacted groups at 20 Mrad; however, this does not necessarily mean that these materials contain unreacted species that are free to diffuse out of the bulk sample. For example, a triacrylate molecule would have a very high probability of reacting with another triacrylate group and becoming part of the network. However, there could easily be unreacted groups on that same molecule which would contribute to residual double bonds and a DSC exotherm from thermolysis, yet would not allow diffusion of this molecule out of the bulk sample. A dose of 20 Mrad was used to cure the cellular materials, for both the surfactant and the mixing method. This dose was chosen after a careful analysis of the radiation cure response of the materials used in the study. Industrial applications typically rely on doses on the order of 4-10 Mrad for curing and crosslinking samples; however, a higher dose was chosen to err on the side of a complete cure vs. optimizing energy usage in an industrial process.

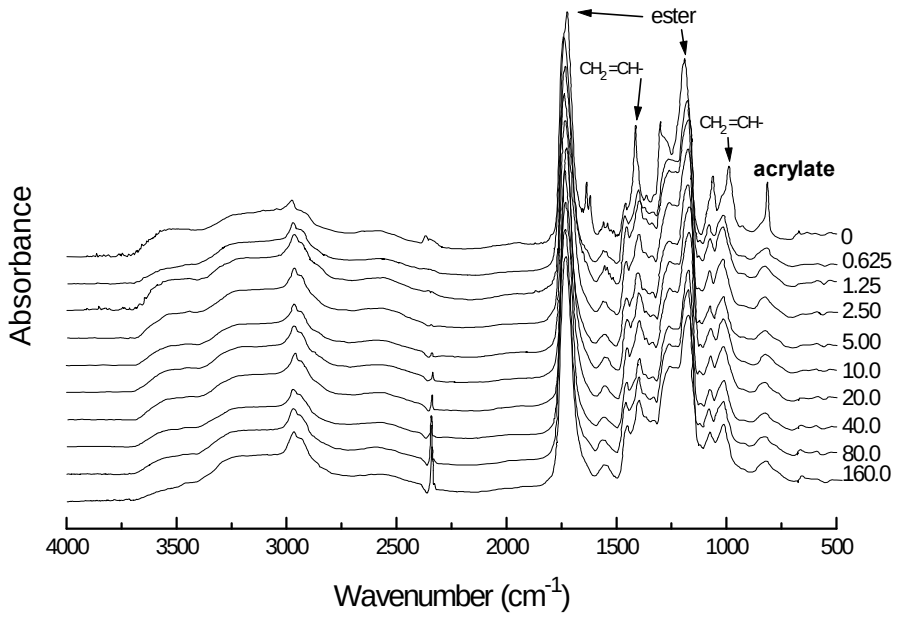

Figure 3-12 β-CEA FTIR scans as a function of dose. Numbers indicate total dose for each sample in Mrad. Plots are normalized on the ester peak at ca. 1750 cm-^{1}.

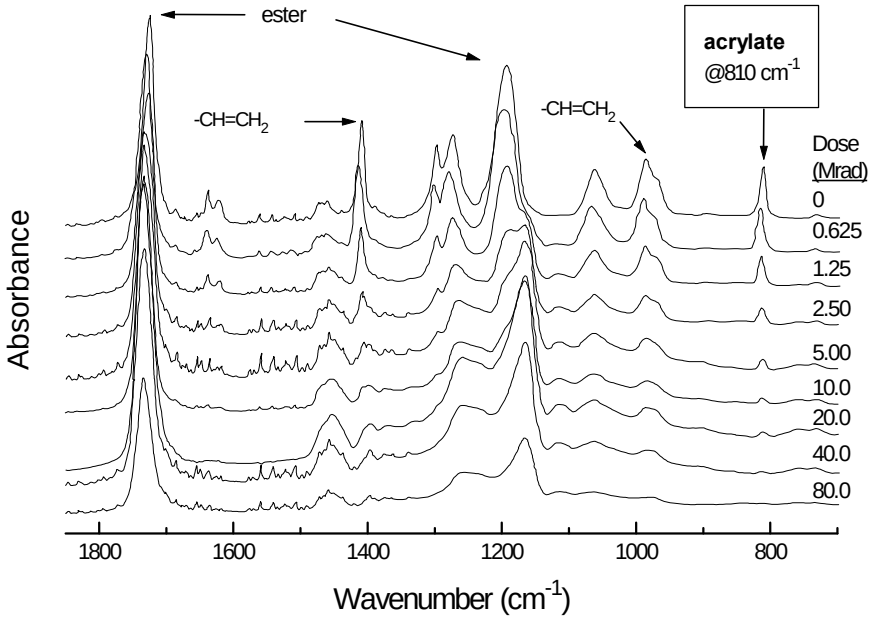

Figure 3-13 FTIR scans for HDODA as a function of dose. . Numbers indicate total dose for each sample in Mrad. Plots are normalized on the ester peak at ca. 1750 cm-^{1}

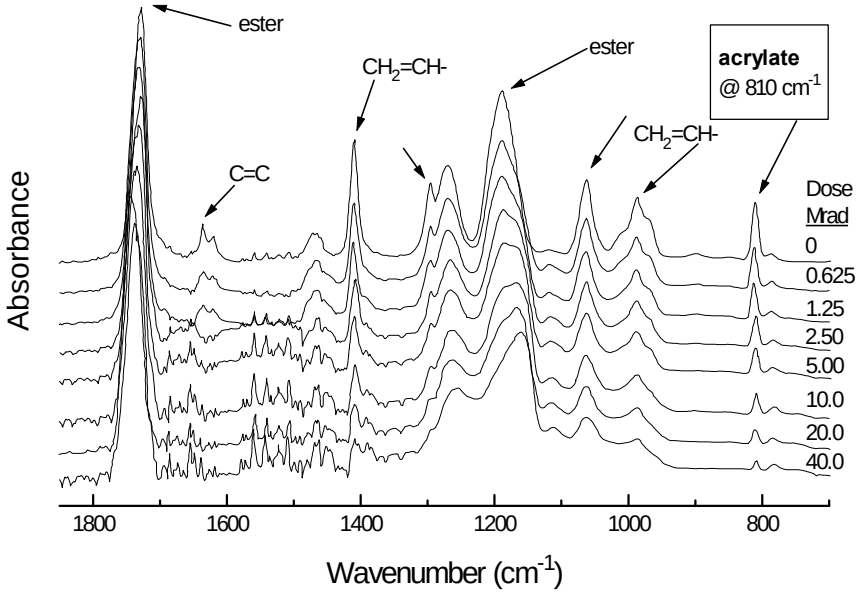

Figure 3-14 FTIR scans for TMPTA as a function of dose. Numbers indicate total dose for each sample in Mrad. Plots are normalized on the ester peak at ca. 1750 cm-^{1}

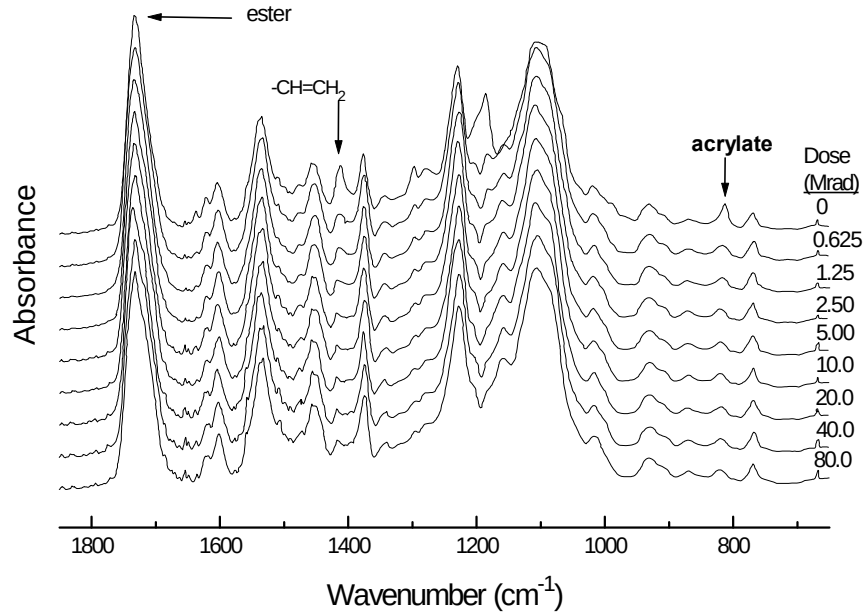

Figure 3-15 FTIR scans for Ebecryl 4827 as a function of dose. Numbers indicate total dose for each sample in Mrad. Plots are normalized on the ester peak at ca. 1750 cm-^{1}

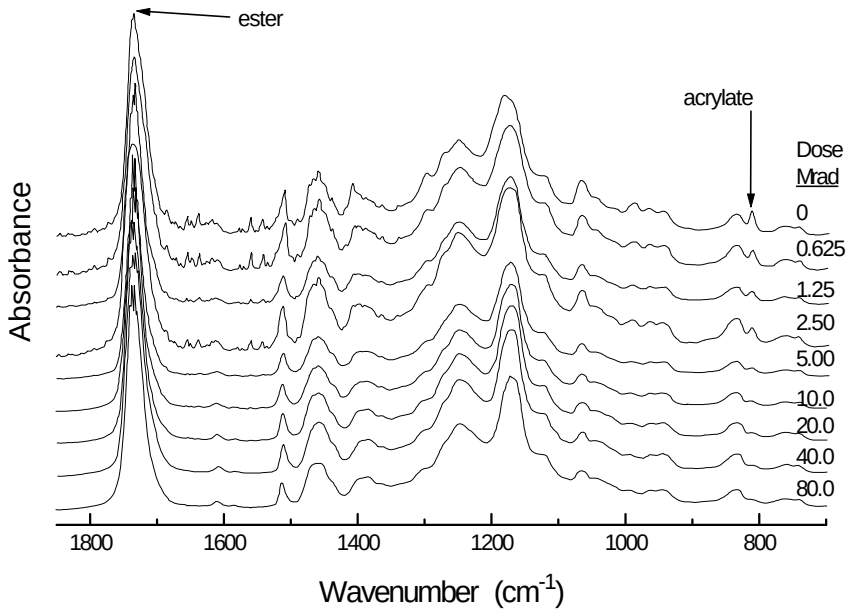

Figure 3-16 FTIR scans for Ebecryl 1701 as a function of dose. Numbers indicate total dose for each sample in Mrad. Plots are normalized on the ester peak at ca. 1750 cm-^{1}

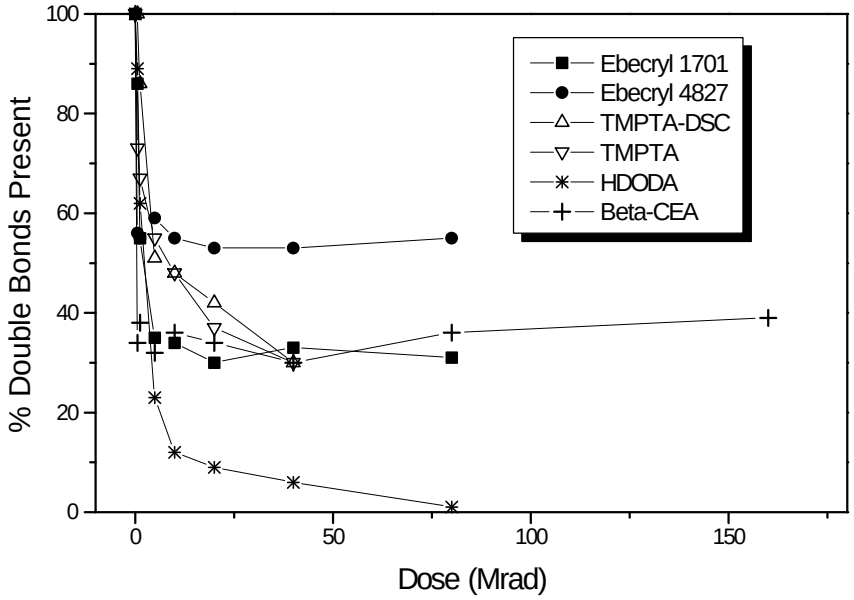

Figure 3-17 Summary of normalized acrylate peak response for all materials also included (for comparative purposes) is the reduction in DSC peak exotherm for TMPTA triacrylate.

3.3.2 Processing Variables

The most important processing variable is the mixture viscosity, which can be controlled by altering mixture composition and, in principal, altering temperature. In this work, temperature is not considered a significant processing variable as excessive heating (to reduce viscosity) can cure the material. However, if one takes the possibility of a thermal cure into consideration, some limited heating would be possible to reduce the system viscosity. In the case where a higher viscosity would be desired, cooling the reactant mixture could also be considered. Figure 3-18-Figure 3-20 show diluent effects on Ebecryl 4827. The most significant feature of these systems is their Newtonian behavior (in the shear rates tested). The tests were performed on a Bohlin CS rheometer using a cone and plate configuration.

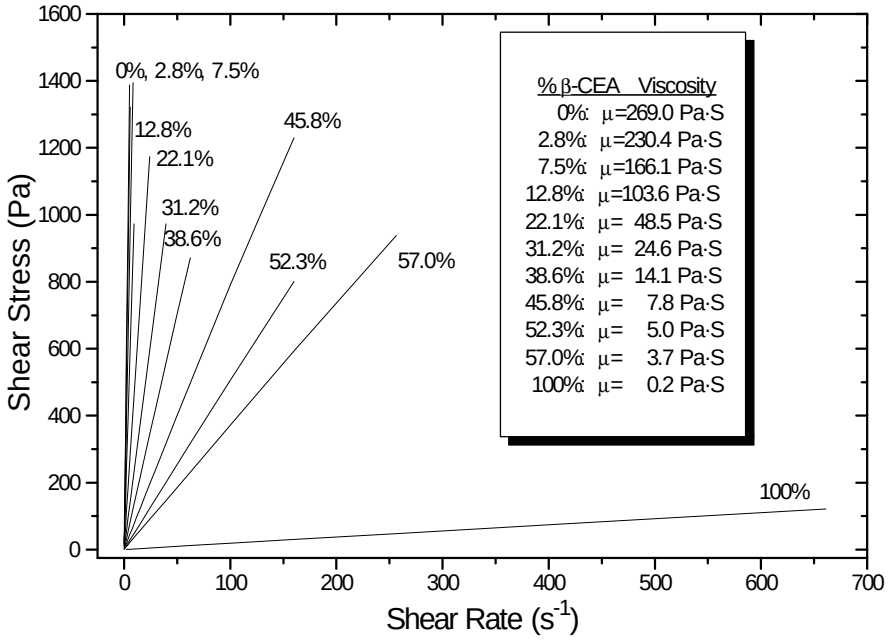

Figure 3-18 Rheology of β-CEA and Ebecryl 4827 blends at 25°C.

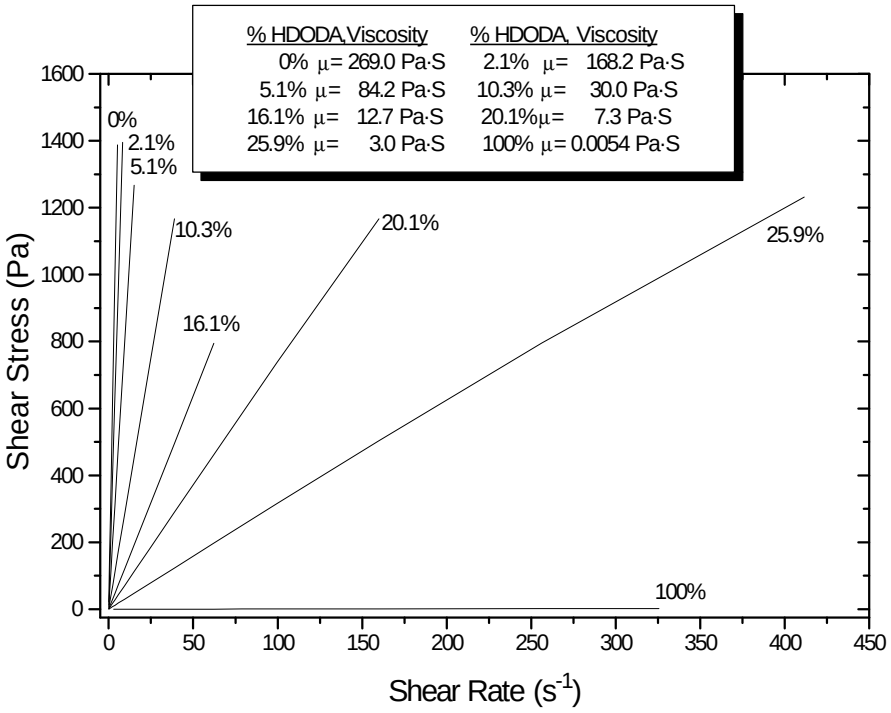

Figure 3-19 Rheology of HDODA and Ebecryl 4827 blends at 25°C.

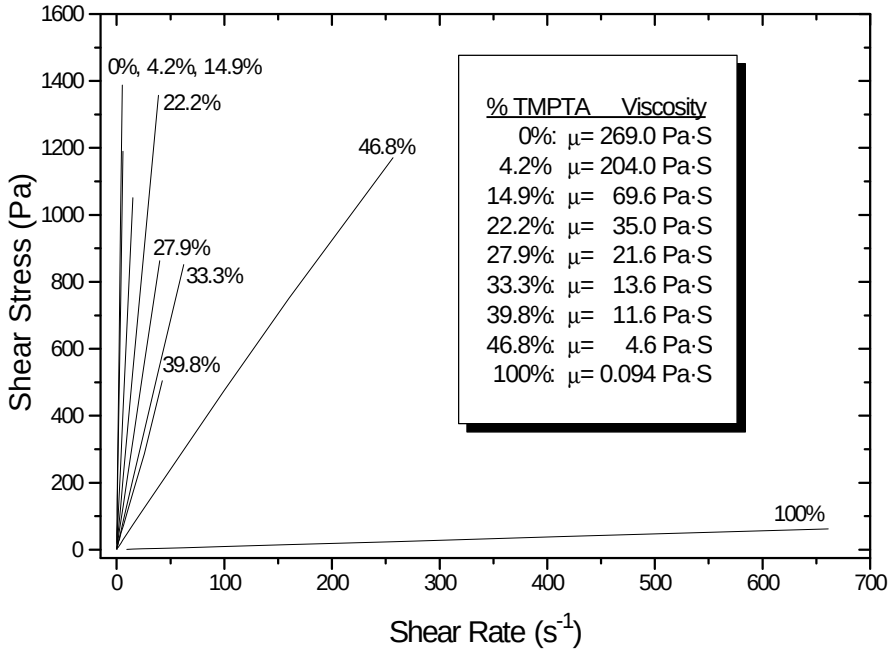

Figure 3-20 Rheology of TMPTA and Ebecryl 4827 blends at 25°C.

Figure 3-21 and Figure 3-22 show diluent effects on the viscosity of Ebecryl 1701 and 4827. One will note deviation from the "straight line" rule of mixtures approach for Ebecryl 1701 and HDODA in Figure 3-18. The rule of mixtures is a simple concept that with respect to a mixture "property" that a blend of substances will have a "property" that is a linear combination of the pure components. However, the exceptions to this are more common than the rule. The rule of mixtures applied to viscosity yields:[249]

$$f(\eta_m)_L = \sum_i x_i f(\eta_i)_L \qquad (3\text{-}2)$$

where: η_m = viscosity of the mixture

η_i = viscosity of the individual component

c_i = volume fraction component *I*

Many modifications of this theory exist. Lobe[250] modified the above equation with an exponential term containing an adjustable parameter. Data from the HDODA and Ebecryl 1701 experiments were fitted to the equation and the results are shown in Figure 3-22. The form of the equation used was:

$$v_m = \sum_{i=1}^{n} \Phi_i v_i \exp\left(\sum_{j=1}^{n} \frac{a_i \Phi_j}{RT} \right)_{j \neq i} \qquad (3\text{-}3)$$

where:

v = kinematic viscosity η/ρ in cSt

Φ_j = volume fraction of component j

a_j = characteristic viscosity parameter for component j in mixture, cal/g·mol·K

R = gas constant = 1.987 cal/g·mol·K

T = temperature, K

All materials tested showed some level of deviation from the rule of mixtures for viscosity, with HDODA showing the strongest deviation and TMPTA and β-CEA showing more mild deviation (see Figure 3-21) in blends with Ebecryl 4827. HDODA was also tested in 14 different compositions with Ebecryl 1701 and showed the same strong deviation from this rule. (see Figure 3-22)

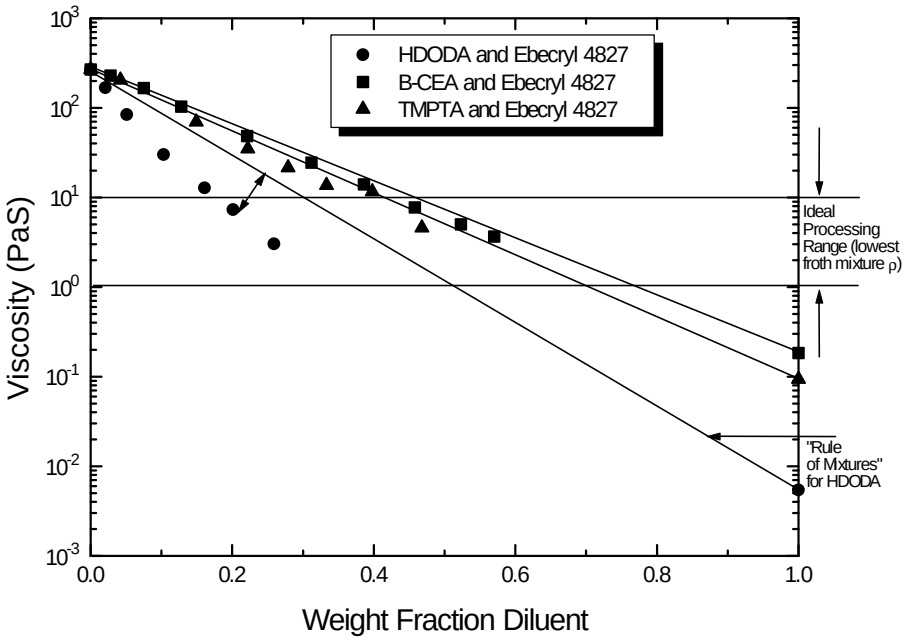

Figure 3-21 Viscosity at 25°C as a function of composition for β-CEA, HDODA and TMPTA monomers with Ebecryl 4827 oligomer. Straight lines are drawn for the rule of mixtures using the viscosities of the pure components for intercepts.

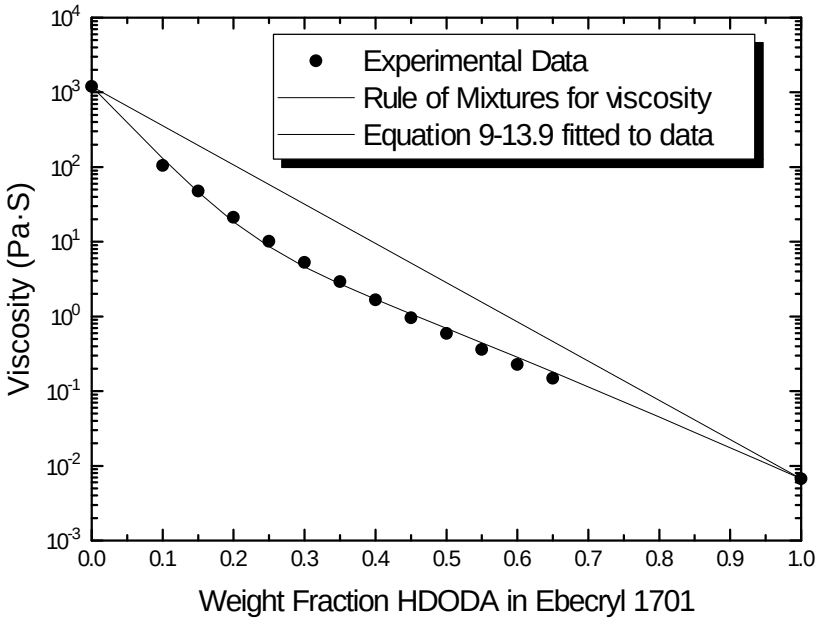

Figure 3-22 Viscosity as a function of diluent concentration for HDODA and Ebecryl 1701 data taken at 25°C..

Additional rheological experiments involving diluting Ebecryl 1701 with acetone to attain the high shear rates necessary for display of shear thinning behavior showed observable non-Newtonian shear thinning behavior at high shear rates. (See Figure 3-23)

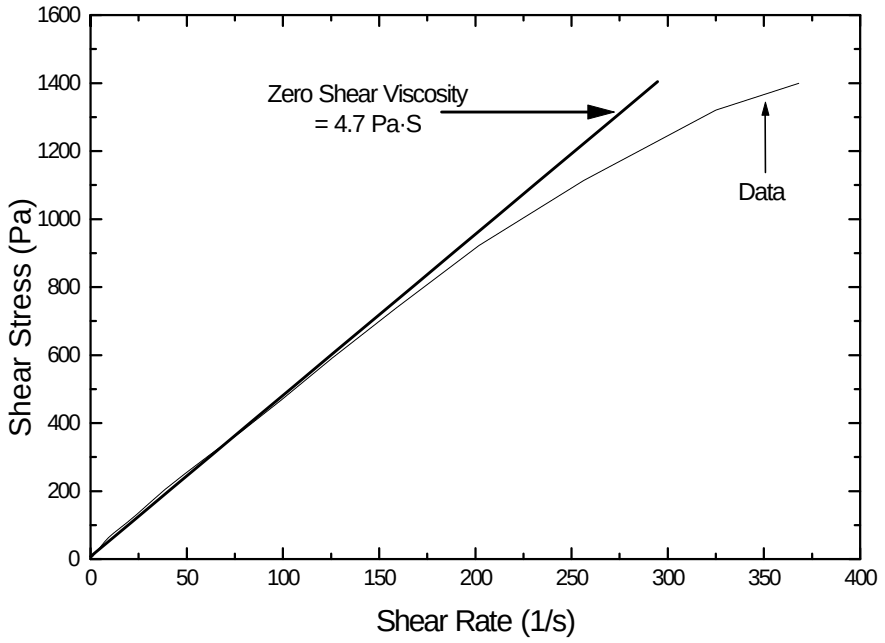

Figure 3-23 Rheology of Ebecryl 1701 with 8.3% acetone as a diluent. Zero-Shear viscosity of the mixture was 4.7 Pa·S. Observe the shear thinning behavior of this system at 400 s^{-1}. Experiment was performed at 25°C.

The consequence of these deviations results in a more difficult process optimization procedure in that prediction of mixture viscosities is more difficult without the full curve. For example, if the desired mixture viscosity for a blend of HDODA and Ebecryl 1701 is 1.0 Pa·S, then based on the straight line approach one would use a composition of approximately 58% HDODA. In reality this composition would give a mixture viscosity of approximately 0.225 Pa·S. This deviation has a dramatic effect on the cellular material generation as will soon be shown.

As discussed in the previous section, the primary method of lowering a mixture viscosity into the appropriate range where processing is possible is by adding a reactive diluent. While viscosity is also a function of temperature, it is important to note that heating these types of monomers and oligomers could result in undesirable reactions from thermally induced

curing. However, slight limited heating could be possible if one is careful to avoid thermal curing. More dramatic heating could be accomplished if one raised the temperature of the froth mixture immediately before irradiation. Raising a mixture viscosity could be accomplished by reducing the amount of reactive diluent or cooling the mixture. Therefore, adding low viscosity diluents to high viscosity oligomers to lower mixture viscosity is the method primarily relied upon to lower mixture viscosity.

Figure 3-24 shows qualitatively the role viscosity plays in the two processes compared in terms of the viscosity ranges over which they effectively operate. The first curve is a qualitative optimization line for the process involving the surfactant and the second line (in the higher viscosity range) is a qualitative optimization line for the process involving mixing a higher viscosity composition. Attempts have been made to lower this processing limit below the 1 Pa·S barrier as it would be desirable to operate the mixing process in a lower viscosity range without the use of a surfactant. It was found that the frothing process utilizing the surfactant had an upper limit of approximately 1 Pa·S where, at which point, it became difficult to generate the froth due to the higher viscosity. As a result the investigation was directed at avoiding this problem by generating the froth by another technique and at the same time eliminating the use of the surfactant. The surfactant did not have any radiation curable functionality, therefore it did not become part of the material after cure and could diffuse out at a later time. It was observed that mechanical mixing would produce a froth, however the mixture was required to be above a certain lower limit of viscosity (also approximately 1 Pa·S) for the mixing technique to work and produce a sufficiently stable froth.

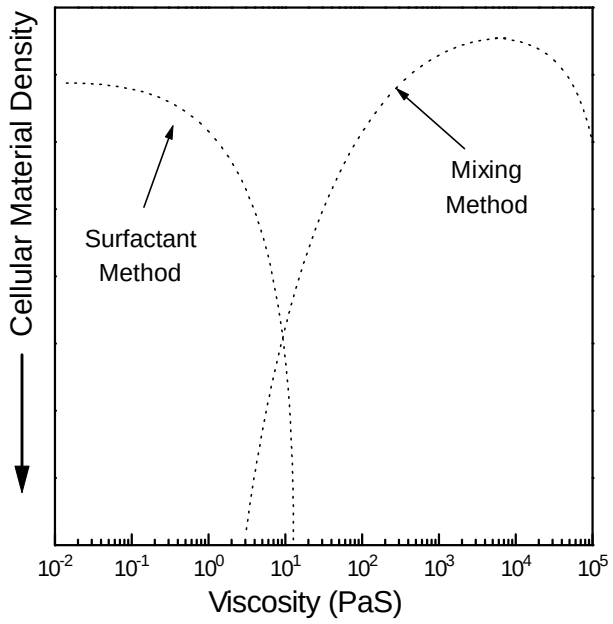

Figure 3-24 Generalized qualitative comparison of the effective processing ranges for the two cellular material generation processes.

While Figure 3-24 shows the effect qualitatively, Figure 3-25 and Figure 3-26 show this effect quantitatively. Figure 3-25 shows froth collapse time data as a function of mixture viscosity. The collapse time increases dramatically with small increases in mixture viscosity and while one might initially assume that this is a desirable effect, Figure 3-26 shows mixture density as a function of viscosity with a minimum in the range of 1 to 10 Pa S. Coupling Figure 3-25 and Figure 3-26 results in a quantitative version of the right half (for the mixing technique) of Figure 3-24.

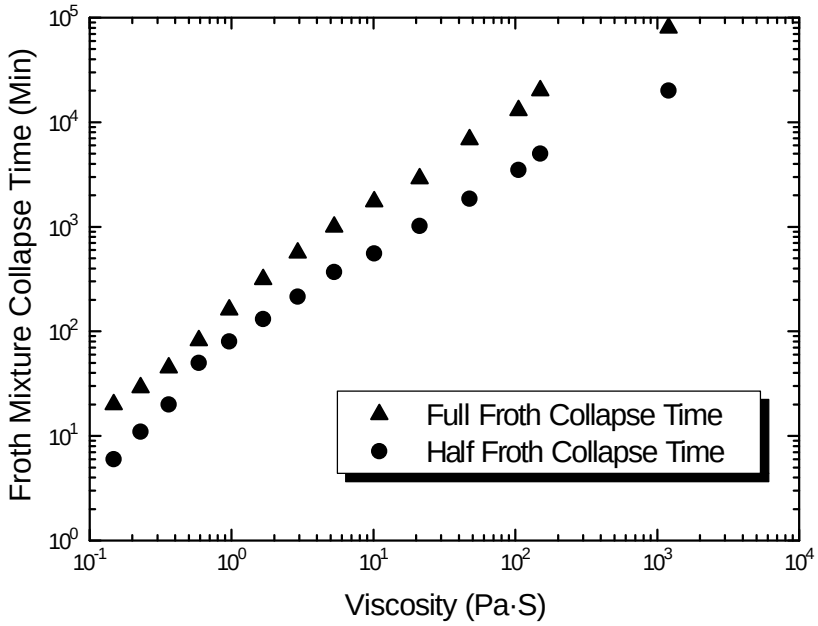

Figure 3-25 Collapse time in minutes as a function of mixture viscosity. Data for the system HDODA and Ebecryl 1701. In the case of shear thinning behavior, viscosities shown are the 0 shear viscosities. Collapse time experiment was performed at 25°C.

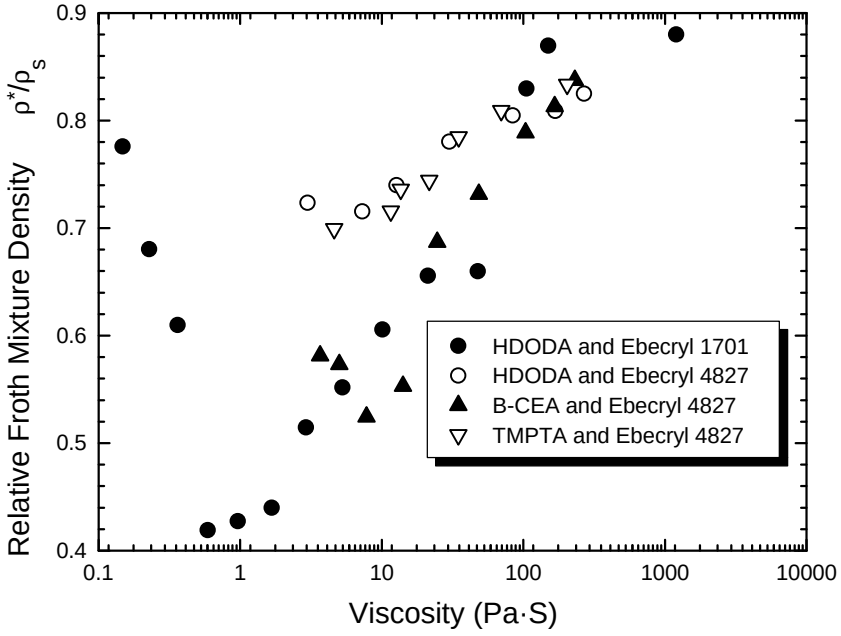

Figure 3-26 Relative mixture density as a function of mixture viscosity for the compositions tested.

If one only considered collapse time as a process optimization variable, then one would assume that a higher viscosity is better in all cases. However as shown in Figure 3-26, the mixture density clearly goes through a minimum value in the range of 1 to 10 Pa S As implied in Figure 3-25, below ca. 1 Pa-S, there is a tremendous reduction in the amount of time one has to cure the material before it collapses utilizing the mixing method. This may be confirmed by observing the collapse time data in Figure 3-25. At this point, a surfactant must be utilized to support the froth until it can be cured in the electron beam radiation source. However, one could also increase the line speed, for example, and decrease the time from froth extrusion until irradiation in the electron beam. As shown in Figure 3-26 the mixture density starts to increase in this same range of 1 Pa S. At higher viscosities (and collapse times), the power of the mixer becomes the limiting factor in generating a low density froth. Although no comparisons among different power mixers were made, at these higher viscosities (100 Pa S and higher) much torque is required of the motor to even stir the mixture. Much lower revolutions are the result of this strain which leads to less entrained air and a higher froth density.

While froth mixture density appears to be the most logical or convenient method for calculating the density of the final product, due to shrinkage and skin affects on these materials, densities were recalculated using a standard weight of a sample divided by it's volume. A micrometer was used to measure 5 samples cut from a standard die and the results are shown in Figure 3-27. Figure 3-27 shows densities of a sampling of E-Beam generated cellular materials produced by the mixing technique and the surfactant technique along with some commercially available foams. Relative density is defined as the density of the cellular material divided by the density of the respective solid.

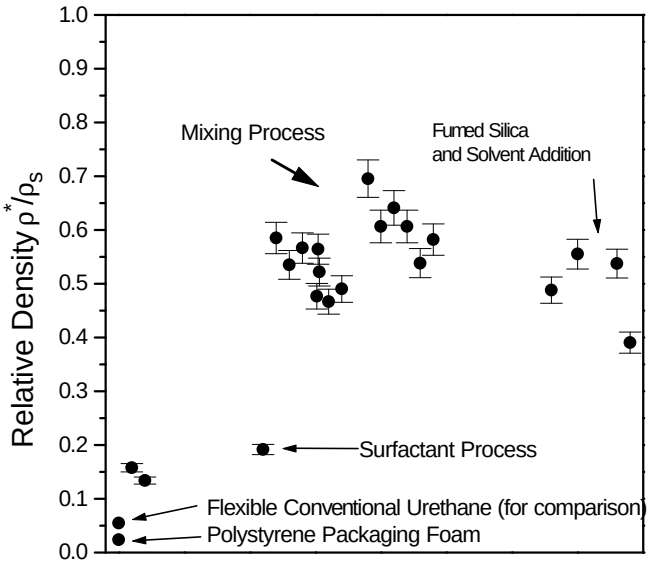

Figure 3-27 Density data for different samples determined by measuring the weight of the final product and dividing by the volume.

It is interesting to note that although these cellular materials are higher in relative density than either the conventional flexible urethane form or polystyrene packaging foams shown in the graph, they appear at least to have densities for closed cell materials that are in the range of what might be thought of as a "theoretical minimum". That is, if one assumes that the cells formed are spherical in nature and treats the density as a packing factor for spheres, appreciation is gained for these materials. For example, the packing factor for random loose spheres is 0.601, which would correlate to a relative density of 0.399. Hexagonal close packing gives a packing factor of 0.7405, or a relative density of 0.2595. To be fair, the cells in these materials are not discrete and many are connected which would give one a lower density as material is not making up the cell wall, however the overall cellular material morphology is one of closed, spherical cells.

3.3.3 SEM

This section is dedicated to showing the microscopic features that exist in the materials generated by the two processes. To familiarize the reader with some of the general microscopic features of cellular materials, scanning electron microscopy on some of the more common materials was performed. First in Figure 3-28, a classic closed cell foam is shown, in this case a common polystyrene "peanut" used in packaging applications. Observe that very little material is utilized in forming the struts and cells resulting in an extremely low relative density. In Figure 3-29, the open cell structure of a slabstock urethane foam is shown, typical of what is used in seating applications. Open cell materials are also used for shipping applications. In Figure 3-30, a foam made from water soluble corn starch is shown. This foam has a higher density (about double) than both the styrene and the urethane foam but has the advantage of being more environmentally friendly from a disposal standpoint.

The next series of figures show the type of cellular structure that is generated by the mixing technique. The cells tend to be closed cell in nature and range from 0.02 to 0.1 mm in size. These materials can be flexible due to the low cure Tg oligomers that can be used in their production. Relative density ranges for these cellular materials are in the range of 0.38 to 0.70. Relative density is defined as the density of the cellular material divided by the density of the solid material. Figure 3-35 shows a cellular material generated by the technique involving the surfactant. This process produces a rigid, open cell material with relative densities in the range of 0.2. The cells in this material are much larger than obtained from the mechanical mixing process, tending to range from 0.3 to 2 mm in size. There is also much lower uniformity in the cell sizes for these materials. For this process to work, low viscosity materials (low molecular weight) are required which typically cure

to form high Tg systems (e.g. low molecular weight diacrylates and triacrylates). Therefore, these materials tend to be rigid and would therefore be more useful in structural applications. The reactive materials that do have the low cured Tg (the oligomers) have viscosities that are too high to be used in this process because it impossible to bubble and froth such a mixture. As mentioned previously, heating the mixture might be possible to lower the viscosity provided the heating process did not thermally cure the mixture prematurely.

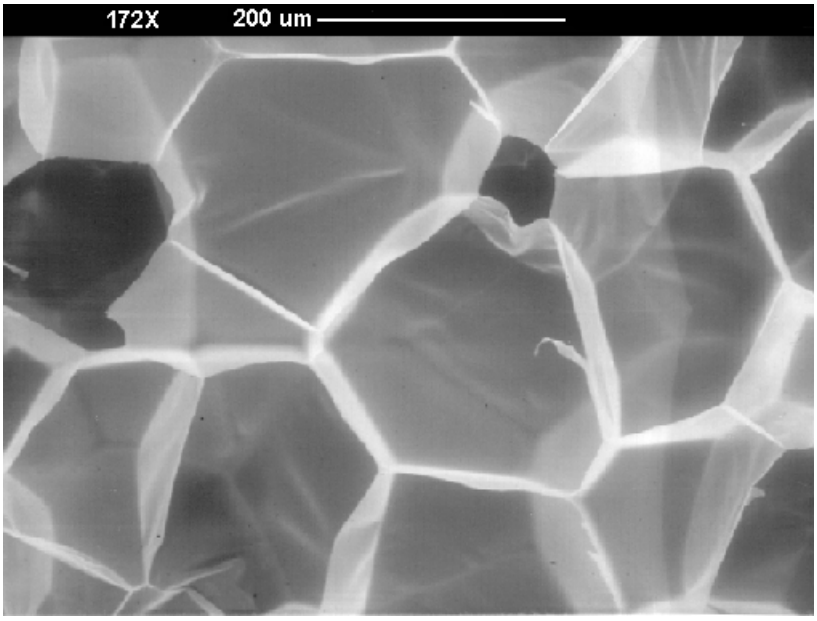

Figure 3-28 SEM of polystyrene packaging foam.

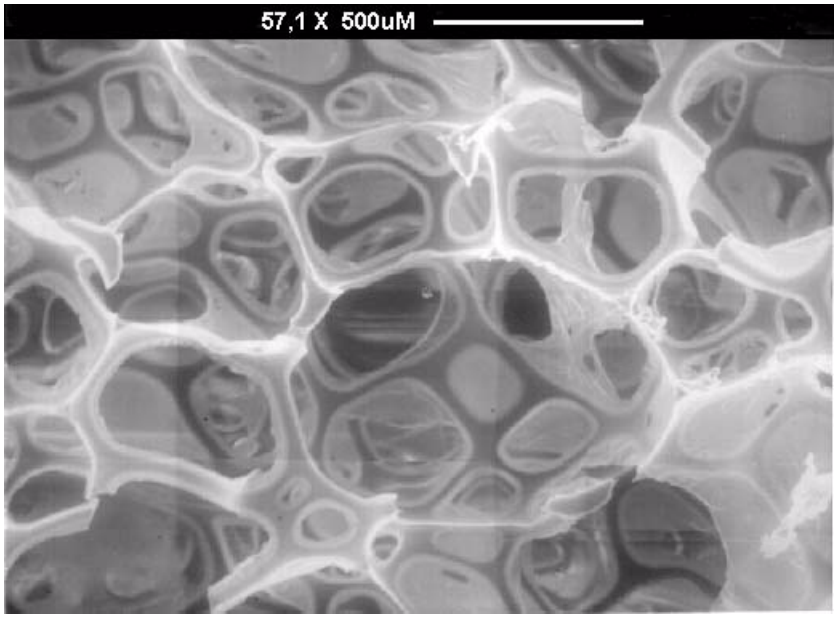

Figure 3-29 SEM of a slabstock urethane foam.

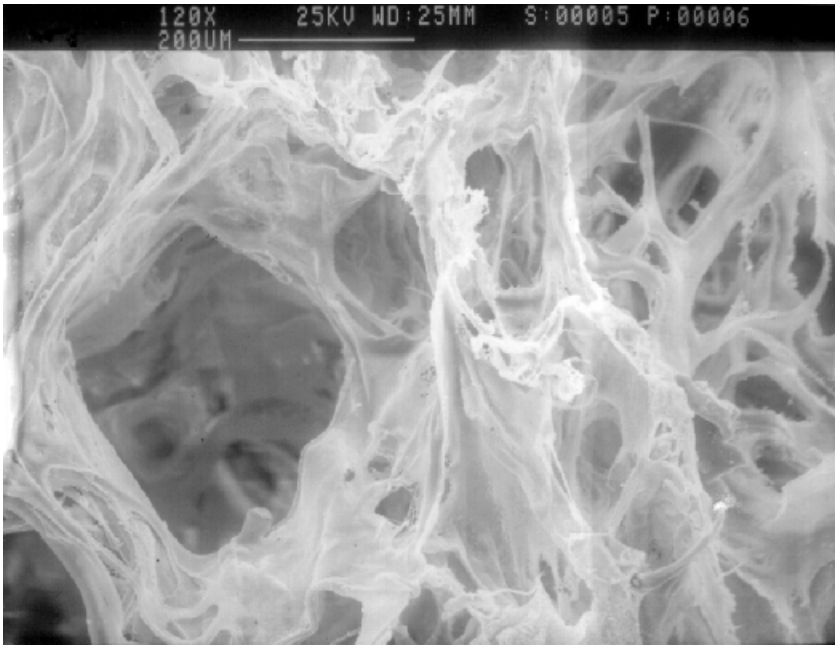

Figure 3-30 SEM of water soluble starch packaging foam.

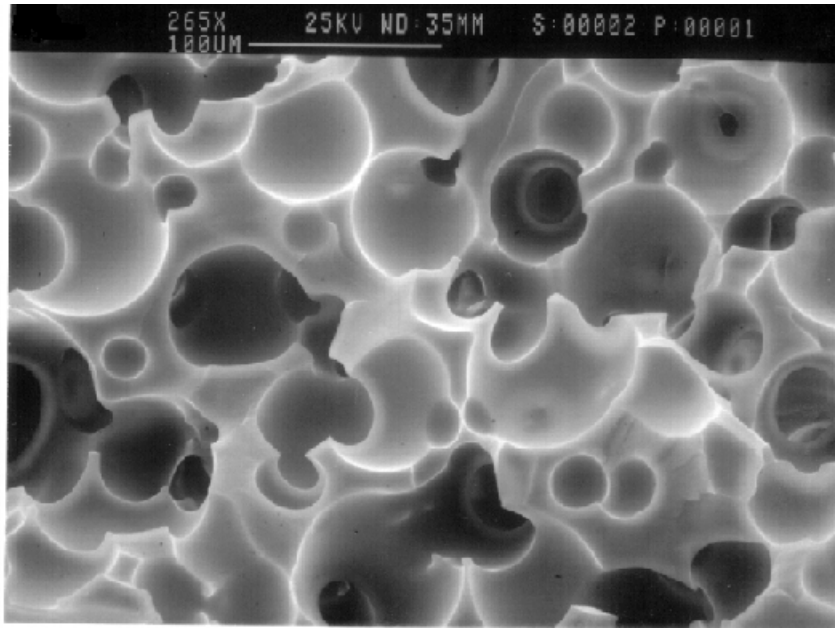

Figure 3-31 SEM of a blend of 75% Ebecryl 4827 and 25% β-CEA. System was mixed and then cured as described in figure 2. Scale = 0.1mm.

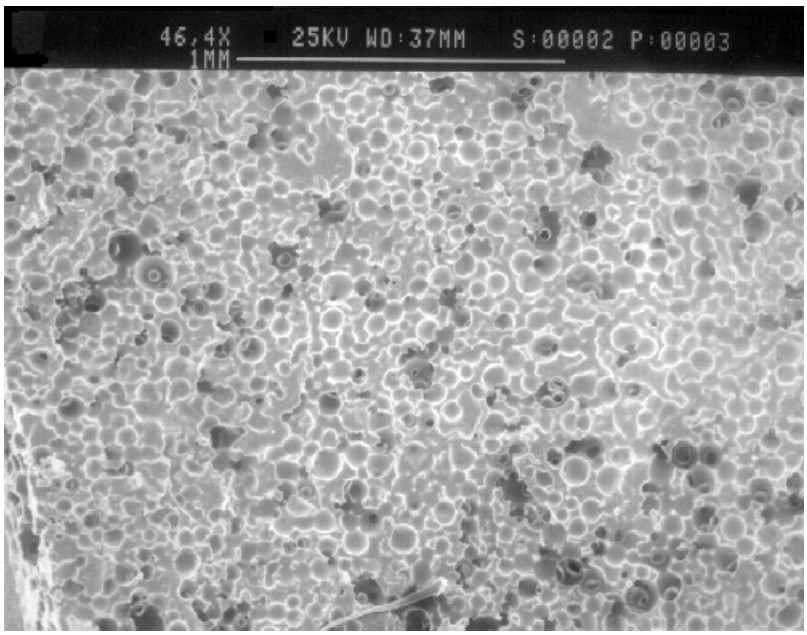

Figure 3-32 SEM of same material as in Figure 3-33. Scale = 1mm.

Figure 3-33 SEM of cellular material produced by the mixing technique showing edge view perspective.

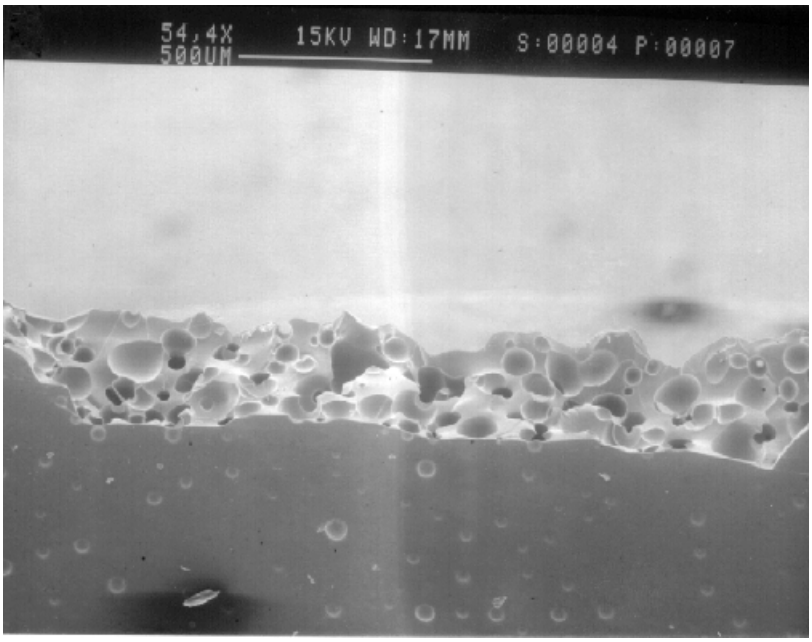

Figure 3-34 SEM of cellular material produced by the mixing technique showing edge view perspective.

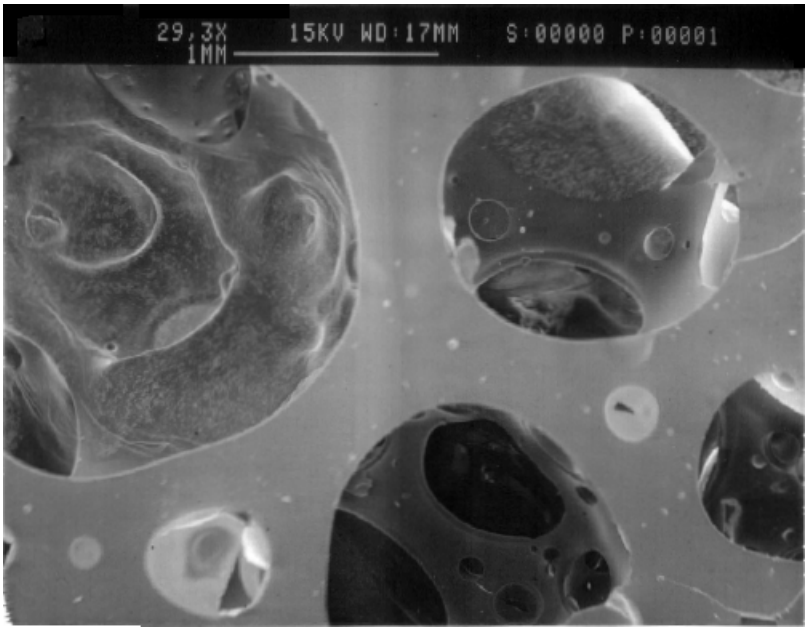

Figure 3-35 SEM of material produced using 3% Fluorad FC-430 fluorochemical surfactant and 97% TMPTA.

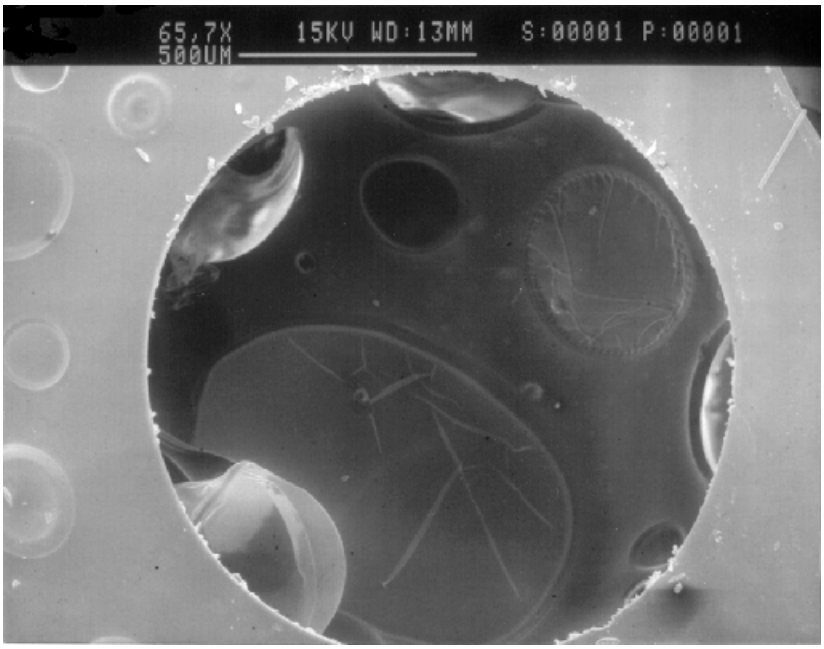

Figure 3-36 SEM of material produced using 3% Fluorad FC-430 fluorochemical surfactant and 97% TMPTA showing higher magnification.

The next series of micrographs display an unusual phenomena that was observed in several early experiments. For some samples, a wavy surface phenomena was observed in and around the cells in the center of the materials. Causes such as phase separation were ruled out as this phenomena was also observed in pure oligomers. After ruling out phase separation, it was thought that it might be related to the curing process. At this point in the research, no curing optimization experiments had been performed, so an optimum dose had not been established for this process. At this point, only a 10 Mrad (per side) dose was being used, so experiments were performed on a series of materials, using curing doses of 10, 20, and 30 Mrad (per side). It was hoped that this series of experiments could not only help understand the phenomena, but serve as a basis for the beginnings of a series of cure optimization experiments. Figure 3-43 through Figure 3-46 show the unusual structures seen in these materials and the results of these experiments. These materials were cured with a dose of 10 Mrad per side. Figure 3-47 through Figure 3-49 show the results of increasing the dose to 20 and 30 Mrad per side, the phenomena disappeared. After performing these experiments, a dose of 20 Mrad/side was used for all cellular materials. It should be noted that 20 Mrad is a particularly high dose, even for these materials as to what would be used in industry. It was desired to produce the thickest material possible to eliminate any skin/core gradient effects in the mechanical property experiments, so to compensate for the limited depth dose profile in our electron beam (4 mils) a higher dose was used than what might be used for thinner materials. As one can see from the FTIR section, no major chemical changes occur in these materials from 2 Mrad through 40 Mrad, so assurance of not altering chemical structure beyond simple curing was assured.

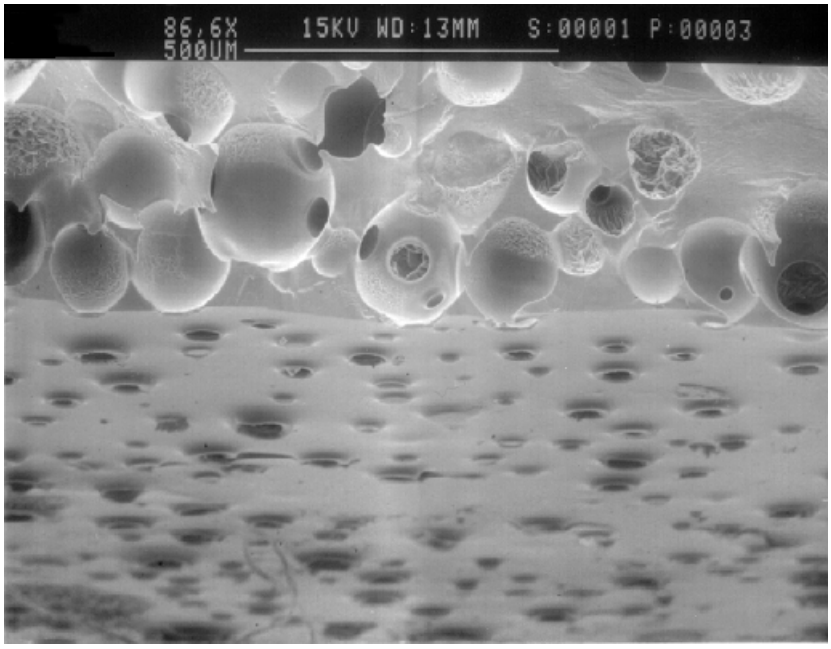

Figure 3-37 SEM of cellular material produced by the mixing method. Composition is 50% β-CEA and 50% Ebecryl 4827. Dose was 10 Mrad/side.

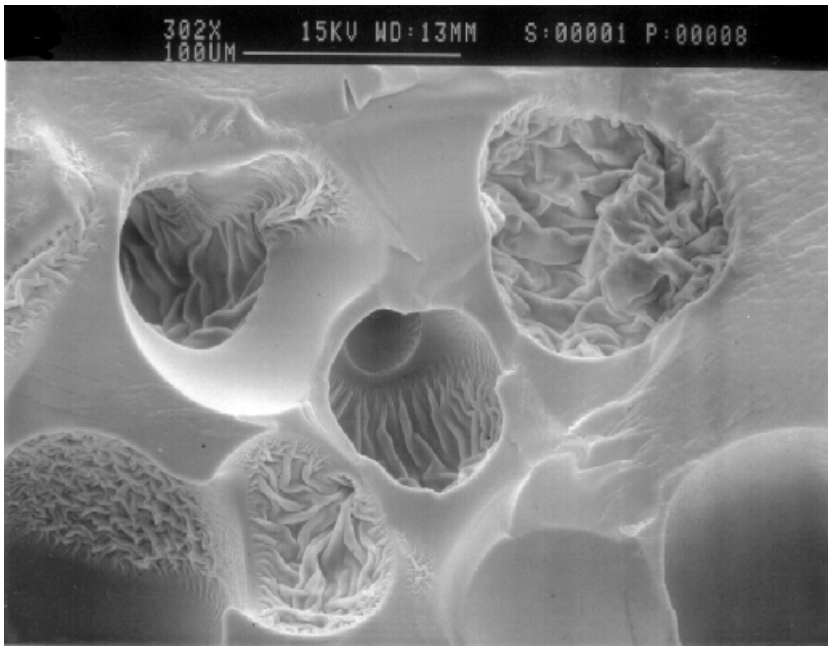

Figure 3-38 SEM of cellular material produced by the mixing method. Composition is 50% β-CEA and 50% Ebecryl 4827. Dose was 10 Mrad/side.

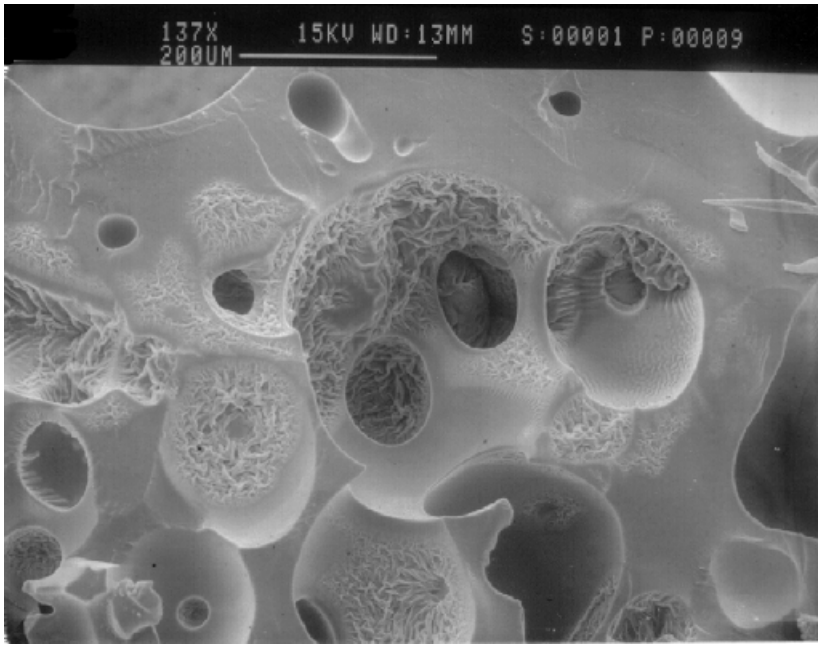

Figure 3-39 SEM of cellular material produced by the mixing method. Composition is 50% β-CEA and 50% Ebecryl 4827. Dose was 10 Mrad/side.

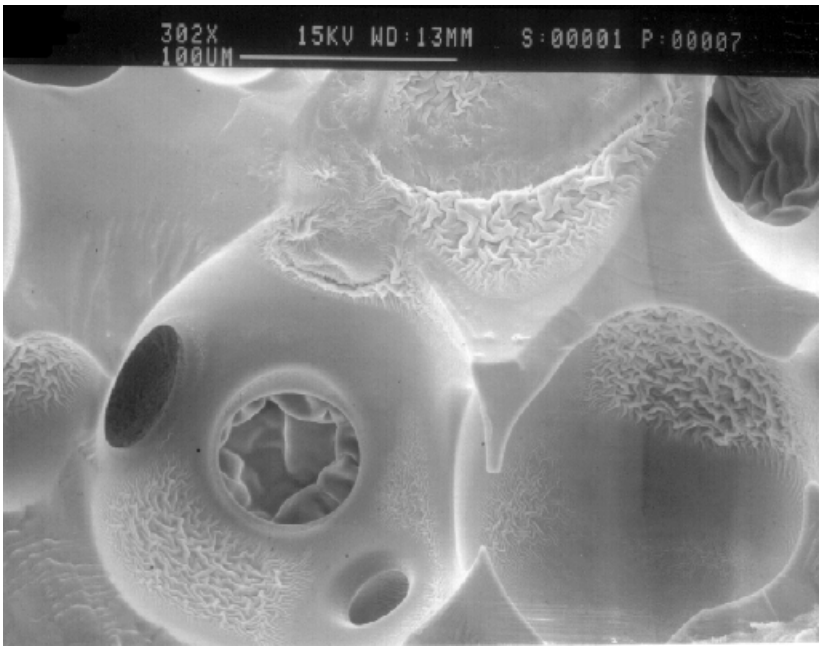

Figure 3-40 SEM of cellular material produced by the mixing method. Composition is 50% β-CEA and 50% Ebecryl 4827. Dose was 10 Mrad/side.

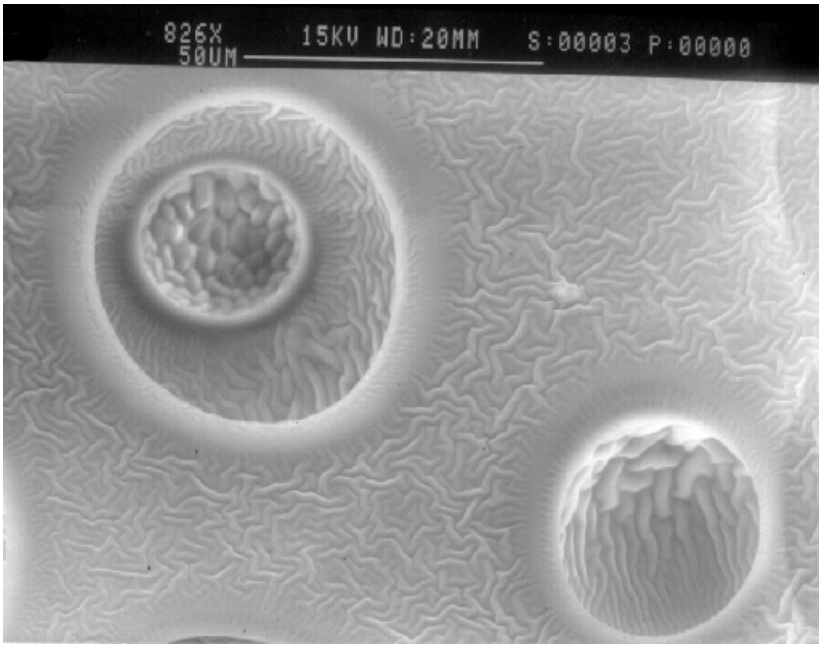

Figure 3-41 SEM of cellular material produced by the mixing method. Composition is 100% oligomer. Dose was 10 Mrad/side.

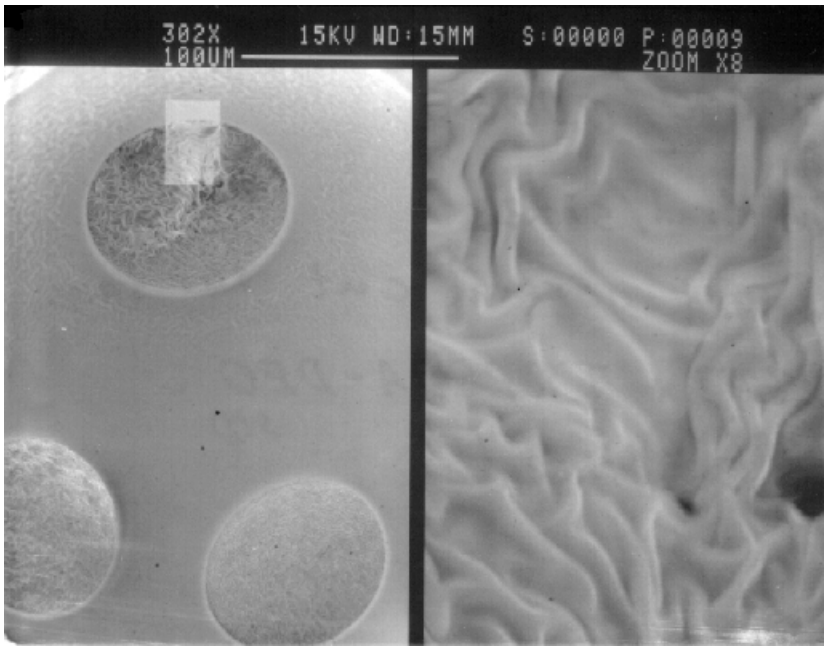

Figure 3-42 SEM of cellular material produced by the mixing method. Composition is 50% β-CEA and 50% Ebecryl 4827. Dose was 10 Mrad/side.

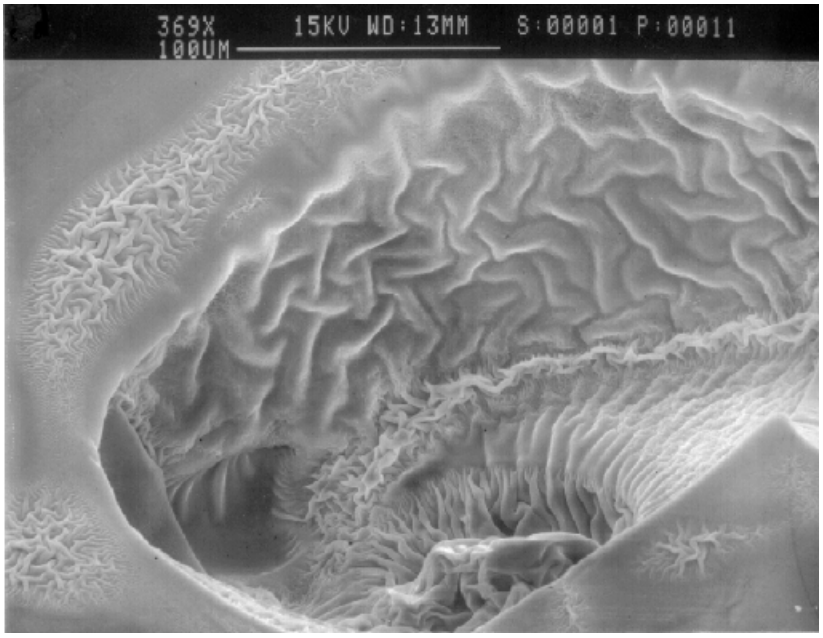

Figure 3-43 SEM of cellular material produced by the mixing method. Composition is 50% β-CEA and 50% Ebecryl 4827. Dose was 10 Mrad/side.

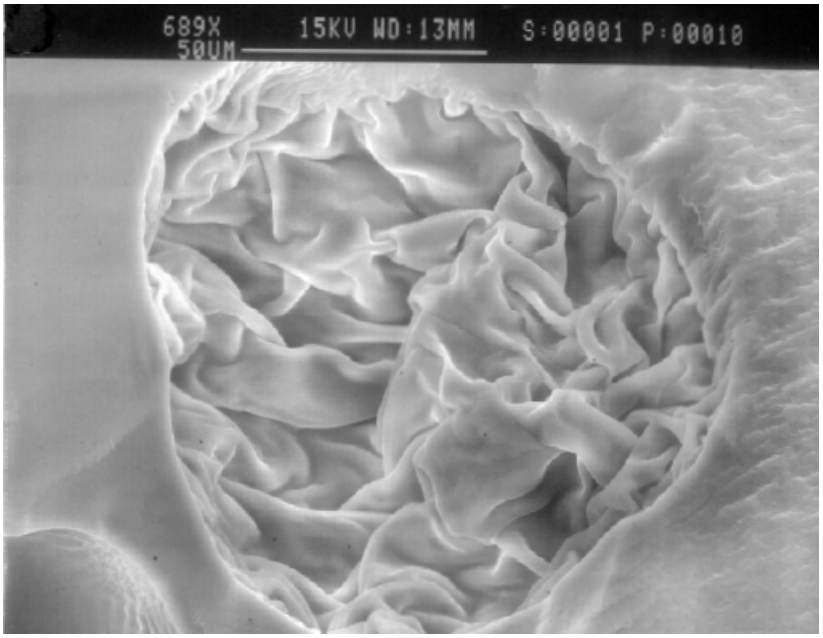

Figure 3-44 SEM of cellular material produced by the mixing method. Composition is 50% β-CEA and 50% Ebecryl 4827. Dose was 10 Mrad/side.

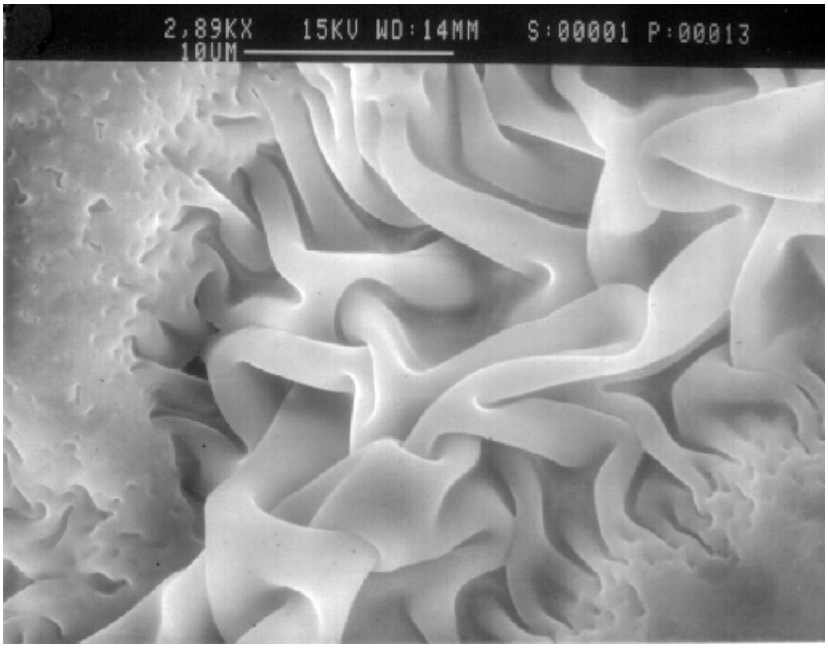

Figure 3-45 SEM of cellular material produced by the mixing method. Composition is 50% β-CEA and 50% Ebecryl 4827. Dose was 10 Mrad/side.

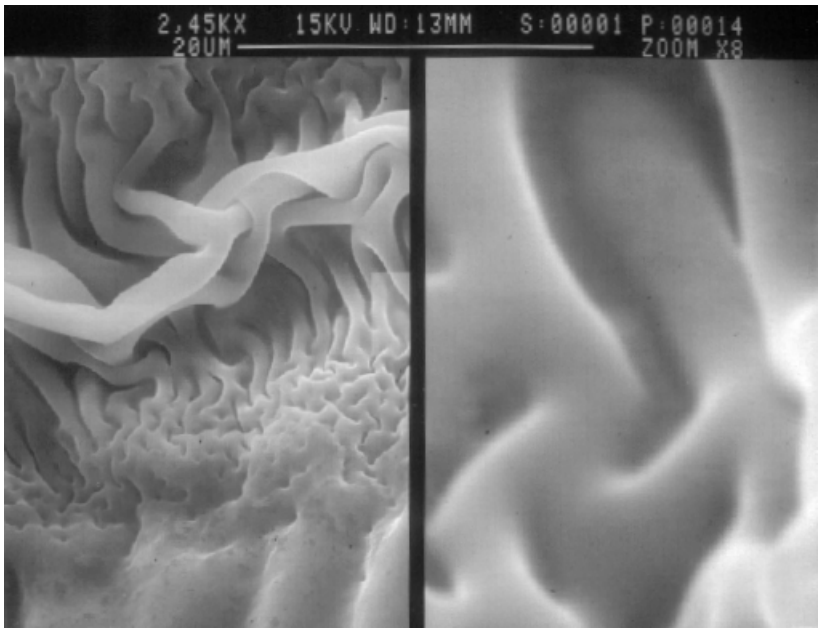

Figure 3-46 SEM of cellular material produced by the mixing method. Composition is 50% β-CEA and 50% Ebecryl 4827. Dose was 10 Mrad/side.

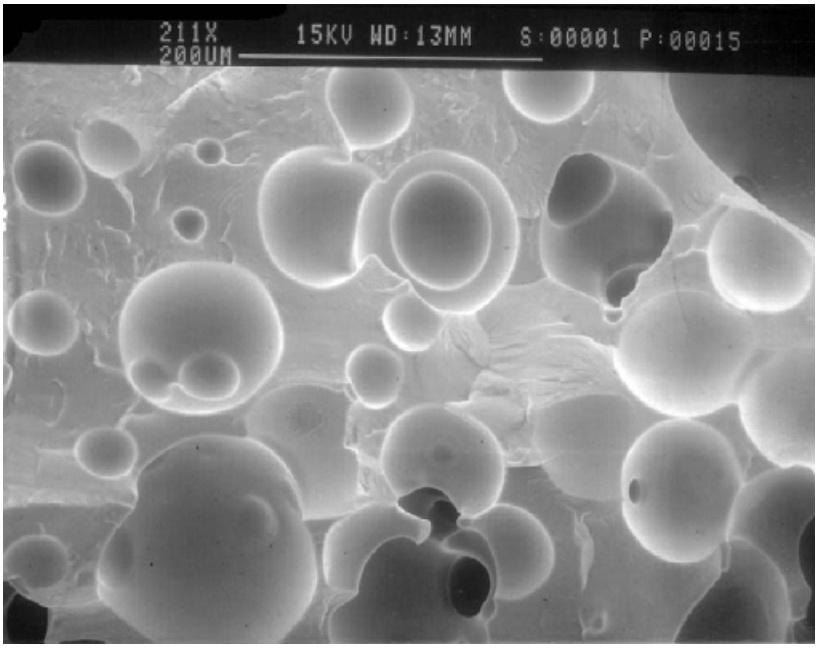

Figure 3-47 SEM of cellular material produced by the mixing method. Composition is 50% β-CEA and 50% Ebecryl 4827. Dose was 20 Mrad/side.

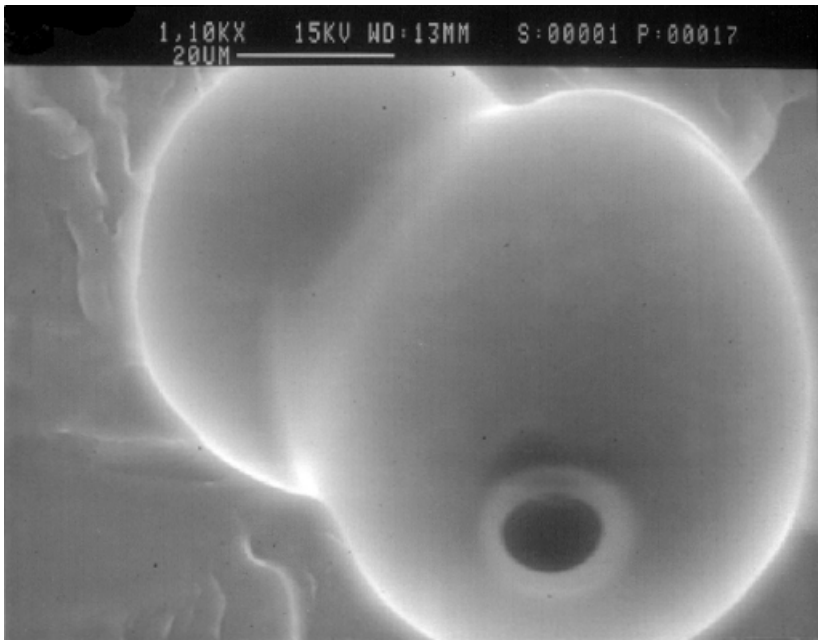

Figure 3-48 SEM of cellular material produced by the mixing method. Composition is 50% β-CEA and 50% Ebecryl 4827. Dose was 20 Mrad/side.

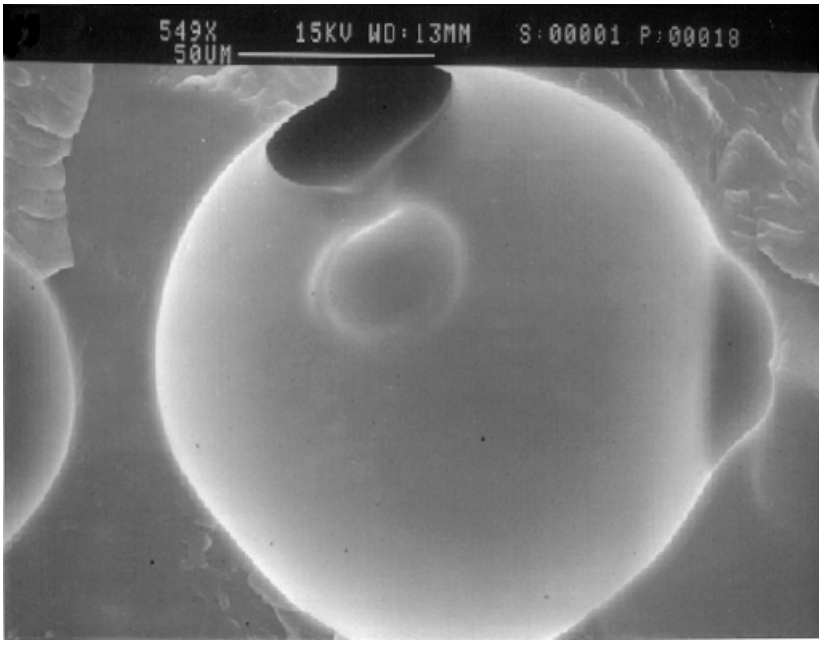

Figure 3-49 SEM of cellular material produced by the mixing method. Composition is 50% β-CEA and 50% Ebecryl 4827. Dose was 30 Mrad/side.

3.3.4 Mechanical Properties

To illustrate the ability to tailor the modulus of the cellular material by increasing the content of a reactive diluent group, a systematic series of experiments were carried out. Ebecryl 4827 oligomer was selected for blending monoacrylate (β-CEA), diacrylate (HDODA), and triacrylate (TMPTA) and measuring tensile modulus as a function of monomer concentration. Both films and cellular materials were produced at each selected composition for comparison with theories which correlate these properties with density. Figure 3-50 through Figure 3-63 show the results of these experiments. Depending on the chemistry of the diluent, very different changes in the tensile modulus of these materials result. Figure 3-50 through Figure 3-52 illustrate the ability to systematically modify tensile modulus by the addition of a reactive diluent. In these figures the modulus displayed is the actual tensile modulus of the material as measured. Normalization on relative density will be dealt with next.

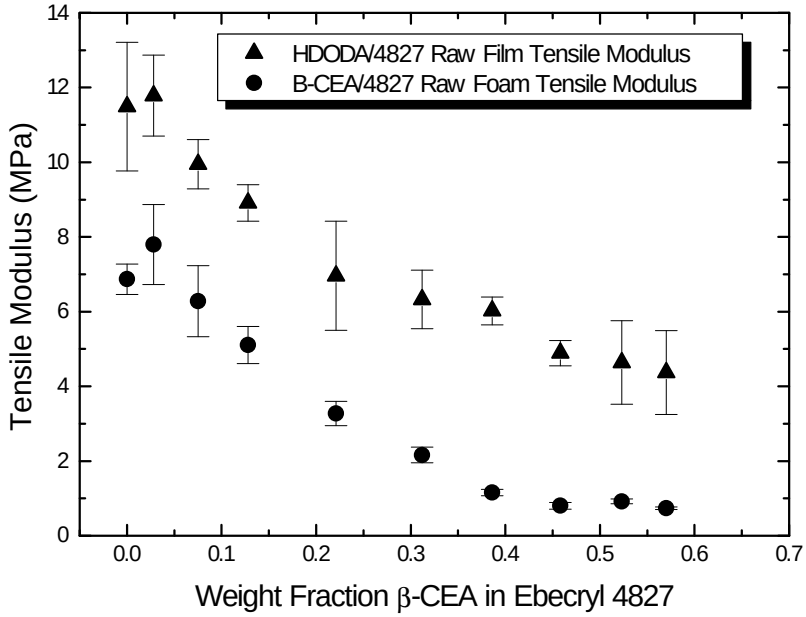

Figure 3-50 Film and cellular material tensile modulus as a function of weight fraction β-CEA.

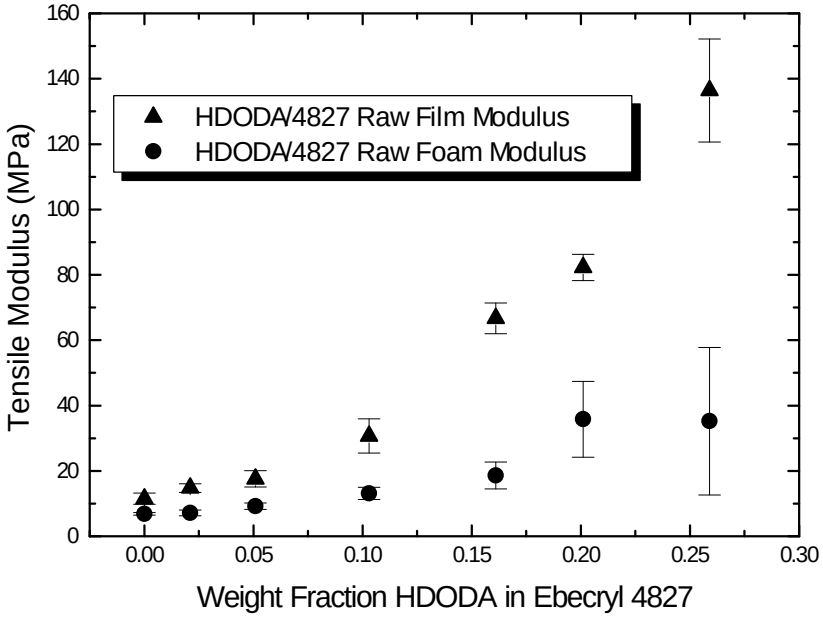

Figure 3-51 Film and cellular material tensile modulus as a function of weight fraction HDODA in the blend.

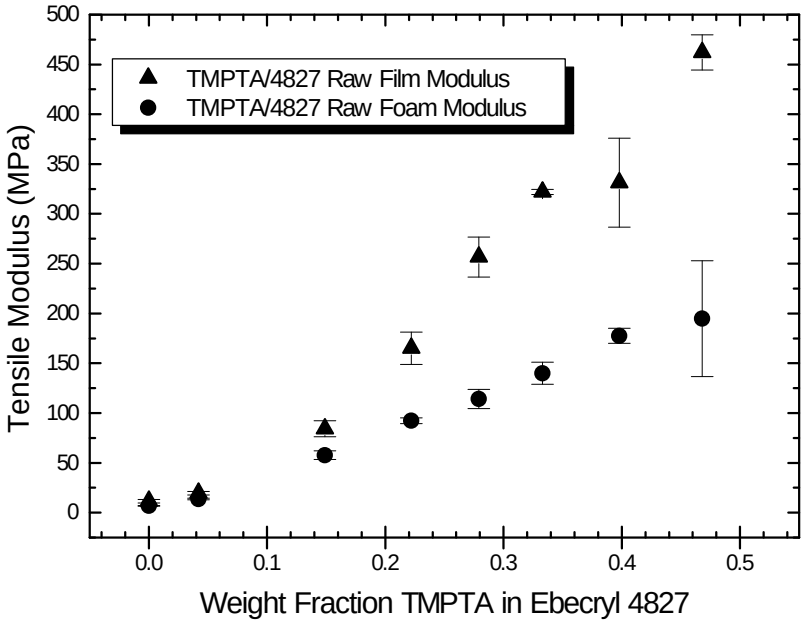

Figure 3-52 Film and cellular material tensile modulus as a function of weight fraction TMPTA in the blend.

The next series of figures show stress and strain at break for the same series of experiments as the previous three figures. For a material in which the modulus increases as a function of decreasing molecular weight between cross-links, one would expect the stress at break to increase with increasing modulus and the strain at break to decrease with increasing modulus. In the series of experiments involving β–CEA monoacrylate, the tensile modulus decreased with increasing β–CEA content. For this series, the stress and strain at break showed the opposite trend (within experimental error) as would be expected. It is believed that β–CEA reacts with the ends of Ebecryl 4827 oligomer preventing oligomer endlinking, which would reduce the molecular weight between crosslinks and produce a looser network. Because β–CEA has a functionality of two, at best it can only form linear species (assuming no other cross-linking reactions take place other than via the acrylate group). This reduces the chances of linking up unreacted oligomer

acrylate endgroups with the network and basically leaves network defects. This must be taken into account in optimizing the process as increasing β–CEA content lowers the cellular material density but at the same time lowers the tensile modulus and decreases the stress at break.

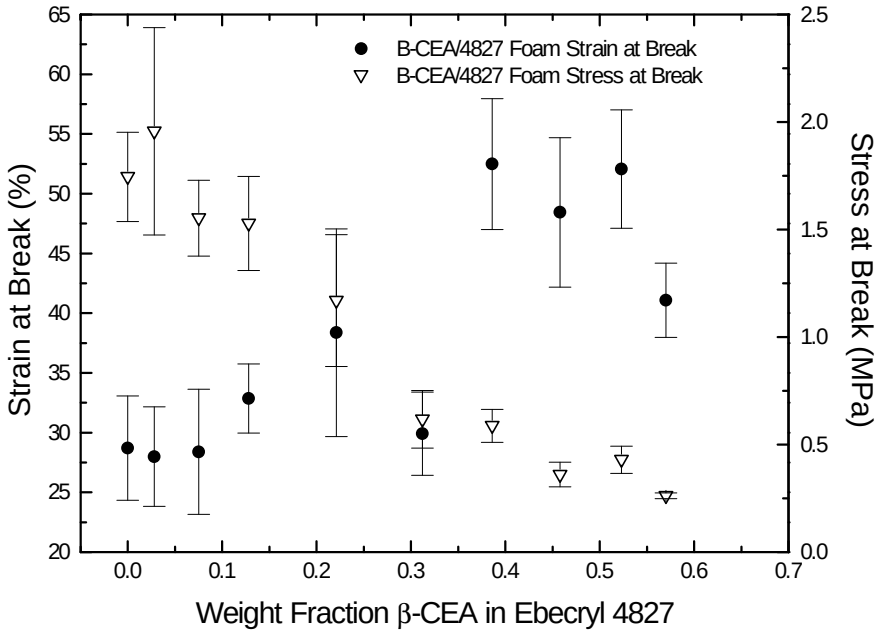

Figure 3-53 β-CEA and Ebecryl 4827 cellular material blend stress and strain at break.

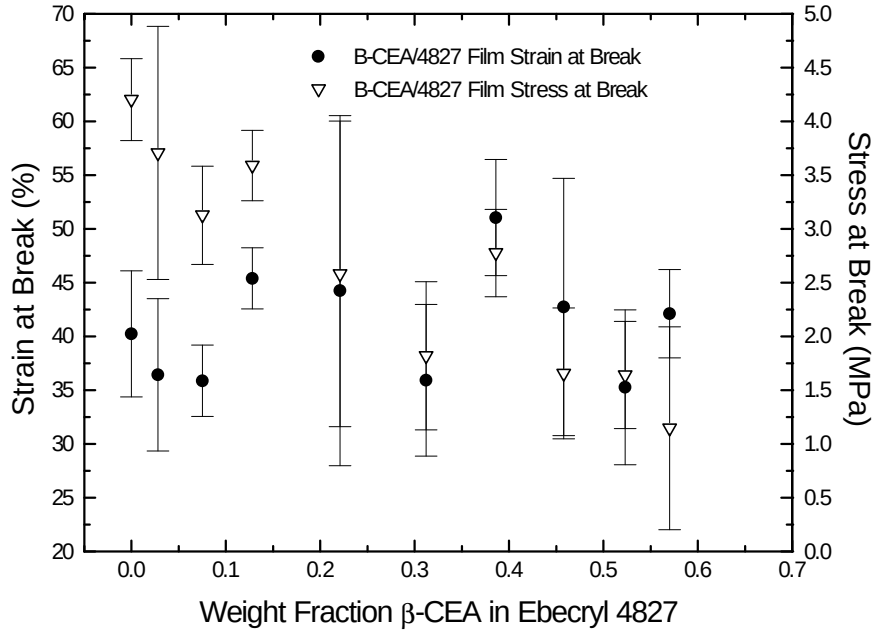

Figure 3-54 β-CEA and Ebecryl 4827 film material blend stress and strain at break.

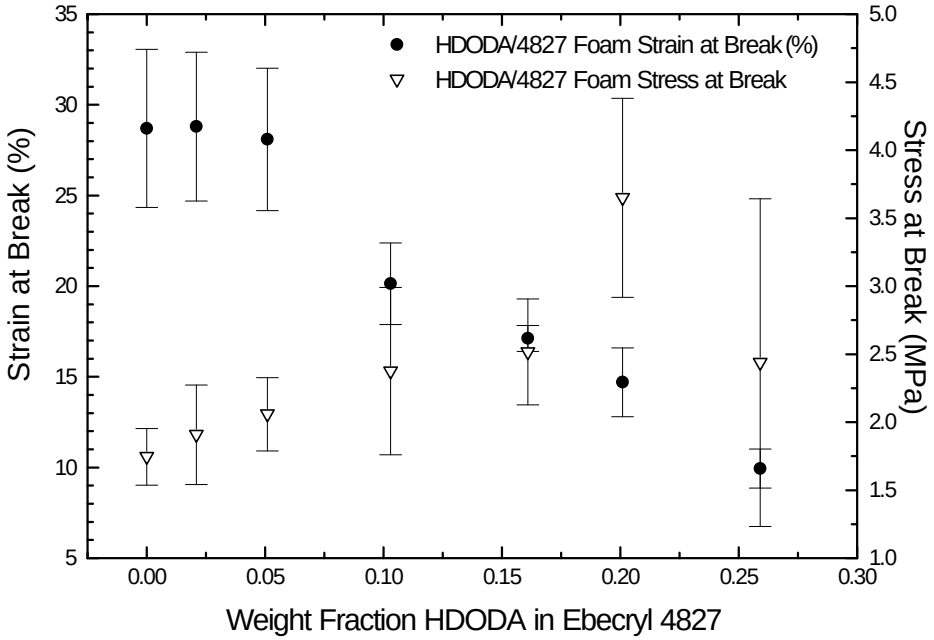

Figure 3-55 HDODA and Ebecryl 4827 cellular material blend stress and strain at break.

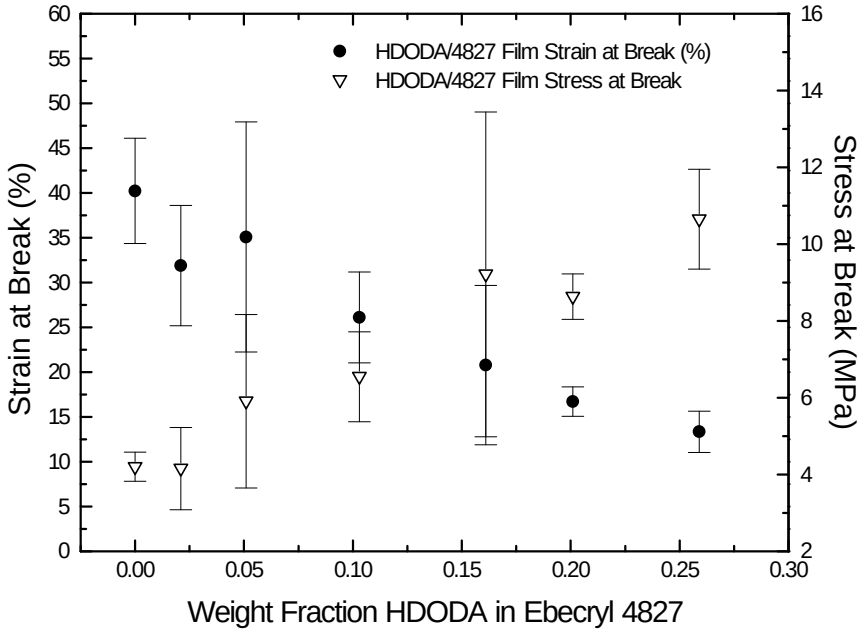

Figure 3-56 HDODA and Ebecryl 4827 film blend stress and strain at break.

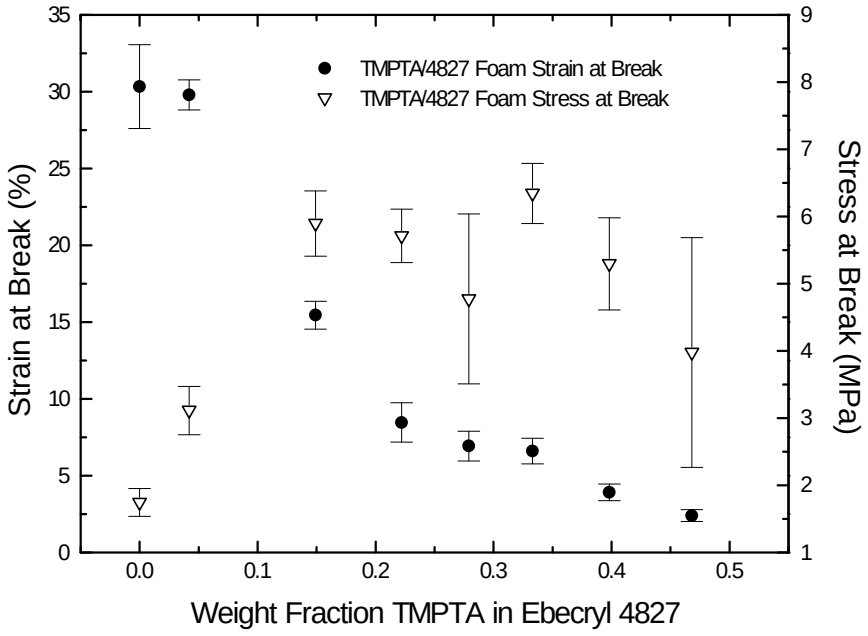

Figure 3-57 TMPTA and Ebecryl 4827 cellular material blend stress and strain at break.

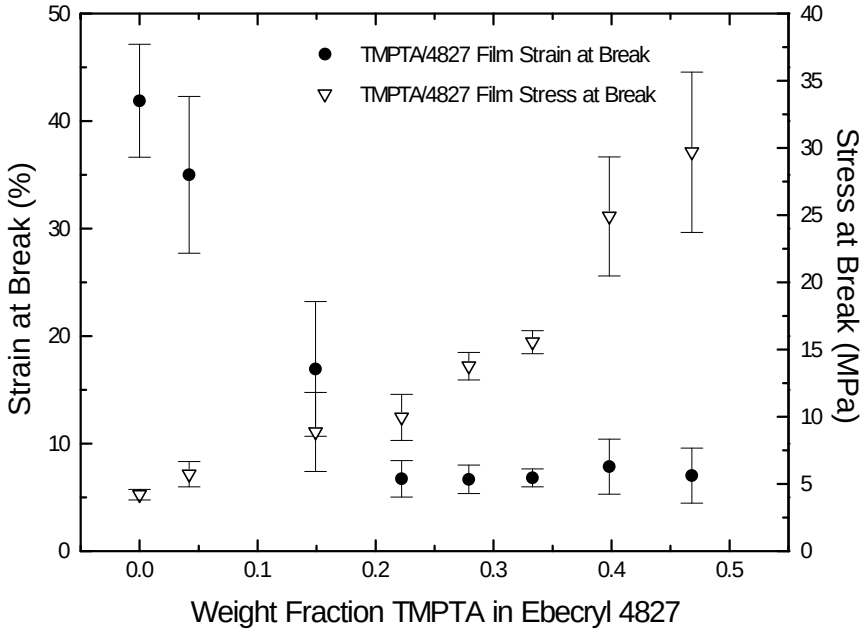

Figure 3-58 TMPTA and Ebecryl 4827 film blend stress and strain at break.

Gibson and Ashby[251] provide an excellent analysis of both closed and open cell materials. Their approach takes into account the density of the cellular material as an important factor in comparing the tensile moduli of different materials. They found the following equations to be adequate for modeling the tensile moduli of cellular materials. For open cell foams:

$$\frac{E^*}{E_S} = \left(\frac{\rho^*}{\rho_S} \right)^2 \qquad (3\text{-}4)$$

Where E^*/E_s is defined as the relative modulus (the modulus of the foam divided by the solid material) ρ^*/ρ_s is defined as the relative density of the cellular material.

For closed cell foams, the gas pressure in the cells, the composition of the cell faces and Poisson's ratio of the material must be taken into account.

Experimental data from Gibson and Ashby have been found to correlate well with the following equation:

$$\frac{E^*}{E_S} \approx \Phi^2\left(\frac{\rho^*}{\rho_s}\right) + (1-\Phi)\frac{\rho^*}{\rho_s} + \frac{p_o(1-2v)^*}{E_s\left(1-\frac{\rho^*}{\rho}\right)} \qquad (3\text{-}5)$$

Where Φ= the variable fraction of solid in the cell faces.
p_0 = the gas pressure in the cells (assumed to be 1 atmosphere)
v = Poisson's ratio (assumed to be 1/3)

Experimental data from the literature shows close agreement with these two equations. Data is shown in Figure 3-59.

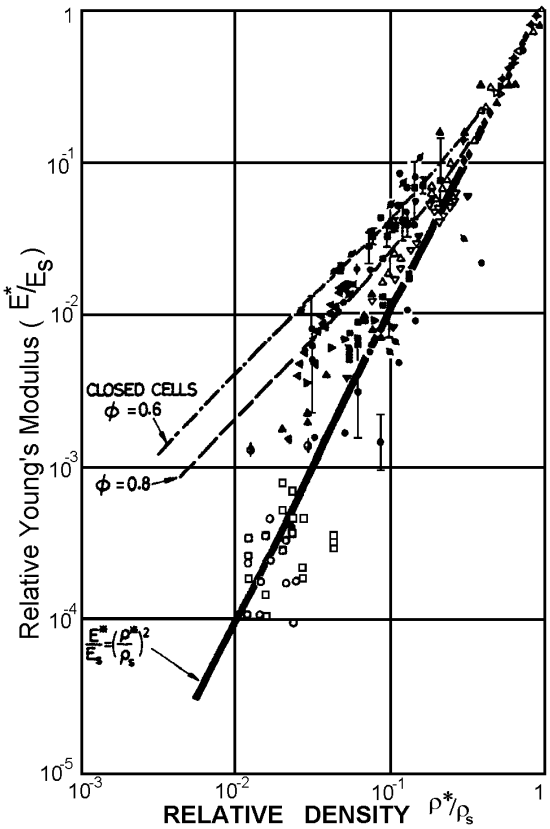

Figure 3-59 Data for relative Young's modulus of foams plotted against relative density. The solid line represents the theory for open cell foams. The two dashed lines represent the theory for closed cell foams with Phi = 0.8 and 0.6. (from ref. 16)

The next four figures compare experimental data with these two theories. In Figure 3-60 through Figure 3-62 data for the relative froth mixture density was used along with the modulus of the film to predict the modulus of the cellular material. Actual data for the cellular material modulus is displayed for comparative purposes. For Gibson and Ashby's closed cell equation, a value for Φ=0.7 was used for all three systems. As can be seen from Figure 3-60 through Figure 3-62, normalizing a cellular material modulus on density deviates strongly from actual data. Normalizing on density squared shows a better approximation and the closed cell equation shows the best correlation for experimental data. In Figure 3-63, experimental data is fit to Equation 4. The equation provided a good fit for blends with β-CEA and TMPTA, however the HDODA blends did not fit well. One possible explanation for this deviation could be found in the struts of the cells in these materials. They are not typical for closed cell materials as would be observed in polystyrene (see Figure 3-28) or the other extreme of an open celled foam as shown in

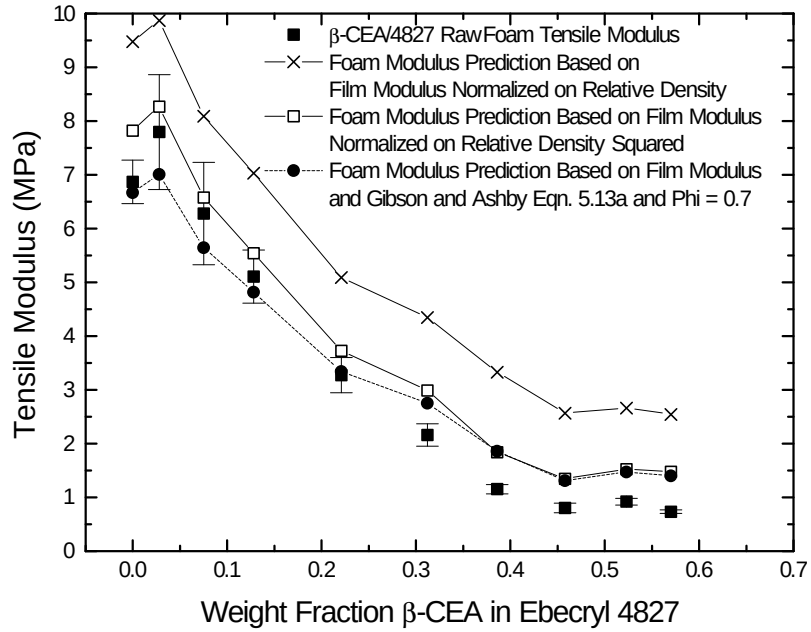

Figure 3-60 Theoretical tensile modulus prediction by various theories as compared with experimental data for β-CEA monoacrylate and Ebecryl 4827.

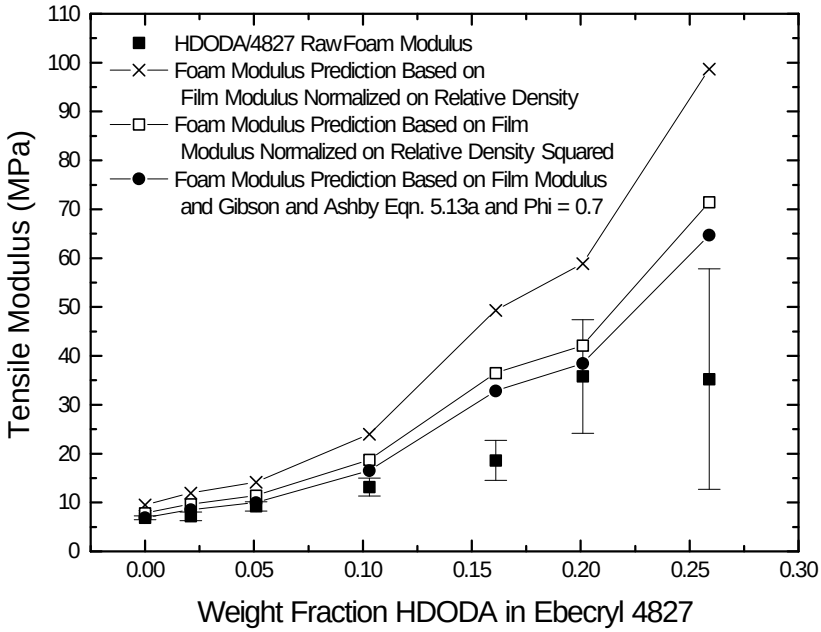

Figure 3-61 Theoretical tensile modulus prediction by various theories as compared with experimental data for HDODA diacrylate and Ebecryl 4827.

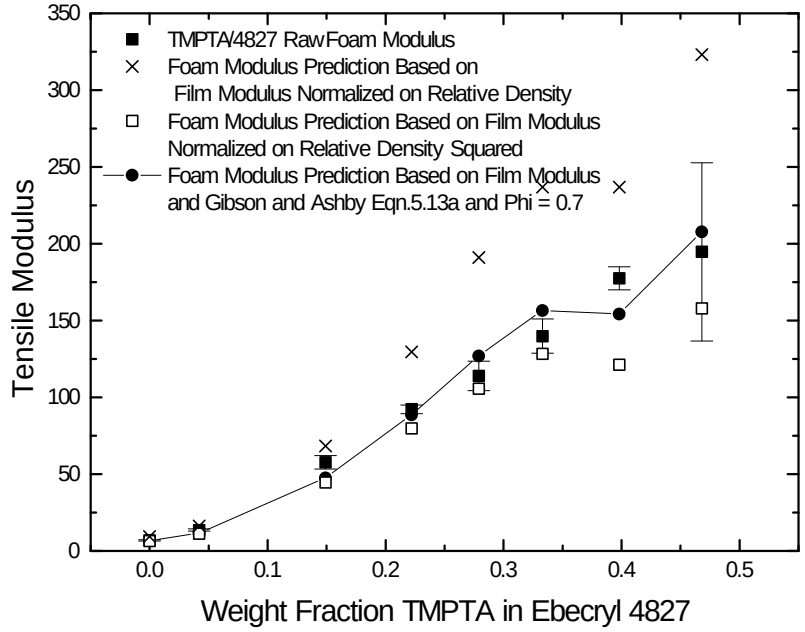

Figure 3-62 Theoretical tensile modulus prediction by various theories as compared with experimental data for TMPTA monoacrylate and Ebecryl 4827.

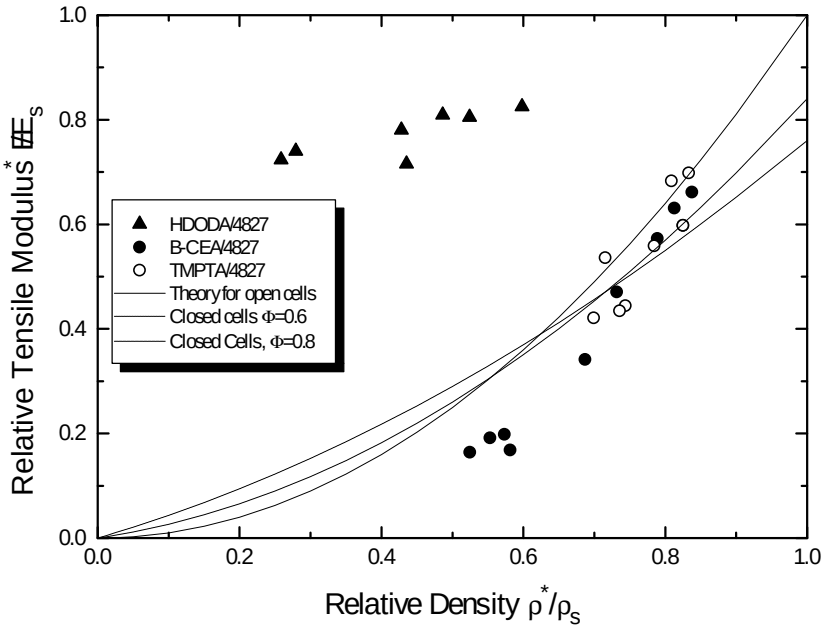

Figure 3-63 Relative modulus vs. relative density for all materials.

3.3.5 Process Modification

An attempt at reducing the 1 Pa·S processing limit was made by adding fumed silica to a low viscosity system with the hope that the increase in viscosity would allow processing of lower viscosity systems. TMPTA was selected (μ~0.1 Pa·S) and various amounts of fumed silica, up to 6% by weight were added. While qualitative observations of viscosity increase were noted, the type of mixing changed from what was observed in the oligomers/monomer blends at about 1.4%(w/w) fumed silica in TMPTA. At this point, the system failed to "froth" as before but instead climbed the mixer which made it impossible to froth the system. Rheological experiments showed a non-Newtonian Bingham plastic behavior of these fluids, which explains the transition behavior at 1.4%. (See Figure 3-64). While the results were disappointing, they did provide insight to one of the important areas of this process. Future attempts at reducing the lower processing limit for the mixing process must take into account the fact that non-Newtonian behavior may not allow the material to froth sufficiently to generate a cellular structure. As noted previously, the monomers and oligomers (with a small exception of Ebecryl 1701) all tested as Newtonian fluids.

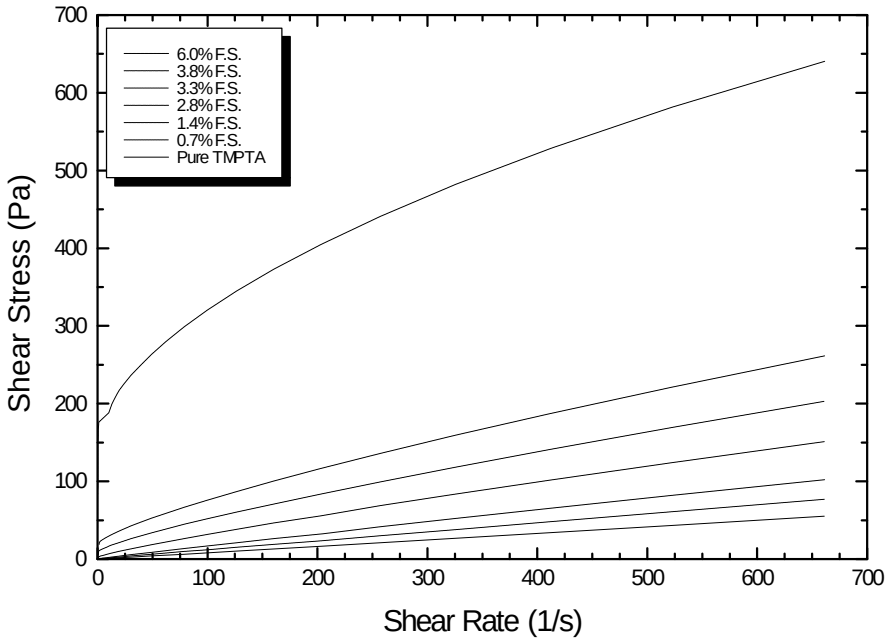

Figure 3-64 Constant rate rheology experiments as a function of weight% fumed silica with TMPTA.

3.4 Other Applications

3.4.1 Layered/Laminate Materials

Interest in producing a material that had a core cellular structure with a skin of a solid material generated two experiments involving curing a mechanically frothed radiation curable mixture on top of a film of either polyethylene or nitrile rubber. This experiment had two goals. First, it was desired to show that such novel materials could be produced. Next, it was desired to show that different materials could be used as the film in the materials. Motivations for materials such as these may come from a desire to have a material that had a lower bulk density than without the cellular core; to have a lower density structural material; to have a material with an integral skin, but of lower density and to improve combined properties of the materials such as toughness, tear resistance, and damping. Figure 3-65 and Figure 3-68 show scanning electron micrographs of these materials. The

thickness of the films was approximately 1 mil for the PE film and 3 mils for the NBR rubber film. A froth composition of 50/50 β-CEA and Ebecryl 4827 was used to produce the cellular structure. The most notable difference between the two materials was the adhesion between the film material and the cellular material. The PE film had relatively poor adhesive properties as expected, while the NBR rubber material was significantly better, as expected since the rubber could allow the monomer to diffuse into the surface before curing while the PE would not due to its limited solubility at room temperature.

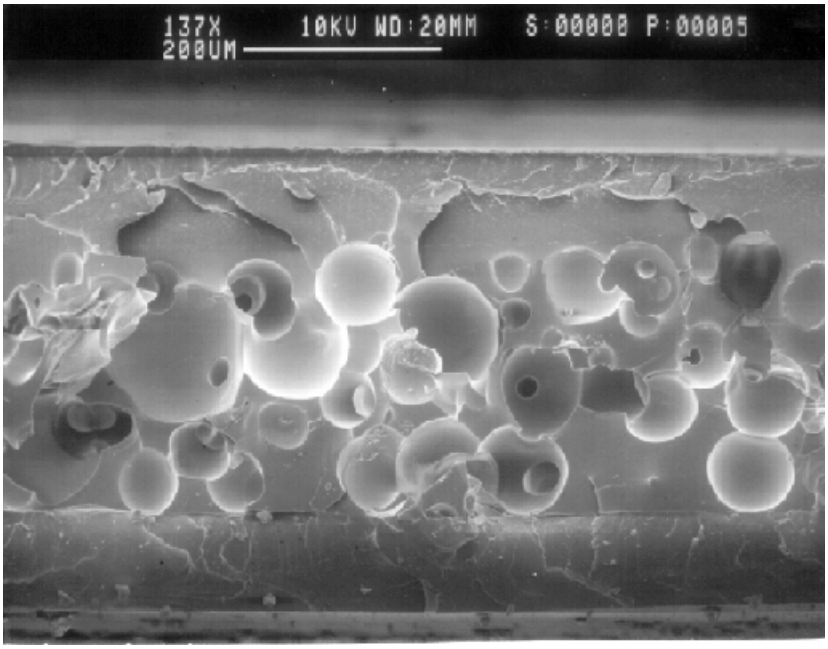

Figure 3-65 Scanning electron micrograph of layered material utilizing a nitrile rubber skin with E-Beam generated cellular material core with a composition of 50% β-CEA and 50% Ebecryl 4827.

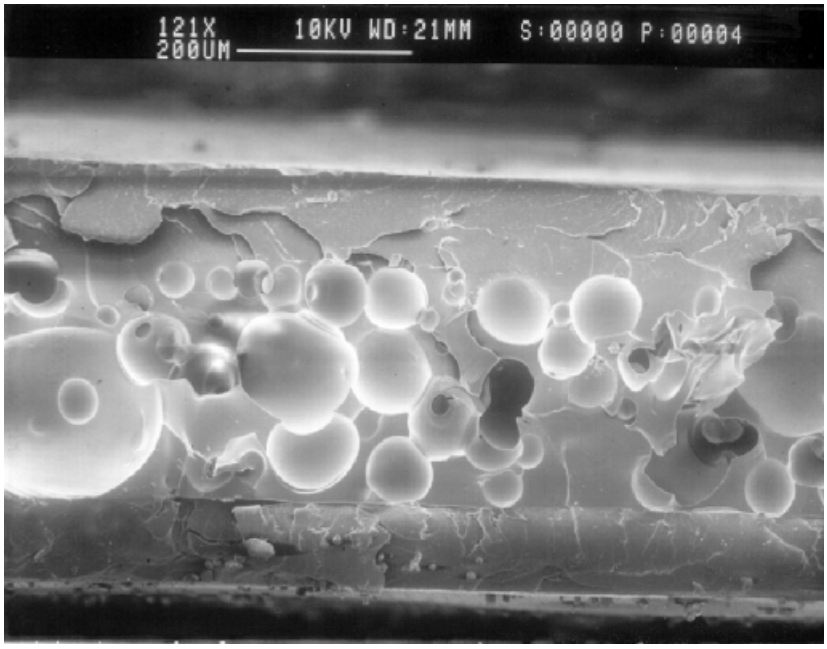

Figure 3-66 Scanning electron micrograph of layered material utilizing a nitrile rubber skin with E-Beam generated cellular material core with a composition of 50% β-CEA and 50% Ebecryl 4827.

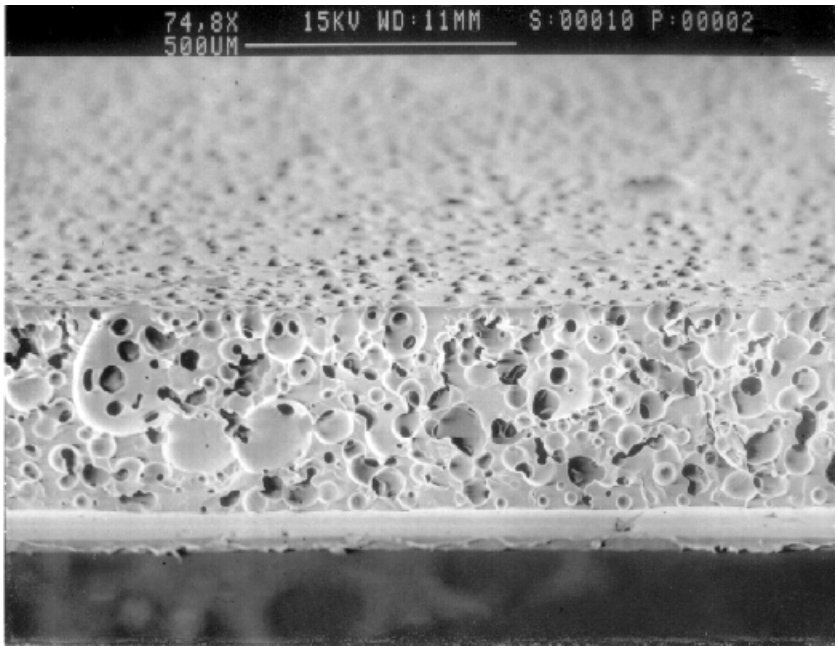

Figure 3-67 Scanning electron micrograph of layered material utilizing a polyethylene skin with E-Beam generated cellular material core with a composition of 50% β-CEA and 50% Ebecryl 4827.

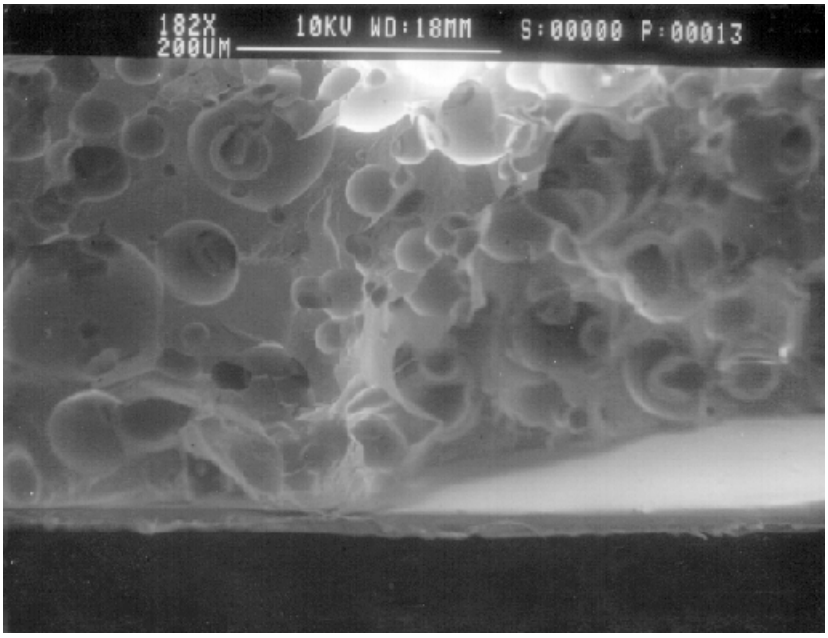

Figure 3-68 Scanning electron micrograph of layered material utilizing a polyethylene skin with E-Beam generated cellular material core with a composition of 50% β-CEA and 50% Ebecryl 4827. "Shelf" appearance on the right side of this material shows the poor adhesion the core material had to the polyethylene skin.

3.4.2 Carbon Fiber Addition

In another experiment, 4% chopped carbon fibers by weight were added to a 50/50 blend of β–CEA and Ebecryl 4827 and frothed in the manner described before. The goal of this experiment was to retain the cellular structure of the material and to add a fiber material with the hope that the fibers could add stability to the froth and provide enhanced mechanical properties to the cured system. Fibers were on the order of 1-5mm in length. A considerable increase in viscosity was observed after the addition of just 4%(w/w) of the carbon fiber. After curing of the material, some orientation of the carbon fibers was observed on the surface of the material that was drawn against the doctor blade. No orientation of fibers was visible on the surface contacting the glass plate. Attempts to produce a material with a "high" (50%

w/w fiber content or greater) material were unsuccessful as mechanical frothing of the carbon fiber/acrylated urethane oligomer could not be maintained. Figure 3-70 shows SEMs of the resulting materials. The fibers did not appear to nucleate cell sites, as was hoped, however the froth mixture collapse time was increased via the increase in mixture viscosity. Figure 3-72 shows that the adhesion between the PVP sized carbon fibers and the acrylated urethane oligomer was generally poor which is not a desired property in carbon fiber composite materials.

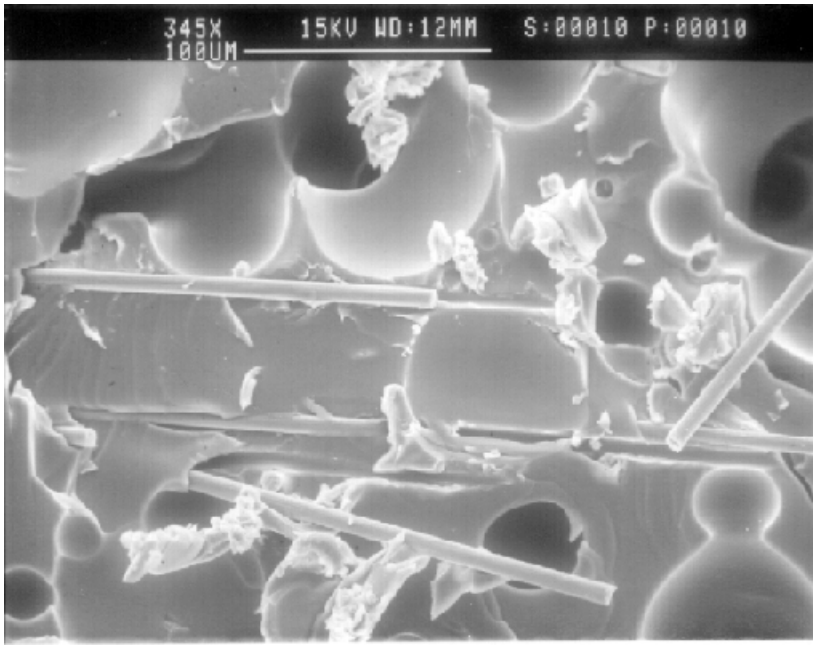

Figure 3-69 SEM of carbon fiber containing electron beam prepared cellular materials.

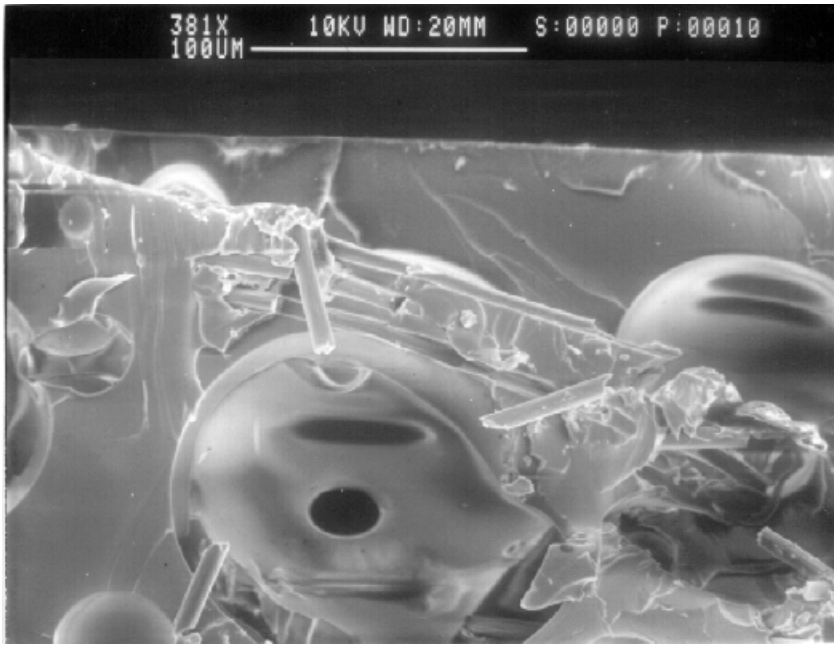

Figure 3-70 SEM of carbon fiber containing electron beam prepared cellular materials.

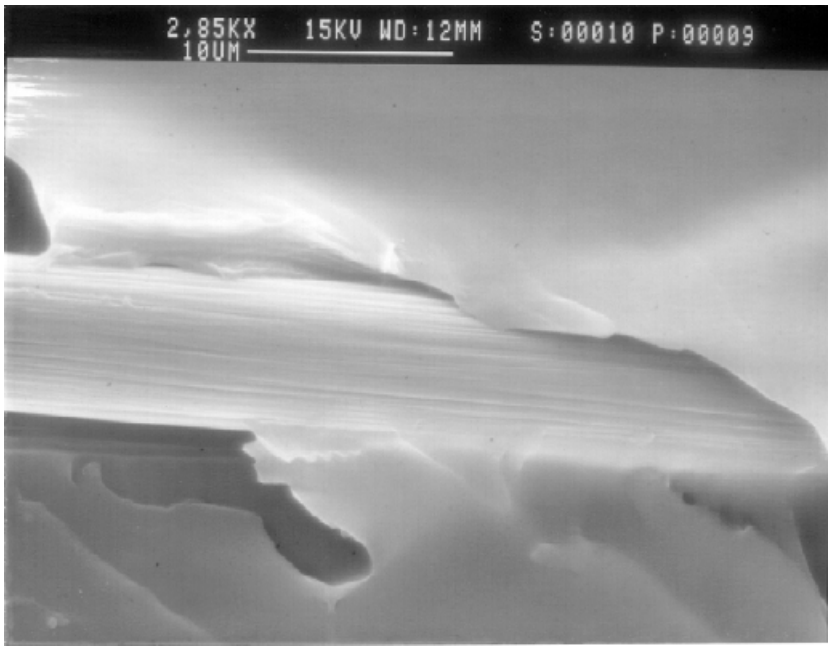

Figure 3-71 SEM of carbon fiber containing cellular materials showing the general poor adhesion between the carbon fiber and acrylated urethane oligomer.

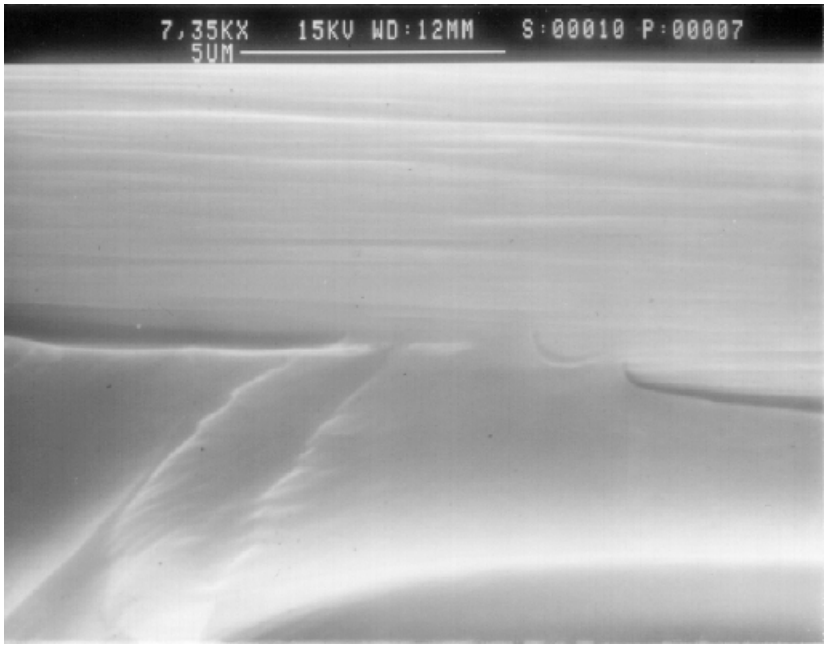

Figure 3-72 SEM of carbon fiber containing cellular materials showing the general poor adhesion between the carbon fiber and acrylated urethane oligomer.

3.5 Conclusions

A technique has been developed that produces closed cell materials by a mixing technique followed by a radiation cure from a radiation curable composition of a suitable viscosity. This process eliminates the need for surfactant to be used as well as heat and/or blowing agents. Comparison of this process with the technique involving a surfactant shows much smaller cell size as well as a tighter control over cell size distribution. Changes in process and cellular material property can be accomplished in the mixing process through the addition of reactive diluents which change the mixture viscosity. Addition of a triacrylate or diacrylate to a mixture of an aromatic urethane diacrylate oligomer increases the modulus of the cellular material while addition of a monoacrylate decreases the modulus but increases the elongation at break. Modeling of these mechanical properties with the Gibson and Ashby analysis show the same trends but do not fit well possibly due to

differences in cell strut structure in these materials. Any addition of reactive monomers to radiation oligomers were observed to decrease the viscosity of the blend in a systematic fashion. The densities of the materials are higher than that of other types of commercially made foam products, however they are in the range of similar processes. Finally, it was shown that these cellular materials can be modified to include novel bilayered composite materials composed of a cellular core with an integral skin.

3.6 Acknowledgments

3M and Radcure are gratefully acknowledged for providing the chemicals used in this study.

4 Apparent Reversal of Physical Aging by Electron Beam Irradiation - Further Investigations

4.1 Introduction

This chapter combines two important aspects of polymer science, radiation chemistry and physical aging of glassy polymers. Radiation chemistry of polymers is the overall focus of this dissertation and the relevant literature was reviewed in Chapter 2. A brief review of the general aspects of the glass transition and physical aging is included in section 2.10 of Chapter 2. Work specific to the observed phenomena is reviewed here.

In previous work from our laboratory[252], it was shown that aged samples of polystyrene (PS), poly(methyl methacrylate) (PMMA), and polycarbonate (PC) will all show, upon sub Tg annealing, a typical physical aging endotherm, as expected. However, when irradiated with electron beam radiation, it was shown that the enthalpic relaxation peak could be reduced and the rate of reduction of this peak was proportional to the dose the sample received (see Figure 4-1). In addition it was observed that PS took a much higher dose to completely eliminate the endotherm than for either PMMA or PC (see Figure 4-2). At that time it was also assumed, based on the knowledge base of radiation chemistry, that PS was predominately crosslinking as a result of being irradiated while PC and PMMA were predominately undergoing main chain scission. Therefore, this apparent reversal of physical aging occurred in aged, glassy samples of very different radiation chemistry.

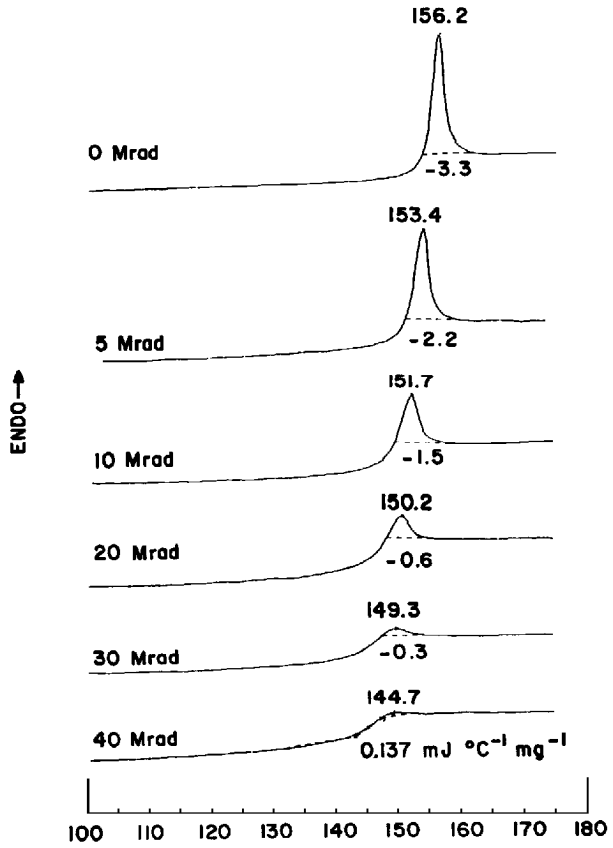

Figure 4-1 DSC scans of aged PC after exposure to the indicated dose.[252]

The issue of the sample being heated (which does occur during irradiation) and therefore possibly being heated above Tg was disproved by comparing the results between PC and PS. PS (Tg = ca. 105°C) required a dose of ca. 400 Mrad to eliminate the enthalpic relaxation peak and PC (Tg = ca. 150°C) took only 40 Mrad to do the same (see Figure 4-2). If sample heating above Tg was causing the deaging to occur, it would have to happen in PS before PC, since PS has a Tg 50°C below that of PC and one would arrive at that polymer's Tg well before that of PC. Note that all samples received the same dose rate of 10 Mrad/pass in the electron accelerator.

One can also consider the following calculation for a theoretical temperature rise per Mrad - which assumes no heat loss to the environment -

and is highly idealized to err on the side of excessive heating. Based on the following input data:

Heat capacity of a typical organic glassy polymer = 0.5 - 0.7 cal/g °C
1 rad = 0.01 Joule/kg
10^6 rad = 1 Mrad
1 Joule = 0.23901 cal
1 kg = 1000g

The heat rise per Mrad of absorbed radiation is 3.4 to 4.8 °C, based on a closed and adiabatic system.

Clearly there must be some heat loss as there were polystyrene samples irradiated in this study to 1400 Mrad that still displayed enthalpic relaxation. Even so, for a 10 Mrad sample of polycarbonate, heating from room temperature would result in a maximum temperature of 73°C, clearly well below the glass transition temperature for this polymer.

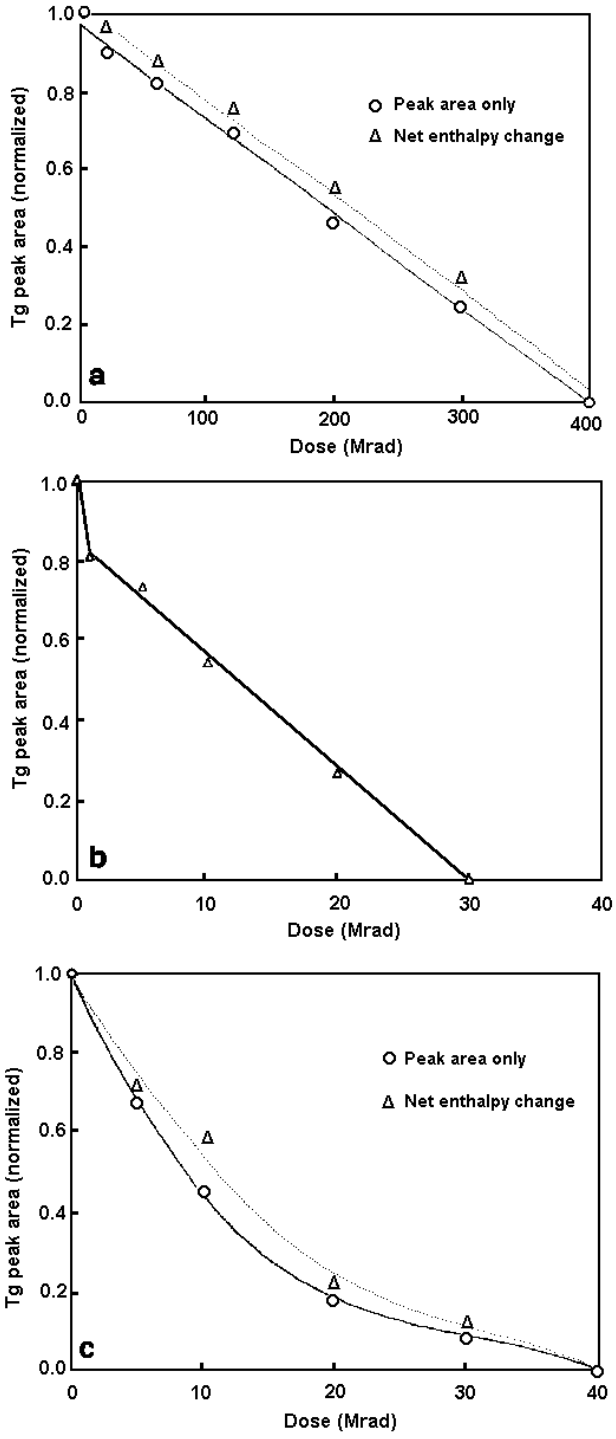

Figure 4-2 Plots of endothermic peak area vs. dose for (a) PS, (b) PMMA and (c) PC.[252]

A tentative explanation was proposed to account for the observed behavior at the time of the earlier report. Specifically, it was conjectured that the polymers were being impregnated with gas which was produced as a result of the radiation chemistry events. Either a main chain scission or a crosslinking event can produce a gas molecule, although there are different gases produced for different events. For example, crosslinking typically produces H_2 through hydrogen abstraction and scission can produce larger molecules such as CO_2. The first piece of evidence in support of this hypothesis was the polymers G_{gas} values found in the literature.[252] PS had a much lower G_{gas} formation value than PMMA and PS took a much higher dose to "deage" therefore, gas generation could be responsible for the observed effect.

The second, and most convincing, piece of evidence in support of the gas generation theory was found in a series of what was termed "time delay" experiments on irradiated and aged polycarbonate. In these experiments thin, solvent cast PC films were irradiated to a total dose of 10 Mrad in increments of 2 Mrad per "pass" through the electron accelerator. Different elapsed times were allowed between passes for the films. When an elapsed time of 5 minutes was used per 2 Mrad pass, the deaging phenomena was not observed by enthalpy relaxation. In other words, the DSC scan was identical to that of an unirradiated, aged sample. However, when a short time delay was used, the deaging phenomena was observable by DSC. (see Figure 4-3) It was therefore assumed that the gas that was generated during irradiation was diffusing out of these thin films during the delay time. When the sample was scanned in the DSC, it was not as "pumped up" by the internally generated gas as the sample that did not receive as long a time delay.

Rationale for the prior conclusions can be found in the definition of enthalpy at constant pressure.

$$\Delta H_P = \Delta U + P\Delta V \qquad (4\text{-}1)$$

Where: H = Enthalpy
U = Internal Energy
P = Pressure
V = Volume

The justification for the gas generation theory was that the gas which theoretically "pumps up" the system should change ΔV. Measured changes in enthalpy correspond to this change in density. Internal energy changes were not considered.

Volumetric changes as a result of the proposed gas generation were not studied; however, it was hypothesized that the density of these polymers should decrease and that this decrease should be proportional to the dose that the polymer received. It was desired to follow up this work by first studying what, if any, volumetric changes could be observed and then to follow up with any additional experiments to support or disprove the gas generation hypothesis.

At this point, the deaging phenomena with radiation has been observed in four polymers. Further testing was required to prove or disprove the gas generation hypothesis. First volumetric studies were proposed, then the enthalpic measurements were repeated. It was assumed in the initial study that PS was crosslinking, and PMMA and PC were undergoing scission. This also needed to be verified though experimental measurements. What follows are the results of this newer work.

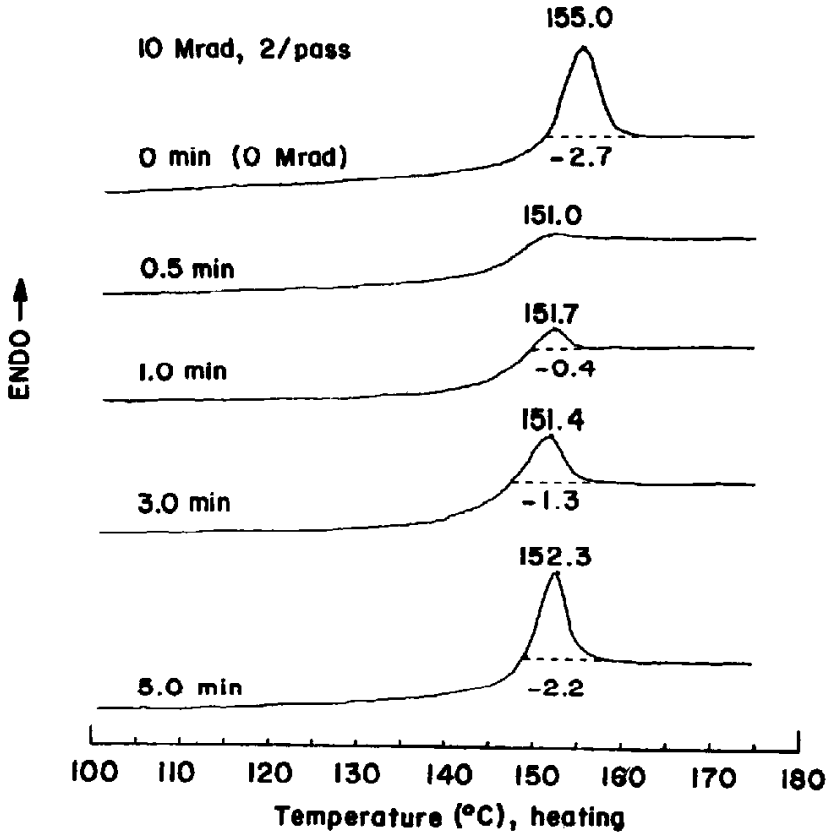

Figure 4-3 Series of DSC scans of physically aged, solvent-cast PC films that have been irradiated to 10 Mrad a 2 Mrad/pass. The times indicated represent the elapsed time between successive exposures to radiation.[252]

In reviewing the literature in this area, one study was found that did not recognize the phenomena of reducing enthalpy relaxation with radiation but did confirm the earlier findings.[253] In that specific study, samples of a poly(arylene ether) were irradiated to two different doses and then DSC scans were made of the materials, along with tensile property measurements. Apparently, some physical aging did occur in their materials to the extent that a small enthalpic aging peak can be observed at Tg in their "0 Mrad" DSC scan. The DSC data published shows the same phenomena observed in our laboratory for PS, PC, and PMMA. One can clearly see in Figure 4-4 the enthalpic aging peak in the first scan of the 0 Mrad sample - and then, upon

reheating, elimination of this aging peak. It's difficult to see any reduction of this peak in the 50 Mrad sample, however, the 1000 Mrad sample's first scan clearly shows a smaller enthalpic aging peak which is very similar to the behavior previously observed in our laboratory. The authors of this study did not comment on the physical aging of their samples nor on the enthalpic reduction with dose but it is encouraging to see this phenomena observed in yet another polymer, with a different radiation source and by other workers.[253]

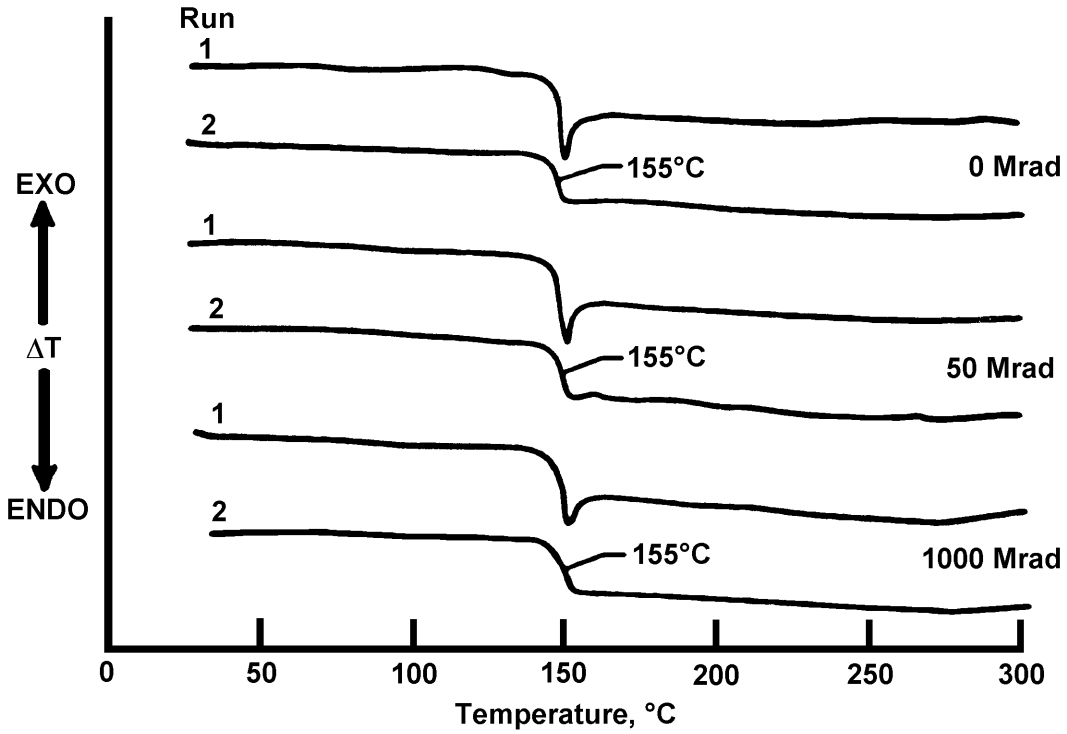

Figure 4-4 DSC scans from poly(arylene ether) before and after radiation exposure displaying the physical aging endotherm reduction.[253]

4.2 Experimental

4.2.1 Materials and Sample Preparation

Samples of PC (Macralon 2608 DR=2 M_n = 16,000), PS (DR=2, M_w = 300,000) were acquired in order to reproduce the previous work as these same polymers of similar molecular weight were used at that time. As will become evident later, polymers with a low radical yield and/or a high crosslinking propensity were desired in order to test a 100% crosslinking system. Therefore, polyethyleneterephthalate (PET) (M_n = 21,500) and *cis*-polybutadiene (Aldrich, M_w = 2,000,000-3,000,000) were acquired for this segment of the study. PET is known to have a low radical yield and is used as a backing material in many industrial radiation processes and was assumed not to undergo degradation when irradiated. Although physical aging of *cis*-polybutadiene was difficult due to its low Tg, (-105°C) it's high double bond content was hoped to yield only crosslinking when irradiated. Thin films (ca. 1 mil) of PC were solvent cast from methylene chloride on Teflon and dried at 60°C in vacuum for 72 hours. Samples of PS and PET were compression molded to 4mil on smooth metal plates and quenched in ice water. PET samples were scanned by DSC to insure that no crystallization had occurred. C*is-p*olybutadiene was cast from THF onto Teflon and vacuum dried at room temperature for 72 hours. DSC experiments were performed on the as received samples in comparison to the solvent cast samples to verify that the solvent had been removed. The observed Tg's for each material (10°C heating rate) were 150°C for PC, 85°C for PET and -103°C for *cis*-polybutadiene. It should be noted that the DSC was not calibrated for low temperature operation and the Tg for *c*-PBD could be off by as much as 10°C.

Once formed, each film was physically aged for approximately 1 week in vacuum ($1x10^{-3}$ Torr) at a temperature 30°C less than the Tg of the

material. Polybutadiene samples were aged in the DSC at a temperature of -118°C for up to 500 minutes.

4.2.2 Radiation Exposure

All films were irradiated using an Energy Sciences (ESI) CB150 175keV Electrocurtain as the radiation source under a nitrogen blanket of 200ppm oxygen. Samples were irradiated from 2 to 10 Mrad per pass to avoid excessive sample heating. Samples were exposed to air between passes if more than a total dose of 10 Mrad was required.

4.2.3 Thermal Analysis

Enthalpy relaxation measurements for PET and PC were performed in a Perkin Elmer DSC 7 system using a heating rate of 10°C/min and cooling rate of 30°C/min. A baseline scan was performed using an empty pan and lid in the reference cell and another pan and lid in the sample cell. The pan and lid in the sample cell were used for the scan after the baseline was performed. In the case of polybutadiene, samples were analyzed using a Seiko DSC 210 apparatus. For all samples, the second heating was subtracted from the first heating and the resultant peak area measured. (see Figure 4-5) In several cases the slopes of the first and second heats did not match up perfectly, resulting in some curvature in the resultant curve after subtraction. In these cases, y-axis values of 0 were picked before and after the physical aging peak to draw the baseline for subtraction. This was done for consistency purposes and most runs were all repeated from 3-8 times to reduce experimental variability.

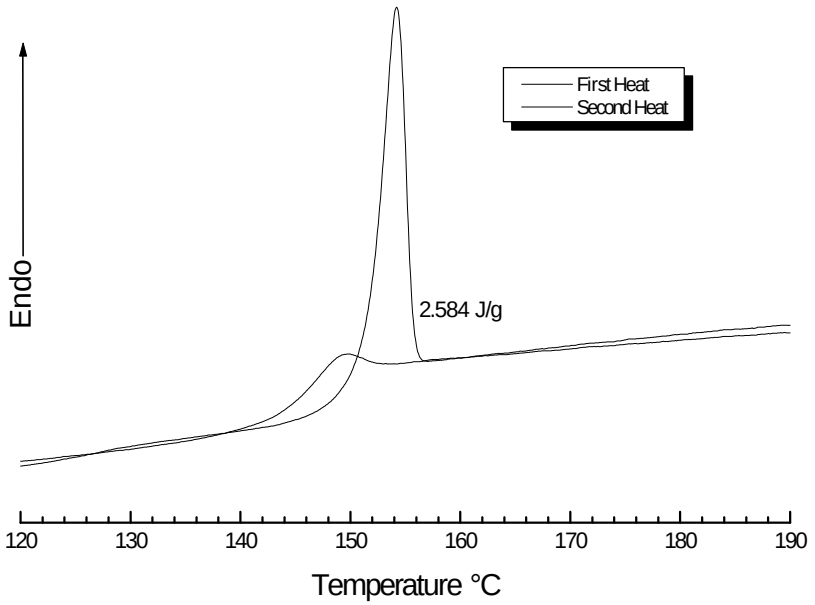

Figure 4-5 Typical DSC trace (first and second heats) of bisphenol-A polycarbonate aged for eight days at 120°C.

4.2.4 ESR/EPR

Electron spin resonance spectroscopy/Electron paramagnetic resonance spectroscopy was performed in a EPR ERC-200 x-band (9.3 GHz) Bruker Electron Magnetic Resonance Spectrometer. EPR can detect the number of spins per gram of material for cylindrical or liquid samples which fill the sample tube. Due to the depth/dose profile of the electron beam accelerator, it was necessary to use film materials which have a flat profile. Therefore, an absolute number of spins per gram was not recorded due to the asymmetric nature of the film samples used. Relative radical decay times were recorded using the peak heights of the resultant ESR curves.

4.2.5 Density Determination

A density gradient column was designed utilizing a NaBr/water mixture with a column range from ρ=1.130 to 1.300 g/cc. A cathatometer was used to note the position of the calibration beads (ρ=1.1600, ρ=1.2000 and ρ=1.2300) as well as film samples. Sample position was recorded as a function of time. The times noted as "zero" were recorded as the times the film sample was placed into the top of the column, as opposed to the times of the start of radiation exposure. Two column setups were utilized, the first covering the broad range mentioned above and the second more sensitized column set up from 1.1300 to 1.2000 g/cc. The first cruder density column utilized a meter stick to reference sample position while the second precision density column utilized a Geartner Scientific Corporation cathatometer to record sample position.

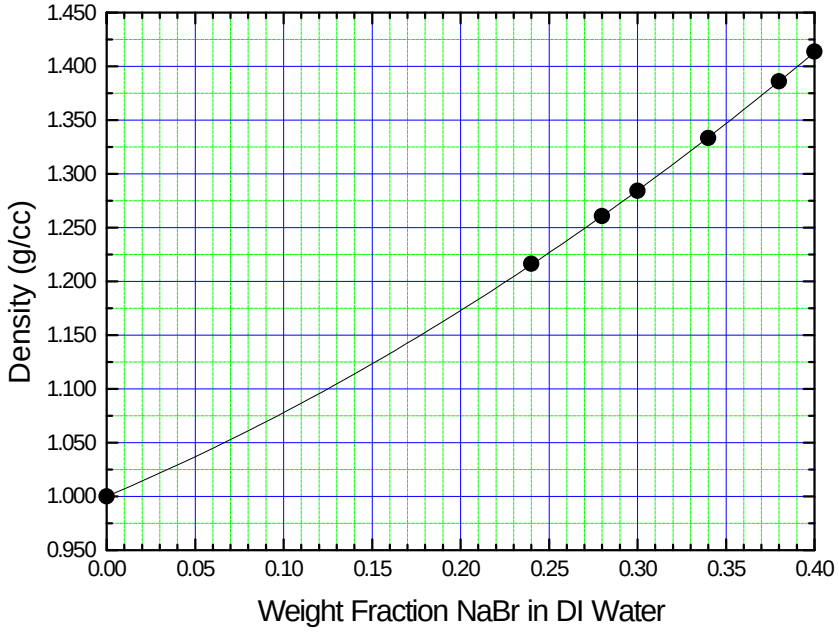

Figure 4-6 Relationship between solution density and weight fraction of NaBr for the $NaBr/H_2O$ mixture at 25°C.

4.2.6 Sol/Gel Analysis

Soluble portions of irradiated films were extracted using a fritted glass cylinder and THF solvent. Vials were removed periodically, dried and the weights recorded and then the vial (with the film) placed back into solution. Care was taken so that the solvent did not reach the top of the vial and the film remained below the level of the solvent. This procedure was repeated until a constant weight of the vial was achieved.

4.3 Results and Discussion

4.3.1 Volumetric Changes

As stated in the introduction, it was a primary goal of this work to determine what, if any, volumetric changes after irradiation were occurring in order to support the gas generation hypothesis. Referring back to equation 4-1, it was thought that volumetric changes could be responsible for enthalpic changes, as is the typical case. It was hoped that an aged, and subsequently irradiated polymer would show a density similar to that of a freshly quenched sample, since they had similar endothermic responses and that an aged polymer sample would have a density significantly greater than either of them. In the first experiment, a column with a density range of ρ=1.130 to ρ=1.275 g/cc was set up with three calibration beads. Samples were irradiated with doses from 5 to 40 Mrad. After irradiation, each sample was immediately placed in the top of the column, starting with the low dose sample (5 Mrad) and ending with the high dose sample (40 Mrad). It was observed that the film samples did not drop to a fixed point and then stay there, instead, they appeared to be moving as a function of time. Figure 4-7 shows data from this initial set of experiments.

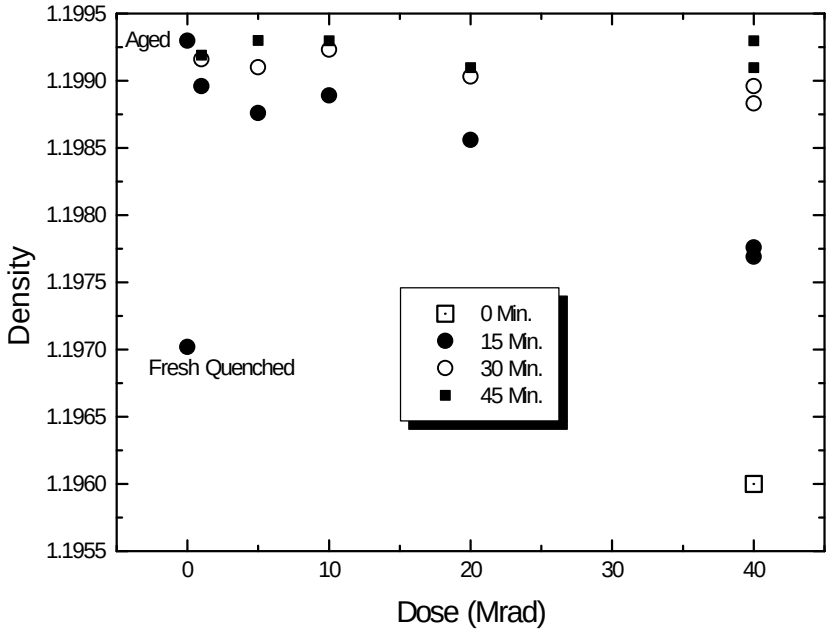

Figure 4-7 Density gradient column data for PC samples. The legend indicates the time difference from irradiation.

The initial observations of this data supported the gas generation theory very well, especially in light of the time delay experiment data shown in Figure 4-3. The samples appeared to show lower densities initially, however then were observed to drift slowly and all eventually showed densities similar to that of an aged sample. Even more convincing was the time scale of the apparent observed changes in film density in the gradient column data compared with the time delay experiment. For the 10 Mrad time delay experiment, 20 minutes of delay elapsed (5 minutes per pass) before the DSC run. In the density column, approximately 15 minutes elapsed before a 10 Mrad (1 pass) PC sample, which appeared to show a low density initially, indicated it had a density of that of an aged sample.

Unfortunately, follow up experiments with a more "sensitized" column utilizing the cathatometer showed that what was actually observed was simply the films (including aged and quenched controls) were undergoing

"settling" as they approached (in the column) a fluid density similar to the film density. Since the films were irradiated starting with lower doses and ending with the 40 Mrad sample, and they were immediately placed in the column after irradiation, they did not have identical "start times" in the column. Hence, when the first data points were taken, it appeared that the 5 Mrad sample had a higher density than that of the 40 Mrad sample, when actually the 5 Mrad sample had started settling in the column well before the 40 Mrad sample. Figure 4-8 and Figure 4-9 both show data from the second series of density gradient column experiments. Figure 4-8 shows raw position data as a function of time in the column. Figure 4-9 shows the same data, with the densities computed for each data point based on the column calibration.

As expected, there is a significant observable difference between the quenched PC sample and the aged PC sample; however, *there is no observable difference between the aged, then irradiated samples and the aged samples*. One would initially expect that PC samples that have similar enthalpy relaxation behavior would show similar densities based on the expectation that ΔH typically scales with ΔV. Indeed, samples with identical aging history did show identical densities when experiments were repeated. However, irradiated samples *did not* show densities similar to that of quenched samples, even though their enthalpy relaxation behavior was similar.

There could certainly be very small changes in density beyond the sensitivity of the column when samples were irradiated. If there was any significant trend when aged PC samples were irradiated, it was a very small increase in density. To be consistent with the observed enthalpic observations, the density of an aged and then irradiated PC sample should be similar to (or at least decrease in the direction of) a quenched sample since

they had similar enthalpic behavior. Recall that in the case of the non-irradiated polymer, changes in ΔH correspond to changes in ΔV. i.e. an aged sample (with lower volume) will display a higher ΔH than that of an unaged sample (with higher volume). Because changes in the chemistry of the system are occurring when irradiated, one would not necessarily expect the two to behave identically due to possible internal energy changes. However, this seems to work against the gas generation theory as that would indicate that the enthalpy relaxation changes are a result of internal energy changes, not volumetric changes as the gas generation hypothesis would predict.

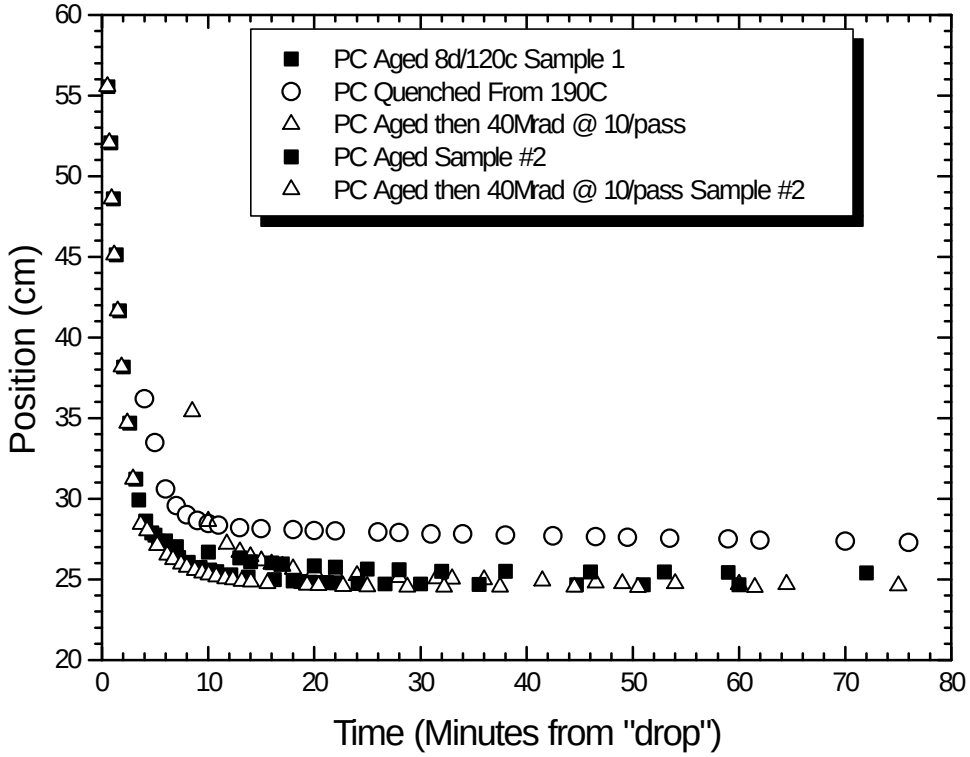

Figure 4-8 Density gradient column “raw data” showing film position as a function of time.

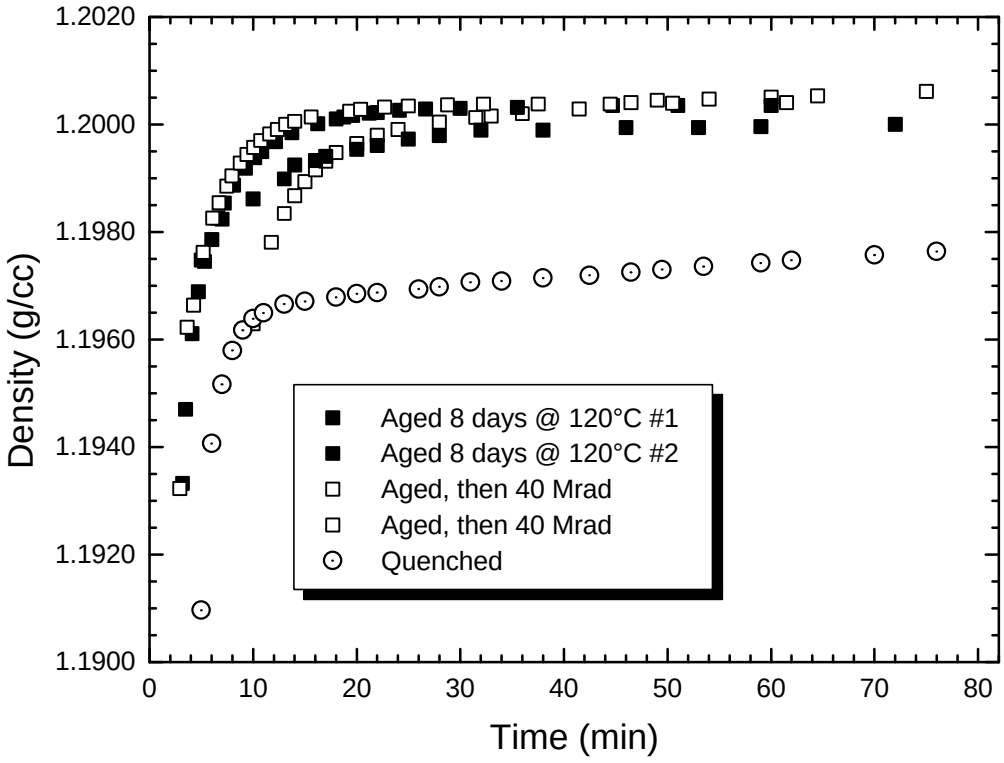

Figure 4-9 Apparent density as a function of time for Bisphenol-A polycarbonate.

4.3.2 Enthalpy Relaxation Changes

Enthalpy relaxation changes in PC, PS and PET were measured after exposing them (after physical aging) to radiation. After the puzzling results from the density gradient column, it was decided to reproduce all of the previous experiments performed on polycarbonate. The only significant changes in the reproduced experiments were that a different DSC was used, and a different sample of PC was used of different molecular weight from the previous work. In this case a Perkin-Elmer DSC was utilized and the previous work utilized a Seiko DSC and previously polycarbonate of M_n = 13,250 and DR = 3.4 and in this work M_n = 16,000 and DR was = 2. The first set of experiments reproduced were the dose vs. endotherm reduction experiments. These experiments were reproduced several times with

excellent repeatability despite the equipment and slight material differences. PC films were irradiated at 10 Mrad per pass and then immediately (within 10 minutes) cut, weighed and then started in the DSC. Sample DSC traces are shown in Figure 4-10. Figure 4-11 summarizes all aged, irradiated PC data. Results are similar to those observed by McHerron previously in this laboratory.[252]

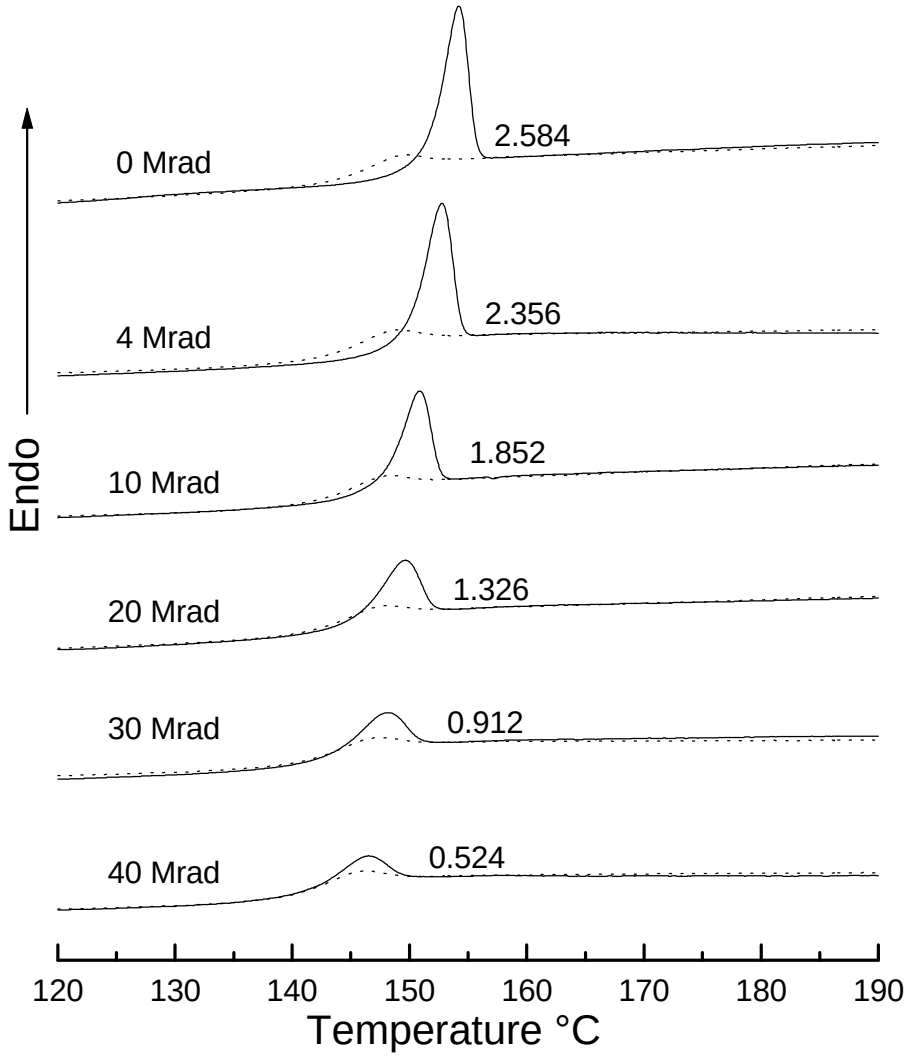

Figure 4-10 DSC scans of polycarbonate irradiated to the doses indicated. Numbers indicate the value of peak area in J/g.

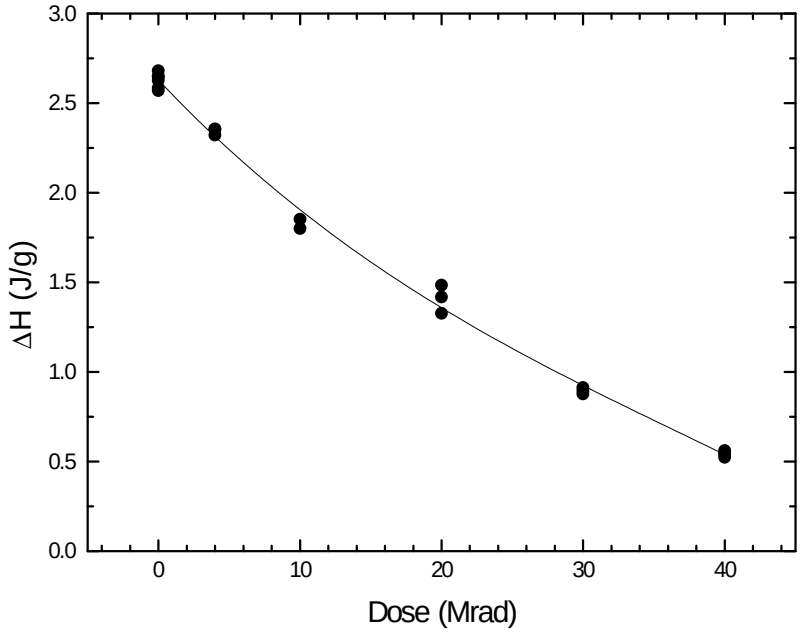

Figure 4-11 Summary of all PC DSC enthalpy relaxation data.

In addition to repeating the dose - endotherm experiments, the time delay experiments previously performed were repeated. As before, films were irradiated to 10 Mrad at 2 Mrad/pass with times increasing from 0.5min to 5 minutes between passes. These experiments were repeated a total of three times and failed to reproduce the results observed previously. In further experiments, times between passes as long as 30 minutes were observed. The total dose was increased to 40 Mrad and the dose per pass at 8 Mrad/pass to be consistent with the total number of passes and time delays from experiment to experiment. Films were cast on both Teflon and glass. An experiment letting the film rest in a nitrogen blanket vs. ambient lab air between passes was also performed. A total of 42 separate experiments were attempted with the goal of reproducing the previously observed time delay effect - all failed to reproduce the previous results of McHerron. Figure 4-12 shows data from time delays of 5 minutes (repeated twice) and 30 seconds

(repeated twice). Although these experiments were repeated several more times, typical data is shown in the resultant subtracted curves.

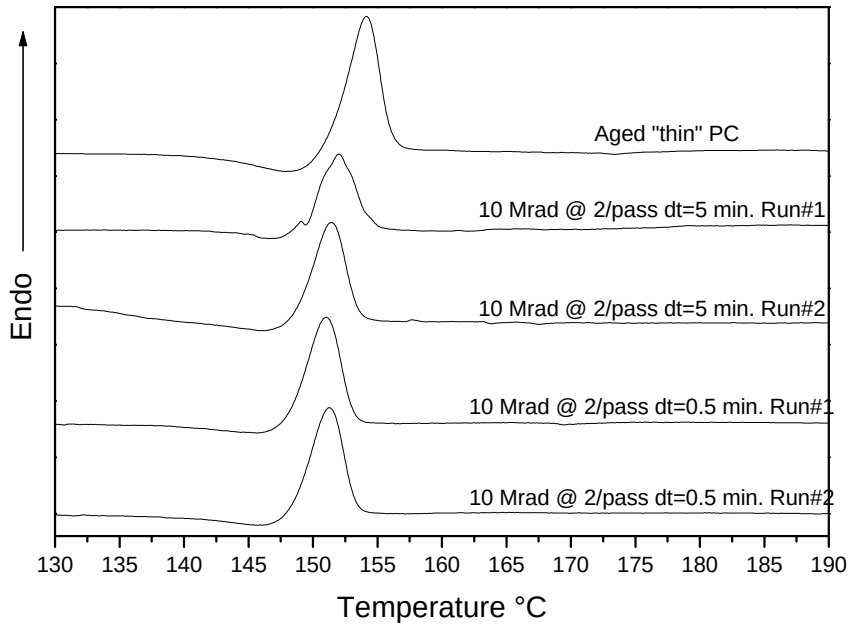

Figure 4-12 Subtracted curves showing endotherm values for the time delay experiments on thin, solvent cast polycarbonate. Experimental details are recorded on each curve.

It was unfortunate that the time delay experiment could not be reproduced. The original student who performed the work was contacted for suggestions, which resulted in casting the polycarbonate on Teflon vs. glass. As before, no significant difference was observed in the resultant enthalpy relaxation behavior of the irradiated films.

Additional DSC studies on PC resulted in further evidence against the gas generation hypothesis. If gas generation was responsible for the reduction in the endotherm at Tg, then, as this gas diffused out of the film, the endotherm should increase in the direction of an aged film. Gas generated by both scission and crosslinking reactions are found in very low

concentrations in the atmosphere; therefore, a high concentration gradient should exist for the generated gas to diffuse out. For this series of experiments, larger pieces of aged PC film were irradiated and then samples cut for DSC experiments. All samples were scanned immediately after irradiation then additional samples were scanned up to 120 hours after being irradiated. Figure 4-13 summarizes these experiments by showing the resultant peak area as a function of time after film exposure to radiation. There is simply no change in the endotherm as a function of time. Whatever gas was generated seems to have had a small effect on the film volume and diffused out without changing the enthalpy relaxation behavior of the film.

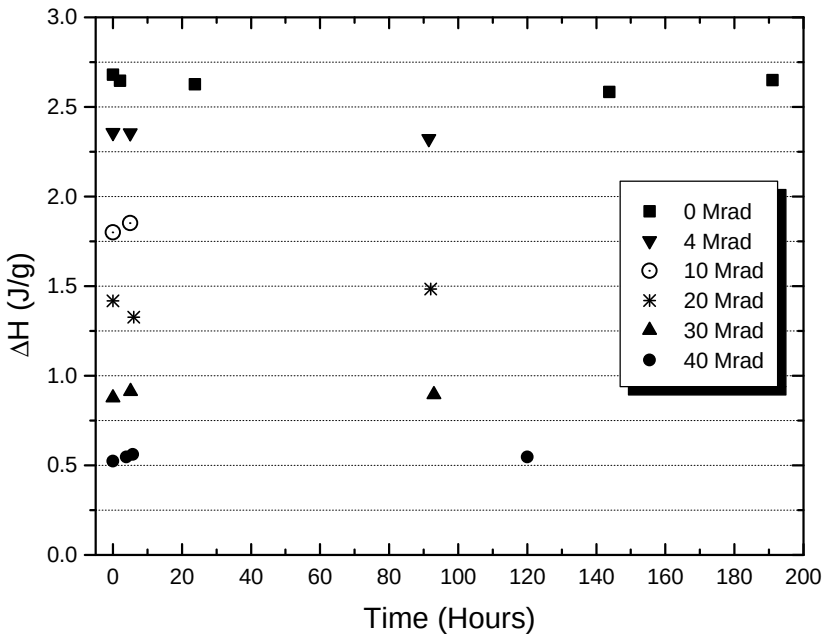

Figure 4-13 Summary of delayed DSC runs after irradiation showing that no significant changes in enthalpy relaxation behavior of irradiated films occurs as a function of time after irradiation exposure.

4.3.3 ESR Results

It appeared at this point that gas generation was not the probable cause of the observed enthalpy relaxation changes. It was thought that trapped radicals or radical decay effects could play a role in the time delay experiments so some qualitative ESR work was performed. It was desired to find out what the decay rate of radicals was in the amorphous PC after irradiation. For instance, if full radical decay was on the order of seconds, cumulative 2 Mrad passes (in the time delay experiments) would result (for long time delays) in a total radical yield no greater than that for a single 2 Mrad pass. However. those passes which occurred with little or no time delay could result in much higher radical yield; therefore, different radical yields could result in the different enthalpic behavior. If, however, radical decay was on the order of hours or days, there would be no reason to think radical decay could play a role in the mystery of the time delay experiments.

Noting the large size of the ESR device and its distant location from the authors laboratory, radical measurements immediately after radiation were deemed impractical; however, data was taken in times of as little as 10 minutes after irradiation. Since the samples were in film form, it was not possible to accurately calculate the number of spins per gram as would normally be done due to the asymmetric nature of the films. Instead, the general shape (height) of the radical spin count decay was observed (see Figure 4-14) In addition, some elevated temperature experiments were performed. Figure 4-15 through Figure 4-17 show data from these experiments. Figure 4-15 shows data from a 4 Mrad PC sample at room temperature. If one were to measure the entire radical lifetime, one would observe a typical exponential decay of the radicals. Since the line for the 4 Mrad sample is relatively linear, one can assume that the radical decay is occurring as only the initial portion of the exponential decay curve.

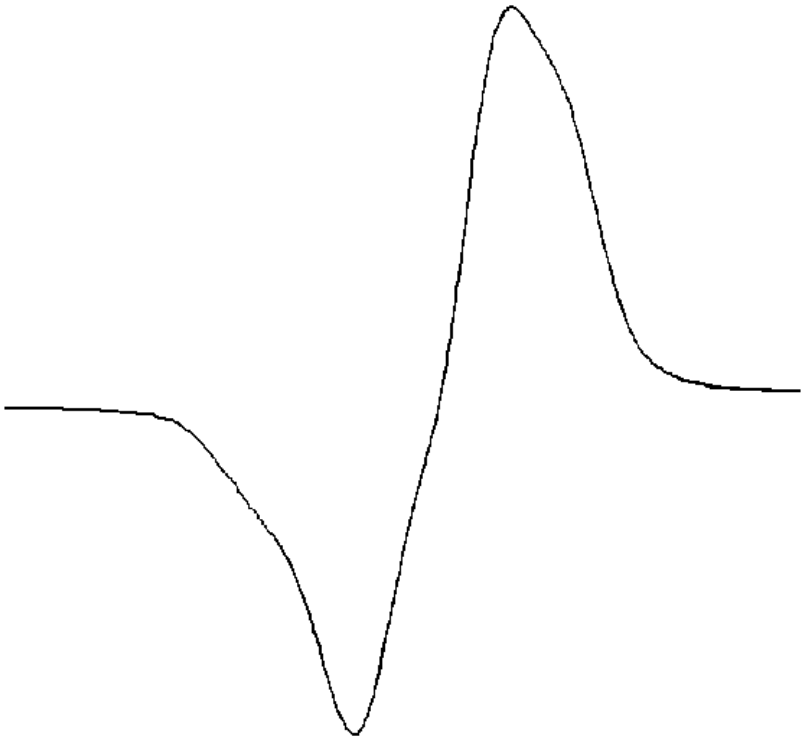

Figure 4-14 ESR experimental results from PC exposed to 10 Mrad. The resultant curve is typical of other doses, however, the peak height of the measured radical is reduced greatly in lower doses.

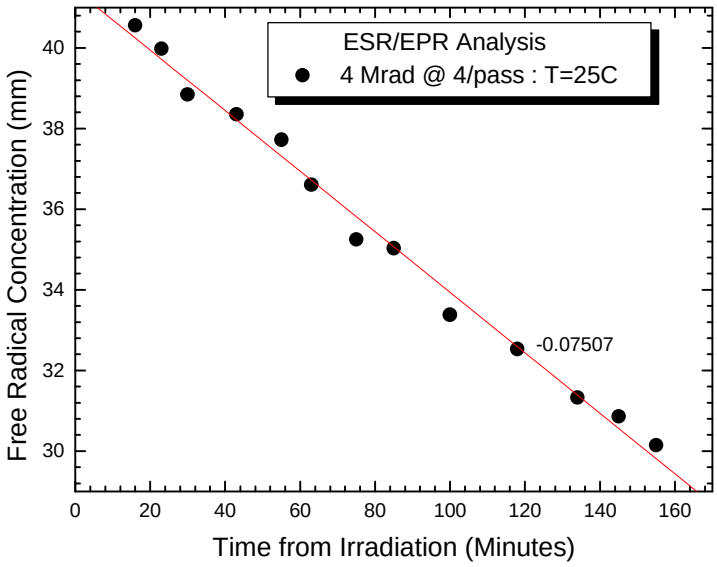

Figure 4-15 Data extracted from an ESR spectra at 25°C for a 4 Mrad PC sample. Relative free electron spin concentration is reported as proportional to the peak height, in mm.

In Figure 4-16, a sample was irradiated to 2 Mrad and is shows the beginnings of a shoulder in an exponential decay curve. These two figures indicate that higher doses produce large radical counts and that these radical counts exist at high concentrations for a very long time relative to any time delay experiment. This seems possible for the 2 Mrad sample, but since quantitative radical count data immediately following radiation exposure was logistically impossible, it is difficult to draw any definitive conclusions from these experiments that would help explain the time delay experiments. Learned from these experiments is that radical lifetime in PC is very significant - likely on the order of months for complete decay. It is therefore unlikely that radical decay has anything to do with the prior observed phenomena of endothermic relaxation peak dose-rate dependence.

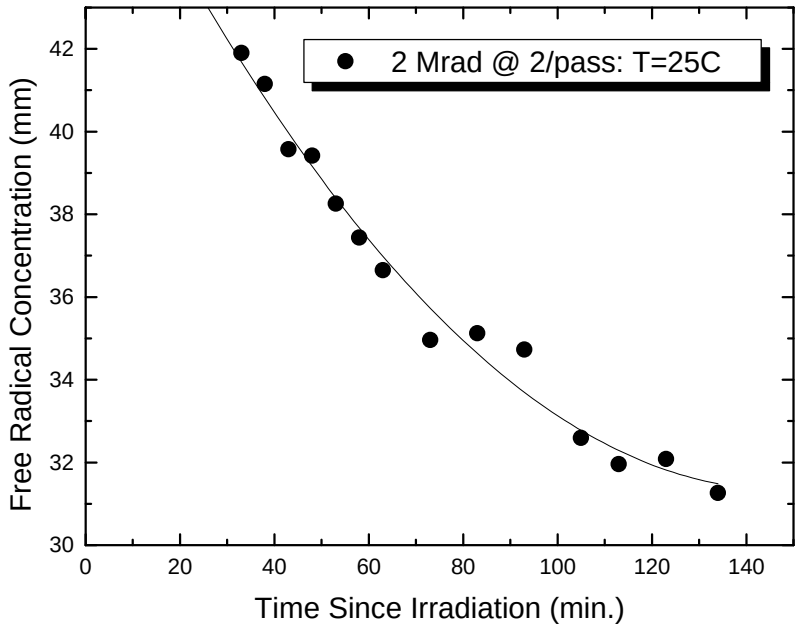

Figure 4-16 ESR peak height data for a 2 Mrad PC sample measured at 25°C.

Finally, an experiment to note the effect of temperature on radical decay was performed. A PC film sample was irradiated to 10 Mrad in 1 pass and then placed in the ESR apparatus. This particular ESR device had temperature control ability, so the temperature was raised to 120°C which took approximately 2 minutes. The sample was removed during heating and no significant radical decay occurred during this time. A radical count was obtained before heating occurred for a "zero time" value and then the sample was removed, noting it's approximate positioning in the sample cell. The sample was placed back in the cell and data taken until the radical count dropped to almost zero. Figure 4-17 shows data from this experiment.

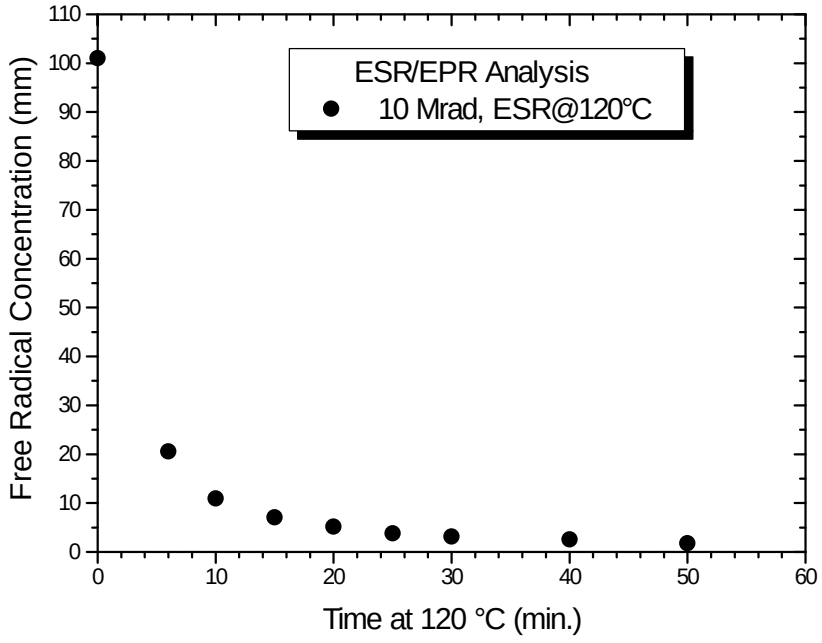

Figure 4-17 ESR data for a PC film irradiated to 10 Mrad and then heated in the ESR apparatus to 120°C. Data is plotted for relative radical concentration (measured as the height of the ESR trace in mm) as a function of time.

The failure of the ESR experiments to help explain the time delay enthalpic experiments still left a much larger question. If observable density changes could not explain the deaging phenomena then only one other possibility could exist to explain the deaging phenomena this being internal energy changes.

At this point, the central focus of the work shifted to the possibility that *endgroup creation* could be causing these enthalpic changes which manifest themselves in the observed deaging phenomena. For endgroup changes to occur, polystyrene would have to scission to some extent during irradiation in the electron beam accelerator. Recall that PS is considered in the literature to have a radiation chemistry of a "predominant crosslinker". Initially, experiments to prove PS was scissioning were based on the thought that if scissions were taking place, the Tg should drop since the molecular weight would decrease. The initial experiments along these lines involved low molecular weight samples of PS that would show a Tg depression if scissioning occurred due to a decrease in molecular weight. Figure 4-18 shows data from several monodisperse low molecular weight polystyrene standards.

Let us assume that one were to irradiate one of the lower Tg PS samples and the Tg increased by 10°C, for example. This would unfortunately reveal nothing conclusive or quantitative about the amount of scission that took place. In fact, one could not tell if scissioning took place at all. One method used to precisely quantify the amount of scission or crosslinking that occurs in a sample is to go through a Charlesby-Pinner analysis which will be outlined in the next section.

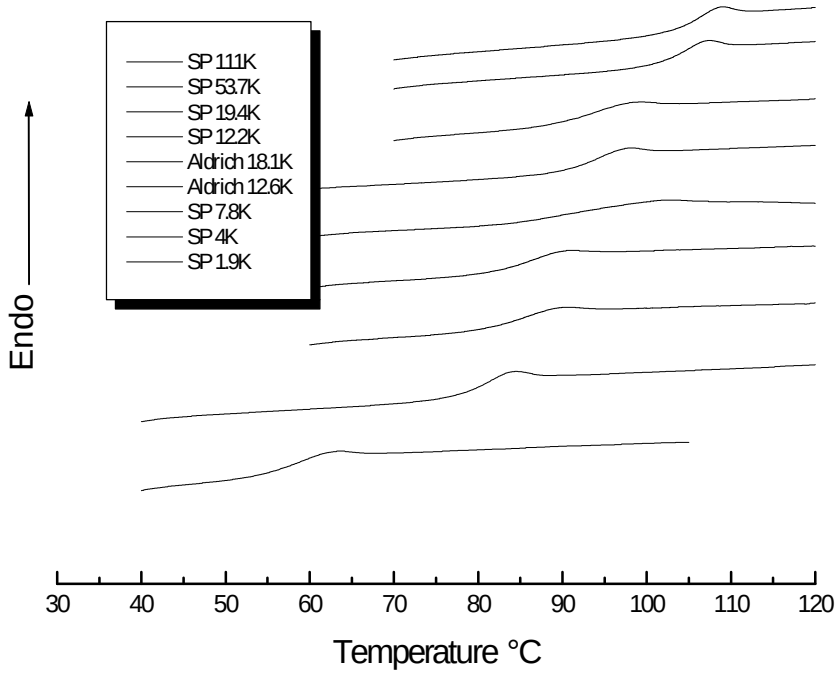

Figure 4-18 DSC traces of PS standards. Heating rate was 10°C/min.

4.3.4 G Value Determination

What follows is a classical to quantifying the degree of scission or crosslinking in polymers first proposed by A.Charlesby.[254-256] First some parameters and assumptions must be stated. A crosslink is to be considered as follows:

-A-A-A'-A-A-
|
-A-A-A'-A-A-

Where the -A-'s represent the chain of a polymer and each A' represents the crosslinking junction point. For purposes of this study, the following assumptions were made:

- Each crosslinked unit is considered to be tri-functional.
- Charlesby-Pinner Theory involves only networks which formed at these tri-functional junction points.
- Radiation induced crosslinks/scissions are randomly distributed.
- The propensity towards crosslinking/scission by a given unit is assumed to be independent of the absorbed radiation dose.

The number of crosslinked units per weight average molecule i.e. the crosslinking coefficient, δ, is then a function of the radiation dose, r, by:

$$\delta = q_0 u_2 r \qquad (4\text{-}2)$$

where:

q_0 = a constant representing the susceptibility of a polymer to crosslinking.
r = radiation dose in megarads
u_2 = weight average degree of polymerization (wu_2 = Mw: w = equivalent weight of chain unit)

q_0 can be related to G(x), the number of units crosslinked per 100 eV absorbed, by the following relationship:

$$1 \text{ Mrad} = 0.624 \times 10^{20} \text{ eV/mole} \qquad (4\text{-}3)$$

$$1 \text{ Mrad} = 10^6 \text{ rads} = 10^4 \text{ J/kg} = 10^4 \text{ gray} = 10 \text{ kGy}$$
$$(0.624 \times 10^{20} \text{ eV/mole w})(1.66 \times 10^{-24} \text{ moles/chain})$$
$$= 1.04 \times 10^{-4} \text{ w eV} \qquad (4\text{-}4)$$
per chain unit of molecular weight w

An energy absorption of 100 eV will yield:

$$100q_0/1.04 \times 10^{-4} \text{ w crosslinked units}$$

which, by definition is the G(crosslink) value, or G(x) for two molecular chains.

For a single crosslink:

$$G(x) = 0.482 \times 10^6 \, q_0/w \qquad (4\text{-}5)$$

The gel point (shown by Flory and Charlesby) occurs when:

$$\delta = qu_2 = 1.0 \qquad (4\text{-}6)$$

where q can be related to the radiation dose for gelation:

$$q = q_0 r_{gel} \qquad (4\text{-}7)$$

Therefore, (Equation 4-5) becomes:

$$\begin{gathered} q_0 u_2 r_{gel} = 1.0 \\ r_{gel} = 1/q_0 u_2 \\ w/q_0 = r_{gel} Mw \end{gathered} \qquad (4\text{-}8)$$

By (Equation 4-4), q_0 can be expressed in terms of G(x):

$$r_{gel} = 0.482 \times 10^6/G(x)wu_2 = 0.482 \times 10^6/G(x)Mw \qquad (4\text{-}9)$$

which can be written in terms of G(x):

$$G(x) = \frac{4.82 * 10^6}{Dg * Mw} \qquad (4\text{-}10)$$

where:

Dg = dose at which the gel first forms (in kGy)
Mw = weight average molecular weight

Equation 4-10 assumes:

1) No scission occurs
2) G(x) is not a function of molecular weight
3) Network formation occurs immediately upon irradiation
4) Dg can be precisely determined
5) Mw can be accurately determined

At this point, one needs an accurate way of determining Dg which is where the Charlesby-Pinner analysis and plot can be utilized.

Charlesby and Pinner showed that for initially random and random crosslinking polymers:

$$S + S^{1/2} = 2/\delta \qquad (4\text{-}11)$$

where:

s= soluble portion of the polymer
δ= crosslinking density

Because $\delta = qu_2$ and $q = q_0 r$

$$S + S^{1/2} = \frac{2}{q_0 u_2 r} \qquad (4\text{-}12)$$

Hence, a plot of $S+S^{1/2}$ vs. 1/r will have a slope = $2/q_0u_2$. To obtain the Dg value, one extrapolates to $S + S^{1/2} = 2$. Deviations based on other than random distributions have also been studied.[257]

If both crosslinking and scission occur it can be shown that:

$$S + S^{1/2} = \frac{1}{2}\lambda + (2 - \frac{1}{2}\lambda)\frac{Dg}{r} \qquad (4\text{-}13)$$

where:

λ = the ratio of G(s) to G(x)

and

$$G(x) = \frac{100 * Na}{Dg * Mw}\left(\frac{2}{4 - \lambda}\right) \qquad (4\text{-}14)$$

A y-axis intercept greater than 0.3 indicates significant deviations in accuracy because condition 1 in equation 4-9 is no longer valid.

Utilization of the above analysis was required for accurate determination of the radiation chemistry of polystyrene. Irradiated samples were extracted to constant weight as shown in Figure 4-19 and these final

weights used to compute the Charlesby - Pinner plot for 300k PS as shown in Figure 4-20. The Charlesby-Pinner plot shows a non-zero y intercept which indicates that some scission occurred in the irradiated sample. In this case, Dg was found to be 83 Mrad, G(x) = 0.02 and G(s) = 0.009 which means that roughly 1 main chain scission occurred for every 2.2 crosslinks. *Therefore, significant scission occurred when PS was irradiated in the electron beam in a 200 PPM oxygen atmosphere.*

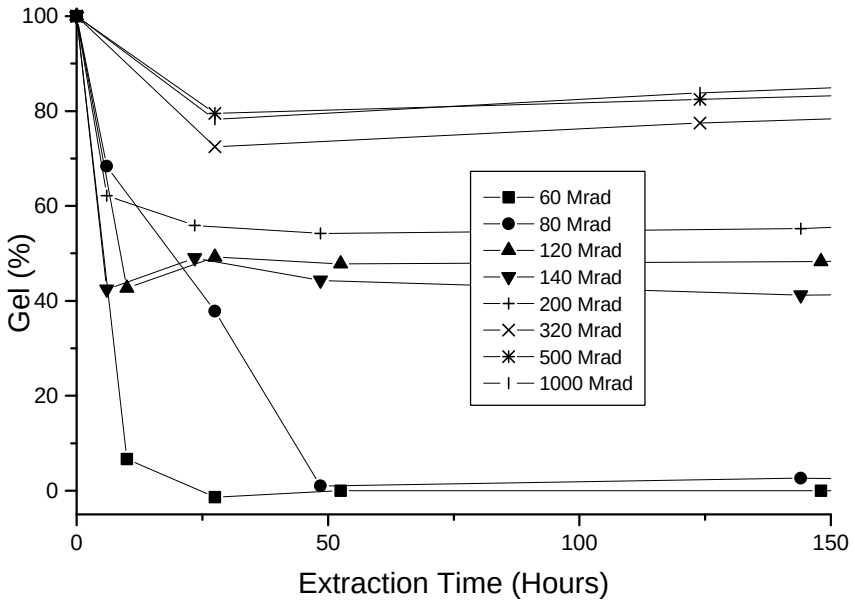

Figure 4-19 Apparent %gel as a function of extraction time and dose for 300K PS.

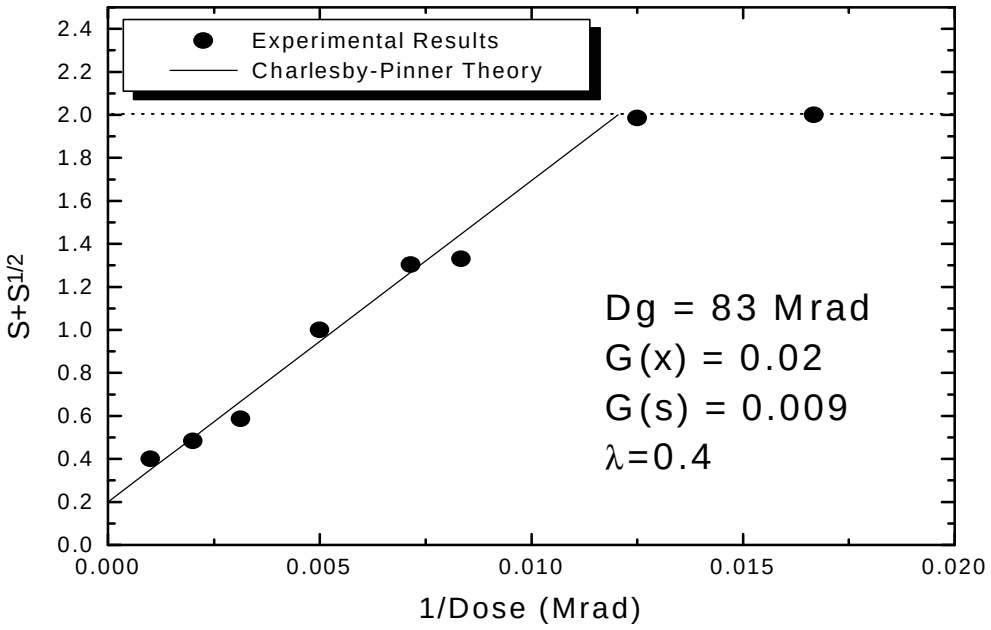

Figure 4-20 Charlesby-Pinner plot for 300K PS.

It has now been shown that the apparent reversal of physical aging with electron-beam radiation occurs in a purely scissioning polymer (PMMA), a predominately scissioning polymer (PC) and a 2.2:1 crosslinking to scissioning polymer (PS). The one type of polymer radiation chemistry that had not been studied at this point was a purely crosslinking polymer. Such a system (100% crosslinking) should, in principal, not produce any new endgroups when irradiated. If the endgroup creation hypothesis is correct, then such a polymer should not display the deaging phenomena when irradiated. What would be desired is a glassy polymer with a high Tg and a high concentration of double bonds. Unfortunately, no polymer of this type was available to the investigator, so samples of *cis*-polybutadiene were acquired and physically aged at -118°C for up to 500 minutes. Longer aging times were difficult to obtain as the DSC would have to have been unavailable for the entire aging period and large amounts of nitrogen would

have been consumed. Figure 4-21 shows data that an aging peak does appear in *cis*-PBD after 500 minutes at -118°C.

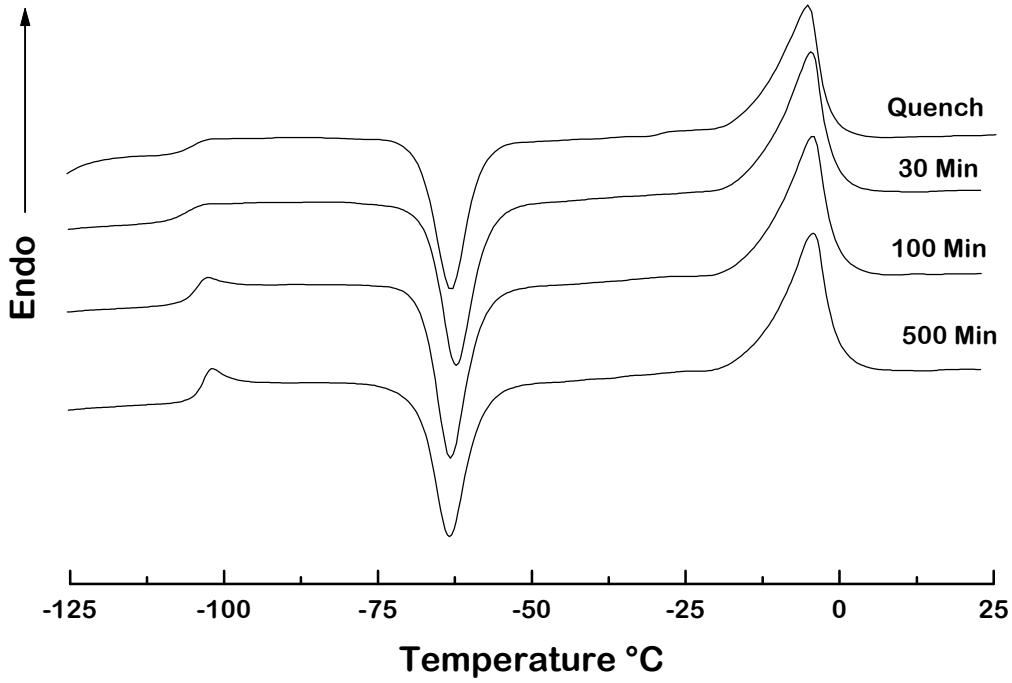

Figure 4-21 Physical aging of cis-polybutadiene at -118°C for the times indicated.

The next step was to show that this polymer did not have a y-axis intercept in a Charlesby-Pinner plot. The final step was to age a sample of polybutadiene in the DSC cell, irradiate the sample, then prepare the sample in the DSC sample pan, and to accomplish this without letting the sample heat above it's Tg (-103°C). This last experiment was not undertaken as a result of the Charlesby-Pinner plot for *cis*-polybutadiene having an intercept of 0.3 (see Figure 4-22). It would also be difficult to calculate reasonably accurate G values (due to the lack of precise molecular weight information) for this polymer since the sample came labeled from Aldrich "*cis*-polybutadiene, 98% Mw=2,000,000-3,000,000. In Figure 4-22, the indicated

G(x) and G(s) values are for the extremes of the molecular weight range as reported on the sample.

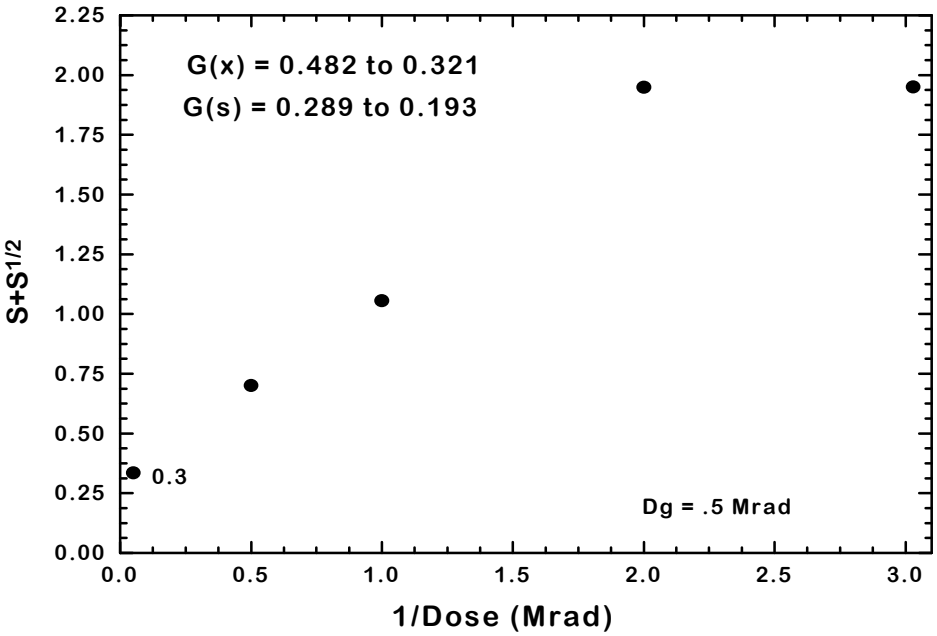

Figure 4-22 Charlesby-Pinner plot for *cis*-polybutadiene.

One final polymer was analyzed upon the suggestion of a well known pioneer of polymer radiation chemistry.[258] PET was selected to help finalize and round out this series of experiments. PET was favored because its low radical yield placed it (in terms of G values) somewhere between PS and PC. Hot pressed and quenched samples of amorphous PET were aged for 93 hours at 60°C and then irradiated. Due to the propensity of PET to crystallize, extreme care was taken to insure that overheating (and thus crystallization) of the polymer did not occur. Indeed, one can observe from Figure 4-23 that no reduction in the crystallization exotherm occurred with dose, which would happen if crystallization had occurred due to excessive heating during radiation. Although PET was recommended as another possible low-

scissioning polymer, it turned out to be the opposite, likely due to the presence of 200ppm oxygen in the electron beam radiation source. As shown in Figure 4-24, the Tg for PET appears to drop at higher doses, indicating that significant scission was occurring in this polymer. Interestingly, there were no corresponding increase in crystallinity, as one would tend to expect in a polymer that scissions when irradiated and is capable of crystallizing. The similarity of the PET molecular weight to PC, and the responding slightly higher dose requirement for endotherm reduction as a function of dose (see Figure 4-25) allows one to make a very rough estimate of a G(s) value for PC in the range of 1 based on the literature value of the G(s) for PET = 0.8.

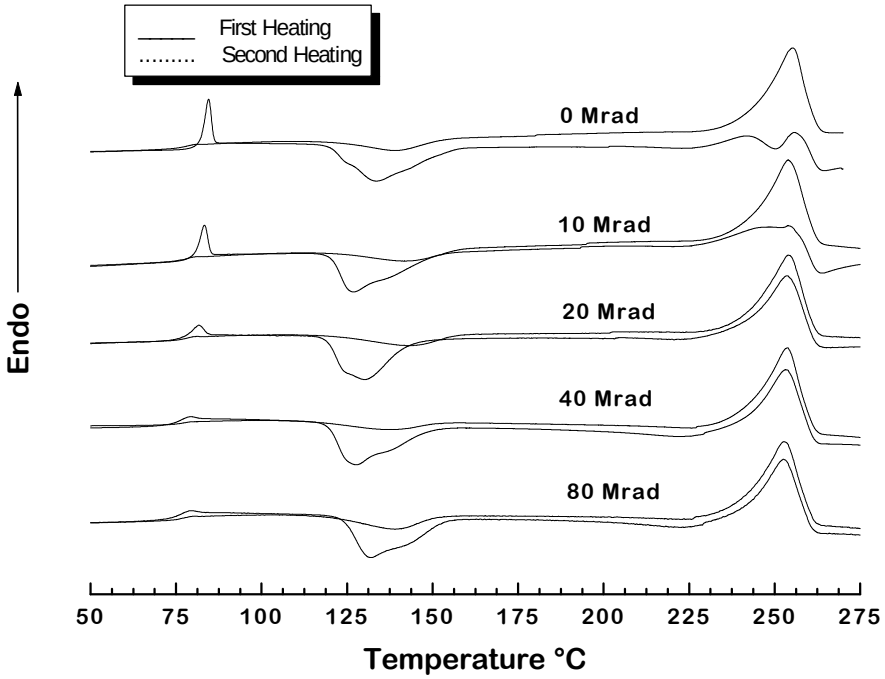

Figure 4-23 Full scan DSC traces for physically aged then irradiated amorphous PET films.

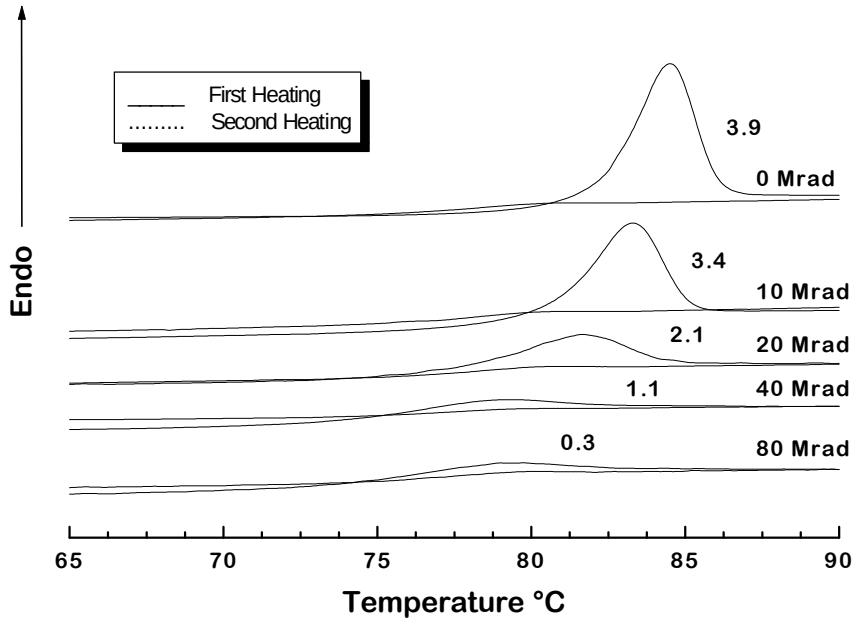

Figure 4-24 Blowup of Tg region of previous figure for PET. Numbers indicate the value of the endotherm peak area at Tg.

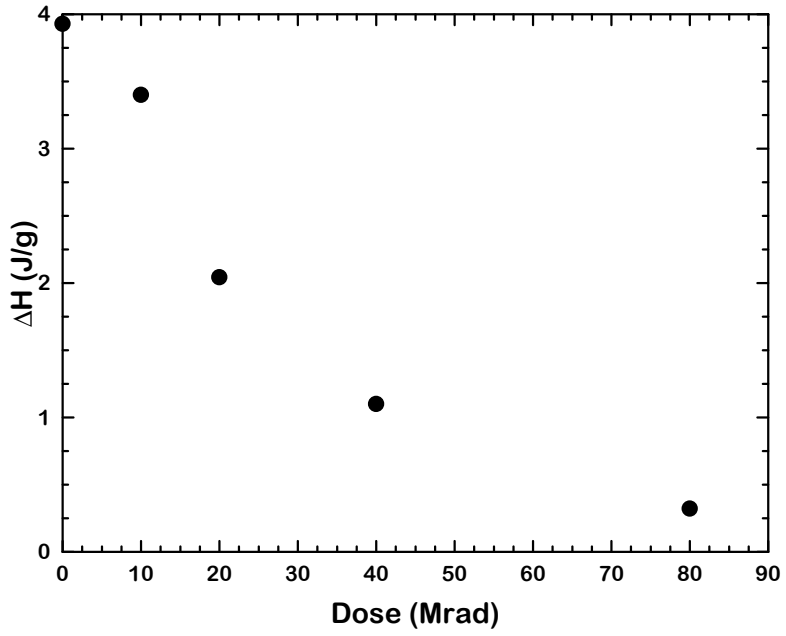

Figure 4-25 Endotherm value as a function of dose for physically aged and irradiated amorphous PET films.

4.3.5 G Value Correlation

We have distinctly shown that electron beam irradiation of aged polymers reduces the observed enthalpic relaxation peak. This reduction increases with increasing dose. It has also been shown that in higher G value polymers, this reduction occurs at lower doses than with low G value polymers (recall PS). Since there are only two possible final events that can occur, crosslinking or scissioning, then there may be a correlation with G(x) or G(s).

Possible correlations of G(x) or G(s) with radiation exposure would intuitively result in the following relationship. Since either G value (by definition) indicates the number of events per given unit of absorbed dose, more events (for correlation) would intuitively result in more thermodynamic changes. Therefore, for a polymer with a high G value, a low dose would be required for the enthalpy relaxation response. For a polymer with a low G value, a high dose would be required for the enthalpy relaxation response.

To summarize all our radiation chemistry and enthalpy relaxation data to this point for analysis and correlation, Table 4-1 is provided.

Table 4-1 Summary of G value and endothermic relaxation data for this study.

Polymer	G(x) range	G(s)	G value source	Dose for 50% endotherm reduction	Source for endotherm reduction data
PC	0	~1	est. by DSC	20 Mrad	This Study
PMMA	0	1.6	Polymer handbook[259]	13 Mrad	McHerron[252]
PS	0.02	0.009	Current work	200 Mrad	McHerron[252]
PET	~0	0.8	Polymer Handbook	25 Mrad	This study
cis-PBD	0.3-0.5	0.2-0.3	Current work	unknown	N/A

In Figure 4-26, the G(x) values are plotted as a function of dose required for reduction of 50% of the enthalpy relaxation endotherm. The 50% value was chosen arbitrarily but is representative of other values. Data representing PET is marked with an asterisk because it is uncertain whether it has a truly zero G(x) value. However, since its Tg dropped when irradiated in a similar fashion to that of PC, it is thought that its G(x) value is small or very close to zero. In Figure 4-26, there is no correlation between G(x) and the dose required for endotherm reduction. What this indicates is that crosslinking does not appear to significantly change the enthalpic state of the polymer - at least not to the point where enthalpic relaxation changes are observable. It would be desirable to have a 100% crosslinking polymer to prove this point definitively; however, the four data points shown do strongly indicate that there is no correlation with crosslinking.

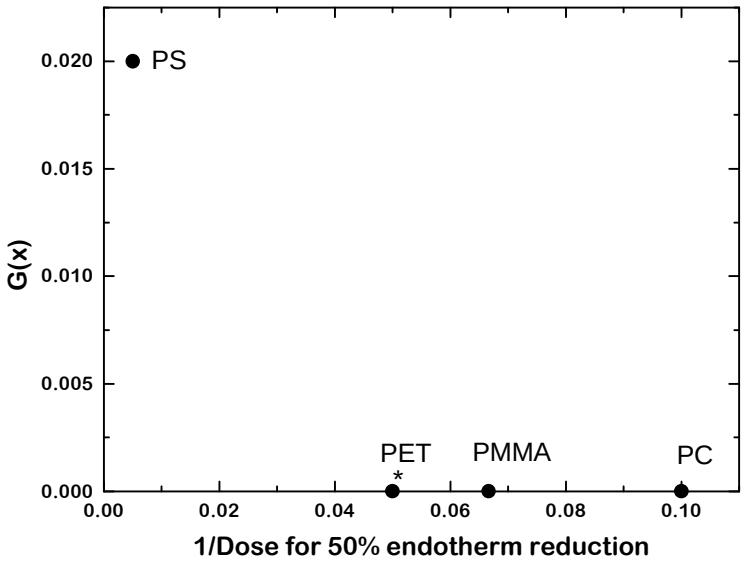

Figure 4-26 Physical aging endotherm reduction correlation with G(x).

In Figure 4-27, G(s) values for each polymer are plotted vs. 1/Dose for 50% reduction in the enthalpy relaxation peak. PC is marked with an asterisk because its G(s) value was not directly calculated. One can see the strong correlation shown on this plot thereby supporting the endgroup creation hypothesis. On a thermodynamic level, this indicates that the resultant observed enthalpic changes in these polymers manifest themselves through internal changes principally caused by the creation of these new endgroups. New endgroups would also increase the disorder (entropy) of the system which would drive the system towards a higher internal energy state at constant volume.

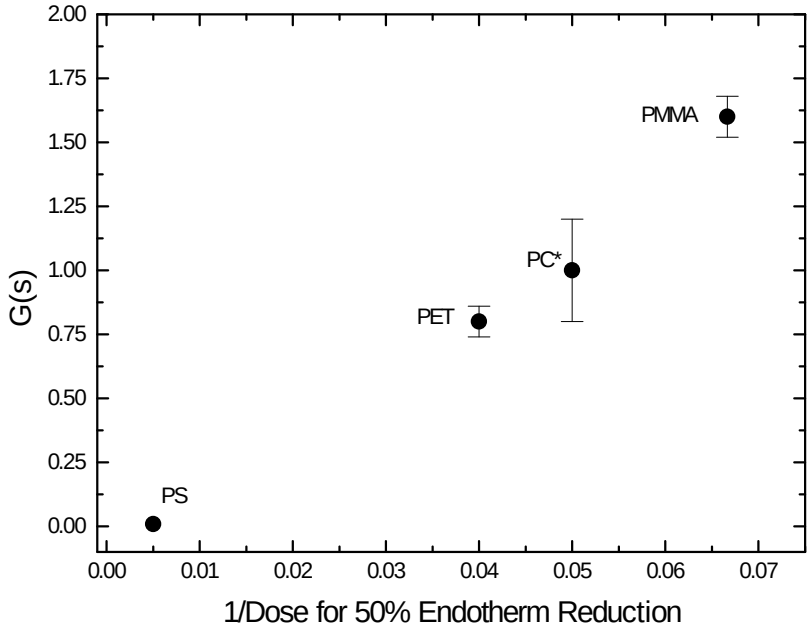

Figure 4-27 Physical aging endotherm correlation with G(s). Dose in $Mrad^{-1}$. Error bars indicate the range of G(s) values based on radiation chemistry data from the literature[259] and from this work.

4.4 Summary/Conclusions

This work has served to further investigate and clarify previous work performed in the area of irradiating physical aged glassy polymers. A phenomena was observed for aged amorphous polymers exposed to electron beam irradiation. An apparent reversal of physical aging through enthalpy relaxation was observed. This "deaging" does not involve heating above the glass transition temperature of the polymer. It was found that there was not an expected reduction in density that accompanied this deaging phenomena. It was further observed that irradiated films did not regain their enthalpy relaxation aged status in the time scale that would normally be associated with any diffusion of gases out of the films. Indeed, it was found that this deaging phenomena had a strong correlation with the radiation G values; i.e. low G(s) and G(x) value polymers such as polystyrene took a much higher dose to deage than PMMA or PC. It was concluded through experimental determination of G values associated with scission and crosslinking [G(s) and G(x)], that there is a very strong correlation of this phenomena with G(s) and little, if any correlation with G(x) indicating that the number of endgroups play an important role in entropy and therefore can play a principal role in the internal energy state of the glassy polymer.

The ramifications of this study to the mechanical behavior of amorphous polymers used in environments where they are exposed to radiation are of interest. Suppose a physically aged amorphous polymer is irradiated with no corresponding change in volume (as we have shown). Normally, one would expect an amorphous material that does not display an enthalpic aging peak to be more ductile than one that shows the peak. However, one would also expect an amorphous material with a higher density to behave in a more brittle fashion than the same material with a lower density (more free volume). How will such a system behave if it then

undergoes deformation? DSC measurements would predict more ductile behavior relative to the non-irradiated and aged sample but density measurements would predict a more brittle behavior. Predictions of such behavior based on enthalpic or volumetric data alone, however, are further complicated by the issue of main chain scission as reductions in molecular weight would also be expected to lead to more brittle behavior.

Finally, the most significant conclusion reached in this work is the important role internal energy can play in physical aging. It is typically observed in aging studies that enthalpic changes are a least proportional to volumetric changes due to small internal energy changes. In this work, it has been shown that this assumption is not always valid and that in this study, when chain scission occurs, internal energy changes can dominate the changes in the enthalpic state of polymers and are not accompanied by significant density changes.

5 Structure-Property Relationships in Electron Beam Irradiated Linear High Density Polyethylene Extruded Tubular Films Having a Well Defined Stacked Lamellar Morphology

5.1 Introduction and Background

In this chapter, characterization of irradiated linear polyethlyene having a well defined stacked lamellar morphology is presented. The goals of this work were to irradiate these polyethlyene films and then to measure water permeability of the films - and to explain why any observed changes occur via standard characterization techniques. In addition, use of these materials as precursors for later development into membrane battery separators dictate that mechanical property changes with irradiation must be investigated along with tests specific to these types of materials. The affects of annealing these materials was also investigated. The reader should note that this chapter will not entail an exhaustive study on the level of the preceding two chapters but will focus on a few specific areas involving the goals outlined above as a preliminary investigation for the response of this oriented material to radiation. Inspiring this study are observations by several workers is which certain polymers, when irradiated, have shown an increase in their barrier properties[260] or in some cases, display an increase in crystallinity and a corresponding decrease in permeability to various gases.[261] Interest in the properties of irradiated polyethylene has increased in recent years with increasing utilization of polyethylene in applications from medical sterilization, solvent barriers, and membrane applications.

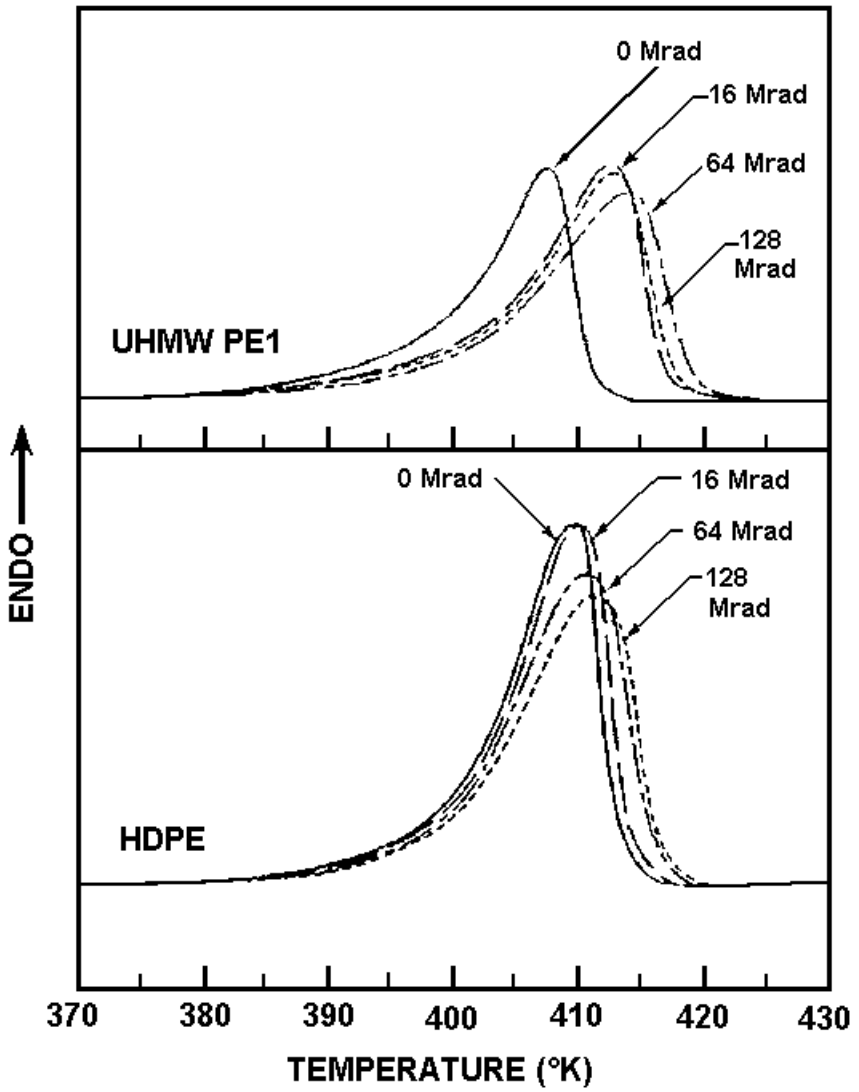

Figure 5-1 DSC traces for two different irradiated linear polyethylenes. UHMW PE1 had Mw = 3 x 10^6 g/mol and the HDPE sample had Mw = 2 x 10^6 g/mol.[261]

From the literature in Figure 5-1, DSC data from irradiated ultra high molecular weight (UHMWPE) and high density (HDPE) polyethlyenes are shown as taken from Bhateja.[261] Neither polymer was processed in a manner

which would induce orientation. For both polymers, an increase in both the melting peak area and melting point is shown (although more dramatic increases were observed in the UHMWPE sample than the HDPE sample). In this study, the UHMWPE had a Mw = 3 x 10^6 g/mol and the HDPE had Mw = 2 x 10^6 g/mol. Higher molecular weight linear polyethylenes tend to have lower percent crystallinity due to the presence of increasing restrictions on the chains primarily due to the increase of entanglement density with increasing molecular weight. Entanglements may not only restrict the number of crystals that may form, but also prevent the chains from forming perfect crystals by introducing physical restrictions to crystallization. In addition, between lamellae are tie chains that are prevented from crystallization by physical restrictions. In this case the authors conclude based on the DSC data, that scission of some of the amorphous tie chains then allowed them to then crystallize and that the resultant increase in lamella thickness was responsible for the observed increase in melting point and peak area.

In addition, it is well known that gas transport occurs for the vast majority of semicrystalline polymers in the amorphous phase. Increasing crystallinity effectively increases the path length for diffusion, and therefore increases the overall barrier properties. While increasing crystallinity may or may not be desired in considerations of other polymer properties, it is well known that for polymers with a higher crystalline density than amorphous density, increasing the percent crystallinity is one way to decrease its permeability. Figure 5-2 schematically shows detail of a process involving ionizing radiation that results in an increase in crystallinity. The first step is for ionization and excitation to occur in the presence of oxygen and water vapor (A) which will result in scission of some amorphous polymer. Statistically with respect to consideration of which chains will scission as a

result of ionizing radiation, a tie chain under strain will preferentially scission and in (B) one can see that that chain is no longer restricted by the lamella which will then allow it to relax and crystallize (C). Although this illustration shows that the crystallization of these chains may result in an epitaxial structure, it should be noted that free amorphous chains which have scissioned and are not restricted by lamella could also result in non-epitaxial crystallization. As one can see from the data shown earlier in Figure 5-1, it is advantageous to have higher molecular weight molecules for this process to occur with any significance, for in general, lower molecular weight linear polyethylenes will tend to not only have a higher percent crystallinity, but will possess more perfect crystals and fewer entangled tie chains capable of crystallization once scissioned. In the case addressed above (again recall Figure 5-1), the ultra high molecular weigh polymer had a level of crystallinity equal to 35% before irradiation, much lower than that typically seen for more conventional linear polyethylenes of lower molecular weight.

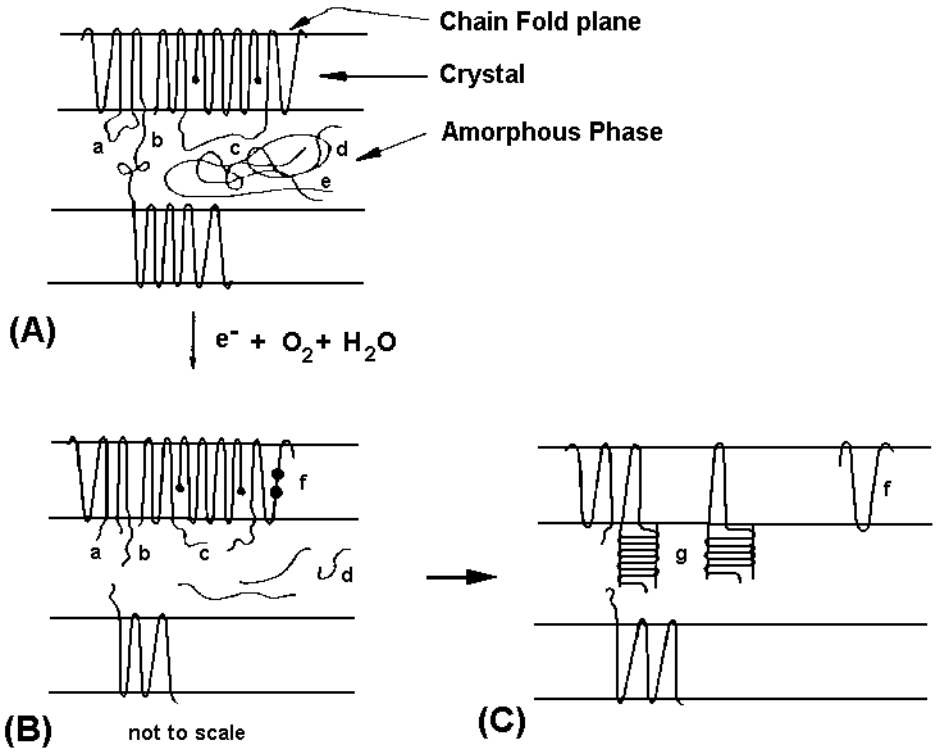

Figure 5-2 Schematic representation of the process of chain scission of amorphous interlamella tie chains and their subsequent crystallization. [261]

Another way that the process of ionizing radiation can influence barrier properties of irradiated polymers is through crosslinking. Figure 5-3 shows data from a study focusing on the CO_2 permeability in various films of both amorphous and semicrystalline polymers. Note that in this study, the polypropylene sample was the only polymer to *increase* its permeability to CO_2, likely resulting from PP's tendency to predominately scission with little crosslinking when irradiated.[260]

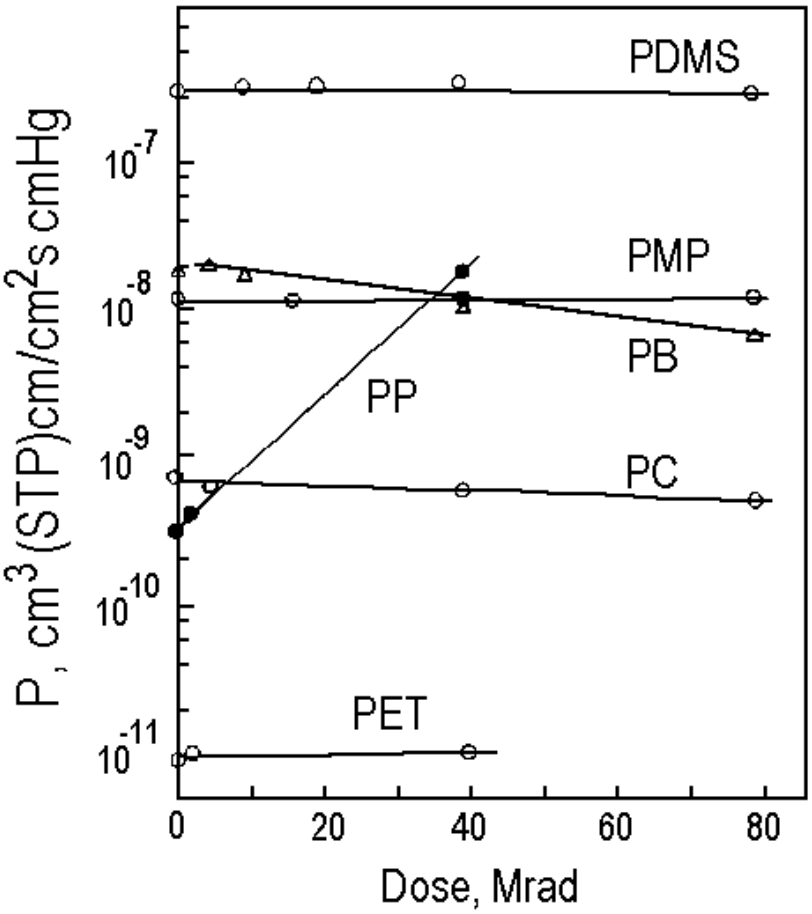

Figure 5-3 The effects of irradiation dose on the permeability coefficients of CO_2 gas through selected irradiated polymer films at 35°C. Data for polydimethlysiloxane (PDMS), 1,2-polybutadiene (PB), poly(4-methylpentene-1) (PMP) polypropylene (PP), polycarbonate (PC), and polyethyleneterephthalate (PET) is shown.[260]

Curing a functionalized oligomer into a network via irradiation also increases in barrier properties as shown in Figure 5-4 and Figure 5-5. In this example, water permeability was shown to decrease with increasing EB dose for all the materials tested which were commercially available materials (Sartomer C-2000, Celrad 3500, Photomer 6019, T4EGDA, and Photomer 5018). Recall from Chapter 3 in this dissertation that these materials are designed to crosslink (i.e. "cure") through the addition of radiation sensitive side and endgroups. In this case, the *decrease* in water permeability is due to

further crosslinking with dose which results in additional restrictions on polymer chain motion and an increase in Tg due to the lower molecular weight between crosslinks in the resultant network which was formed when the system was irradiated. None of these materials are semicrystalline.

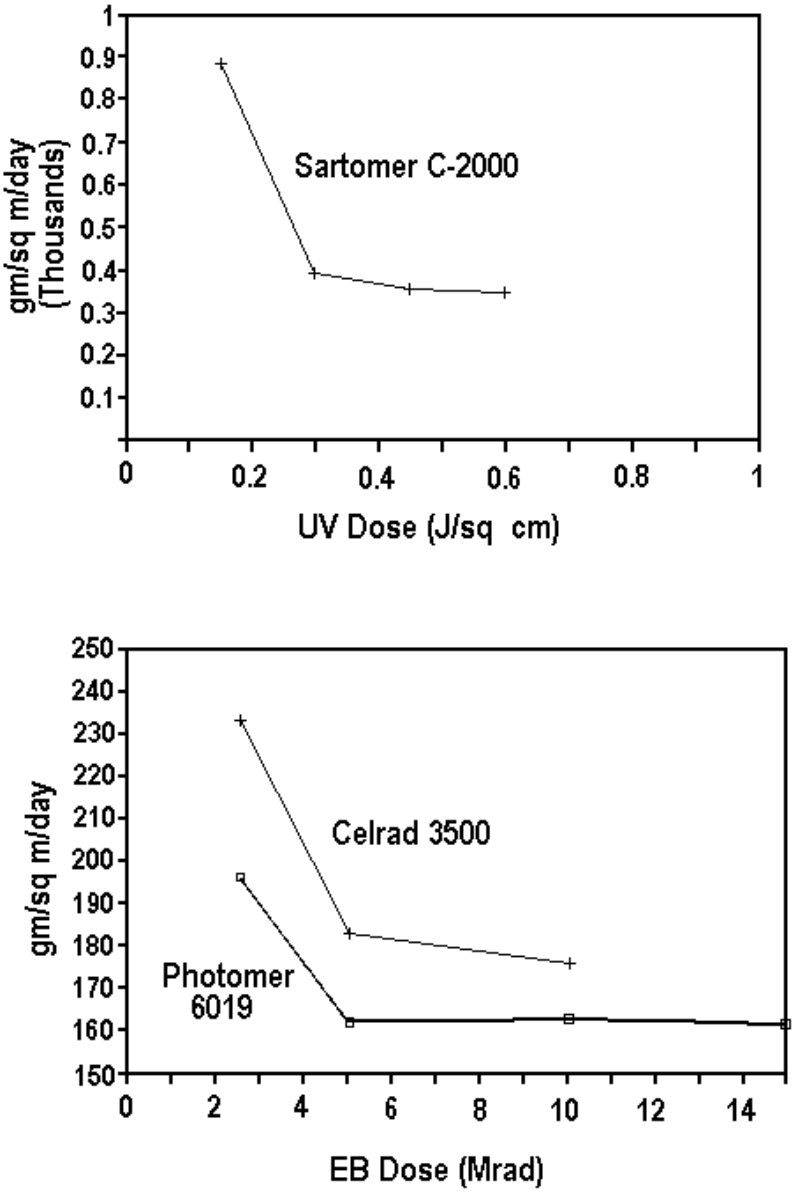

Figure 5-4 Water permeability as a function of dose of EB cured oligomers.[262]

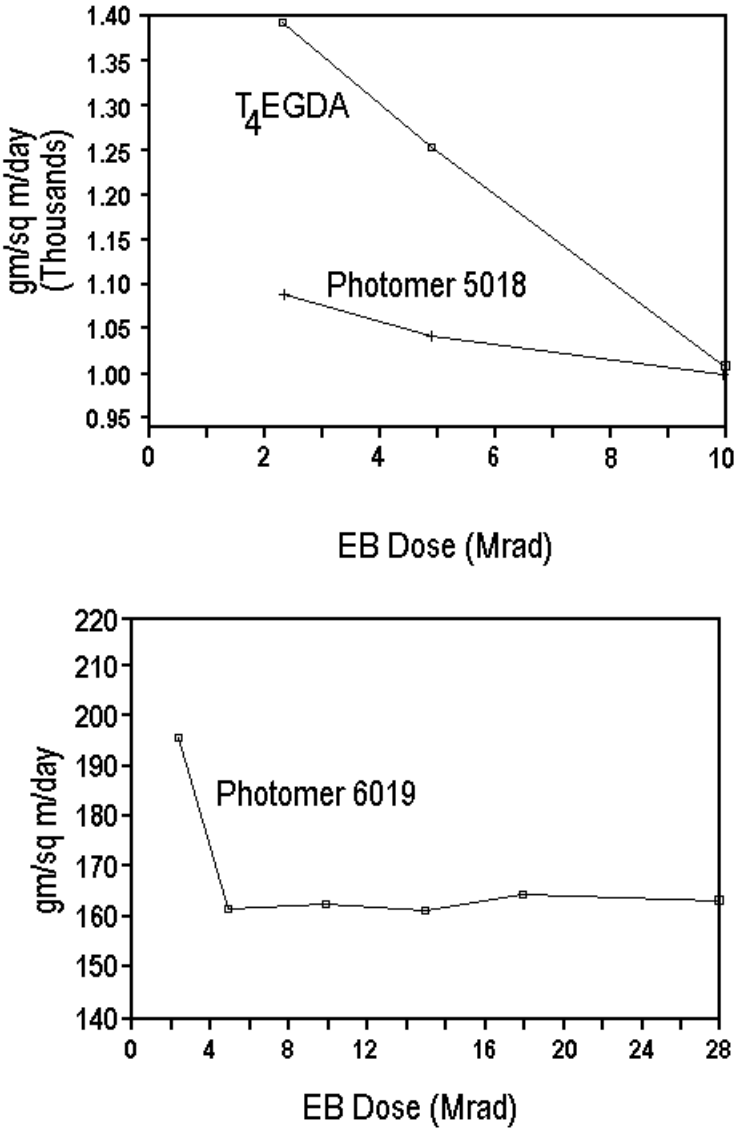

Figure 5-5 Water permeability as a function of dose of EB cured oligomers.[262]

In the previous two examples, one can see how completely different morphological changes (further crystallization or crosslinking) can lead to changes such as permeability. In the following study, permeation changes in irradiated polyethlyenes will be presented along with examination of the role both crosslinking and/or scission play in this specific case.

5.2 Experimental

5.2.1 Materials and Sample Preparation

For this study, a commercial high density linear polyethylene (HDPE) resin was melt extruded through an annular die with a blow-up ratio of one resulting in essentially uniaxially oriented extruded tubular films. This polymer resin has been well characterized in previous work[263] and it was shown to have a Mn of 14,600 and a dispersity ratio of 10.3. The process which produced these films did not result in any visually observed fibril nuclei by TEM studies over a wide range of processing conditions and levels of orientation. Two films were produced by Hoechst Cellanese by production through the process outlined in Figure 5-6 under two slightly different processing conditions which resulted in different levels of orientation. The following table compares the processing conditions for the two films.

Table 5-1. Comparison of the processing conditions for the two films utilized in this study

Sample	Melt Temp(°C)	Quench Height (inches)	Air Flow Rate in Air Ring	Line Speed (ft/min.)	Die Gap (inches)
Film A	195	1.75	medium	60	0.07
Film B	185	1.50	high	80	0.14

As indicated, these two films will be designated “film A” and “film B” in this study. Due to a lack of sufficient material, film A was only utilized only for DSC and mechanical testing to see what general kinds of changes occur in these materials when irradiated. A larger sample of film B was obtained for the full study and focus on the second material will be the emphasis of this chapter. While there is some differences in the level of crystalline orientation of the two films A and B, it will be shown, in fact, that these two films are

very similar in terms of radiation response, level of crystallinity, orientation, and morphology.

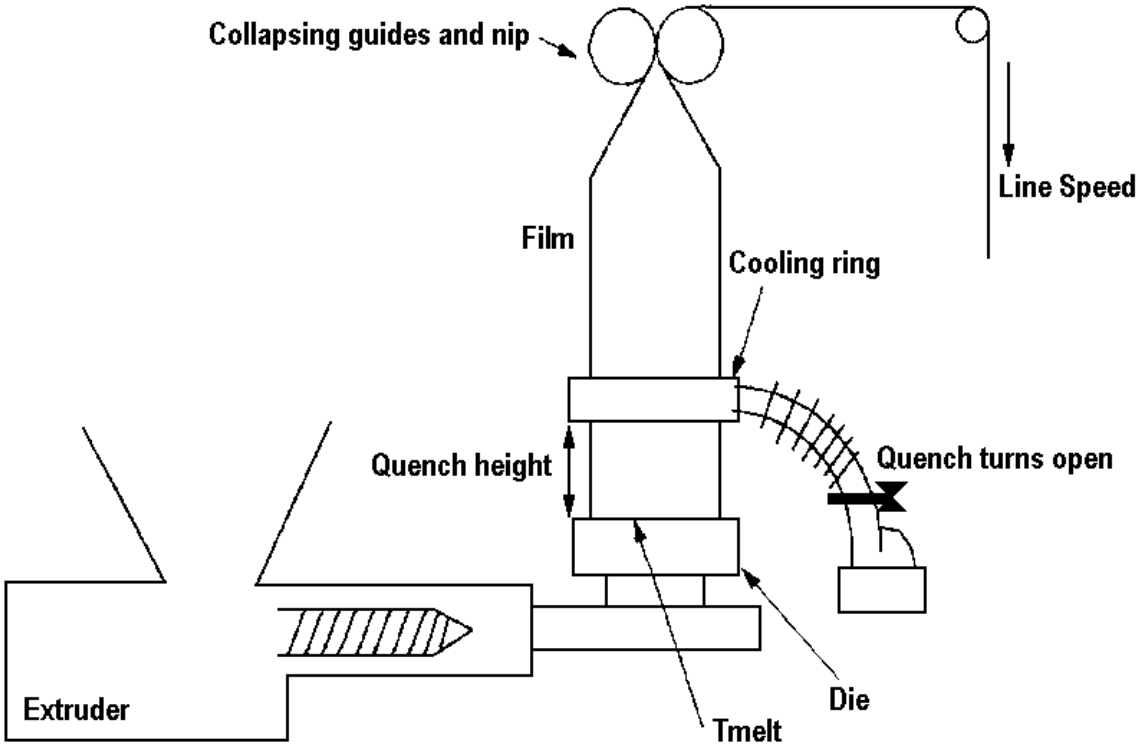

Figure 5-6 Process schematic for production of the tubular polyethlyene tubular films which result in a stacked lamella morphology showing all processing variables. A previous study fully analyzed these variables to determine which ones have the largest effect on the orientation behavior of the film.[263]

Figure 5-7 shows the morphology for film B. It is noted that this morphology is nearly identical to film A which has been previously characterized[263]. Note that the stacked lamella are nearly perpendicular to the machine direction resulting in a well defined morphology. The procedure for characterizing this material by TEM will be outlined in a following section and the effects of radiation will be discussed as well. It is important, though that the reader understand specifically what kind of morphology these films possess which will help understand some of the properties of these materials.

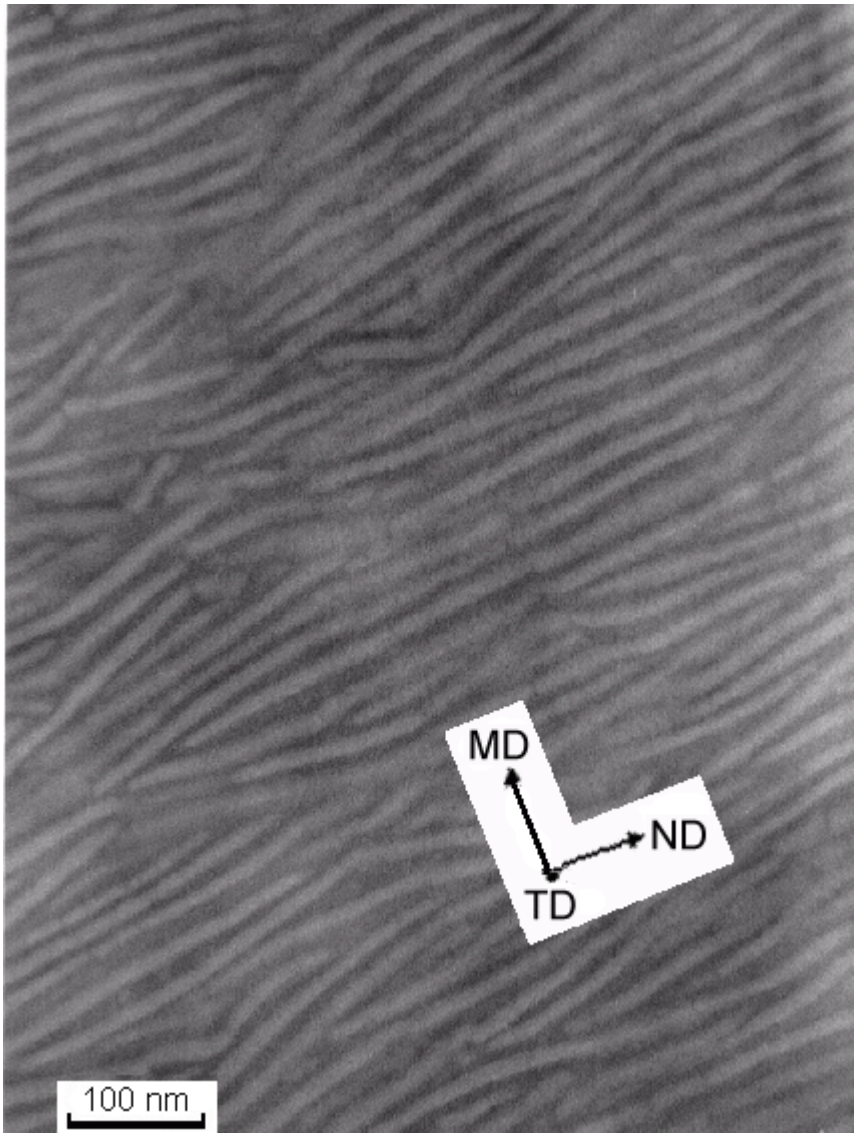

Figure 5-7 Film B 0 Mrad 187,500x. Scale indicated.

These 1.0mil thick films were irradiated at doses up to 80 Mrad and then tested to determine what, if any changes in their morphology, thermal properties, level of crystallinity, mechanical properties, and water permeability had occurred.

The morphological features and state of orientation in these films were examined by transmission electron microscopy (TEM), high resolution

scanning electron microscopy (HSEM), SAXS, WAXS, DSC, FTIR dichroism, and tensile properties.

5.2.2 Radiation Exposure

Films were cut to approximately 4 inches square and irradiated using an Energy Sciences (ESI) CB150 Electrocurtain as the radiation source under a nitrogen blanket containing 200ppm oxygen and a beam voltage of 175 keV. Samples were irradiated at no more than 10 Mrad per pass to avoid excessive heating. Doses utilized were 0.5, 1, 2, 4, 5, 6, 10, 20, 40, and 80 Mrad. Samples were exposed to air between passes if more than a total dose of 10 Mrad was required.

5.2.3 Thermal Analysis

A Perkin Elmer DSC 7 system was used to determine the melting peak temperatures and the approximate degree of crystallinity by calculation of the area under the melting peak. Baselines were taken before every experiment and the aluminum sample pans used for the baseline runs were used for the experimental runs. The heating rate was 10°C/min. In some cases multiple runs of similar material were performed to determine the degree of experimental error for ΔH and the melting peak temperature. Fractional crystallinity (mass fraction) X_c was calculated based on DSC data according to the following equation:

$$X_c = \frac{\Delta H}{\Delta H_0} \tag{5- 1}$$

where ΔH_0 is the specific heat of melting of an ideal crystal for which the commonly accepted value of 293 J/g was used.[263]

5.2.4 Wide Angle X-ray Scattering

Wide angle X-ray scattering (WAXS) experiments were performed in a Phillips table-top X-ray generator model PW1170 equipped with a standard vacuum sealed Warhus photographic pinhole camera. WAXS is often capable of providing the complete orientation distribution for the crystalline phase, however, orientation functions for the two films were not calculated. WAXS was primarily utilized in this study to qualitatively assess if any new crystallization had occurred after irradiation and if so, what corresponding changes in c-axis crystal orientation may have taken place.

5.2.5 Small Angle X-ray Scattering

Small angle X-ray scattering (SAXS) experiments were conducted to detect the presence of any lamella thickening generation (again, due to tie chain scission and subsequent crystallization). These experiments were performed using Ni filtered Cu K_α radiation (λ=1.54A) on a compact Kratky camera with slit geometry, equipped with a Braun position sensitive detector. After corrections for parasitic scattering and absorption were made, the scattering curves were normalized to the main beam intensity and sample thickness. The results were plotted against the angular variable, s. where

$$s = 2(\sin\frac{q}{2})/l \qquad (5\text{-}2)$$

where theta is the radial scattering angle.

5.2.6 Transmission Electron Microscopy

Samples of film B were treated with 99% chlorosulfonic acid at 60°C for six hours. These samples were then washed with sulfuric acid and water, dried, and embedded in a low viscosity Spurr epoxy which was cured at 70°C

for 12 hours. Following embedding and curing, the sample was microtomed at ambient conditions. Thin sections were then examined by a Philips EM-420 scanning transmission electron microscope operated in transmission mode at 100 kV. Samples for the HSEM experiments were coated with a thin layer of gold and examined by the same device operating in the scanning mode at 100 kV.

5.2.7 Tensile Analysis

An Instron Model 1122 tensile testing machine was utilized for determination (in both transverse-TD and machine direction-MD) of modulus, toughness, yield stress and strain and stress and strain at break. Uniform 10mm dogbone samples were cut in MD and TD from the 1 mil films and a crosshead speed of 12.7mm per minute was used for all samples. A minimum of seven samples to a maximum of 12 samples were tested at each condition.

5.2.8 Permeability

Water vapor permeability experiments were performed by Eastman Chemical in Kingsport Tennessee utilizing a Mocon W600 water permeability test apparatus. Room temperature testing followed ASTM procedure number F1249. Two to three samples from each radiation dose were utilized in the permeation testing and an average water permeability at room temperature reported as a function of dose.

5.2.9 Linear Dichroism

One method commonly utilized for measuring orientation is linear dichroism. This method can often be employed to detect the degree of molecular orientation in a specific phase or component for multiphase or multicomponent systems.[264] The basic principle of dichroism is that an

oriented sample is subjected to plane-polarized light at a given frequency in two perpendicular directions which can yield different absorbances. The sample must have chromophore with an known association with the chain axis, and must absorb in the infared region. Ultimately, the orientation of the chains with respect to the reference axis is desired. In order to accomplish this, first the dichroic ratio, D, is calculated by:

$$D = \frac{A_{\parallel}}{A_{\perp}} \tag{5- 3}$$

Where $A_{||}$ and $A_{\perp}$ correspond to the IR absorbances resulting when the sample is exposed to polarized IR energy parallel and perpendicular to a specific reference axis, that is often the orientation or deformation axis. $A_{||}$ and $A_{\perp}$ are calculated by the Beer-Lambert Law:

$$A = \log_{10}\left(\frac{I_0}{I}\right) = -\log_{10}(T) \tag{5- 4}$$

Where I_0 is the intensity of the incident IR beam, I is the transmitted intensity, and T is the transmittance. The dichroic ratio of the absorbing chromophoric groups is quantitatively related to the state of orientation for the chain axis through the second-moment average, Hermans' orientation function, f which is defined as:

$$f = \frac{3 < \cos^2 \beta > -1}{2} \tag{5- 5}$$

where β is the angle between the reference axis and chain axis. The dichroic ratio, D, is related to f by:

$$f = \left(\frac{D_0 + 2}{D_0 - 1} \right) \left(\frac{D - 1}{D + 2} \right) \tag{5- 6}$$

where D_0 is defined as $2\cot^2\alpha$ and α is the angle between the transition moment of the chromophoric group and the chain axis. For the case of polyethylene, the CH_2 rocking vibrations in the crystalline phase give absorptions at 720 cm^{-1} and 730 cm^{-1} which are associated with the b axis and a axis, respectively. For these two transition moments, $D_0=\infty$ which simplifies Equation 5-6 to:

$$f = \frac{D - 1}{D + 2} \tag{5- 7}$$

Once the orientation functions for the a and b axis are calculated, then f_c can be calculated (assuming orthagonal unit axes) by:[263]

$$f_c = -(f_a + f_b) \tag{5- 8}$$

In this work, a Nicolet 510 FTIR spectrometer with a DTGS KBr detector was utilized to measure the absorbances at 720 and 730 cm^{-1} with 32 scans per sample at 4 wavenumber resolution with a laser frequency of 15798.0 cm^{-1}, mirror velocity of 1.5825, and Happ-Genzel Apodization.. The IR beam was polarized with a Cambridge Physical Sciences TGP225 polarizer.

5.3 Results and Discussion

5.3.1 Mechanical Properties

In order to investigate the effect of radiation on the mechanical properties of each film, a series of tensile Instron experiments were conducted with samples of both machine direction (MD) and transverse direction (TD). MD and TD directions were tested in order to show what property differences result from the anisotropic stacked lamellar morphology along with the effects of radiation on those properties.

To illustrate the dramatic differences in behavior in the two directions, Figure 5-8 and Figure 5-9 show typical raw data from MD and TD testing. These figures illustrate not only the contrast between the two testing directions but the dramatic effect of ionizing radiation. Note that the TD direction seems more dependent on radiation than the machine direction.

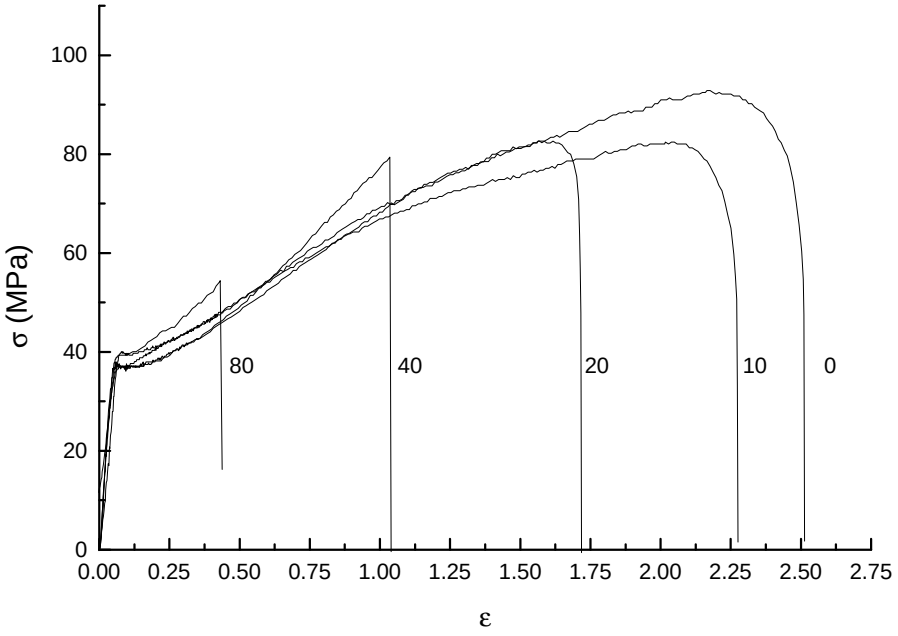

Figure 5-8 Typical stress strain data for machine direction MD tests. Numbers indicate the E-Beam dose the sample received in Mrad.

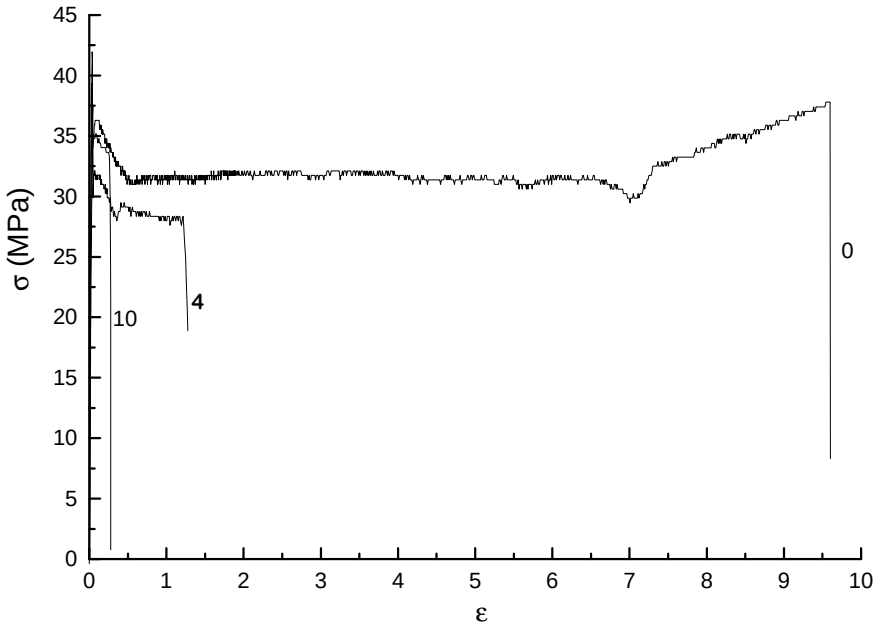

Figure 5-9 Typical stress strain data for transverse direction tests. Numbers indicate the E-Beam dose the sample received in Mrad.

The first series of experiments were performed on the material referred to earlier as film A. The following figures show data from these experiments. The results indicate that a slight maximum in machine direction toughness and machine direction tensile modulus at 2 Mrad. While these results seem to indicate a maximum exists at low dosages, no other maximum was observed for MD or TD properties in film A. Further dosages beyond 10 Mrad have a dramatic degradation effect on both tensile modulus and toughness.

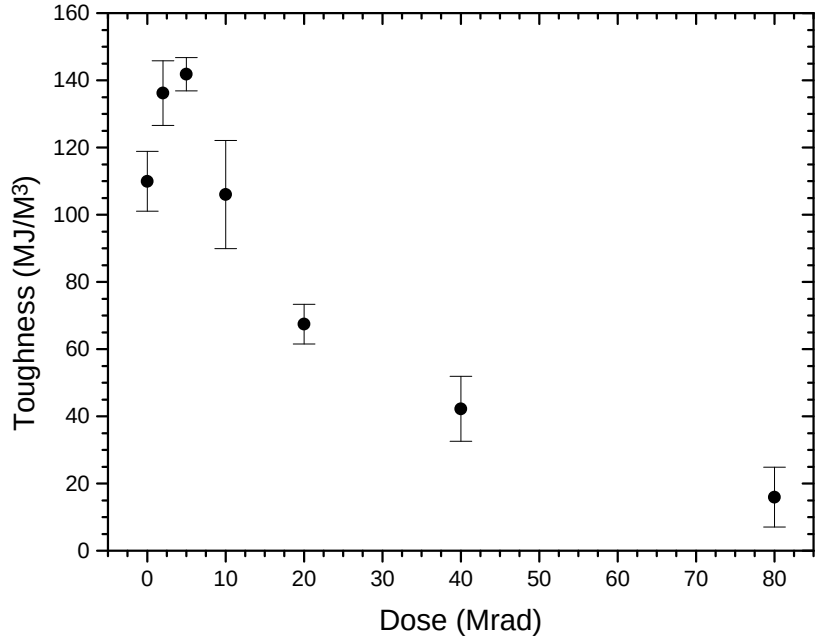

Figure 5-10 PE Film A machine direction toughness as a function of dose.

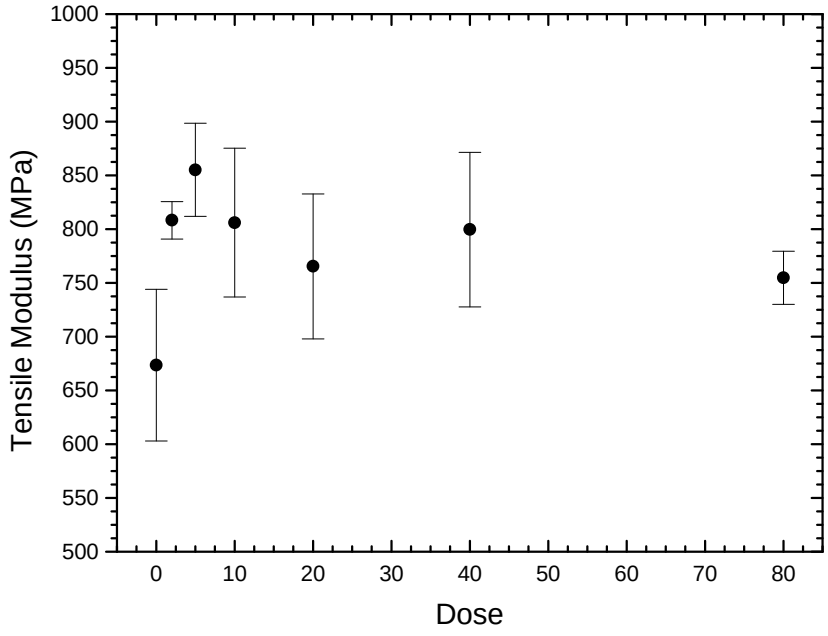

Figure 5-11 Film A machine direction tensile modulus as a function of dose.

Figure 5-11, shows data from machine direction tensile modulus experiments. Note that radiation does not seem to have as dramatic an effect on MD tensile modulus as MD toughness. Undoubtedly some tie chains did scission at 80 Mrad, but not enough were cut to reduce the tensile modulus.

The next series of figures show, the transverse direction (TD) testing of the same materials. While there is no observed maximum in any TD property, note that scission of tie chains would have more of an effect on MD properties than on TD properties since in TD, the strain is mostly parallel to the lamellae. Toughness is the one property that seems to degrade the most with radiation while modulus and yield stress seem to be relatively independent of radiation dose over the range and conditions addressed (within the scatter of the data).

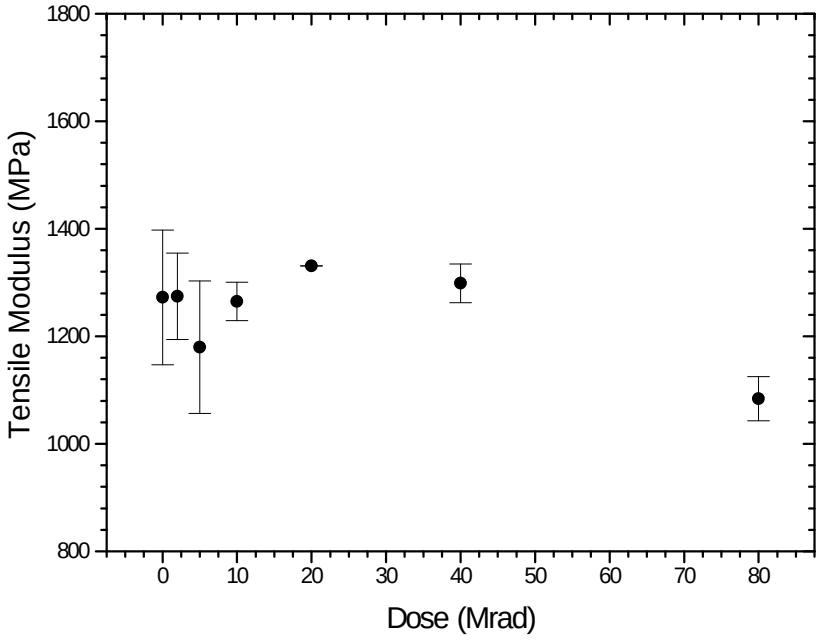

Figure 5-12 Film A transverse direction tensile modulus as a function of dose.

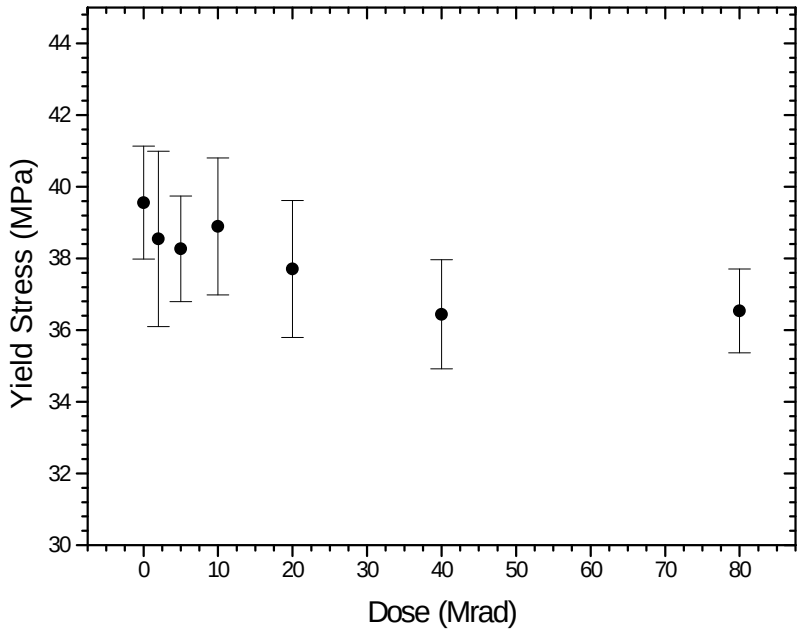

Figure 5-13 Film A transverse direction yield stress as a function of dose.

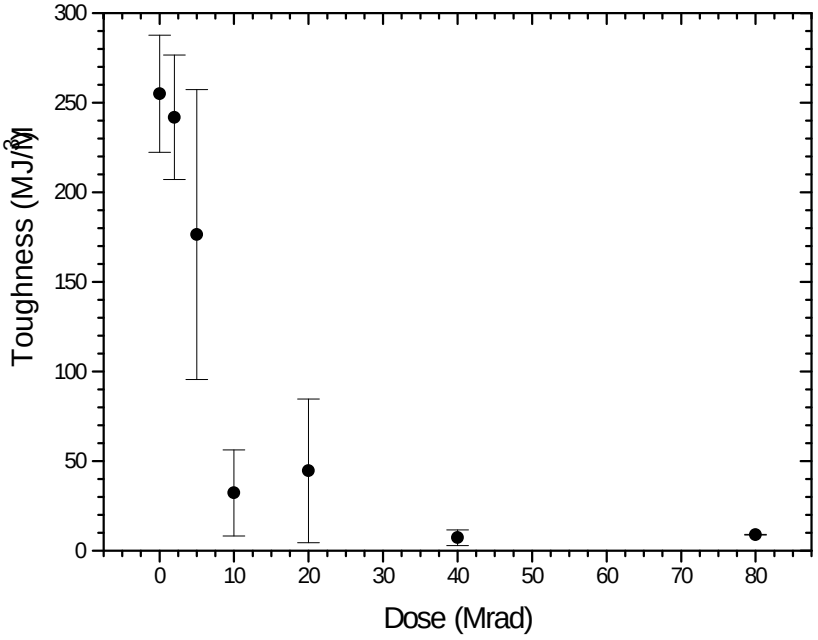

Figure 5-14 Film A transverse direction toughness as a function of dose.

The following series of figures show results for similar experiments performed on film B. For this material, it appears that irradiation serves to degrade every property except the yield strength. Modulus and toughness (MD and TD) seem especially sensitive to radiation, which was not the case for film A. There is no indicated maximum in any property with dose as was observed in film A. Note that although no maximum in the machine direction tensile properties was observed, the results for properties other than the MD and TD modulus over the range of experimental electron beam radiation dosages are within experimental error of film A. One interesting finding was that the machine direction modulus for film B suffered much more with radiation than film A, perhaps (as will be shown later) due to it's higher orientation function and thus more lamellae and tie chains in a position where tie chain scission could have a more deleterious effect on MD properties.

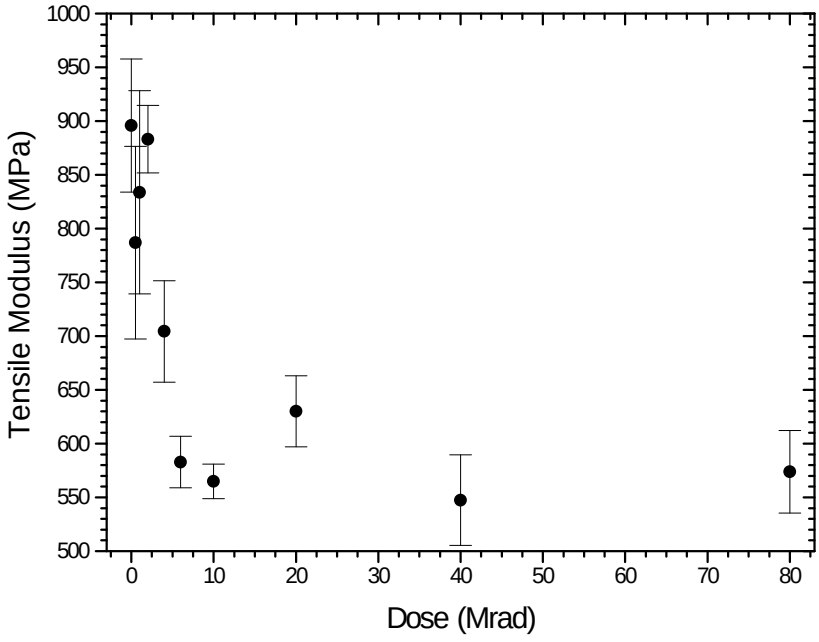

Figure 5-15 Film B machine direction tensile modulus as a function of dose.

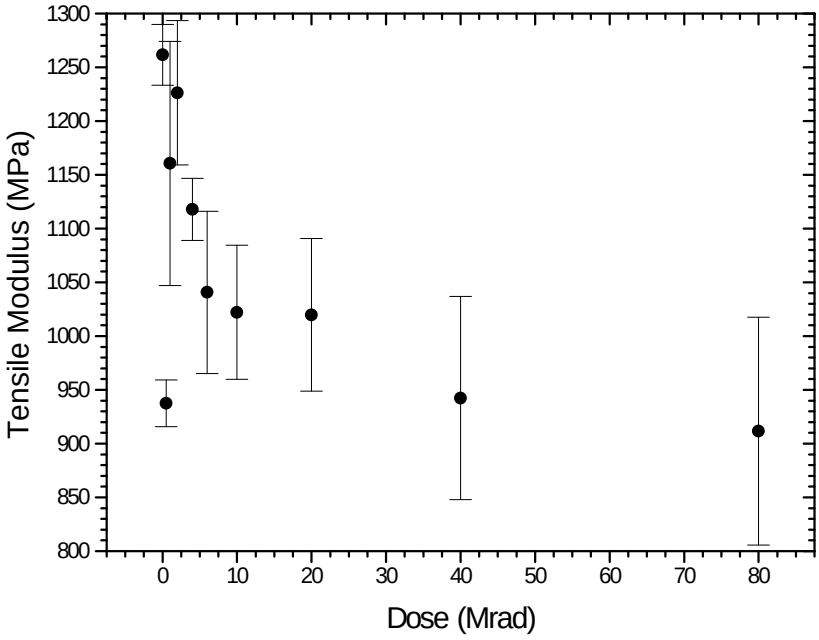

Figure 5-16 Film B transverse direction tensile modulus as a function of dose.

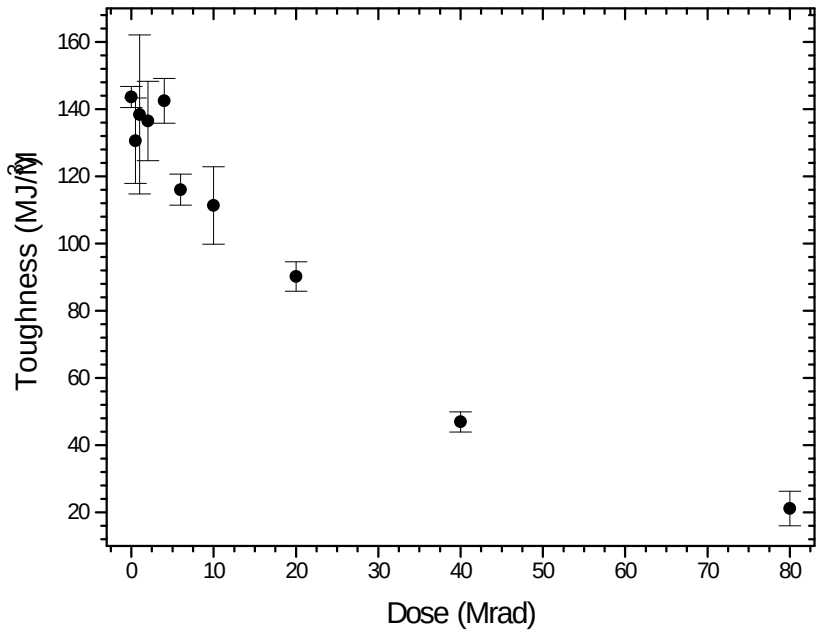

Figure 5-17 Film B machine direction toughness as a function of dose.

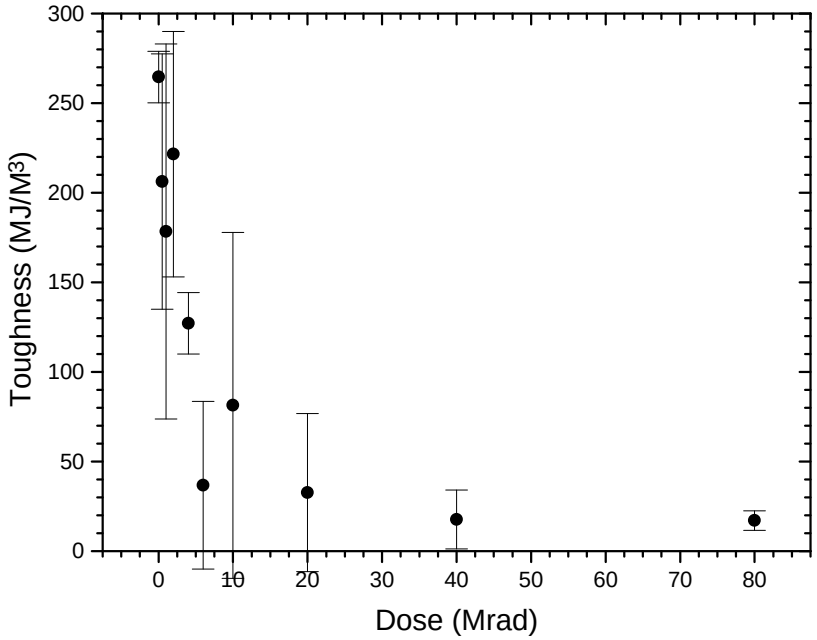

Figure 5-18 Film B transverse direction toughness as a function of dose.

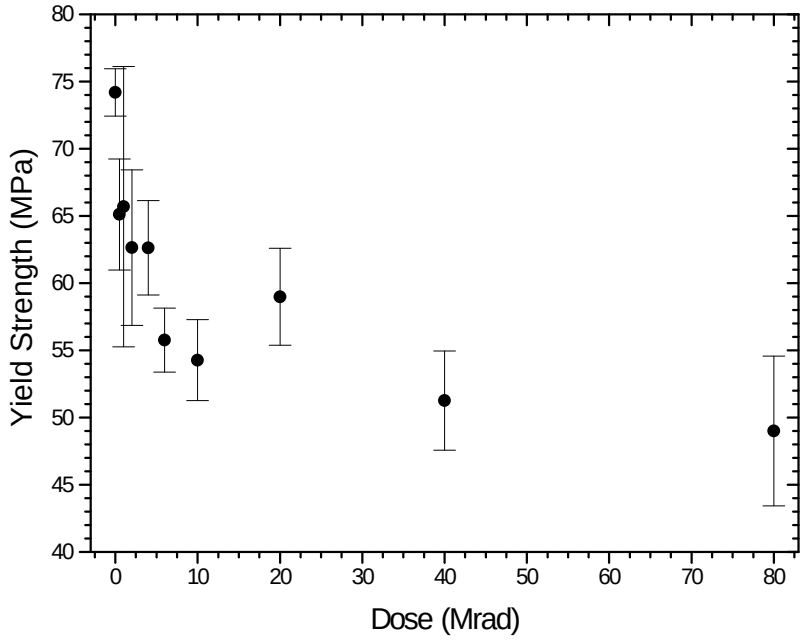

Figure 5-19 Film B machine direction yield strength as a function of dose.

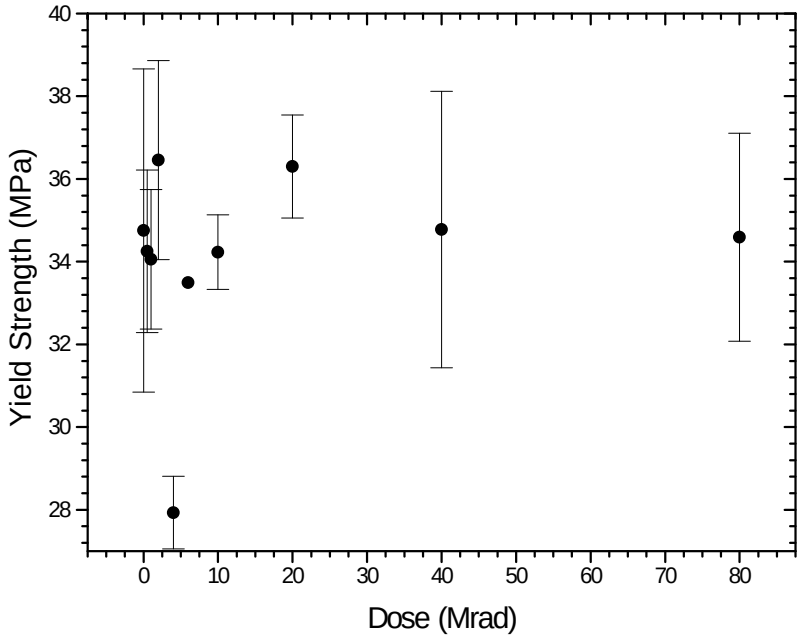

Figure 5-20 Film B transverse direction yield strength as a function of dose.

Finally, the effect of annealing at 120°C for 20 minutes (before irradiation) was investigated for film B in order to elucidate if annealing could improve mechanical properties or alter radiation effects through an increase in crystallinity, lamella perfection, or lamellar thickening. In a previous study utilizing polyethylene films made from the same resin,[263] it was shown that annealing at 120°C can increase the level of crystallinity and yield a sharper secondary SAXS peak. In the following figures, mechanical results somewhat similar to the unannealed samples are found. Comparative results from all three sets of experiments can be found in Table 5-2 at the end of this section.

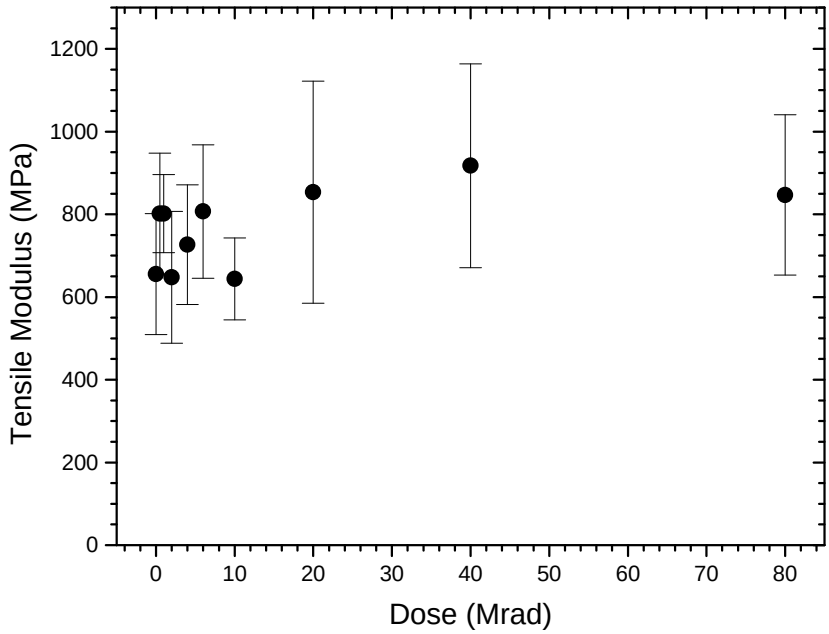

Figure 5-21 Free annealed Film B machine direction modulus for as a function of dose.

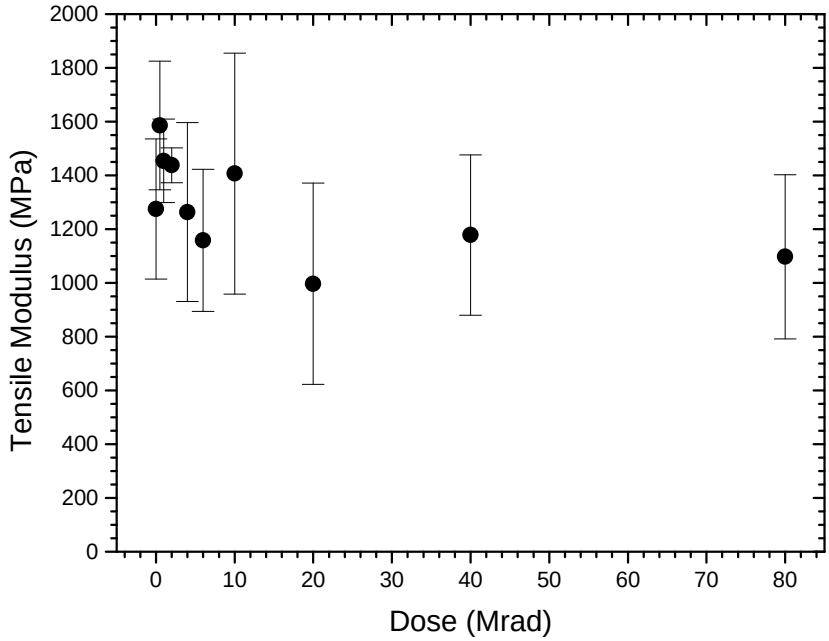

Figure 5-22 Annealed film B transverse direction tensile modulus as a function of dose.

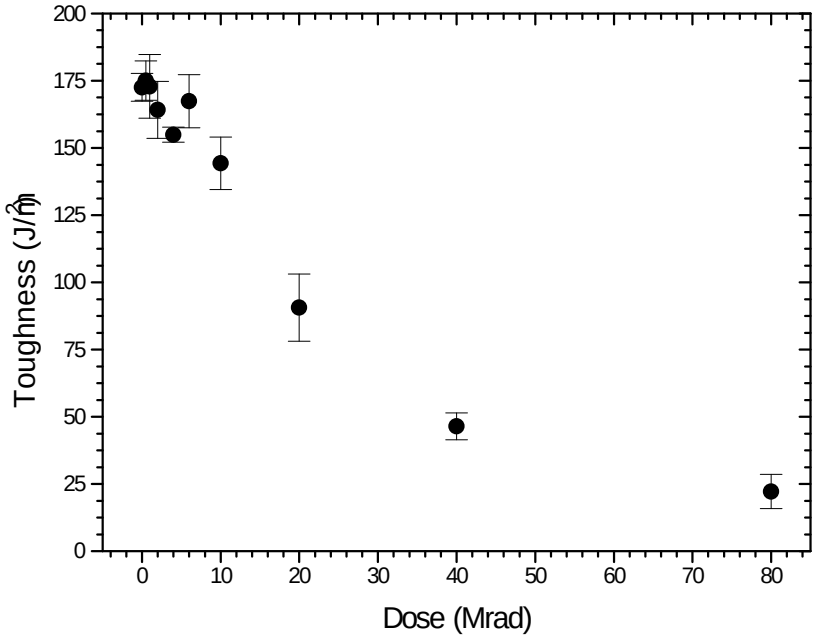

Figure 5-23 Annealed film B machine direction toughness as a function of dose.

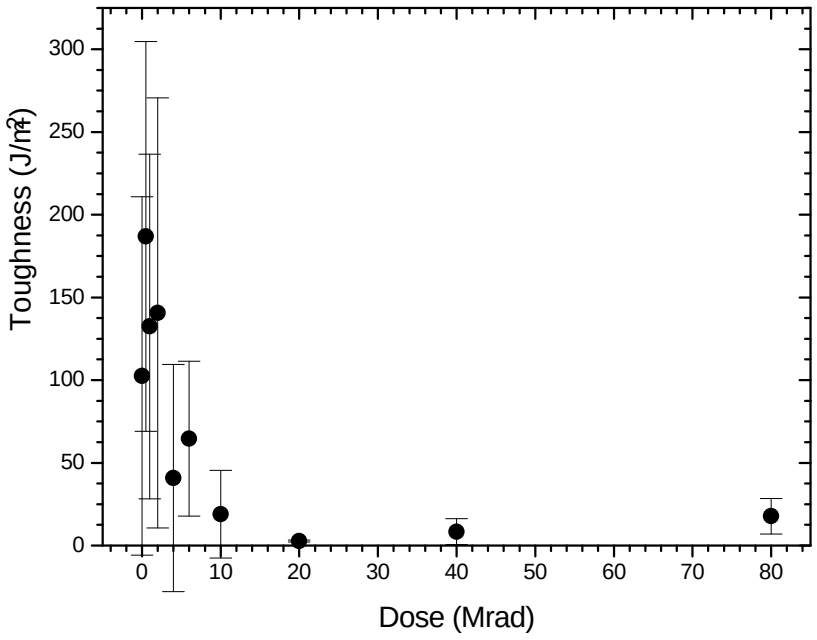

Figure 5-24 Annealed film B transverse direction toughness as a function of dose.

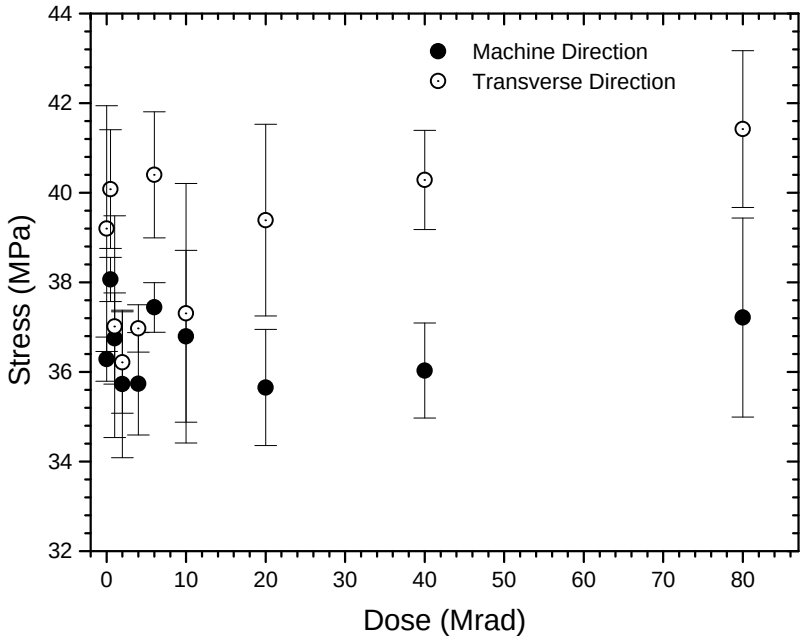

Figure 5-25 Annealed film B yield stress for both TD and MD tests.

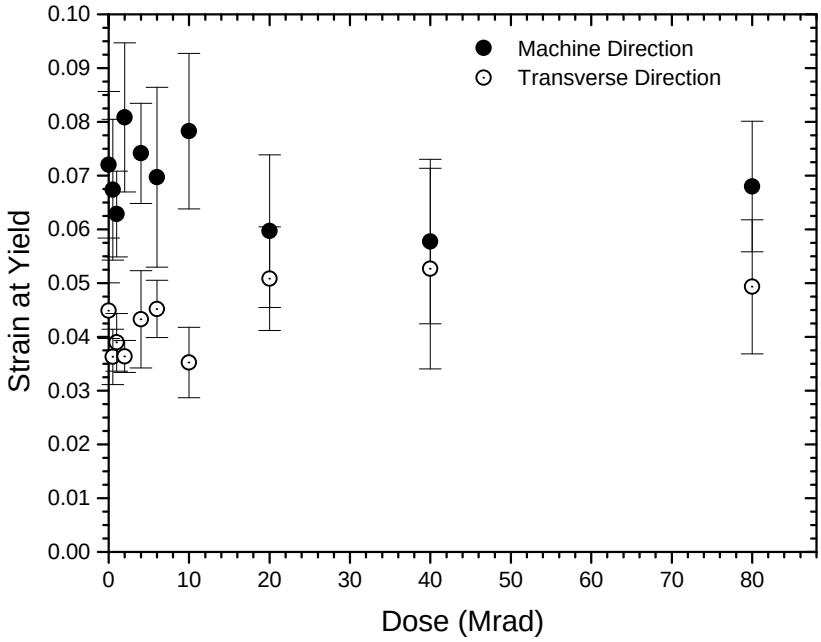

Figure 5-26 Strain at yield for annealed film B. MD and TD results are shown.

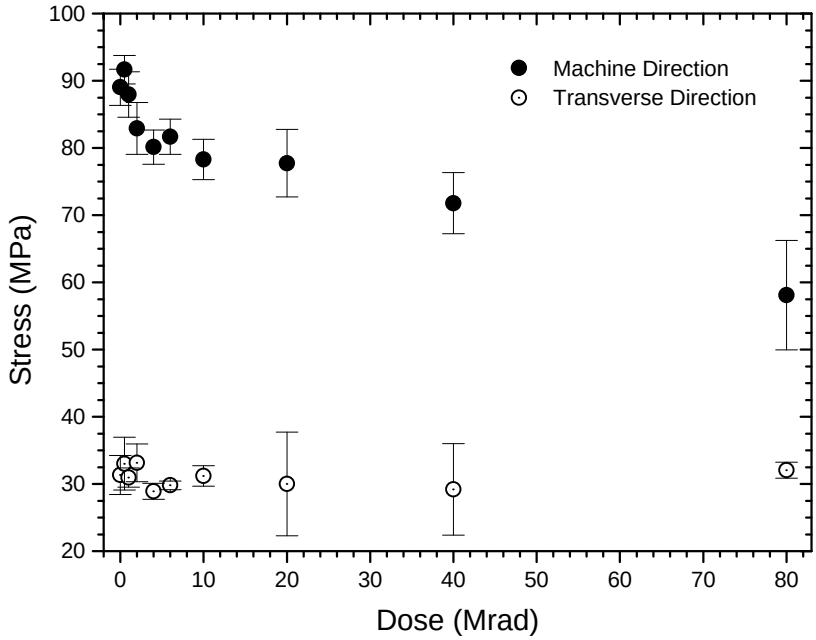

Figure 5-27 Stress at break for annealed film B. MD and TD results are shown.

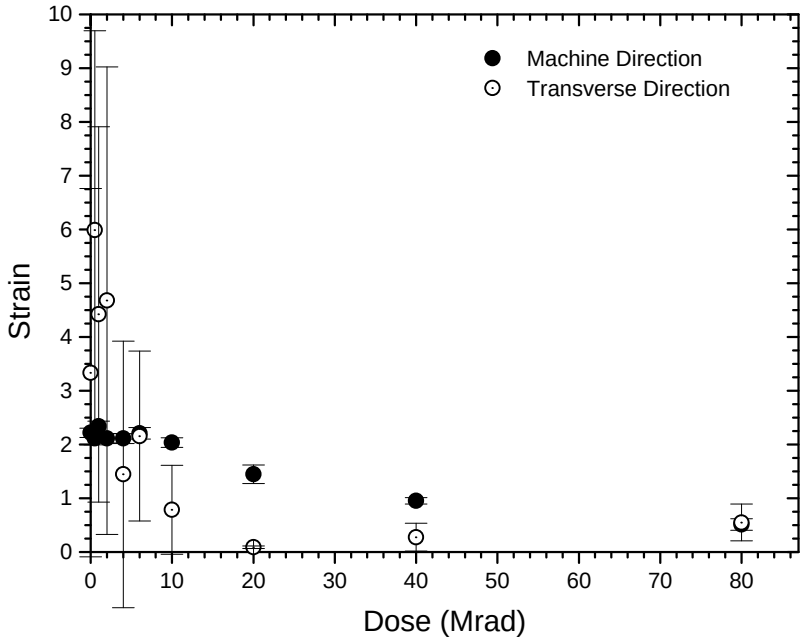

Figure 5-28 Strain at break for annealed film B. MD and TD results are shown.

To summarize some of the mechanical property results, the following table is provided. The table contains data summarizing the mechanical property results from the three experiments performed on film A, film B, and film B annealed. Four properties representing toughness and modulus in MD and TD were selected for comparison. The first number in each column indicates the approximate property value with no radiation and the second indicated the value at 80 Mrad. Both radiation resistance and relative property values can therefore be directly compared.

Table 5-2. Summary of mechanical property experiments

	Film A	Film B	Film B Annealed
MD Modulus (MPa)	800....750	900....600	800....
TD Modulus (MPa)	1300....	1250....950	1500....1200
MD Toughness (MJ/m^3)	120....20	140....20	175....25
TD Toughness (MJ/m^3)	250....0	250....10	200....0

Modulus values seemed the most affected by annealing and the small differences in morphology between film A and film B. For MD modulus, annealing appears to have the effect on film B of making the film more radiation resistant. while the unannealed film B had a slightly higher MD modulus than A but appears to be more affected by radiation. Annealing showed the strongest affect on TD modulus as comparison of film B data shows. The same degradation in this TD property occurs but annealing seems to have increased the TD modulus - not to the point of increasing resistance to radiation. Small changes in the lamellar morphology (e.g. perfection) could account for this increase, but is unknown why the same increases do not show up in TD toughness. As one can see from the table, trends in toughness (are under the stress-strain curve) seemed the most consistent from one

condition to another. Radiation seemed to make these films much more brittle with dose. As for the actual magnitude of the toughness values, it is difficult to say that these results are much outside of experimental error.

5.3.2 Differential Scanning Calorimetry

Differential scanning calorimetry (DSC) was utilized to characterize films A and B with respect to their melting distributions and percent crystallinity. The goals of this study were to determine to what extent the percent crystallinity changes with dose and to what extent the melting peak temperature is altered with dose. The first series of DSC scans on film A are presented. The first three figures are DSC scans of the as received material with the same experimental conditions for the purposes of indicating the degree of scatter. For film A it was observed that +/- 1°C in the melting peak temp and up to +/- 4 J/g in the melting endotherm was typical.

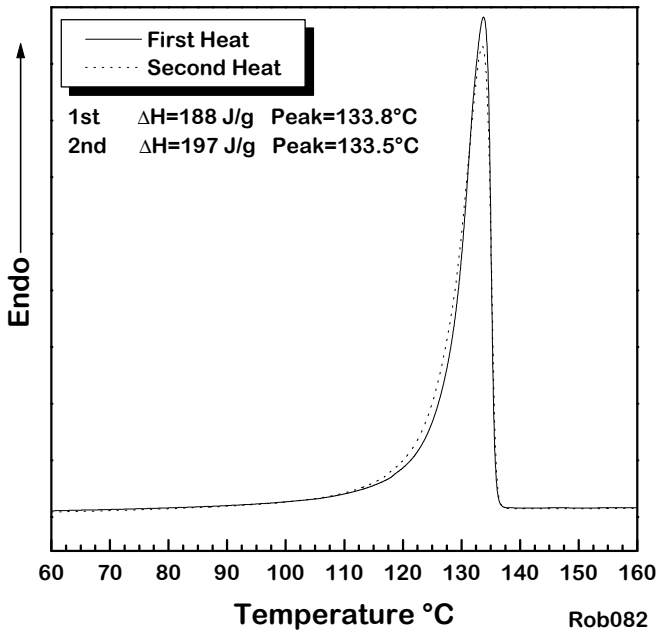

Figure 5-29 As received film A DSC scan sample one of three.

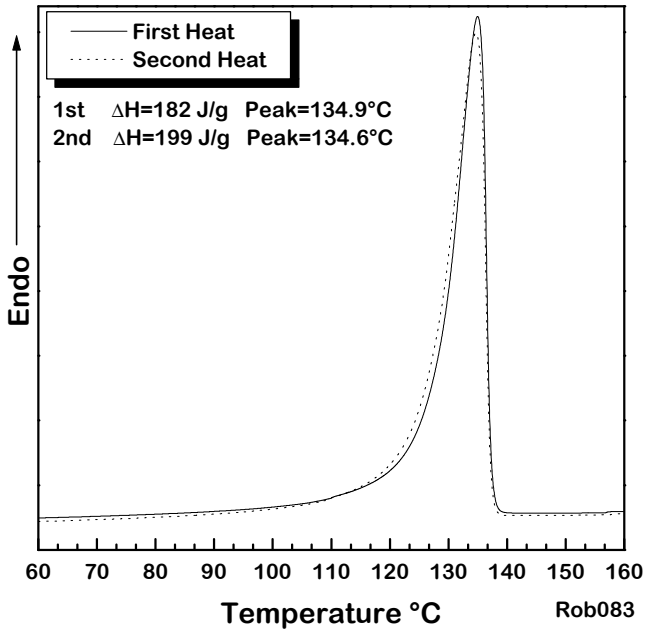

Figure 5-30 As received film A DSC scan sample two of three.

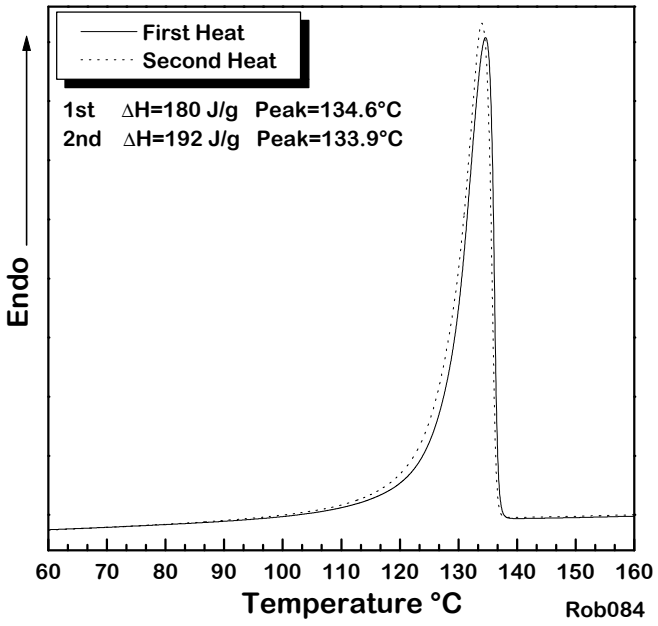

Figure 5-31 As received film A DSC scan sample three of three.

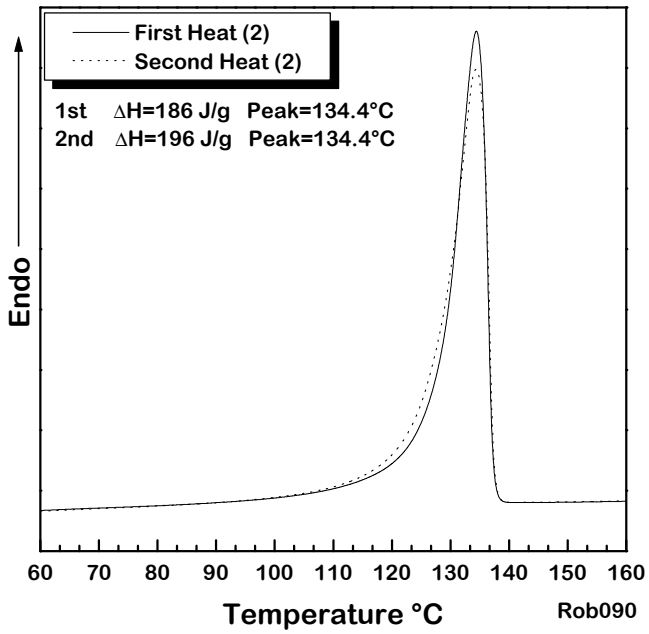

Figure 5-32 PE film A irradiated to 2.0 Mrad.

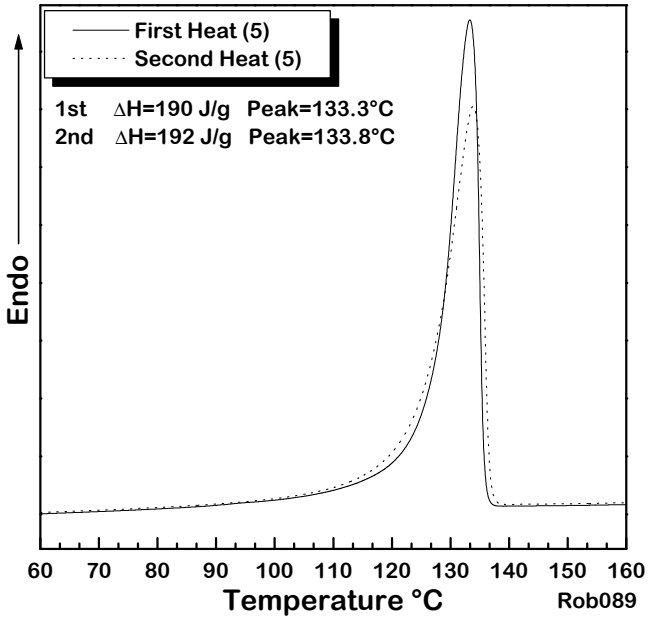

Figure 5-33 PE film A irradiated to 5.0 Mrad.

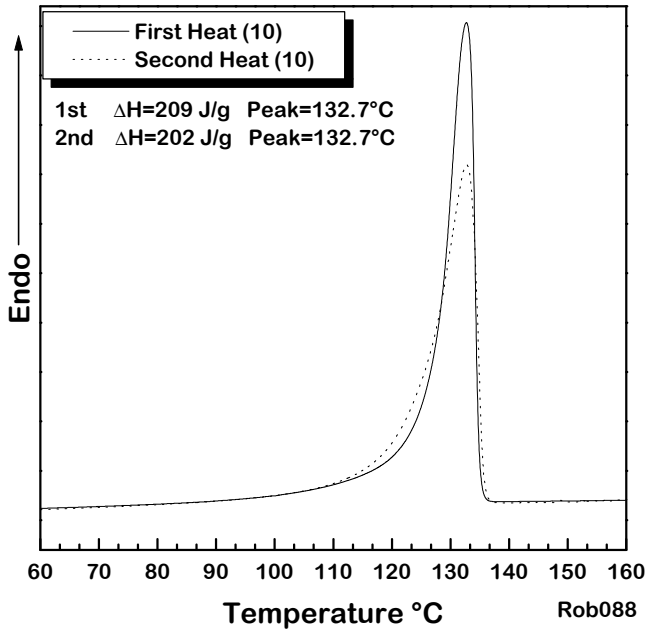

Figure 5-34 PE film A irradiated to 10.0 Mrad.

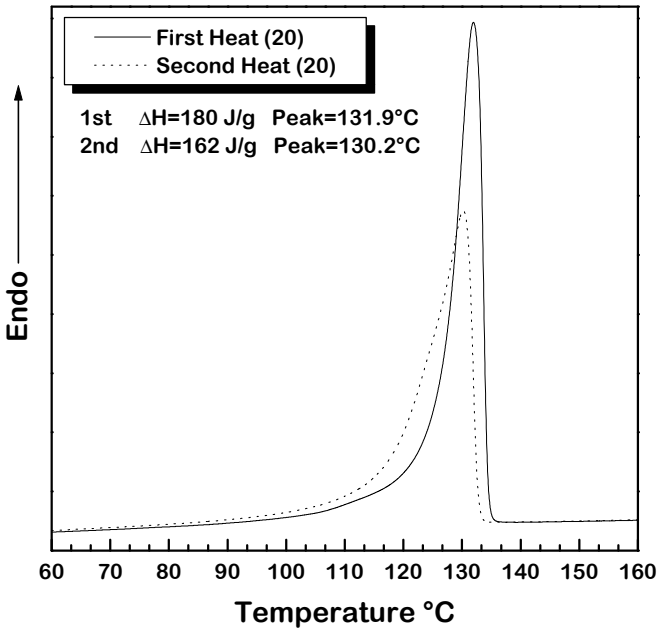

Figure 5-35 PE film A irradiated to 20.0 Mrad.

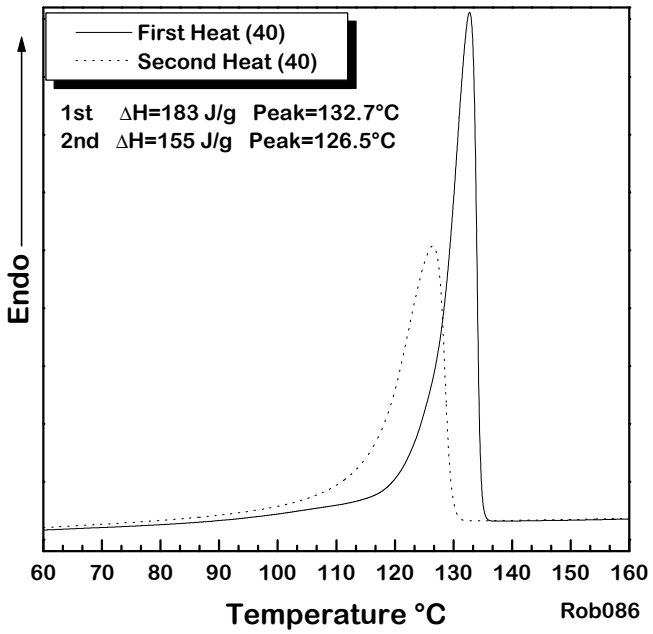

Figure 5-36 PE film A irradiated to 40.0 Mrad.

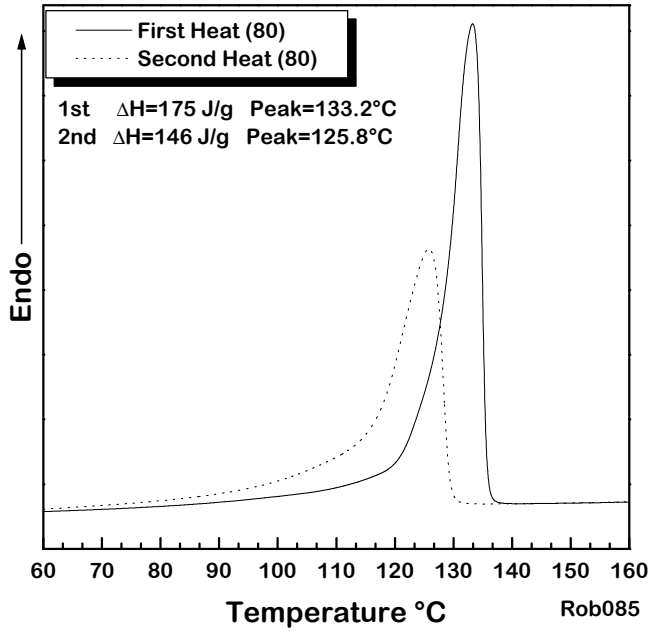

Figure 5-37 PE film A irradiated to 80.0 Mrad.

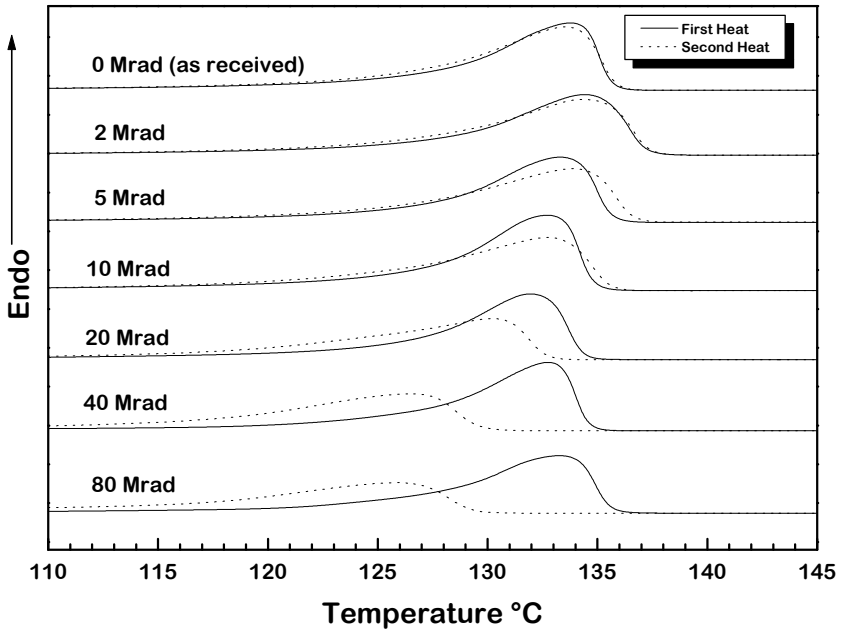

Figure 5-38 Summary of DSC traces for film A. Numbers indicate the E-Beam radiation dose in Mrad for each sample.

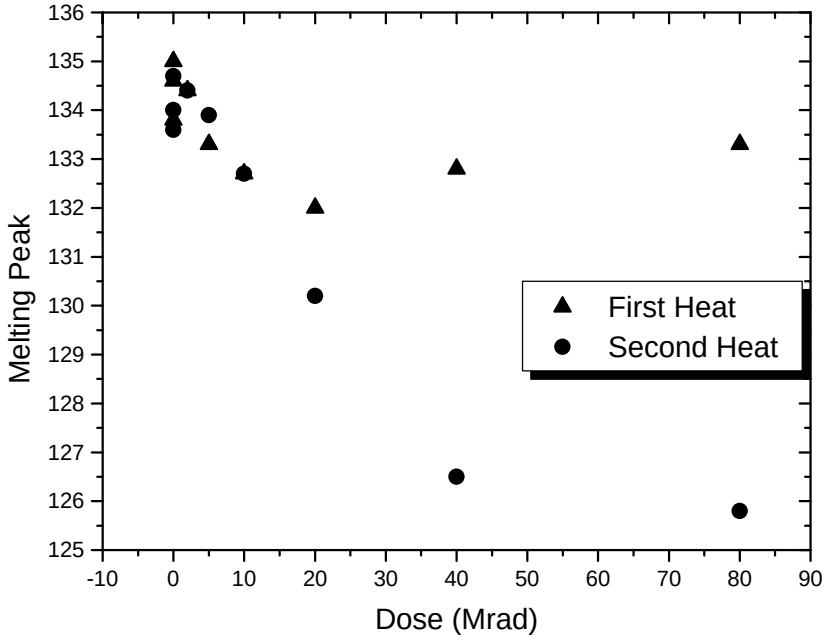

Figure 5-39 Summary of melting peak data vs. dose for film A.

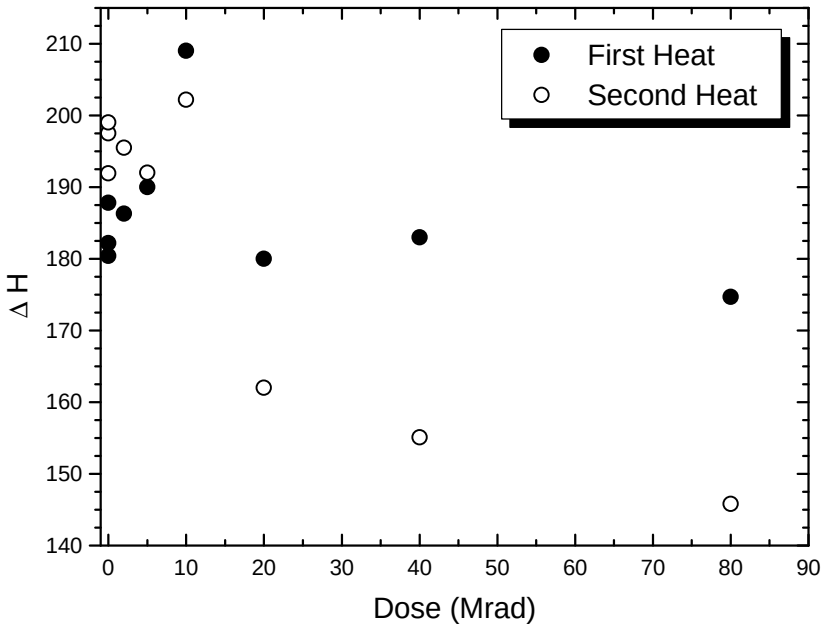

Figure 5-40 Melting endotherm area as a function of dose for film A.

As with the mechanical property testing on the film A PE films, there is a trend of a small maximum at low doses that could be argued is not within experimental error. As with the mechanical properties, radiation dramatically alters the thermal properties of film A. The first and second heating melting peak decreases with dose, although the second melting endotherm decreases much more with dose (as expected due to crosslinking) than the first. Recall the earlier studies (see Figure 5-1) that show an increase in peak area and peak location for UHMWPE. It appears that for the film A material, ionizing radiation dose not cause enough tie chain scission (and subsequent tie chain crystallization) to measure an increase in crystallinity by DSC - of course there is much less amorphous material available for crystallization in these materials than the ones utilized in Figure 5-1.

Next, similar DSC studies on film B (with additional dosages selected below 10 Mrad) were performed. After these studies were complete,

additional DSC experiments were performed on film B to determine what changes in crystallinty and/or radiation response occur when samples are annealed at 120°C for 20 min. before being irradiated. Individual scans were similar to those of film A shown at the beginning of this section, therefore individual DSC scans from film B film are not shown.

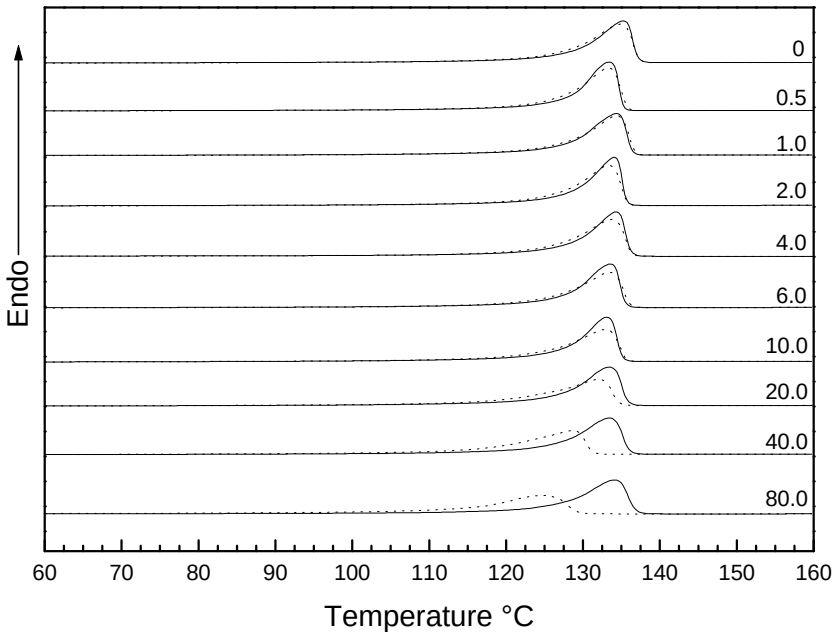

Figure 5-41 Film B DSC summary. Numbers indicate the dose in Mrad.

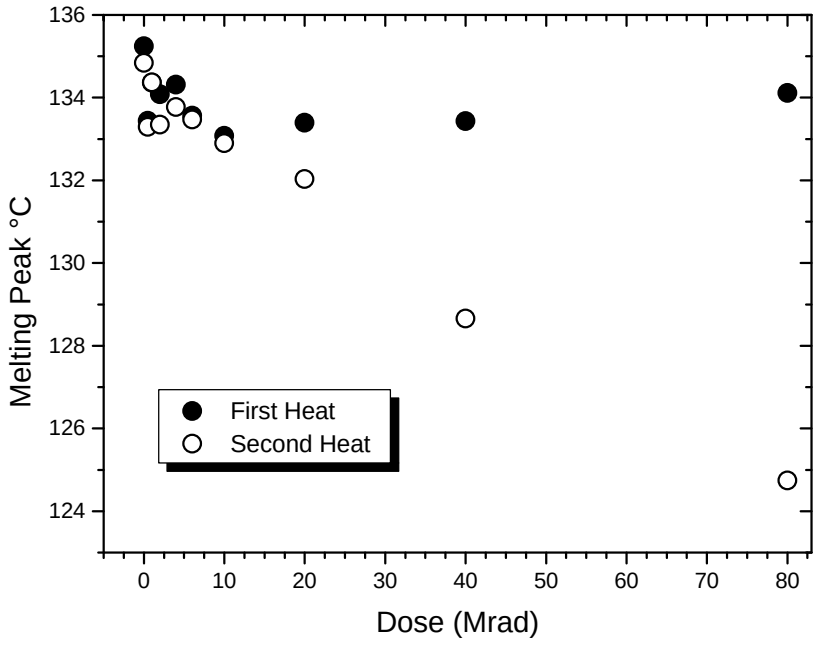

Figure 5-42 Film B DSC melting peak summary as a function of dose.

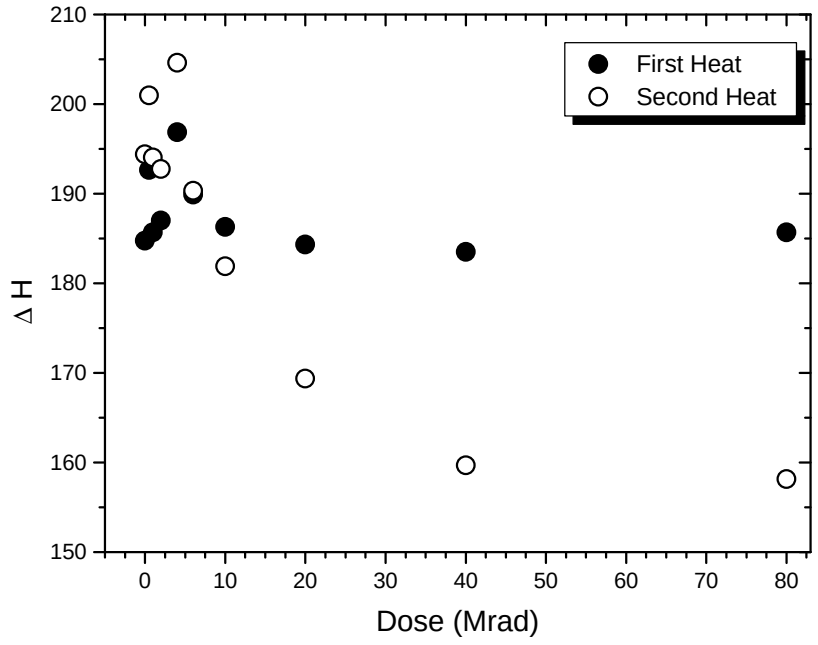

Figure 5-43 Summary of Film B endotherm area data as a function of dose.

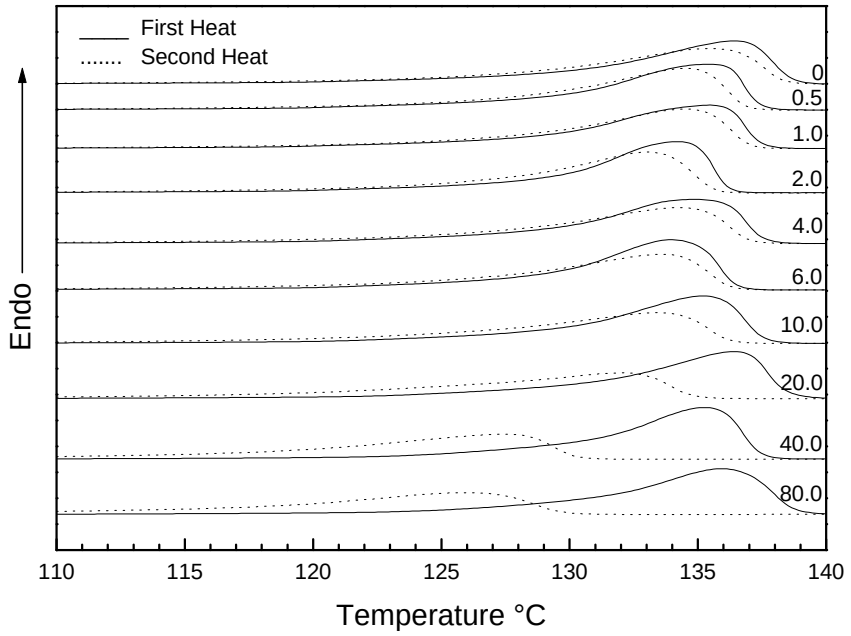

Figure 5-44 Annealed film B DSC summary. Numbers indicate the E-Beam dose the sample received in Mrad.

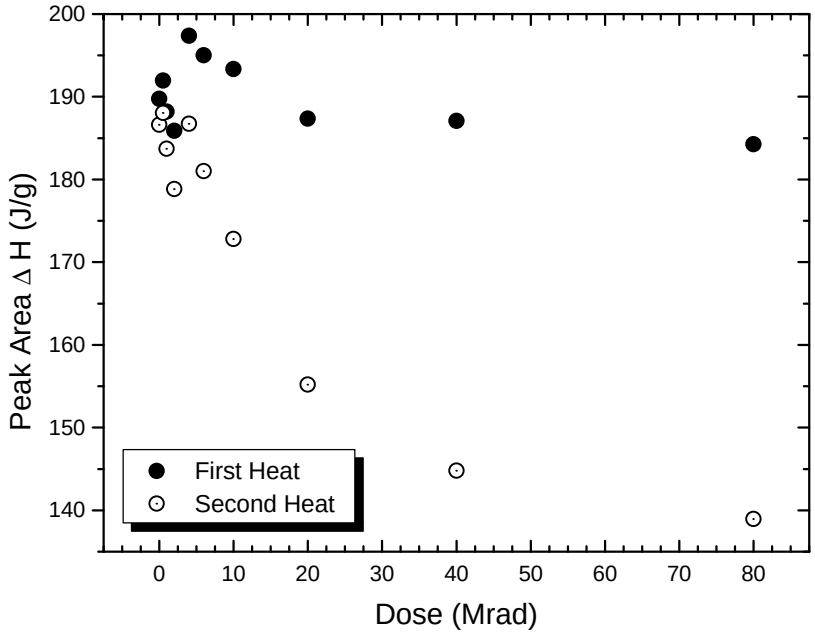

Figure 5-45 Annealed and irradiated film B melting endotherm area vs. dose.

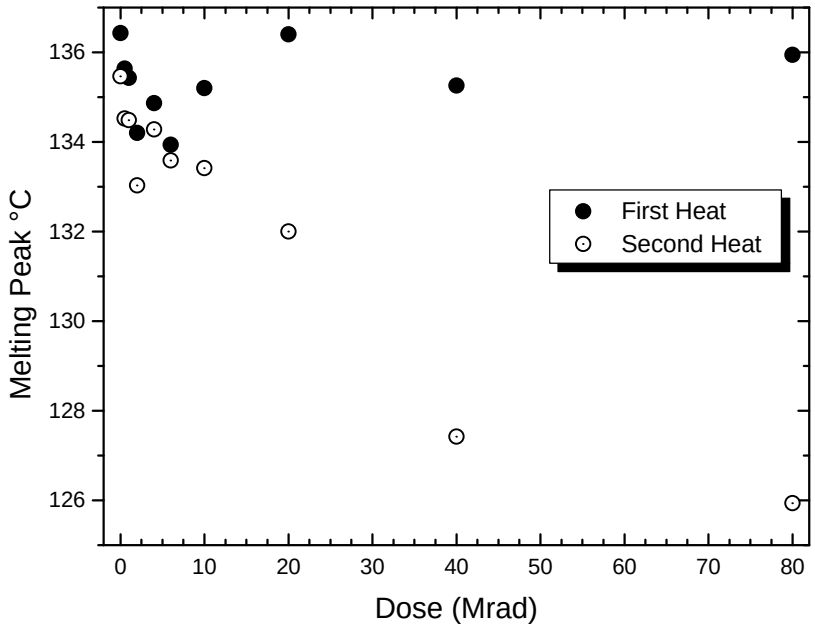

Figure 5-46 Annealed and irradiated film B melting peak vs. dose.

To summarize the results of the DSC study, no increase in crystallinity with radiation dose was observed for film A, or for film B both annealed and as received. In addition, free annealing did not appear to increase the level of crystallinity (within the scatter of the data as observed by DSC) though a previous study[263] showed that annealing these materials under strain does increase crystallinity. Indeed, radiation steadily decreased the melting peak and melting peak area both for first and second heats for all three PE samples. The second heats for all samples showed evidence of crosslinking as marked reductions in their peak areas were observed. This decrease was proportional to the dose the sample received (see Figure 5-47, Figure 5-48, and Figure 5-49). Similar levels of crystallinity were found in both film A and B.

5.3.3 Linear Dichroism

As outlined in the experimental section, linear dichroism experiments were performed to determine the orientation behavior of film A and film B. Results of these experiments were important to not only understand what effect the different processing conditions had on orientation, but to discover what, if any, changes in orientation occurred with radiation. Both films were analyzed as a function of radiation dose and it was found that radiation had *no effect* on the orientation of the crystal a, b, or c axes. Typical results for these experiments are shown in Figure 5-47 and Figure 5-48. Figure 5-49 shows the orientation data for all of the linear dichroism experiments. In addition, it was found that radiation had no effect on the orientation behavior of the amorphous phase in both films by observation of the 1368 cm^{-1} absorption band and was very close to zero. Film B did display, however, a slightly higher c axis orientation function than film A.

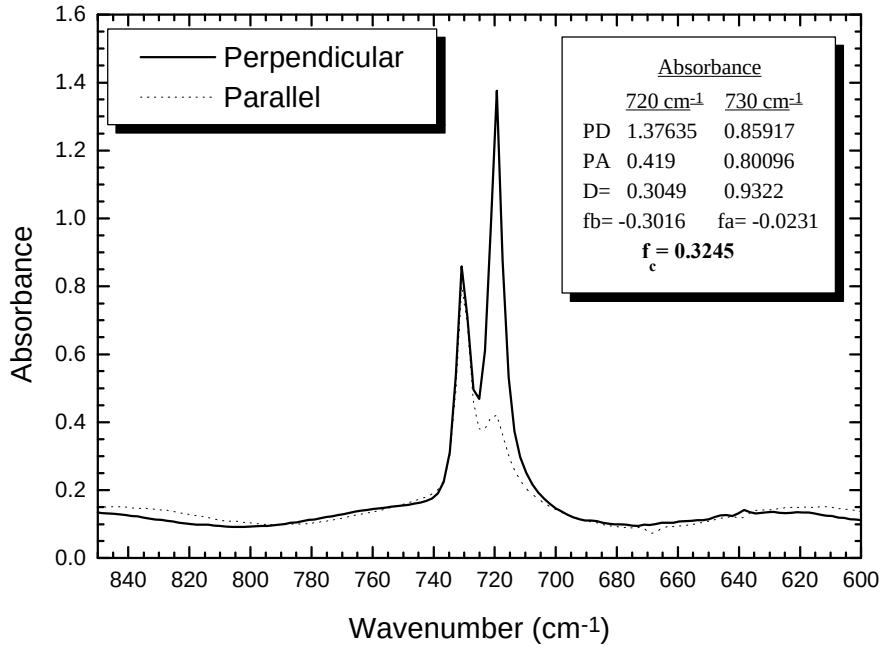

Figure 5-47 Film A linear dichroism experimental data showing parallel and perpendicular scans and peaks at 720 and 730 cm^{-1}.

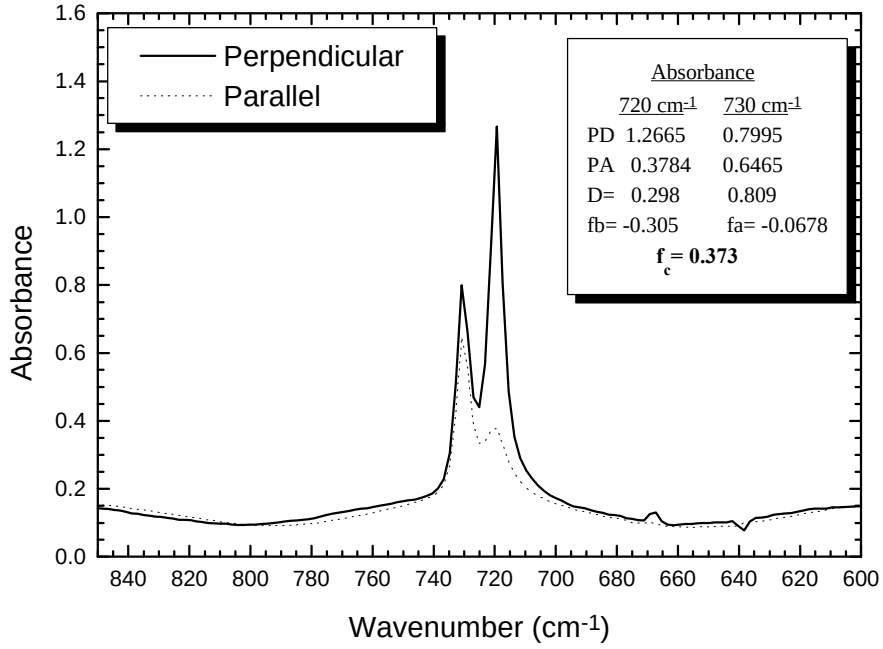

Figure 5-48 Film B linear dichroism experimental data showing parallel and perpendicular scans and peaks at 720 and 730 cm^{-1}.

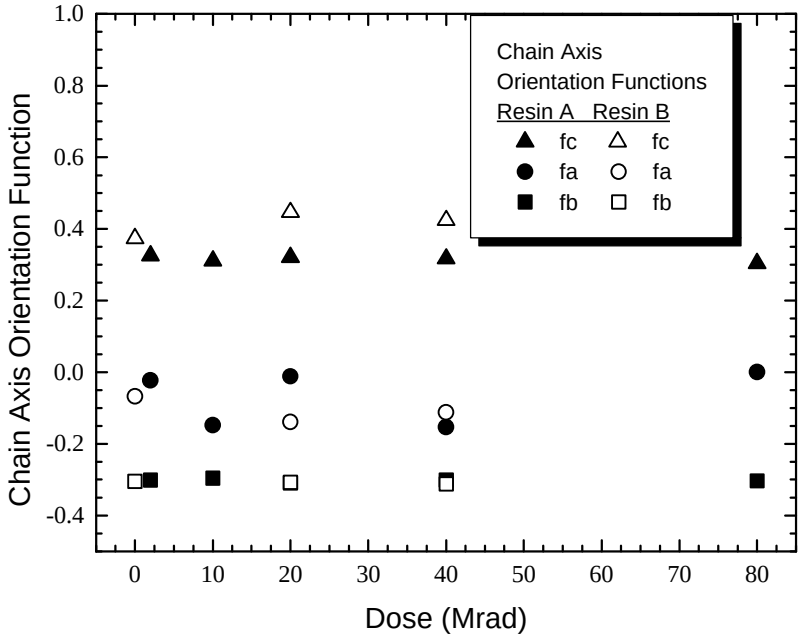

Figure 5-49 Unit cell orientation data for Film A and Film B.

5.3.4 Water Permeability

As received film A PE films were irradiated to 2, 10, 20, and 40 Mrad and then tested as outlined in the experimental section for changes in water permeability. Figure 5-1 shows the data from these experiments. It should be noted that for the 2 and 40 Mrad samples, several months passed between irradiation time and for the 10 and 20 Mrad samples, approximately one week passed in between irradiation and permeability testing. It does not appear from this or any other data (DSC, mechanical properties, FTIR, SAXS, WAXS, TEM, etc.) that there is any time dependency after irradiation on any measured property. What one observes from this experiment is that (1) there is a dramatic decrease in water permeability with dose - reducing by half at 40 Mrad the results from the unirradiated sample and (2) there is no "maximum" in the data. Since there was no indicated increase in the level of crystallinity by DSC, this leaves one to speculate that either very small increases in crystallinity have occurred since there is undoubtedly *some* level of scission occurring in the film - but obviously not enough to result in a significant increase in crystallinity that could be measured by DSC or any other technique (TEM, SAXS) in this work. What is most probable since there is no evidence of an increase in crystallization and there is, just from the DSC results but in a moment more evidence will show that crosslinking of the amorphous regions have reduced the water permeation by restricting chain motion. I

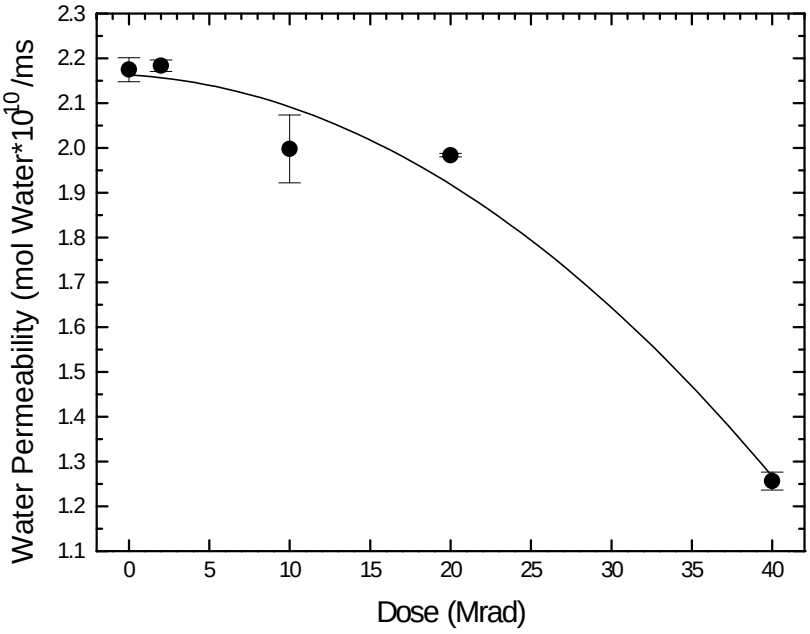

Figure 5-50 Water permeability as a function of dose for film B.

5.3.5 Small Angle X-Ray Scattering

Small angle X-ray scattering (SAXS) experiments at 0, 20, 40 and 80 Mrad were performed on film B to determine if any changes in lamella spacing or peak intensity were occurring with annealing and/or with radiation. Comparison of Figure 5-51 and Figure 5-52 clearly indicates that annealing affected both primary and secondary peak intensity and long spacing and these results are identical to previous SAXS experiments on film A.[263] No change in lamella thickness or spacing has occurred, however, with radiation.

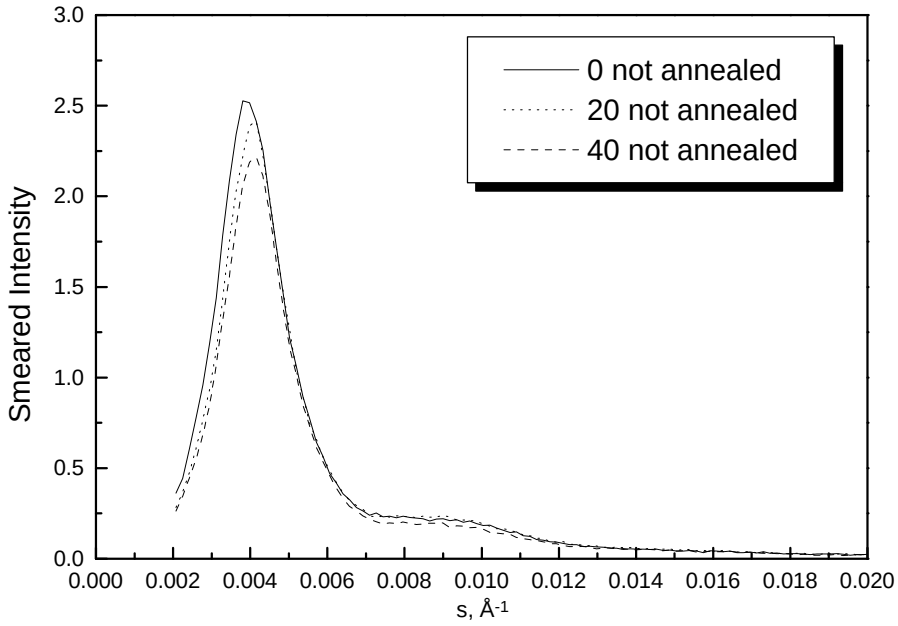

Figure 5-51 SAXS for film B at 0, 20 and 40 Mrad.

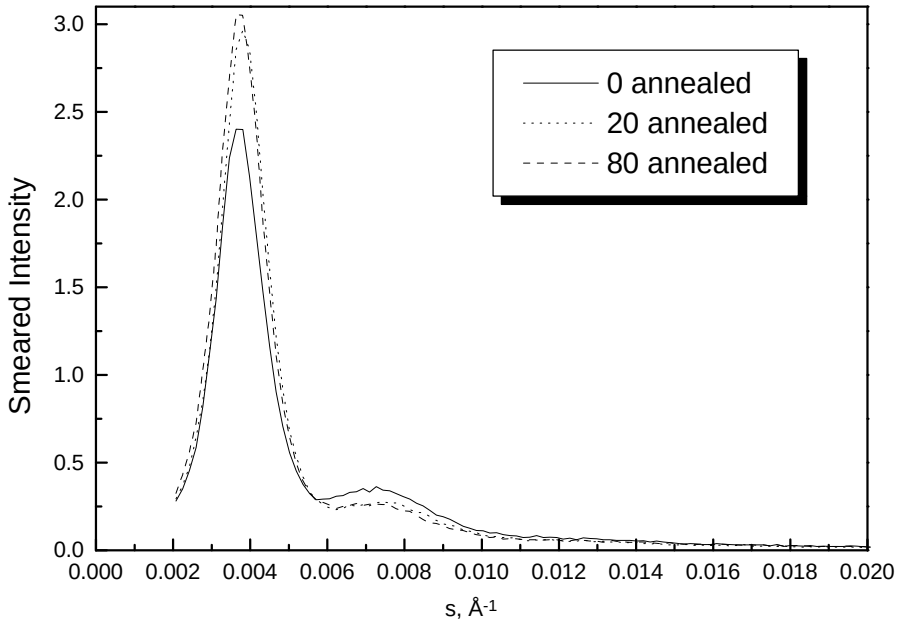

Figure 5-52 SAXS for annealed film B at 0, 20 and 80 Mrad.

5.3.6 Transmission Electron Microscopy

TEM experiments were also carried out to examine the morphology of film B and to determine if any other morphological changes take place when this particular polyethlyene is irradiated at such a high dose level. The extremes (0 and 80 Mrad) were again examined and, there appears to be little difference between the irradiated and unirradiated samples. The 80 Mrad samples are essentially identical to TEM's in a previous study[263] on film A which was unirradiated.

The main conclusions derived from the TEM study are that the highly crystalline stacked lamella morphology withstands radiation treatment surprisingly well and that no visible changes of the lamella occurred as a result of irradiation. This finding is well supported by the DSC evidence which showed little difference in crystallinity level with dose for either film sample.

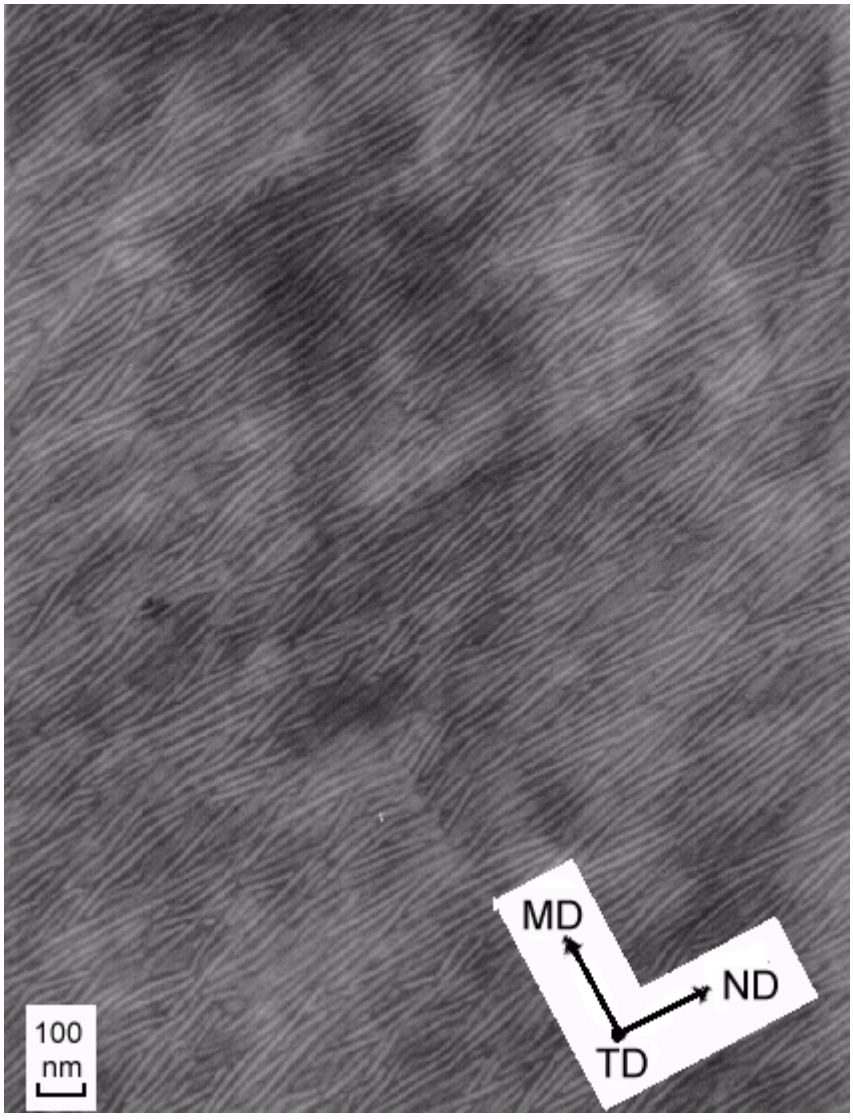

Figure 5-53 Film B 0 Mrad sample. 67,000x scale indicated.

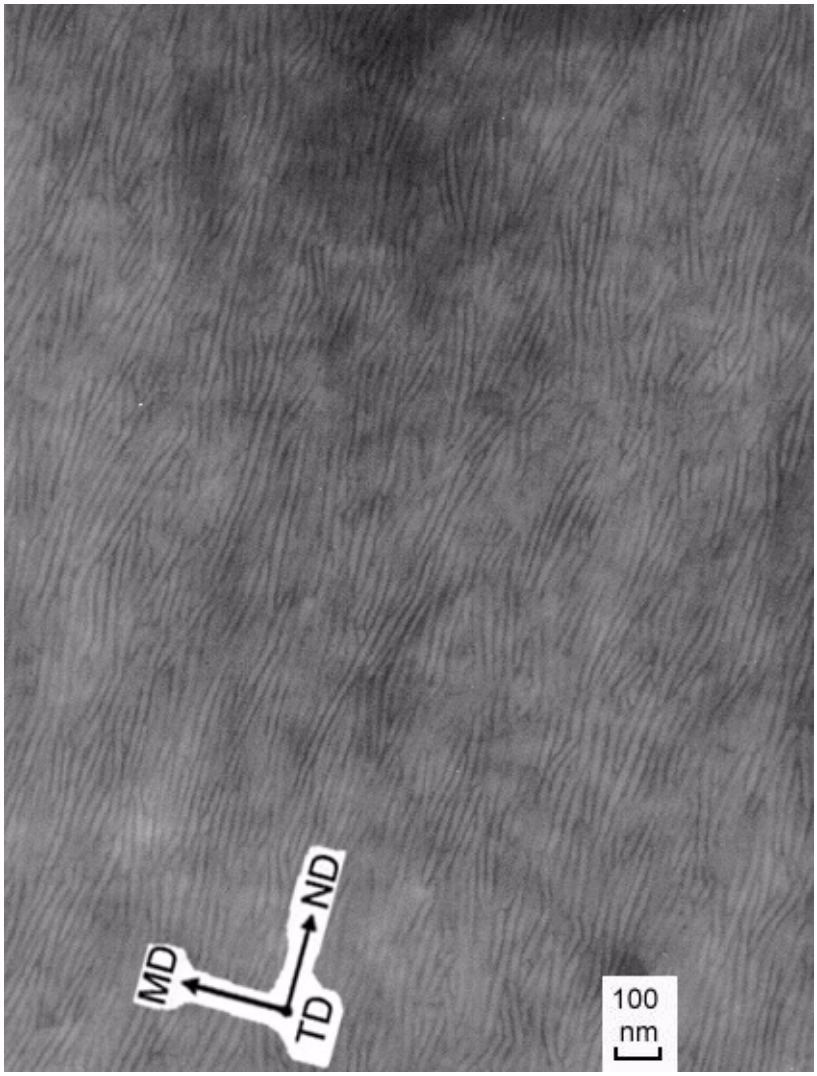

Figure 5-54 Film B 80 Mrad sample 67,000x scale indicated.

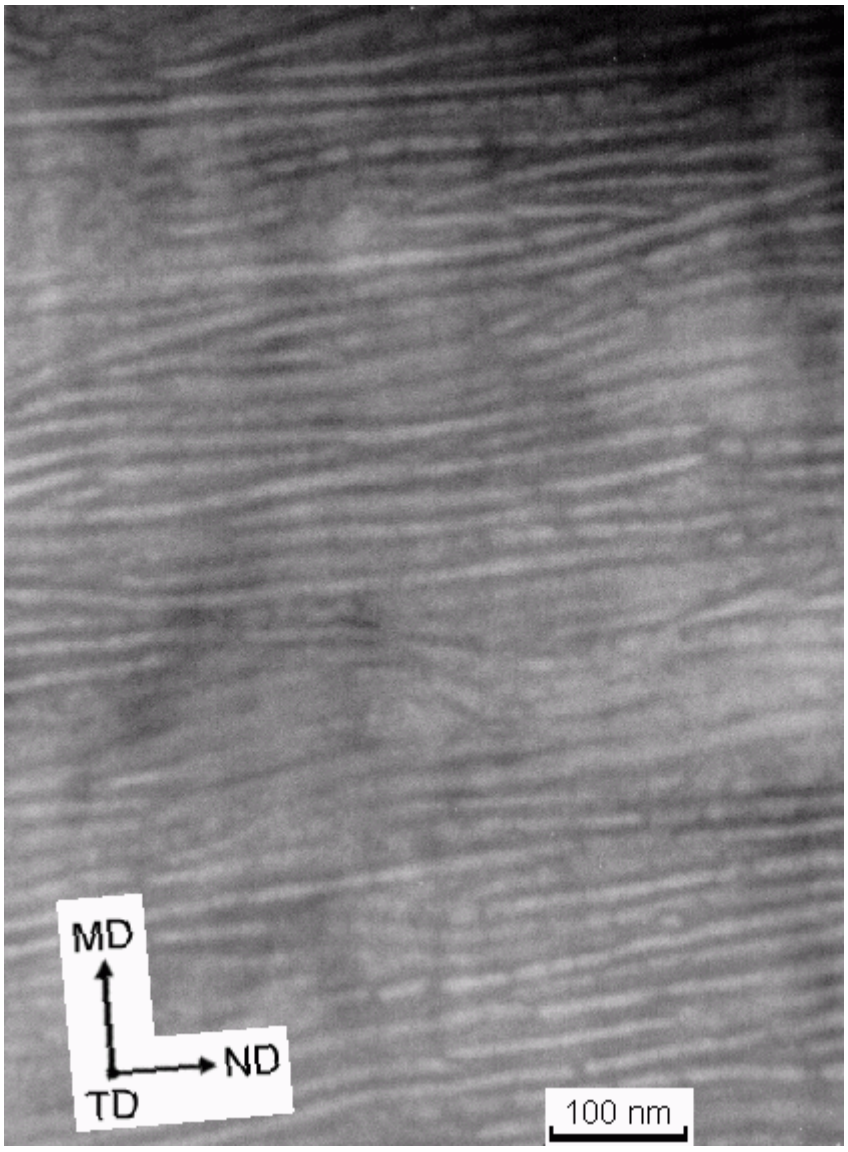

Figure 5-55 Film B 80 Mrad. 187,500x. Scale Indicated.

5.3.7 Wide Angle X-Ray Scattering

WAXS experiments were performed to study the unit cell orientation behavior in film B. In general. if crystallization of any amorphous chains occurred during irradiation as a result of scission, then these chains would be more or less free to crystallize in any random orientation. In the case of an oriented material of a stacked lamellar morphology, possible epitaxial (as shown in Figure 5-2) crystallization might result in additional or more diffuse reflections. However, as can be seen from Figure 5-56 and Figure 5-57 there are no significant differences between the 80 Mrad and 0 Mrad WAXS patterns.

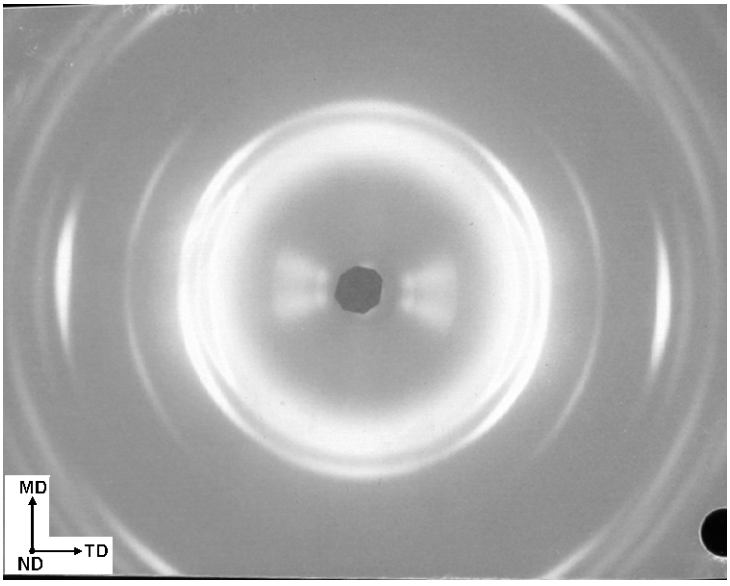

Figure 5-56 Film B 0 Mrad WAXS pattern.

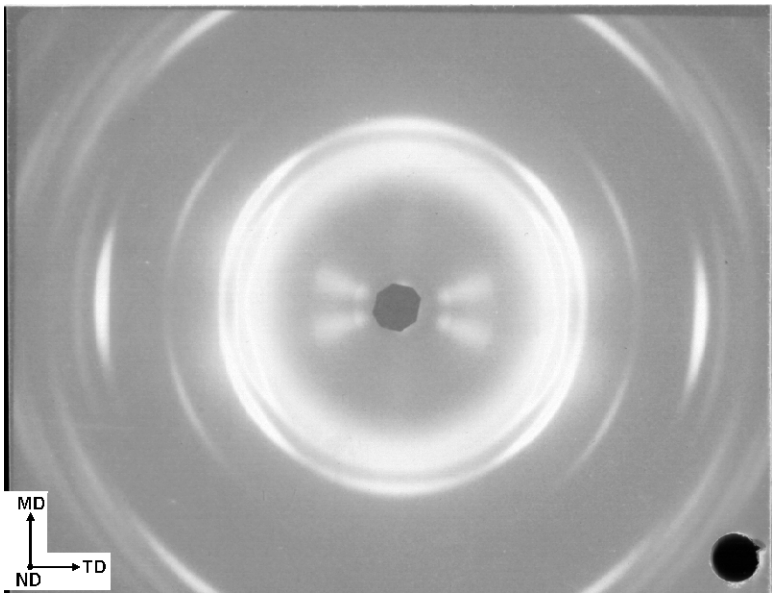

Figure 5-57 Film B 80 Mrad WAXS pattern.

5.3.8 Dynamic Mechanical Analysis

DMA experiments on 80 and 0 Mrad film B films along the MD, TD and 45° to MD were performed and the results shown in the next three figures. It is known in polyethylene that the gamma relaxation is associated with crankshaft motion in the amorphous region, higher amorphous content (or amorphous polymer of a different nature, i.e. crosslinked) should result in different gamma relaxation behavior. For theses experiments 10mm by 5mm samples from the 1 mil films were cut. Frequencies from 0.1 to 10 Hz were selected and a temperatures were scanned from -150°C to melting at a rate of 0.5°C/min. It should now be clear that the decrease in water permeability is not a result of any change in the crystal structure in the polymer. The one other likely explanation for this decrease is crosslinking of the amorphous phase. Recall the definition of permeability:

$$P = SD \tag{5-9}$$

Where S= solubility and D= diffusivity. Solubility is a thermodynamic parameter and may affect permeation by a change in chemistry or percent crystallinity. Diffusivity is a kinetic parameter and is typically affected by changes involving molecular motions (e.g. crosslinking).

The data discussed to this point strongly leads to crosslinking reducing the chain mobility in the amorphous phase - where the majority of permeation occurs and the diffusivity (the kinetic parameter) is decreasing. DMA testing along the transverse direction (basically pulling directly along the lamella) should be the least sensitive to crosslinking while machine direction testing and 45° testing should be more sensitive to crosslinking. Although not definitive, the scans do all show differences in Tan δ in the in the gamma relaxation region indicating that there are differences between the amorphous molecular behavior. The β region is associated with branching

and the unirradiated materials are linear. In every case, the irradiated sample had a higher β relaxation than the unirradiated sample. Since a crosslink is a tri-functional junction, these are basically very long branches and the β relaxation shows strong evidence of crosslinking in these samples. The lower α relaxation for the irradiated samples could possibly be explained by considering the addition of some defects which could slightly lower the percent crystallinity. The DSC data for this material showed evidence of a small decrease in ΔH, with increasing dose which a small reduction in crystallinity from a few defects could be responsible.

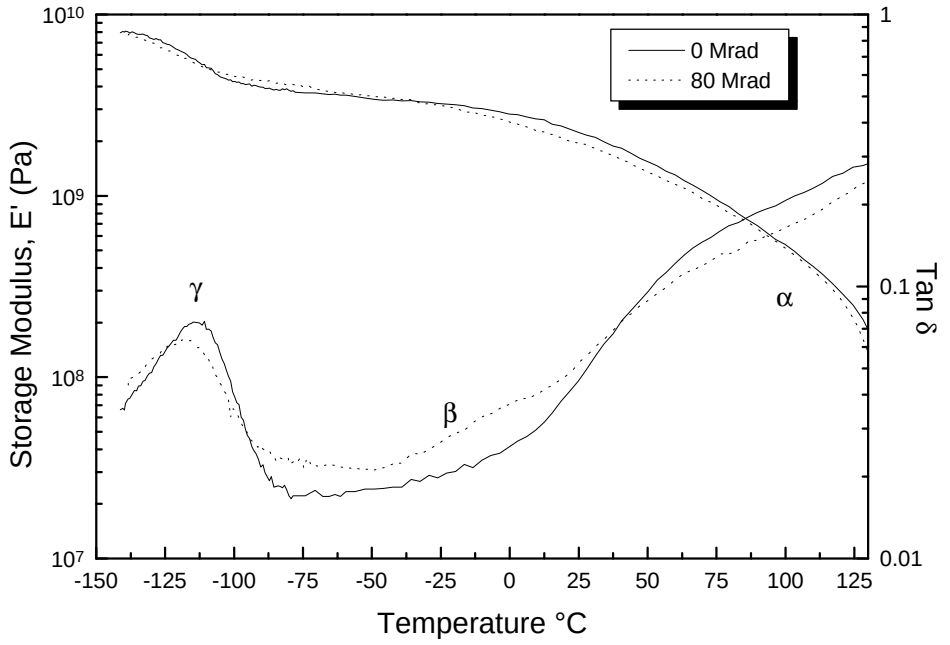

Figure 5-58 Film B machine direction 10Hz DMA for 0 and 80 Mrad doses. Heating rate was 0.5°C/min.

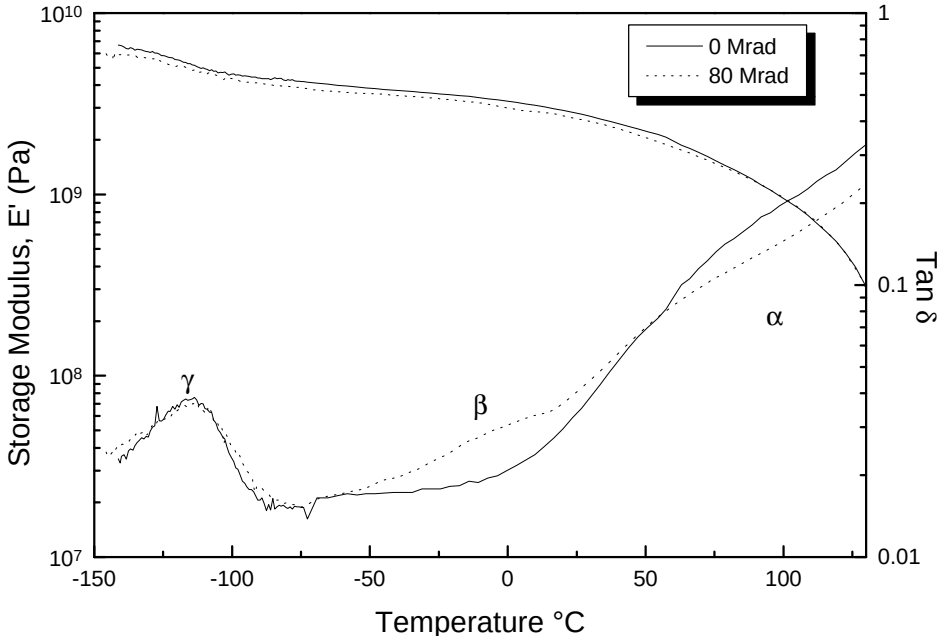

Figure 5-59 Film B transverse direction 10Hz DMA for 0 and 80 Mrad doses. Heating rate was 0.5°C/min. Note the similarity in the gamma region for the two doses. The TD gamma relaxation for this type of morphology is the least sensitive to crosslinking of the amorphous phase.

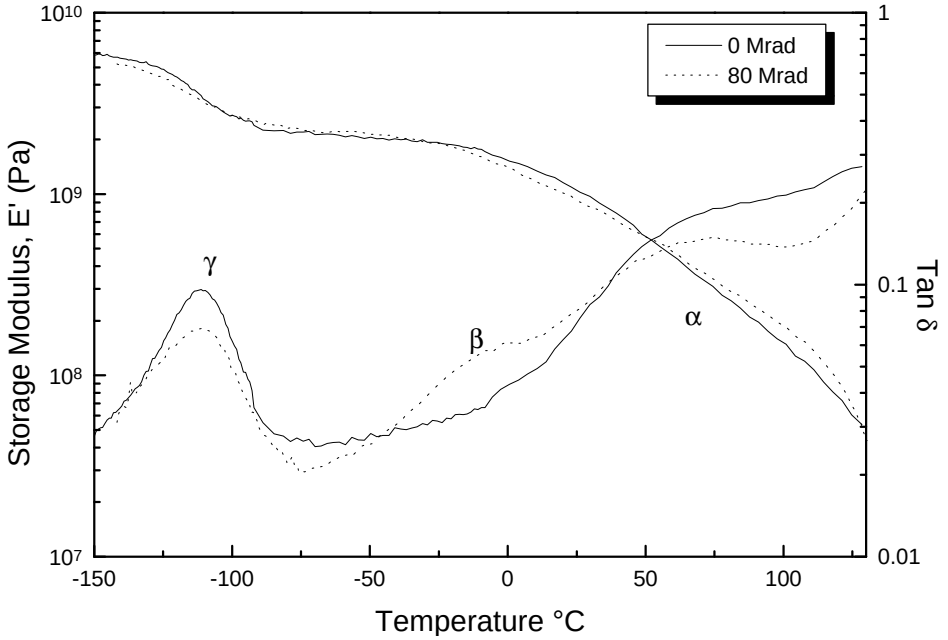

Figure 5-60 Film B 45° direction 10Hz DMA for 0 and 80 Mrad doses. Heating rate was 0.5°C/min.

5.4 Summary/Conclusions

A study is presented of the effects of electron beam irradiation on a HDPE polyethylene precursor having a simple and well defined stacked lamellar morphology used commercially to produce microporous membranes. In other work[261], radiation has been shown to increase the degree of crystallinity in ultra high and high molecular weight polyethylenes which should be noted were not oriented films. In this study, no observable increase in crystallinity was observed by DSC and the second heatings showed lower melting endotherms. There were no significant change in morphology as observed by TEM, SAXS, or WAXS. However, there was a dramatic reduction in water permeability of 50% at 40 Mrad in irradiated film B. DMA indicated that there is a difference in the nature of the amorphous phase in film B and that the irradiated films showed evidence of branching (i.e. crosslinking). Therefore, the main conclusion of this work is that the decrease in water permeability is a result of a change in the diffusion coefficient of the interlamellar amorphous phase in polyethlyene as a result of amorphous chain crosslinking.

6 Recommendations for Future Work

6.1 Process Structure Property Relationships in Electron Beam Generated Cellular Materials

This study has shown that it is possible to generate cellular materials by electron beam processing in a continuous manner. Fairly extensive process optimization was completed with respect to material properties as well as density. However, only one mixer was utilized to create these materials and, in general, one mixer speed. For the higher molecular weight oligomers, the mixer speed slowed considerably due to their higher viscosity. It would be interesting to see how the process optimization (mix viscosity vs. density) changed, if at all, with different mixer speeds and a stronger mixer. Note that limitations were observed for the utilized mixer when mix viscosities reached a 1200 Pa·S which is fairly high for oligomers - but no where near the viscosity of typical melt polymers. It also would be interesting to see if the frothing process could work for non-Newtonian polymers in the melt. If shear rates were kept down to where "mixer climb" was not a problem - it might be possible to froth a polymer in the melt and quench (or extrude) it thus producing a cellular polymer without blowing agent. One would likely be limited to a reduction in density of approximately 50% - and that, while not approaching that of foamed PS for example, could potentially have some applications for structural foam applications. Indeed one attempt was made with PET, and it did produce a somewhat frothed material but the viscosity of molten PET was too high to sufficiently froth the material to a suitable density.

6.2 Apparent Reversal of Physical Aging by Electron Beam Irradiation - Further Investigations

This study showed that there exists a strong correlation between G(s) and the dose required to deage a physically aged polymer. One obvious suggestion is to find a polymer that (1) is capable of physical aging and (2) as a G(s) value = 0 and a large G(x) value. This polymer should, in principal, display no deaging as observed in scissioning polymers (assuming no heating above Tg occurs during irradiation). Attempts along this line were made with a very low Tg polymer, however, it is doubtful that any polymer does exist that will not have any chain scissioning when EB irradiated. It is suggested, therefore, that if such a polymer exists, gamma irradiation under ultra high vacuum (10^{-7} Torr) be attempted as very low concentration of oxygen relative to the EB source would help reduce the number of scissions. Note, though, that a 40 Mrad experiment in EB takes only minutes to complete, it might take months to complete a gamma experiment, as dose rates can differ by 5 orders of magnitude in the case of Co^{60} gamma source. One would then have to complete the Charlesby-Pinner plot for the polymer in question (to prove that no scission took place) and then complete the deaging study. While this could take considerable effort, it could prove more distinctly, if the endgroup creation theory is valid.

6.3 Structure-Property Relationships in Electron Beam Irradiated High Density Polyethylene Extruded Tubular Films

There are no specific suggestions. It would be interesting to utilize some ultra high molecular weight oriented film with crystallinity in the range of 35% for a study. It is thought that along with the scission and crystallinity that has been shown to take place, a more dramatic increase in permeability would be observed. For the same materials used in the study, permeability to different vapors might prove interesting.

References

1 A.Charlesby, Atomic Radiation and Polymers, Pergamon Press, 1960.

2 J.H. O'Donnell, "Radiation Chemistry of Polymers", *ACS Symposium Series # **381** Chapter 1*, American Chemical Society, Washington, DC 1989.

3 Farhataziz, and M.A.J. Rodgers, Radiation Chemistry, Principles and Applications, VCH Publishers, New York, 1987.

4 J. Silverman, and A.R. Van Dyken, (Eds.), Radiation Processing Volume 1, Pergamon Press, New York, 1977, p.2.

5 G. Földiák,(ed.), Radiation Chemistry of Hydrocarbons, Elsevier Scientific Publishing Company, New York, 1981, p.2.

6 J.H. O'Donnell, "Chemistry of Radiation Degradation of Polymers", in Radiation Effects on Polymers, eds. Roger L. Clough and Shalaby W. Shalaby, ACS symposium series # **475**, American Chemical Society, Washington D.C., 1991.

7 Frank A. Bovey, The Effects of Ionizing Radiation on Natural and Synthetic High Polymers, Interscience Publishers, Inc., New York, 1958, p.2.

8 J.F. Kinstle, "Electron Beam Curing of Polymeric Materials" in Radiation Curing of Polymeric Materials, C.E. Hoyle, and J.F. Kinstle, (Eds.), ACS Symposium Series #**417**, American Chemical Society, Washington, D.C., 1990, p.18.

9 J.H. O'Donnell, and D.F. Sangster, Principles of Radiation Chemistry, American Elsevier Publishing Company, Inc., New York, 1970.

10 A. Charlesby, "The Effects of Ionizing Radiation on Polymers", Irradiation Effects on Polymers, ed. by D.W. Clegg and A.A. Collyer, Elsevier Applied Science, England, 1991.

11 Gordon Hughes, Radiation Chemistry, Clarendon Press, Oxford, 1973.

12 W.C. Roentgen, *Sitzungosberichte der Physikalisch-Medizinishen Gesellshaft zu Wurzburg*, 1895.

13 A.R. Denaro and G.G. Jayson, Fundamentals of Radiation Chemistry, The Butterworth Group, England, 1972, p.8.

14 H. Becquerel, "Sur quelques effets chimiques produits par le rayonnement du radium", *Compt. rend.*, **133**, 709-12, (1901).

15 Eugene P. Bertin, Introduction to X-ray Spectrometric Analysis, Plenum Press, New York, 1978, p.2.

16 M. Curie, *Compt. Rend.*, 1899, *129*, 823.

17 A.R. Denaro and G.G. Jayson, Fundamentals of Radiation Chemistry, The Butterworth Group, England, 1972, p.10.

18 G.W. Salmon, Polymers for High Technology, American Chemical Society, Washington, D.C., 1987.

19 W.P. Jorrisen and W.E. Ringer, *Brigchte*, 1906, *39*, 2093.

20 W.P. Jorrisen and H.W. Woudstra, *Ziet. Chem. u. Industrie d. Kolloid 1912*, *10*, 280.

21 W.D. Collidge, *Science*, 1925, **62**, 441

22 E.G. Newton, U.S.P. 1, 1929, 402 to the B.F. Goodrich Co.

23 Gordon Hughes, Radiation Chemistry, Clarendon Press, Oxford, 1973.

24 M. Dole, *Chemistry and Physics of Radiation Chemistry*; Report of Symposium IX, Army Chemical Center, Maryland, 1950.

25 A. Charlesby, *Proc. Roy. Soc.* 1952, **A215**, 1987.

26 E. Reichmanis and L.F. Thompson, in Polymers in Microlithography, Materials and Processes, E. Reichmanis, S.A. MacDonald, T. Iwayanagi, (eds.) ACS Symposium Series #**412**, American Chemical Society, Washington DC, 1989. p.1.

27 L.F. Thompson, C.G. Wilson, J.M.J. Fréchet, (Eds.), Materials for Microlithography, ACS Symposium Series #**266**, American Chemical Society, Washington, D.C., 1984.

[28] R. Clough and S.W. Shalaby, eds., "Radiation Effects on Polymers," *ACS Symposium Series* **475**, ACS Washington D.C., 1991.
[29] E. Reichmanis, C.W. Frank, and J.H. O'Donnell, eds., "Irradiation of Polymeric Materials, Processes, Mechanisms, and Applications", *ACS Symposium Series*, **527**, ACS, Washington D.C., 1993.
[30] W.M. Moreau, *Semiconductor Lithography Principles, Practices, and Materials,* Plenum Press, New York, 1988, p. 7.
[31] A. Charlesby, "The Effects of Ionizing Radiation on Polymers", D.W. Clegg and A.A. Collyer, (eds.), Irradiation Effects on Polymers, Elsevier Applied Science, London, 1991, p.76-77.
[32] A. Charlesby, "The Effects of Ionizing Radiation on Polymers", Irradiation Effects on Polymers, ed. by D.W. Clegg and A.A. Collyer, Elsevier Applied Science, England, 1991.
[33] J.H. O'Donnell and D.F. Sangster, Principles of Radiation Chemistry, American Elsevier Publishing Company, Inc., New York, 1970.
[34] Ibid, O'Donnell, p.404 (ACS #475).
[35] J.H. O'Donnell, "Radiation Chemistry of Polymers", *ACS Symposium Series # 381 Chapter 1*, American Chemical Society, Washington, DC 1989.
[36] H.C. Biggin, *An Introduction to Radiation Units and Measurement*, in Irradiation Effects on Polymers, Ch 1, D.W. Clegg and A.A. Collyer, eds, Elsevier Applied Science, London and New York, 1991.
[37] Gordon Hughes, Radiation Chemistry, Clarendon Press, Oxford, 1973.
[38] Farhataziz and M.A.J. Rodgers, (Eds.) Radiation Chemistry-Principles and Applications; VCH: New York, 1987.
[39] I.G. Kaplan, A.M. Miterev, Advances in Chemical Physics; vol. LXVIII; I.Prigogine, S.A.Rice, Eds.; Interscience: New York, 1987; pp.255-386.
[40] J.H. Baxendale, F.Busi, Eds.; The Study of Fast Processes and Transient Species by Electron Pulse Radiolysis; D. Reidel: Dordrecht, 1982.
[41] Linear Energy Transfer; International Commission on Radiological Units and Measurements: Washington, D.C., 1970; Report No. 16.
[42] Radiation Quantities and Units; International Commission on Radiological Units and Measurements: Bethesda, 1980; Report No. 33.
[43] "Radiation Dosimetry: Electron Beams with Energies between 1 and 50 MeV;" International Commission on Radiological Units and Measurements: Bethesda, 1980; Report No. 35.
[44] Microdosimetry; International Commission on Radiological Units and Measurements: Washington D.C., 1983; Report No. 36.
[45] David F. Sangster, Early Events in High-Energy Irradiation of Polymers, Chapter 2 in ACS symposium series #381, The Effects of Radiation on High-Technology Polymers, E.Reichmanis and J.H. O'Donnell, eds., American Chemical Society, Washington, DC 1989.
[46] ICRU, Report 31, Average energy required to produce an ion pair, ICRU Publications, Washington, D.C., 1979.
[47] H.C. Biggin, *An Introduction to Radiation Units and Measurement*, in Irradiation Effects on Polymers, Ch 1, D.W. Clegg and A.A. Collyer, eds, Elsevier Applied Science, London and New York, 1991.
[48] F.A.Bovey, The Effects of Ionizing Radiation on Natural and Synthetic High Polymers, Polymer Reviews Series, Vol. I, Interscience, New York, 1958.
[49] A. Charlesby, *Atomic Radiation and Polymers*, Pergamon Press, New York, 1960.
[50] A.R. Shultz, in Chemical Reactions of Polymers, ed by E.M. Fettes, Interscience, 1964.
[51] J.H. O'Donnell, and D.F.Sangster, Principles of Radiation Chemistry, American Elsevier Publishing Company, Inc., New York, 1970, p.9.
[52] Farhataziz, and Rodgers, M.A.J., Radiation Chemistry, Principles and Applications, VCH Publishers, New York, 1987, p.2.
[53] H.C. Biggin, *An Introduction to Radiation Units and Measurement*, in Irradiation Effects on Polymers, Ch 1, D.W. Clegg and A.A. Collyer, eds, Elsevier Applied Science, London and New York, 1991.

[54] I.G. Draganic, and Z.D. Draganic, The Radiation Chemistry of Water, Academic Press, New York, 1971, p.23-29.

[55] A.Charlesby, "The Effects of Ionizing Radiation on Polymers", Clegg, D.W., and Collyer, A.A.eds., Irradiation Effects on Polymers, Elsevier Applied Science, London, 1991, p.73-74.

[56] H.C. Biggin, *An Introduction to Radiation Units and Measurement*, in Irradiation Effects on Polymers, Ch 1, D.W. Clegg and A.A. Collyer, eds, Elsevier Applied Science, London and New York, 1991.

[57] O'Donnell, James H., "Radiation Chemistry of Polymers", *ACS Symposium Series # 381 Chapter 1*, American Chemical Society, Washington, DC 1989.

[58] Adolphe Chapiro, Radiation Chemistry of Polymeric Systems, John Wiley and Sons, London, 1962, p.19.

[59] H.C. Biggin, *An Introduction to Radiation Units and Measurement*, in Irradiation Effects on Polymers, Ch 1, D.W. Clegg and A.A. Collyer, eds, Elsevier Applied Science, London and New York, 1991.

[60] Farhataziz, and Rodgers, M.A.J., Radiation Chemistry, Principles and Applications, VCH Publishers, New York, 1987, p.3-10.

[61] Y.Tabata, Y.Ito, and S.Tagawa, Eds., CRC Handbook of Radiation Chemistry, CRC Press, Boston, 1991, p.3.

[62] Farhataziz, and Rodgers, M.A.J., Radiation Chemistry, Principles and Applications, VCH Publishers, New York, 1987, p.2.

[63] H.C. Biggin, *An Introduction to Radiation Units and Measurement*, in Irradiation Effects on Polymers, Ch 1, D.W. Clegg and A.A. Collyer, eds, Elsevier Applied Science, London and New York, 1991.

[64] Farhataziz, and Rodgers, M.A.J., Radiation Chemistry, Principles and Applications, VCH Publishers, New York, 1987.

[65] J.H.O'Donnell, "Radiation Chemistry of Polymers", *ACS Symposium Series # 381 Chapter 1*, American Chemical Society, Washington, DC 1989, p.2.

[66] I.G.Draganic, and Z.D.Draganic, The Radiation Chemistry of Water, Academic Press, New York, 1971, p.23-29.

[67] A. Einstein, "Uber einen die Erzeugung und Verwandlung des Lichtes betreffenden heuristischen Gesichtspunkt," *Annalen der Physik* 17, 132 (1905).

[68] Farhataziz, and Rodgers, M.A.J., Radiation Chemistry, Principles and Applications, VCH Publishers, New York, 1987, p.4-6.

[69] Eyvind H.Wichmann, Quantum Physics, McGraw-Hill, New York, 1971

[70] H.C. Biggin, *An Introduction to Radiation Units and Measurement*, in Irradiation Effects on Polymers, Ch 1, D.W. Clegg and A.A. Collyer, eds, Elsevier Applied Science, London and New York, 1991.

[71] G.Hughes, Radiation Chemistry, Clarendon Press, Oxford, 1973.

[72] O'Donnell, James H., "Radiation Chemistry of Polymers", *ACS Symposium Series # 381 Chapter 1*, American Chemical Society, Washington, DC 1989 p.2-3.

[73] ICRU, Report 33, Radiation quantities and units, ICRU Publications, Washington, DC, 1980.

[74] G.Hughes, Radiation Chemistry, Clarendon Press, Oxford, 1973.

[75] T.E. Burlin, Cavity chamber theory, in *Radiation Dosimetry I*, F.H. Arrix, W.C. Roesch and E. Tochilin (Eds), Academic Press, London, 1968.

[76] L. Weisner, *Proc. Int. Symp. High Dose Dosimetry*, IAEA, Vienna, 1985, p.95.

[77] James H. O'Donnell, "Radiation Chemistry of Polymers", *ACS Symposium Series # 381 Chapter 1*, American Chemical Society, Washington, DC 1989.

[78] James H. O'Donnell, "Chemistry of Radiation Degradation of Polymers", in Radiation Effects on Polymers, eds. Roger L. Clough and Shalaby W. Shalaby, ACS symposium series # 475, American Chemical Society, Washington D.C., 1991.

[79] G.Hughes, Radiation Chemistry, Clarendon Press, Oxford, 1973.

[80] R.W. Tess, and G.W. Poehlein, (Eds.) Applied Polymer Science, Second Ed., ACS Symposium Series #285, American Chemical Society, Washington, D.C., 1985.

[81] M.S. de. Wilton, *Radiat. Phys. Chem.*, 1985, **25**(4-6), 643

82 A.Miller, *Radiat. Phys. Chem.*, 1986, **28**(5-6), 521.

83 E.M.Fielden and N.W. Holm, Dosimetry in accelerator research and processing, in *Manual on Radiation Dosimetry*, N.W. Holm and R.J. Berry (Eds), Marcel Dekker, New York, 1970.

84 N.Tamura, *Radiat. Phys. Chem.*, 1981, 18(1-2), 281.

85 N.A. Halls, "Gamma-irradiation Processing", D.W.Clegg, and A.A.Collyer, eds., Irradiation Effects on Polymers, Elsevier Applied Science, London, 1991, pp 253-296.

86 James H. O'Donnell, "Radiation Chemistry of Polymers", *ACS Symposium Series # 381 Chapter 1*, American Chemical Society, Washington, DC 1989.

87 M.C. Lagunas-Solar and S.M. Matthews, *Radiat. Phys. Chem.*, 1985, **25**(4-6), 691.

88 Farhataziz, and Rodgers, M.A.J., Radiation Chemistry, Principles and Applications, VCH Publishers, New York, 1987, p.3-10.

89 G.Hughes, Radiation Chemistry, Clarendon Press, Oxford, 1973.

90 James H. O'Donnell, "Radiation Chemistry of Polymers", *ACS Symposium Series # 381 Chapter 1*, American Chemical Society, Washington, DC 1989.

91 J.H.O'Donnell, in *The Effects of Radiation on High-Technology Polymers;* E.Reichmanis, J.H.O'Donnell, Eds.; Symposium Series 381; Amer.Chem.Soc.; Washington, DC, 1989, p.1.

92 A.Charlesby, N.Moore, Int. *J.Appl.Rad.Isotopes* 1964, **15**, 703.

93 K.Wundrich, *J.Polym.Sci., Polym.Chem.Ed.* 1964, **11**, 1293.

94 K.Wundrich, *Europ.Polym.J.* 1971, **10**, 341.

95 R.W.Garrett, D.T.J.Hill, T.T.Le, K.A.Milne, J.H.O'Donnell, S.M.C.Perera, and P.J.Poyery, "Temperature Dependence of the Radiation Chemistry of Polymers, in Radiation Effects on Polymers, Roger L.Clough, and Shalaby W. Shalaby eds., ACS Symposium Series #475, 1991, p.147.

96 T.N.Bowmer, J.H.O'Donnell, *J.Macromol.Sci.Chem.* 1982, **A17**, 243.

97 S.R. Turner, C.C. Anderson, K.M. Kolterman, and D. Seligson, "X-Ray-Sensitive Alternating Copolymers", *ACS Symposium Series # 381 Chapter 11*, American Chemical Society, Washington, DC 1989.

98 A.Chapiro, Radiation Chemistry of Polymeric Systems, John Wiley and Sons, London, 1962, p.394.

99 P.J.Flory, *Am. Chem. Soc.*, **63**, 3096, 1941.

100 W.H. Stockmayer, *J. Chem. Phys.*, **12**, 125, 1944.

101 A.M.Rijke, L.Manderlern, *Macromolecules*, **4**, 594, 1971.

102 B.J.Lyons, F.E. Weir, in *The Radiation Chemistry of Macromolecules*, Ed. M. Dole, Academic Press, New York, **2**, 281, 1973.

103 J.H.O'Donnell, "Radiation Chemistry of Polymers", *ACS Symposium Series # 381 Chapter 1*, American Chemical Society, Washington, DC 1989.

104 E. Reichmanis, "Radiation Chemistry of Polymers for Electronic Applications", *ACS Symposium Series # 381 Chapter 9*, American Chemical Society, Washington, DC 1989.

105 Gordon Hughes, Radiation Chemistry, Clarendon Press, Oxford, 1973.

106 J.H.O'Donnell, "Radiation Chemistry of Polymers", *ACS Symposium Series # 381 Chapter 1*, American Chemical Society, Washington, DC 1989.

107 G.Hughes, Radiation Chemistry, Clarendon Press, Oxford, 1973.

108 A.Charlesby, "Use of High Energy Radiation for Crosslinking and Degradation" in Silverman, J., and Van Dyken, A.R., (Eds.), Radiation Processing Volume 1, Pergamon Press, New York, 1977.

109 H.Kim and G.L. Wilkes, NBR paper...

110 G.A.Chadwick, *Metallography of Phase Transitions*, Crane, Russak & Co., New York (1972).

111 J.Burke, *The Kinetics of Phase Transformations in Metals*, Pergamon Press, Oxford (1965).

112 J.K.Gillham, *Soc.Plas.Eng.Proc.An.Tech.Conf.*, **38**, 238 (1980).

113 J.B.Enns, J.K.Gillham, and R.Small, *Polym. Prepr. Am. Chem. Soc. Div. Polym. Chem.*, **22**(2), 123 (1981).

114 J.B.Enns, and J.K.Gillham, in *Polymer Characterization: Spectroscopic, Chromatographic, and Physical Instrumental Methods*, C.D. Craver, ed., *Adv. Chem. Ser.*, **203**, ACS, Washington D.C. (1983) p.27

115 J.K.Gillham, in *Development in Polymer Characterization-3*, J.V.Dawkins, ed., Applied Science, London (1982) p.159.

116 L.C.Chan, N.H.Nae, and J.K.Gillham, *J.Appl.Polym.Sci.*, **29**, 3307 (1984).

117 X.Peng, and J.K.Gillham, *J. Appl. Polym. Sci.*, **30**, 4685 (1985).

118 J.K.Gillham, *Polym. Eng. Sci.*, **26,** 1429 (1986).

119 C.C.Chan, J.K.Gillham, *J.Appl.Polym.Sci.,* **30**, 4685 (1985).

120 J.H.O'Donnell, "Radiation Chemistry of Polymers", *ACS Symposium Series # 381 Chapter 1*, American Chemical Society, Washington, DC 1989.

121 J.H.O'Donnell, "Radiation Chemistry of Polymers", *ACS Symposium Series # 381 Chapter 1*, American Chemical Society, Washington, DC 1989.

122 G.Hughes, Radiation Chemistry, Clarendon Press, Oxford, 1973.

123 J.O'Donnell, "Radiation Chemistry of Polymers", *ACS Symposium Series # 381 Chapter 1*, American Chemical Society, Washington, DC 1989.

124 F.W.Harris, and H.J.Spinelli, Reactive Oligomers, ACS Symposium Series #282, American Chemical Society, Washington, D.C., 1985.

125 N.Shiraishi, J.L.Williams, V.T.Stannett, *Radiat. Phys. Chem.*, 1982, **19**, 73.

126 M.Suzuki, Y.Tamada, H.Iwata, Y.Ikada, *Physicochemical Aspects on Polymer Surface*; K.L.Mittal, Ed., Plenum, NY, 1983, Vol 2; pp923-941.

127 J.T.Simpson, *Radiat. Phys. Chem.*, 1985, **25**, 483.

128 U.Wang, *Radiat. Phys. Chem.*, 1985, **25**, 491.

129 Japan Kikai Tokkyo Koho; 54-148547.

130 K.Kaji, M.Hatada, I.Yoshizawa, C.Kohara, K.Kimai, *J.Appl.Polym.Sci.*, 1989, **37***,* 2153.

131 *Annual Report of the Osaka Laboratory for Radiation Chemistry Japan Atomic Energy Research Institute*, vol 20 JAEERI-M 88-272, **29,** 1988.

132 H.Omichi, D.Chundury, V.T.Stannett, *J.Appl.Polym.Sci.*, 1986, **32**, 4827.

133 J.D.Andrade, *ACS Polymer Preprint*, 1972, **13**, 290.

134 B.D.Rather, A.S.Hoffman, *J.Appl.Polym.Sci.*, 1974, **18***,* 3183.

135 D.J.Lyman,. *Trans. Am. Soc. Art. Int. Org.*, 1972, **18**, 19.

136 A.Chapiro, M.F.Millequant, A.M.Jendrychowska-Bonamour, Y.Lerke, P.Sadurni, D.Domurado, *Radiat. Phys. Chem.*, 1980, **15**, 423.

137 Y.Sasaki, B.D.Ranter, A.S.Hoffman, *ACS Polymer Preprint*, 1975, **16**, 435.

138 Japan Patent 53-46199.

139 S.B.Vitta, E.P.Stahel, V.T.Stannett, *J. Macromol. Sci. A*, 1985, **22**, 579.

140 S.B.Vitta, E.P.Stahel, V.T.Stannett, *J. Appl. Polym. Sci.*, 1986, **32**, 5799.

141 N.Shiraishi, J.L.Williams, V.T.Stannett, *Radiat. Phys. Chem.*, 1982, **19***,* 79.

142 A.Charlesby, P.J.Fydelor, *Radiat. Phys. Chem.*, 1972, **4**, 107.

143 C.Guimson, *Radiat. Phys. Chem.*, 1979, **14**, 841.

144 J.P.Lawler, A.Charlesby, *Radiat. Phys. Chem.*, 1980, **5**, 595.

145 L.P.Sidorova, A.D.Aliev, V.B.Zlobin, R.E.Aliev, A.E.Chalkh, V.Y.Kabanov, *Radiat. Phys. Chem.*, 1986, **28**, 407.

146 L.N.Grushevskaya, R.E.Aliev, V.Y.Kabanov, *Radiat. Phys. Chem.*, 1990, **36**, 475.

147 I.Ishigaki, T.Sugo, K.Senoo, T.Takayama, S.Machi, J.Okamoto, T.Okada, *Radiat. Phys. Chem.*, 1981, **18**, 899.

148 I.Ishigaki, T.Sugo, T.Takayama, T.Okada, J.Okamoto, K.Senoo, *J. Appl. Polym. Sci.*, 1982, **27**, 1033.

149 I.Ishigaki, T.Sugo, T.Takayama, T.Okada, J.Okamoto, S.Machi, *J. Appl. Polym. Sci.*, 1982, **27**, 1043.

150 S.Tanso, S.Yoshida, K.Senoo, *Yuasa Jiho*, 1985, **59**, 35.

151 H.Omichi, D.Chundry, V.T.Stannett, *J.Appl.Polym.Sci.*, 1986, **32**, 4827.

152 H.Omichi, J.Okamoto, *J. Appl. Polym. Sci.*, 1985, **30**, 1277.
153 J.Okamoto, T.Sugo, A.Katakai, H.Omichi, *J. Appl. Polym. Sci.*, 1985, **30**, 2967.
154 S.Furusaki, J.Okamoto, T.Sugo, K.Saito, *Chemical Engineering*, 1987, 521.
155 K.Saito, S.Yamada, S.Furusaki, T.Sugo, J.Okamoto, *J. Membrane Sci.*, 1987, **32**, 307.
156 S.Furusaki, J.Okamoto, T.Sugo, K.Saito, *Chemical Engineering*, 1987, 521.
157 J.Okamoto, *Membrane*, 1989, **14**, 277.
158 Z.H.Pimg, Q.T.Nguyen, R.Clement, J.Neel, *Membrane Sci.*, 1990, **48**, 297.
159 A.S. Hoffman, *Intern. Meet. Radiat. Process.*, 1989, Tokyo, 297.
160 Kaetsu, I. *Radiation Technology for Immobilization of Bioactive Materials*, 1987, Beijing, 153.
161 J. Hadada, R.T. Chern, and V.T. Stannett,"Acrylic-Acid-Grafted Polyethylene by Electron Beam Preirradiation Method", in Radiation Effects on Polymers, R.L. Clough, and S.W. Shalaby, eds., ACS Symposium Series #475, 1991, p.239.
162 G. Hughes, Radiation Chemistry, Clarendon Press, Oxford, 1973.
163 P.A. Dworjanyn, B. Fields, and J.L. Garnett, "Effects of Various Additives on Accelerated Grafting and Curing Reactions Initiated by UV and Ionizing Radiation", *ACS Symposium Series # 381 Chapter 8*, American Chemical Society, Washington, DC 1989.
164 J. Hadada, R.T. Chern, and V.T. Stannett, "Acrylic-Acid-Grafted Polyethylene by Electron Beam Preirradiation Method", in Radiation Effects on Polymers, Clough, Roger L., and Shalaby, Shalaby W., eds., ACS Symposium Series #475, 1991, p.238.
165 A.Charlesby, "The Effects of Ionizing Radiation on Polymers", Irradiation Effects on Polymers, ed. by D.W. Clegg and A.A. Collyer, Elsevier Applied Science, England, 1991, pp. 68-70.
166 Perry's Chemical Engineer's Handbook, 6th edition, p. 18-57(1984).
167 L.J. Gibson and M.F.Ashby, Cellular Solids Structure and Properties, Pergamon Press, New York, 1988.
168 Berkman and Egloff, *Emulsions and Foams*, Reinhold, New York, 1941 pp. 112-152.
169 Perry's Chemical Engineer's Handbook, 6th edition, p. 18-57(1984).
170 Bikerman, *Foams: Theory and Industrial Applications*, Reinhold, New York, 1953, p.10.
171 Blander and Katz, *Am.Inst.Chem.Eng.J.*, 21, 833 (1975).
172 Wark, *J.Phys.Chem.*, **37**, 623 (1933).
173 Jakob, *Mech.Eng.*, **58**, 643, (1936).
174 Perry's Chemical Engineer's Handbook, 6th edition, p. 18-57(1984).
175 Siberman, *Proceedings of the Fifth Midwestern Conference on Fluid Mechanics*, University of Michigan Press, Ann Arbor, 1957, pp. 263-284.
176 Perry's Chemical Engineer's Handbook, 6th edition, p. 18-59(1984).
177 Ibid, Bikerman, p. 161.
178 Maragoni, *Nuovo cimento*, no. 2, **5-6**, 239 (1871).
179 Ibid, Berkman and Egloff p. 133.
180 Ibid, Bikerman, Ch 11.
181 Bartsch, *Kolloidchem. Beih.*, **20**, 1 (1925).
182 Perry's Chemical Engineer's Handbook, 6th edition, p. 18-59(1984).
183 Fundy and Bates, *Am. Inst. Chem. Eng.*, **9**, 338 (1963).
184 Perry's Chemical Engineer's Handbook, 6th edition, p. 18-65(1984).
185 Allaway et al., U.S. Patent # 4,378,278 (1983).
186 Clines et al., U.S. Patent # 3,484,352 (1969).
187 Minomi et al., U.S. Patent # 3,709,806 (1973).
188 Schisler et al., U.S. Patent # 4,767,793 (1988).
189 Schisler et al., U.S. Patent # 4,771,078 (1988).
190 R. Greiner and F. R. Schwarzl, Rheo Acta 23, 378 (1984).
191 L. C. E. Struik, Physical Aging in Amorphous Polymers and Other Materials, Elsevier, New York, 1978.

192 J. J. Aklonis and W. J. MacKnight, *Introduction to Polymer Viscoelasticity*, John Wiley and Sons, New York, NY (1983).
193 I. M. Ward, *Mechanical Properties of Solid Polymers*, Wiley-Interscience, New York, NY (1971).
194 J. D. Ferry, *Viscoelastic Properties of Polymers*, Wiley and Sons, New York, NY (1971).
195 G. B. McKenna, Comprehensive Polymer Science, Vol 2. Polymer Properties, C. Booth and C. Price, Eds., Pergamon, Oxford, (1990).
196 J. H. Gibbs, *J. Chem. Phys*., **25,** 185, (1956).
197 J. H. Gibbs and E. A. DiMarzio, *J. Chem. Phys*., **28**, 373 (1958).
198 E. A. DiMarzio and J. H. Gibbs, *J. Chem. Phys*., **28**, 807 (1958).
199 R. N. Haward, The Physics of Glassy Polymers, John Wiley and Sons, New York, 26, 1973.
200 A. Bondi, *J. Phys. Chem*., **58**, 929 (1954).
201 M. H. Cohen and D. Turnbull, *J. Chem. Phys*., **31**, 1164 (1959).
202 D. Turnbull and M. H. Cohen, *J. Chem. Phys*., **34**, 120 (1961).
203 R. Simha and T. Somcynsky, *Macromolecules* **2**, 342, (1969).
204 T. Somcynsky and R. Simha, *J. Appl. Phys*., **42**, 4545 (1971).
205 W. Kauzmann, Chem Rev. **43**, 219 (1948).
206 J. H. Gibbs, J. Chem. Phys. 25, 185 (1956).
207 J. H. Gibbs and E. A. DiMarzio, J. Chem. Phys. 28, 373 (1958).
208 E. A. DiMarzio and J. H. Gibbs, J. Chem. Phys. 28, 807 (1958).
209 J. M. G. Cowie and P. M. Toporowski, Eur. Polym. J. 4, 621 (1968).
210 J. A. Faucher, J. Polym. Sci. Pt. B, 3, 143 (1965).
211 R. B. Beevers and E. F. T. White, Trans. Faraday Soc. 56, 744 (1960).
212 K. Uebrreiter and G. Kanig, J. Chem. Phys. 18, 399 (1950).
213 E. A. DiMarzio, J. Res. Natl. Bur. Stand., Sect. A 68A, 611 (1964).
214 E. A. DiMarzio and J. H. Gibbs, J. Polym. Sci. 40, 121 (1959).
215 J. M. Gordon, G. B. Rouse, J. H. Gibbs and W. M. Risen, Jr., J. Chem. Phys. 66, 4971 (1977).
216 T. S. Chow, Ferroelectrics 30, 139 (1980).
217 W. Kauzmann, *Chem. Rev.*, **43**, 219 (1948).
218 M. H. Cohen and D. Turnbull, J. Chem. Phys. 31, 1164 (1959).
219 D. Turnbull and M. H. Cohen, J. Chem. Phys. 34, 120 (1961).
220 R. Simha and T. Somcynsky, Macromolecules 2, 342 (1969).
221 T. Somcynsky and R. Simha, J. Appl. Phys. 42, 4545 (1971).
222 J. A. Faucher, J. Polym. Sci. , Pt. B, 3, 143 (1965).
223 G. Pezzin, F. Zillio-Grandi and P. Sammartin, Eur. Polym. J. 6, 1053 (1970).
224 S. Loshaek, J. Polym. Sci. 15, 391 (1955).
225 T. G. Fox, and S. Loshaek, J. Polym. Sci. 15, 371 (1955).
226 M. Gordon and J. S. Taylor, J. Appl. Chem. 2, 493 (1952).
227 L. C. E. Struik, Physical Aging in Amorphous Polymers and Other Materials, Elsevier, New York, 1978.
228 L.C.E. Struik, Physical Aging in Amorphous Polymers and Other Materials, Elsevier, New York, (1978).
229 K. Neki and P.H. Geil, *J.Macromol.Sci.-Phys. (B),* **8**, 295 (1973).
230 J.H. O'Donnell, "Radiation Chemistry of Polymers", Chapter 1 in *ACS symposium series #381*, E.Reichmanis and J.H. O'Donnell, eds., American Chemical Society, Washington, DC (1989).
231 J.H. O'Donnell, "Chemistry of Radiation Degradation of Polymers", in Radiation Effects on Polymers, eds. R.L. Clough and S.W. Shalaby, ACS symposium series # 475, American Chemical Society, Washington D.C., (1991).
232 A. Charlesby, "The Effects of Ionizing Radiation on Polymers", Irradiation Effects on Polymers, eds. D.W. Clegg and A.A. Collyer, Elsevier Applied Science, England, (1991).
233 M.R. Tant and G.L. Wilkes, *Polym. Eng. Sci.*, **21** (14) (1981).

234 J.M. Hutchinson. *Prog. Colloid Polym. Sci.*, **87**, 69 (1992).
235 Allaway et al., U.S. Patent # 4,378,278, 1983.
236 Clines et al., U.S. Patent # 3,484,352, 1969.
237 Minomi et al., U.S. Patent # 3,709,806, 1973.
238 Schisler et al., U.S. Patent # 4,767,793, 1988.
239 Schisler et al., U.S. Patent # 4,771,078, 1988.
240 Clines, et al., U.S. Patent # 3,484,352 1969.
241 Uejikkoku, et al., U.S. Patent # 5,110,842 1992.
242 Saito, et al., U.S. Patent # 3,709,806, 1973.
243 Shikinami, et al., U.S. Patent # 4,144,153, 1979.
244 Goswami et al., U.S. Patent # 4,187,159, 1980.
245 Schisler et al., U.S. Patent # 4,767,793, 1988.
246 Allaway, et al., U.S. Patent # 4,378,278, 1983.
247 D.C. McHerron and G.L. Wilkes, "Formation of Polymeric Microspheres Using Electron Beam Radiation", *J.Appl.Poly.Sci.,* Vol. 42, 1045-1058 (1991).
248 Allaway et al., U.S. Patent # 4,378,278, 1983.
249 Reid, Prausnitz, and Sherwood, *The Properties of Gases and Liquids, 3rd Ed.*, McGraw Hill, New York, 1977.
250 V.M.Lobe, M.S. thesis, University of Rochester, Rochester, N.Y., 1973.
251 L.J.Gibson and M.F.Ashby, Cellular Solids, Structure and properties., Pergmanon Press, Oxford, 1988.
252 D.C. McHerron and G.L. Wilkes, *Polymer* 1993 **34** (5).
253 J.W. Connell, E.J. Siochi, and *C.I. Croall, High Perform. Polym.*, **5**, 1-14 (1993).
254 A.Charlesby and S.H.Pinner, *Proc.R.Soc.,* London (A222), **60**, 542 (1955).
255 A.Charlesby and S.H.Pinner, *Proc.R.Soc.,* London (A224), **60**, 120, (1954).
256 A.Charlesby and S.H.Pinner, *Proc.R.Soc.,* London (A231), **60**, 521 (1955).
257 A.Charlesby, Atomic Radiation and Polymers, Pergamon Press, 1960.
258 V.T. Stannett, private communication, Raleigh, NC; May 12, 1996; tea time.
259 A. Chapiro, *Polymer Handbook*, 2nd ed., J. Brandrup, E.H. Immergut, eds. John Wiley & Sons, (1975).
260 H. Kita, M. Muraoka, K. Tanaka, and K. Okamoto, *Polymer Journal*, **20**, 6, 485 (1988).
261 S.K. Bhateja, R.W. Duerst, J.A. Martens, and E.H. Andrews, *J.M.S.-Rev. Macromol. Chem. Phys.*, C35(4), 581-659 (1995).
262 J.E. Sax, V.P. Thalacker, T.E. Boettcher, and E.G. Larson, *Radiat. Phys. Chem.*, **31**, 4-6, pp887-896, 1988.
263 Ta-Hua Yu, Ph.D. Dissertation, Virginia Tech, 1996.
264 G.L. Wilkes, *Encycl. Polym. Sci. and Eng.,* John Wiley & Sons, Inc., 1988 **14**, 542.

Vita

Robert William Alonzo Greer IV was born at Fort Belvoir Virginia on June 20, 1969 in between his father's first and second tours of duty in Vietnam. The family eventually moved to Madison, Wisconsin where his brother, Matthew, was born in 1972. Shortly thereafter the family moved to South Bend, Indiana where they lived until 1979. They then moved to Greensboro, North Carolina where his parents still live. Rob attended Western Guilford High School where he enjoyed playing varsity football, band, and science fairs. During his senior year, he started dating Janice Gunn. He left for North Carolina State University in Raleigh that fall. During his sophomore year at NC state, he co-oped with Analog Devices in Greensboro. During his senior year at NCSU he worked for Professor Vivian T. Stannett, a pioneer of diffusion and radiation chemistry of polymers. In May, 1992 he graduated with a BS in Chemical Engineering. After finishing a project for Professor Stannett that led to his first peer reviewed publication, he left for Virginia Tech to attend graduate school under the direction of Professor Garth L. Wilkes. One year later he married the former Janice Gunn. After finishing his work under professor Wilkes, he will join Alcatel in their optical fiber coatings R&D group in Claremont NC.

Rob has enjoyed playing the piano since the age of 6. He plays several other musical instruments with various degrees of competence. He enjoys racquetball and basketball and is arguably highly skilled at both. He spends what spare time he has backpacking, fly fishing, brewing beer, cooking Italian cuisine, maintaining his many aquariums, putting small tightly grouped holes in paper from great distances, spending money on his computer, working on his car, and best of all - playing with his son, Zachary.